

AD-A132 033

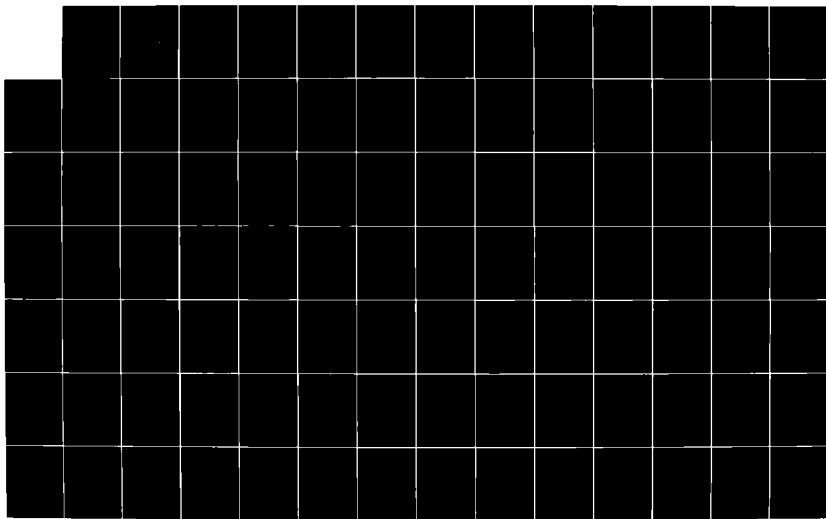
A STUDY OF NORMAL SHOCK-WAVE TURBULENT BOUNDARY-LAYER  
INTERACTIONS AT MAC... (U) ROYAL AIRCRAFT ESTABLISHMENT  
FARNBOROUGH (ENGLAND) W G SAWYER ET AL. OCT 82  
RAE-TR-82099 DRIC-BR-88360

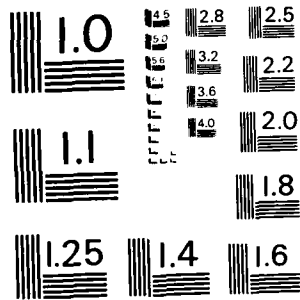
1/2

UNCLASSIFIED

F/G 20/4

NI





MICROCOPY RESOLUTION TEST CHART  
NATIONAL BUREAU OF STANDARDS-1963-A

TR 82099

ADA 132033

UNLIMITED  
PC (30-T) 11-7-83 JH

BR 88360

TR 82099

(4)



ROYAL AIRCRAFT ESTABLISHMENT

\*

Technical Report 82099

October 1982

**A STUDY OF NORMAL SHOCK-WAVE  
TURBULENT BOUNDARY-LAYER  
INTERACTIONS AT MACH NUMBERS  
OF 1.3, 1.4 AND 1.5**

by

W. G. Sawyer  
Carol J. Long

\*

DTIC  
ELECTE  
SEP 01 1983  
S E

Procurement Executive, Ministry of Defence  
Farnborough, Hants

DTIC FILE COPY

UNLIMITED

88 08 17 037

UDC 532.526.4 : 533.6.011.72

R O Y A L   A I R C R A F T   E S T A B L I S H M E N T

Technical Report 82099

Received for printing 27 October 1982

A STUDY OF NORMAL SHOCK-WAVE TURBULENT BOUNDARY-LAYER INTERACTIONS  
AT MACH NUMBERS OF 1.3, 1.4 AND 1.5

by

W. G. Sawyer  
Carol J. Long

SUMMARY

This Report presents the results of a study of seven flows involving the interaction between a normal shock wave and a two-dimensional turbulent boundary layer. The measurements were made at free-stream Mach numbers of 1.3, 1.4 and 1.5 and at Reynolds numbers based on an effective streamwise run of  $10 \times 10^6$  to  $30 \times 10^6$ . The results were obtained from comprehensive traverses with both pitot and static probes.

Standard boundary-layer integral parameters based on wall and measured static pressures are presented, together with velocity profiles and the Mach number distribution over the interaction region.

An investigation has been made of the 'law of the wall' and the 'law of the wake' under the influence of strong normal pressure gradients.

Departmental Reference: Aero 3532

Copyright  
©  
Controller HMSO London  
1982



Accession For	
NTIS GRA&I	<input checked="" type="checkbox"/>
DTIC TAB	<input type="checkbox"/>
Unannounced	<input type="checkbox"/>
Justification	
By	
Distribution	
Availability Codes	
Dist	
<b>A</b>	

LIST OF CONTENTS

	<u>Page</u>
1 INTRODUCTION	3
2 DESCRIPTION OF THE EXPERIMENT	4
2.1 Mechanical arrangement	4
2.2 Experimental measurements	6
2.2.1 Pitot measurements	6
2.2.2 Floor static pressure measurements	6
2.2.3 Reversed pitot measurements	6
2.2.4 Static probe measurements	6
2.2.5 Shock-wave position	7
3 REDUCTION OF DATA	7
3.1 Boundary-layer profiles	8
3.2 Integral parameters	9
3.2.1 Static pressure constant and equal to the measured wall pressure	10
3.2.2 Static pressure variation as measured	11
3.2.3 Equivalent inviscid static pressure together with measured static pressure	12
3.3 Skin friction	12
4 EXPERIMENTAL RESULTS	13
4.1 The general characteristics of the flow	13
4.1.1 Shock-wave patterns	13
4.1.2 Flow visualisation	13
4.1.3 Momentum balance	14
4.2 Edge Mach numbers and boundary layer parameters	16
4.3 Measured static pressures	17
4.4 Mach number distribution	17
4.5 Boundary-layer velocity profiles	18
4.5.1 General	18
4.5.2 Logarithmic velocity profiles	18
4.5.3 The law of the wall	19
4.5.4 Departures from equilibrium and the law of the wake	20
5 CONCLUSIONS	23
Appendix Static pressure probe corrections	25
Tables 1 to 3	30
List of symbols	94
References	96
Illustrations	Figures 1-33
Report documentation page	inside back cover

## 1 INTRODUCTION

A series of experiments<sup>1-4</sup> has been undertaken in the RAE Bedford 3ft x 3ft wind tunnel to investigate the interaction of a normal shock wave and a turbulent boundary layer at nominal upstream Mach numbers of 1.3, 1.4 and 1.5 over a Reynolds number range based on the undisturbed boundary-layer momentum thickness at the start of the interaction of  $12 \times 10^3$  to  $34 \times 10^3$ .

This Report deals with the measurements made at a series of stations upstream and downstream of the interaction using conventional pitot and static probes traversed normal to the flat wall.

The series of experiments was planned because of the lack of knowledge of the interaction between normal shock waves and turbulent boundary layers at high Reynolds numbers and the need to predict the development of the boundary layer through and beyond the interaction region as, for example, in the flow over supercritical aerofoils.

A number of investigations have been reported over the past two decades and broadly speaking three techniques have been used to produce the interaction.

The first and most commonly used technique (Fig 1a) in supersonic tunnels is to position a shock generator with downstream choking flap over a flat plate so that the steady normal shock wave formed by the shock generator interacts with a turbulent boundary layer grown from the leading edge of the flat plate. This is the technique adopted by Seddon<sup>5</sup>, Vidal, *et al*<sup>6</sup> and Kooi<sup>7</sup>.

The second technique<sup>8,9</sup> is used in transonic wind tunnels and involves mounting a two-dimensional bump on the wind tunnel wall so that the shock-wave boundary-layer interaction approximates to that on an aerofoil (Fig 1b). More recently, small supercritical aerofoils have been tested<sup>10</sup> and in fact these two experiments have been combined by Burdges<sup>11</sup> who let the aerofoil into the tunnel floor and bled away the floor boundary layer under its leading edge.

Gadd<sup>12</sup> and more recently Mateer, Brosch and Veigas<sup>13</sup> used a third technique which was to hold the normal shock wave steady in a supersonic tube by the adjustment of a conical choke downstream of the working section as in Fig 1c. The turbulent boundary layer under consideration was allowed to grow naturally along the tube wall.

For the present experiment the facility which was available was the RAE 3ft x 3ft transonic-supersonic wind tunnel. The arrangements of Fig 1a or 1b could have been employed, but it was argued that if the tunnel floor was used, then the measuring techniques would be simpler, a higher Reynolds number could be obtained, and the interference effects of the wall boundary layers should be less than in the technique of Fig 1a where the test boundary layer is of smaller thickness than the interfering wall boundary layers. The simple technique was therefore used of holding a shock wave across the test section, set up to run at supersonic speed, by means of an adjustable sonic throat which was situated far downstream of the test section. The technique is in fact similar to that of Fig 1c.

The 3ft x 3ft wind tunnel has a good Reynolds number capability (up to  $12 \times 10^6/m$  for continuous running) is easily accessible for non-intrusive measurements and, above all, is easy to modify in the working section region having removable supersonic liners and downstream wooden fairings. A further advantage is that the pressure distribution in the working section is not only similar to that over a supercritical aerofoil but also the dimensions and Reynolds numbers approximate to full-scale conditions. A ninth scale (4 in x 4 in) model of the tunnel is also available and this proved invaluable for the development of the experiment.

The most time-consuming aspect of the development has been providing a suitable downstream sonic throat to control the shock-wave position and to keep it acceptably steady. However it was also necessary to design and manufacture a new raised false tunnel floor (to house submerged boundary-layer traverse mechanisms and to raise the boundary-layer interaction region into view above the bottom of the schlieren windows) which would match the three alternative half-nozzle blocks used to generate the required free-stream Mach numbers and which form the upper wall.

During the period of time taken to manufacture the new floor and the necessary associated equipment, two interim experiments were made, the first<sup>2</sup> using a conventional boundary-layer pitot rake and the second<sup>1</sup> using non-intrusive laser-Doppler measurements. The first experiment differed in another important aspect from the present one in that the pitot rake was attached to the tunnel floor in a single, fixed, position and the shock wave moved fore-and-aft of the rake.

For the present experiment the location of the shock wave was fixed for each condition tested and measurements were made with probes which could be traversed both normal to the tunnel floor and streamwise. Measurements of the static pressure distribution along the floor were also made.

## 2 DESCRIPTION OF THE EXPERIMENT

### 2.1 Mechanical arrangement

The general arrangement of the experiment is shown in Fig 2. The unmodified parts of the 3ft x 3ft wind tunnel are shown shaded.

In its standard form, the 3ft x 3ft wind tunnel has a working section with a fixed lower liner and interchangeable upper liners which are matched to the lower liner to give 0.1 incremental steps in Mach number between 1.3 and 2.0. One of the major modifications made to the tunnel was the provision of a new raised bottom liner together with a false floor (Fig 3). This false floor contained two pitot traverse mechanisms so that a region close to the floor centre line could be investigated from approximately 0.8 m ahead of the schlieren window centre line to 3m downstream using a total horizontal traverse movement of little more than 2 m. Because of the interest in the free-stream Mach number range of 1.3 to 1.5, the new bottom liner was designed to match the  $M = 1.4$  upper liner and the consequent slight mismatch with the  $M = 1.3$  and  $M = 1.5$  upper liners had to be accepted. Although raising the floor by 152 mm had the advantage of bringing the shock-wave interaction region into full view through the schlieren windows, it reduced the height of the working section so that the tunnel was no longer square in cross

section. There was however no particular disadvantage in this because the asymmetrical nozzle which generated the supersonic flow inevitably resulted in boundary layers which were not the same on all four walls.

The other major item of redesign as described in Ref 2 involved the careful fairing of the existing 'spoiler door' arrangement\* in the diffuser section to give an adjustable second throat. By adjusting the throat, the normal shock wave could be placed in the desired location within the view through the tunnel windows. Any subsequent small progressive movement of the shock wave could then be corrected by adjusting the tunnel compressor speed. Initially there was a large random movement of the normal shock wave but this was reduced to about 20 mm by the careful fairing of the shape of the second throat. The mean position of the normal shock wave was checked both visually and by means of a differential pressure transducer connected between a wall static pressure hole under the shock wave and a reference tapping near the working section sonic throat.

The region between the working section and diffuser was faired to give smooth side-wall and roof contours. The geometry of the fairing was such as to give an expanding passage, the cross sectional area at the diffuser entry increasing to 1.067 times the area of the working section over a distance of 3660 mm. In the region of the interaction, the standard taper of 0.004 m/m was maintained on the top liner. This is normally combined with a similar taper on the lower liner to allow for boundary-layer growth on all four tunnel walls. However, for this experiment, the taper on the false floor was approximately 0.003 m/m.

The traverse mechanism together with a twin pitot probe is shown in Fig 4. Two identical traverse mechanisms were supported 1800 mm apart from a slide which was approximately 6 m long and sufficiently flexible to submerge, at its upstream end, below the liner surface approximately 1 m ahead of the schlieren window centre line, and at its downstream end to retract into a covered channel between the spoiler doors in the diffuser section. Any leaks around the slide were sealed by two pvc tubes which inflated when the slide was stationary as shown in Fig 3. A chain drive was used to move the slide in the streamwise direction. A total streamwise distance of 3800 mm could be covered using the tandem boundary layer traverses. The slide was positioned 100 mm to the port of the row of static pressure holes on the tunnel centre line and the probes were cranked so that vertical traverses could be made half way between the slide and the tunnel centre line. In this way it was hoped to reduce the various interferences, namely, of the probe on the wall static pressure holes, of the slight irregularity of the slide on the probe measurements, and of the probe stem on the probe measurements.

Repeatability of the probe position was  $\pm 0.02$  mm vertically and  $\pm 3$  mm horizontally.

Details of the static probes can be seen in Fig 5. The pitot probes were designed to be fairly short in order to avoid vibrations in the expected highly turbulent flow. The same overall dimensions were then retained for the twin static probes. With hindsight, the twin static probes might have been lengthened to diminish the interference

---

\* Used in normal testing for controlling the tunnel shock wave during starting or stopping the tunnel.



caused by the supporting structure because the vertical positional accuracy is not quite as important for these probes as for the pitot probes. However this was not done and large corrections had to be applied to the static pressure measurements especially at transonic Mach numbers. These corrections are described in the Appendix.

All the probes were electrically insulated from their vertical traverse mechanisms so that a touch indicator could be used to set the pitot datum at the surface of the false floor. The streamwise datum was set by aligning the tip of a pitot probe or the holes in a static probe with a line marked on the surface of the false floor.

Pressure measurements were made with differential transducers (Druck) of range  $0.69 \text{ kN/m}^2$  in two D-type scanivalves placed outside the tunnel shell. The transducers were calibrated against a Texas Instrument 0-203  $\text{kN/m}^2$  absolute quartz Bourdon-tube pressure-controller. Corrections were made to the primary slopes and zeros of these calibrations for each data point, by comparing the transducer outputs with reference pressures applied to the first and last pairs of scanivalve ports.

## 2.2 Experimental measurements

### 2.2.1 Pitot measurements

Measurements were made at three nominal Mach numbers, 1.3, 1.4 and 1.5 at Reynolds numbers of approximately  $10 \times 10^6/\text{m}$  (the maximum continuous running value permitted for the experiment) and  $3.5 \times 10^6/\text{m}$ . An intermediate Reynolds number was also included for  $M = 1.5$ . Details of the test conditions are given in Table 1.

Traverses normal to the floor were made using the twin-pitot probe over a large number of stations from 0.7 m ahead of the normal shock wave to approximately 3 m downstream of the normal shock wave. In most cases, a vertical distance of 200 mm was covered. The forward pitot was removed while measurements were being made with the rear one, and a flush plug was used to fill the hole left in the slide.

### 2.2.2 Floor static pressure measurements

Measurements of the static pressure distribution on the floor were made with only the rear pitot in place, set at its furthest downstream position. These measurements were used to calculate the wall reference static pressure for each pitot or static pressure probe traverse.

### 2.2.3 Reversed pitot measurements

Measurements were also made with a single reversed pitot probe (rather similar in shape to static probe B (Fig 5) but reversed) for conditions of separated flow which occurred for  $M = 1.5$ . Separation was indicated by the forward-pointing pitot recording a lower pressure than the corresponding wall static pressure hole. The measurements were made with the tip of the reversed pitot in the same streamwise position as the normal pitot tube. Although the flow was probably disturbed by either probe, a simple correction was made to both sets of results as described under section 3.1.

### 2.2.4 Static probe measurements

Before the static pressure measurements in the boundary layer were begun, the static probes were calibrated in the centre of the slotted transonic working section of

the tunnel over a Mach number range of 0.4 to 1.2 and similar free-stream Reynolds numbers to those encountered in the main experiment. Each probe was held at the end of its stem furthest away from the probe tip by a specially manufactured sting. Static probe B was also calibrated while supported at the near end of its stem to check for support interference. This appeared to be negligible. The probe measurements were compared with wall static pressures obtained from a tunnel calibration referred to a  $3^{\circ}$  conical static head probe. This probe has been described in Ref 14 and within the limits of the required accuracy was assumed to have no static pressure errors.

The real problem which arose when using static probes in an environment which invoked the problems of transonic flow combined with pressure gradients, wall interference effects and the presence of boundary layers, lay in obtaining sufficient calibration data in a tunnel which could not be used between  $M = 0.88$  and  $M = 1.3$  while modified to take the false floor and traverse mechanisms.

However some information was forthcoming from twin static probe calibrations made through the floor boundary layer between  $M = 0.66$  and  $0.88$  at similar Reynolds numbers to the main experiment. Additional information was obtained during the actual shock-wave boundary-layer interaction experiment from the static and pitot probe traverses ahead of the interaction, while further data were available from traverses 1 to 3 m downstream of the normal shock wave at  $M = 1.3$ . In all these cases it was assumed that there was no static pressure variation normal to the wall through each vertical boundary-layer traverse, and that the pressure was equal to the estimated wall value. Because the free-stream calibration showed no apparent Reynolds number effects, data at the highest Reynolds number from the experiment were used.

Time limitations meant that nearly all the boundary layer static traverses were made with the twin-static probe rather than the single probes and the static investigation was omitted for  $M = 1.4$  at a Reynolds number of  $3.5 \times 10^6/m$ . Single static probes were in fact used only as a check on the validity of the results obtained from the twin probe. Traverses were made in rather different streamwise positions from those made with the pitot probes and each traverse contained about half the measurements made using the pitot.

#### 2.2.5 Shock-wave position

A careful check was made of the shock-wave position using the output from the shock-position transducer and readings were only taken while the shock wave was within prescribed limits. Subsequently, during the analysis of the results, the average position of the normal part of the shock wave was ascertained from the large number of schlieren photographs taken for each set of tunnel conditions. This was necessary because there was an interval of a year between making the static pressure measurements and the pitot measurements. It was difficult to reset the shock wave in the same position, and so corrections had to be applied to make both sets of results compatible.

### 3 REDUCTION OF DATA

The data have been reduced as follows to produce the boundary layer profiles of Table 2 and the integral parameters of Table 3.

### 3.1 Boundary-layer profiles

These have been tabulated against  $y$  (the equivalent height of the pitot or static tube above the wall) where for pitot measurements

$$y = h + 0.15 d \quad (1)$$

and for static measurements

$$y = h \quad (2)$$

where  $h$  = height of probe centre line above floor  
and  $d$  = diameter of probe.

The profiles have been derived

- (a) assuming constant wall static pressure applied throughout each traverse,
- (b) using measured static pressures after correction (see Appendix).

Standard formulae were used to calculate Mach numbers, velocities and densities from the pitot and static results. Total temperature was assumed constant across the boundary layer except at the wall where a recovery factor of 0.89 was used. Wall static pressures were calculated for each traverse position by linear interpolation of the floor static measurements made with the front pitot removed and the rear pitot as far downstream as possible.

The flow was assumed reversed when the pitot pressure was lower than the wall static pressure. In such cases measurements were also made with the pitot tube reversed in direction. The Mach number was taken as the mean derived from the two sets of measurements. When the pitot tube was effectively facing downstream, it was assumed that the pressure recorded was that for a base with a pressure coefficient of -0.6. The wall static pressure was used for both sets of calculations in the reversed flow region.

Unit Reynolds numbers were calculated using the following formula based on Sutherland's law for viscosity

$$Re/m = \frac{M_\delta p_\delta}{T_\delta^2} (T_\delta + 110.4) \times 47.91 \times 10^3 \quad (3)$$

where subscript  $\delta$  denotes conditions at the edge of the boundary layer

$p$  is the static pressure in  $N/m^2$

and  $T$  is the temperature in K.

A further parameter, namely  $p_i/p_{t0}$  has been presented where  $p_i$  is an estimated static pressure in the 'equivalent inviscid flow' (see Ref 15). The static pressure  $p_i$  is that in the equivalent inviscid flow which is defined as the flow external to the shear layers continued as an inviscid flow to the wall bounding the real flow with the growth of the viscous layer represented by transpiration at the boundary.  $p_i$  has been non-dimensionalised by dividing by the tunnel total pressure  $p_{t0}$ .

An estimate of  $p_i/p_{t0}$  has been attempted in the region ahead of the normal shock-wave. Here, the flow at the edge of the boundary layer is supersonic and influence lines of constant  $p/p_{t0}$  following Mach lines may be constructed back to the wall from the edge of the viscous region. An estimate of  $p_i/p_{t0}$  as a function of  $y$  for each traverse can then be made from the carpet of influence lines which are assumed straight and inclined at the Mach angle  $\mu$  plus the flow inclination at  $\delta_{0.999}$  (the distance from the wall where  $U/U_\delta = 0.999$ ) viz

$$\mu + \tan^{-1}\left(\frac{V}{U}\right)_\delta$$

where 
$$\left(\frac{V}{U}\right)_\delta = \frac{d\delta^*}{dX} - (\delta_{0.999} - \delta^*) \frac{d}{dX} \left(\ln(\rho_\delta U_\delta)\right) \tag{4}$$

- and  $V$  is the vertical component of velocity
- $U$  is the horizontal component of velocity
- $\delta^*$  is the displacement thickness
- $\rho$  is the density.

It will be noted (see section 4.4) that there is a supersonic region at the edge of the boundary layer behind the normal shock wave for  $M = 1.5$ . However estimates of  $p_i/p_{t0}$  have not been included for this region because they become discontinuous in the region of the shock wave.

### 3.2 Integral parameters

Boundary-layer thickness parameters were obtained by trapezoidal integration. Velocity profiles were faired between the wall and the pitot position corresponding to 0.8 mm from the wall by applying East's prediction of the law of the wall<sup>16</sup> in compressible boundary layers as a 20 point curve.

East's prediction is based on an incompressible law of the wall combined with a compressibility factor. For this experiment Cole's law of the wall<sup>17</sup> has been used with the constants recommended at the Stanford conference<sup>18</sup> namely

$$\frac{U}{U_\tau} = 5.62 \log \frac{yU_\tau}{\nu_\delta} + 5.0 \tag{5}$$

where  $U_\tau$  is the friction velocity.

The form of East's prediction which is faired into Cole's law of the wall is

$$\frac{U}{U_\tau} = \frac{1}{F} \sin \left[ F \left\{ 2K \ln \left( y^{*2} \frac{K}{D} + 1 \right) + D \left( 1 - e^{-y^*/D} \right) \right\} \right] \tag{6}$$

where the compressibility factor

$$F = M_{\tau} \sqrt{\frac{\gamma(\gamma-1)}{2}} = \frac{U_{\tau}}{\sqrt{T_w}} \times 0.021033 ,$$

$$D = 8.73(1 + 45F^2) ,$$

$$y^* = y \frac{U_{\tau}}{v_w} ,$$

$$K = 0.41 ,$$

$r$  being the recovery factor, and suffix  $w$  denoting wall values.

A value of  $U_{\tau}$  was obtained at  $y \approx 0.8$  mm using equation (6) and values of  $U/U_{\tau}$  were then calculated for 20 equispaced values of  $y$  between 0 and 0.8 mm.

A linear variation was assumed between  $y = 0$  and 0.8 mm for reversed flow.

The following definitions of the integral quantities have been used as first proposed by Myring<sup>19</sup> and later incorporated in East's modified momentum integral equation<sup>15</sup>.

They are (where suffices  $i$  and  $w$  denote equivalent inviscid flow quantities and wall values respectively)

$$\bar{\delta} = \frac{1}{\rho_{iw} U_{iw}} \int_0^{\delta} (\rho_i U_i - \rho U) dy , \quad (7)$$

$$\bar{\theta} = \frac{1}{\rho_{iw} U_{iw}^2} \int_0^{\delta} \left\{ (\rho_i U_i^2 - \rho U^2) - U_{iw} (\rho_i U_i - \rho U) \right\} dy , \quad (8)$$

shape parameter  $H = \frac{\bar{\delta}}{\bar{\theta}} , \quad (9)$

shape parameter  $\bar{H} = \frac{1}{\rho_{iw} U_{iw}} \int_0^{\delta} \rho (U_i - U) dy . \quad (10)$

The integral parameters were calculated for three different distributions of static pressure across the boundary layers as described in the following paragraphs.

### 3.2.1 Static pressure constant and equal to the measured wall pressure

Equations (7), (8), (9) and (10) reduce to the familiar standard integrals when static pressure is constant across the boundary layer giving

$$\text{displacement thickness } \delta^* = \int_0^{\delta} \left( 1 - \frac{\rho U}{\rho_{\delta} U_{\delta}} \right) dy, \quad (11)$$

$$\text{momentum thickness } \theta = \int_0^{\delta} \frac{\rho U}{\rho_{\delta} U_{\delta}} \left( 1 - \frac{U}{U_{\delta}} \right) dy, \quad (12)$$

$$\text{shape factor } H = \frac{\delta^*}{\theta}, \quad (13)$$

$$\text{shape factor } \bar{H} = \frac{1}{\theta} \int_0^{\delta} \frac{\rho}{\rho_{\delta}} \left( 1 - \frac{U}{U_{\delta}} \right) dy. \quad (14)$$

The energy thickness was also evaluated:

$$\delta_E = \int_0^{\delta} \frac{\rho U}{\rho_{\delta} U_{\delta}} \left[ 1 - \left( \frac{U}{U_{\delta}} \right)^2 \right] dy. \quad (15)$$

### 3.2.2 Static pressure variation as measured

Equations (7), (8), (9) and (10) can be used in an 'intermediate form' as in Cook, McDonald and Firmin<sup>20</sup>. In this form the boundary layer defect thicknesses are referred to a fictitious potential flow having the same static pressure distribution as that for the actual viscous flow and a total pressure equal to that at the edge of the boundary layer ( $p_{t1}$ ).

Thus for example

$$M_p = \sqrt{5 \left[ \left( \frac{p_{t1}}{p} \right)^{\frac{2}{\gamma}} - 1 \right]} \quad (16)$$

where

$$p_{t1} = p_{\delta} \left( 1 + 0.2 M_{\delta}^2 \right)^{3.5}. \quad (17)$$

The revised integral quantities are as follows:

$$\text{displacement thickness } \delta^* = \frac{1}{\rho_w U_w} \int_0^{\delta} (\rho_p U_p - \rho U) dy, \quad (18)$$

$$\text{momentum thickness } \theta = \frac{1}{\rho_w U_w^2} \int_0^{\delta} \left\{ (\rho_p U_p^2 - \rho U^2) - U_p (\rho_p U_p - \rho U) \right\} dy, \quad (19)$$

$$\text{shape factor} \quad H = \frac{\delta^*}{\delta} ,$$

$$\text{shape factor} \quad \bar{H} = \frac{1}{\theta} \frac{1}{\rho_w U_w} \int_0^{\delta} \rho_p (U_p - U) dy . \quad (20)$$

### 3.2.3 Equivalent inviscid static pressure together with measured static pressure

$\bar{\rho}$ ,  $\bar{U}$ ,  $H$  and  $\bar{H}$  have already been defined by equations (7), (8), (9) and (10).

Equivalent inviscid static pressures were estimated as described in section 3.1 for traverse positions ahead of the normal shock. Equivalent inviscid Mach numbers were obtained from these pressures, and the total pressure calculated at the edge of the boundary layer (equation (17)) so that

$$M_i = \sqrt{5 \left[ \left( \frac{P_{t_i}}{P_i} \right)^{\frac{2}{\gamma}} - 1 \right]} . \quad (21)$$

$\rho_i$  and  $U_i$  were obtained from  $M_i$  using a temperature recovery factor of unity while the values of  $\rho$  and  $U$  were identical to those in section 3.2.2 (being calculated from the measured pitot and static pressures).

Linear interpolation was used to obtain  $\rho_i$  and  $U_i$  for the 20 points between the wall and  $y \approx 0.8$  mm .

### 3.3 Skin friction

Three estimates of skin friction are given.

The first estimate  $C_{f_p}$  has been deduced by considering the pitot tube when in contact with the wall to be a Preston tube and applying Patel's<sup>21</sup> calibration as formulated by Head and Vasanta Ram<sup>22</sup> and transformed for compressible flow by the method of Fenter and Stalmach<sup>23</sup>.

The second and third estimates emerge directly from  $U_\tau$  which was calculated by fitting East's law of the wall (equation (6)) to the pitot reading for  $y \approx 0.8$  mm . The second estimate was obtained assuming constant wall static pressure to apply across the boundary layer and the third was obtained using measured static pressures. Because at  $y \approx 0.8$  mm wall static pressure applied for both cases, the differences are entirely due to the boundary layer edge conditions obtained from the different static pressures.

It will be noted that several values of  $C_f$  are missing from Table 3 and these omissions occur where reversed flow is indicated at  $M = 1.5$ .

#### 4 EXPERIMENTAL RESULTS

##### 4.1 The general characteristics of the flow

###### 4.1.1 Shock-wave patterns

Fig 6a shows the vertical cross sections of the main interactions traced from schlieren photographs. Typical photographs have been reproduced in Fig 6b. For completeness, the calculated boundary layer thickness ( $\delta_{0.995}$ ) and the start of the measured reversed flow regions at  $M = 1.5$  have been added to the diagrams. The progression from the pattern at  $M = 1.3$  of a single normal shock wave distorted by the influence of compression curves emanating from the thickening of the upstream boundary layer, to the established triple shock system with the shear layer emanating from the point of bifurcation at  $M = 1.5$ , is well illustrated. The increase in size of the shock system with reduction in Reynolds number can also be seen.

The main interaction region has been described in detail by East<sup>3</sup> and the present results at high Reynolds numbers agree with his at  $M = 1.3$  and  $1.4$ . However there is a discrepancy between the sets of results at  $M = 1.5$ . The shock bifurcation point for the present experiments is at 180 mm from the floor compared with a value, presumed to be erroneous, of 215 mm given by East.

###### 4.1.2 Flow visualisation

After the completion of the traverse measurements the interaction region was examined by oil flow\*.

Photographs of the surface oil flow were taken for all three Mach numbers at a Reynolds number of  $10 \times 10^6/m$ . These photographs, reproduced in Fig 7, were taken after shutting down the tunnel and removing the roof and therefore suffer from slight blurring. The viewpoint looks downstream. The photographs reveal mild three-dimensional effects for  $M = 1.3$  and  $M = 1.4$  but a much more complex pattern for  $M = 1.5$  when the flow is separated. The photograph for  $M = 1.5$  is shown in more detail in Fig 8 together with an attempted interpretation of the wall streamlines.

The nature of the flow in this case appears to be such that there is flow along the arch of a vortex connecting a position on the port side, denoted by B in Fig 8, to a position denoted by A on the starboard side. Thus in a sense A is an attachment node and B a separation node. It should be remarked that whilst the streamwise extent of this region is roughly 300 mm the probe measurements suggest its depth to be only 7 mm.

Near the tunnel centre line between the two vortex patterns, the flow is tolerably two-dimensional except in the immediate regions of the saddle points at the start and end of the separation region.

Presumably because of the non-uniform boundary-layer thickness on the tunnel side wall arising from the flow field associated with the asymmetrical nozzle, the separation line on the sidewall is swept and a single vortex node only of separation type is formed.

---

\* The oil-flow mixture was an amalgam of the following in the ratio of 4 cc Vitrea F2, to 2 cc Limea 931, to 3 cc TiO<sub>2</sub>, to 2 drops of oleic acid.



The vortex arising from this node is presumed to create the strong convergence towards the tunnel centre line occurring in the corner regions downstream of the interaction. The lines D in Fig 8 have the appearance of separation lines but may in fact indicate only a locally strong convergence of the boundary layer.

#### 4.1.3 Momentum balance

Momentum balance calculations have been made using a rearranged form of East's modified momentum integral equation<sup>15</sup>

$$\begin{aligned} \frac{d\bar{\theta}}{dX} + (H + 2 - M_{iw}^2) \frac{\bar{\theta}}{U_{iw}} \frac{dU_{iw}}{dX} - \frac{\tau_w}{\rho_{iw} U_{iw}^2} \\ = - \frac{1}{2\rho_{iw} U_{iw}^2} \frac{d}{dX} \left\{ \rho_{iw} U_{iw}^2 \left( \frac{d^2 \bar{\delta}}{dX^2} + \kappa \right) (\bar{\theta} + \bar{\delta})^2 \right\} + \kappa (\bar{\theta} + \bar{\delta}) \frac{d\bar{\delta}}{dX} \\ + \frac{1}{\rho_{iw} U_{iw}^2} \frac{d}{dX} \left\{ K \rho_{iw} U_{iw}^2 \bar{\theta} \left( \frac{\bar{H} - 1}{\bar{H}} \right) \right\} + \frac{M_{iw}^2 \bar{\theta} v_{iw}}{U_{iw}^2} \frac{dv_{iw}}{dX} \end{aligned} \quad (22)$$

The last term has been neglected in the analysis because it is small and in any case cannot be evaluated with any reliability. The remaining terms in the right hand side of the equation are:

- ① the normal pressure gradient effect arising from the wall and stream curvature;
- ② the approximation to the direct effect of wall curvature on the flow momentum;
- ③ the approximation to the normal stress terms.

The integral parameters,  $H$ ,  $\bar{H}$ ,  $\bar{\theta}$  and  $\bar{\delta}$  are defined in equations (7) to (10) while  $\rho_{iw}$ ,  $U_{iw}$  and  $M_{iw}$  are respectively the equivalent inviscid values of density, horizontal component of velocity and Mach number at the wall.

The surface curvature  $\kappa$  is zero for this example leaving

$$\begin{aligned} \frac{d\bar{\theta}}{dX} + (H + 2 - M_{iw}^2) \frac{\bar{\theta}}{U_{iw}} \frac{dU_{iw}}{dX} - \frac{\tau_w}{\rho_{iw} U_{iw}^2} \\ = - \frac{1}{2\rho_{iw} U_{iw}^2} \frac{d}{dX} \left\{ \rho_{iw} U_{iw}^2 \frac{d^2 \bar{\delta}}{dX^2} (\bar{\theta} + \bar{\delta})^2 \right\} + \frac{1}{\rho_{iw} U_{iw}^2} \frac{d}{dX} \left\{ K \rho_{iw} U_{iw}^2 \bar{\theta} \left( \frac{\bar{H} - 1}{\bar{H}} \right) \right\} \end{aligned} \quad (23)$$

After multiplying throughout by  $\rho_{iw} U_{iw}^2$  and rearranging, the equation becomes

$$\frac{d}{dX} (\rho_{iw} U_{iw}^2 \bar{\theta}) = \tau_w - H \rho_{iw} U_{iw} \bar{\theta} \frac{dU_{iw}}{dX} + \frac{d}{dX} (f \rho_{iw} U_{iw}^2 \bar{\theta}) \quad (24)$$

where  $f = f_1 - f_2$ ,

$f_1 = 0.072 \left( \frac{\bar{H} - 1}{\bar{H}} \right)$ , and is the contribution due to the normal stress,

and  $f_2 = \frac{1}{2} \frac{d^2 \bar{\delta}}{dX^2} \frac{1}{\bar{H}} (\bar{H} + \delta^2) = \frac{1}{2} \frac{d^2 \bar{\delta}}{dX^2} (1 + H) (\bar{\theta} + \bar{\delta})$  and is the contribution due to the stream curvature

If suffix 0 represents the conditions at the start of the interaction, then dividing through by  $\rho_{iw0} U_{iw0}^2 \bar{\theta}_{iw0}$  and integrating, results in the form of the momentum integral equation used in the momentum balance calculations shown in Fig 9:

$$\left[ \frac{\rho_{iw} U_{iw}^2 \bar{\theta}}{\rho_{iw0} U_{iw0}^2 \bar{\theta}_0} - 1 \right] = \int_{X_0}^X \frac{C_f}{2} \frac{\rho_e U_e^2}{\rho_{iw0} U_{iw0}^2 \bar{\theta}_0} dX - \frac{1}{2} \int_1^{\left( \frac{U_{iw}}{U_{iw0}} \right)^2} \frac{\rho_{iw} \bar{\delta}}{\rho_{iw0} \bar{\delta}_0} d \left( \frac{U_{iw}}{U_{iw0}} \right)^2 + \left( \frac{f \rho_{iw} U_{iw}^2 \bar{\theta}}{\rho_{iw0} U_{iw0}^2 \bar{\theta}_0} - f_0 \right) \quad (25)$$

In Figs 9 and 11  $\left( \frac{\rho_{iw} U_{iw}^2 \bar{\theta}}{\rho_{iw0} U_{iw0}^2 \bar{\theta}_0} - 1 \right)$  is called the left hand side while the remainder

of the expression is called the right hand side. The numbered terms are identified later (in Fig 12) as the contributions due to

- ④ skin friction
- ⑤ pressure gradient.

Both sides of equation (25) were calculated using the alternative assumptions of section 3.2 which were (for traverses across the boundary layer):

- (a) static pressure constant and equal to the measured wall pressure;
- (b) static pressure as measured;
- (c) equivalent inviscid static pressure together with measured static pressure. The equivalent inviscid static pressure was calculated for traverses ahead of the shock wave only.

Fig 9 shows the comparison between the left hand side and the right hand side of equation (25) plotted against the streamwise position. The calculations were made using assumption (c). It will be seen that the momentum balance is good over the main interaction region and only becomes significantly in error at approximately 800 mm downstream of the normal shock wave. Downstream of this point, the left hand side actually reduces for Mach numbers ahead of the interaction of 1.4 and 1.5. This indicates a flow divergence and it is interesting to calculate its magnitude.

In terms of equation (22) Green *et al*<sup>24</sup> showed that a flow divergence could be accounted for by subtracting the local rate of divergence  $\bar{\theta}(d\phi/dz)$  from the right hand side. This quantity represents the rate of the deviation relative to the nominal flow direction with respect to distance Z perpendicular to the flow but parallel to the surface.

In equation (25) this divergence takes the form

$$\int_{X_0}^X \frac{\rho_{iw} U_{iw}^2 \bar{\theta}}{\rho_{iw_0} U_{iw_0}^2 \bar{\theta}_0} \frac{d\phi}{dz} dX$$

and this can be added to the left hand side. It is therefore easy to make an estimate of  $d\phi/dz$ .

This estimate is shown in Fig 10a-c in degrees per metre. For points further downstream of the normal shock wave than 300 mm the figures show a flow divergence of  $7^\circ/\text{m}$  at  $M = 1.3$  rising to  $15^\circ/\text{m}$  at  $M = 1.5$  (equivalent to  $7^\circ$  and  $15^\circ$  over the tunnel width). The wild fluctuations within the main interaction region are of course due to the rapidly changing conditions and the close streamwise spacing of the traverse positions.

Assumptions (a), (b) and (c) were used to provide comparisons of both sides of the momentum integral equation as shown in Fig 11. There appears little to choose between the momentum balance using any of these assumptions. However it is possible to see some improvement using assumption (b) rather than (a). If the region ahead of the shock wave is examined there is again some improvement if calculation assumption (c) is used.

Fig 12 shows the individual contributions to the right hand side of equation (25).

#### 4.2 Edge Mach numbers and boundary layer parameters

Fig 13a-c shows the development of the Mach number at the edge of the boundary layer,  $M_\delta$ , the boundary-layer displacement thickness,  $\delta^*$ , the shape factor  $H$ , defined by equation (13), the boundary layer thickness,  $\delta_{0.995}$ , the skin friction coefficient  $C_{f_p}$  (section 3.3), and the shape factor  $\bar{H}$  defined by equation (14), all plotted against the longitudinal distance  $X$  from the normal part of the shock wave. The results in Fig 13 were calculated assuming constant static pressure,  $p_w$ , across the boundary layer normal to the tunnel wall. Further graphs of  $M_\delta$ ,  $\delta^*$ ,  $H$  and  $\bar{H}$  (Fig 14a-c) show the effect of using measured static pressures to calculate these parameters. The longitudinal region covered by these figures is from 500 mm ahead to 500 mm downstream of the normal shock wave. Outside this region it was assumed that the static pressures were constant normal to the wall and equal to the static pressures used in the first set of calculations (see Fig 15a&b and the Appendix).

Overall there appears to be little effect of variation of Reynolds number on the shape factors and the normalised variation of  $\delta^*$  and  $\delta_{0.995}$ . A separation bubble occurs under the interaction region at  $M = 1.5$  and its extent is indicated by the zero values of  $C_{f_p}$ . The bubble size decreases slightly with increase in Reynolds number. The shape of the bubble can, however, be seen in the plots of Mach number distribution, Fig 16a-f, and will be described in section 4.4.

The results agree broadly with those obtained in Ref 2 where a fixed pitot rake was used on the standard tunnel floor. However discrepancies begin to creep in 1 m downstream of the normal shock wave where in Ref 2 the Mach number at the start of the interaction was affected by the proximity of the tunnel throat. The results from Ref 2 at  $M = 1.5$  were much more sensitive to Reynolds number in the interaction region and this was probably due to pitot-rake interference. One other point should be noted (and it can be seen in nearly all the following figures) and that is that the rehabilitation process behind the normal shock wave has not been completed after 3 m. This distance is equivalent to at least 400 times the undisturbed displacement thickness ahead of the interaction. It can be seen in Fig 13a-c that the edge Mach numbers, shape factors and boundary layer thicknesses have not yet reached their asymptotic values at the furthest downstream traverse positions.

#### 4.3 Measured static pressures

Static pressure distributions normal to the wall are plotted on scale diagrams of the main interaction region in Fig 15a&b as the difference from the corresponding wall static pressure non-dimensionalised by dividing by the undisturbed stagnation pressure. Zero values are located at the appropriate streamwise station.

As described in the Appendix, the static pressure results have usually been made to merge into the appropriate wall values at floor level, however wall static values have been assumed to apply throughout the separated region in the absence of reliable local values. Static pressures recorded very close to the shock wave may have been affected by its movement and so local pressure gradients may have been reduced.

The diagrams show the expected static pressure variation throughout the main interaction region. The static pressures are fairly constant across the inner part of the shear flow and then decrease outwards across the compression region ahead of the normal shock wave to free-stream values. Behind the main shock wave they increase from one fairly constant level near the wall to a second level behind the normal part of the shock wave.

#### 4.4 Mach number distribution

Mach number contours are plotted in Fig 16a-f over the main interaction region and over the whole of the region investigated downstream of the normal shock wave (note the change of streamwise scale). Measured pitot and the corrected static pressures were used to calculate Mach numbers and the figures result from linear interpolations of Mach number profiles in the vertical direction and from horizontal plots of Mach numbers at constant distances from the wall,  $y$ .

The results are therefore dependent on the accuracy of the corrected static pressure measurements and the interpolation procedures which are affected most critically by the smearing effect of the slightly unsteady shock wave. However the results in the interaction region are broadly confirmed by the laser-Doppler anemometer measurements of East<sup>3</sup> and the results of Kooi<sup>7</sup> at  $M = 1.4$ . A particular feature is the development of the supersonic tongue beneath the downstream shock wave for  $M = 1.5$ .

If East's and the present results at a Reynolds number of  $10 \times 10^6/m$  are compared in slightly more detail, the Mach number contours are in good agreement ahead of the normal shock wave if due allowance is made for the smearing effect of the unsteady shock wave (see above). Very similar supersonic tongues may be seen behind the shock wave and they continue downstream (in both experiments) for 100 mm near the edge of the boundary layer. East's results at  $M = 1.5$  do not cover the full extent of the supersonic tongue but show that it is more extensive than at  $M = 1.4$ . In fact the present experiment confirms that it persists near the edge of the boundary layer for 400 mm downstream of the shock wave while at a Reynolds number of  $3.5 \times 10^6/m$  it persists for 600 mm.

It is difficult to be specific about the shape of the supersonic tongue immediately downstream of the trailing shock wave, but the present results agree well with Kooi<sup>7</sup> who also used pitot and static pressure measurements. The rear shock wave appears to terminate at the edge of the boundary layer so that supersonic flow appears to exist above the boundary layer behind a normal shock wave.

There is evidence to suggest that the thin shear layer formed downstream of the shock bifurcation point is still intact 3 m behind the normal shock wave, and even at  $M = 1.3$  there is no sign that the inviscid flow has recovered sufficiently to provide a uniform Mach number contour across the tunnel.

The other point of interest is the separation region at  $M = 1.5$ . There appears to be a small decrease in the overall dimensions of the separation bubble with increase in Reynolds number. In fact the length of the separation bubble is reduced from 300 mm at  $Re/m = 3.5 \times 10^6$  to 200 mm at  $Re/m = 10 \times 10^6$  while the height is reduced slightly from just over 9 mm at the lowest Reynolds number to 7 mm at the highest Reynolds number. This result is in disagreement with Sawyer *et al.*<sup>2</sup> where a much greater reduction in bubble size was indicated although as stated in section 4.2 the conditions were somewhat different.

#### 4.5 Boundary-layer velocity profiles

##### 4.5.1 General

Boundary-layer profiles are shown in Fig 17a-f plotted on a scale diagram of the main interaction region together with an extended diagram on a compressed scale showing the whole region of measurement behind the normal shock wave.

The figures indicate the general characteristics of the boundary-layer development. They show the progression from the undisturbed state through the leading compression which influences the shape of the outer part of the boundary layer, through the subsequent separation or near-separation region, to the final recovery towards a zero-pressure-gradient form for the profiles. It can be seen even on the small scale diagrams that the profiles are still disturbed after a distance of nearly 3 m downstream of the normal shock wave, or approximately 400 times the undisturbed displacement thickness.

##### 4.5.2 Logarithmic velocity profiles

Representative velocity profiles are plotted in the logarithmic form adopted by Winter and Gaudet<sup>25</sup> as  $(U/U_\tau^i)$  against  $\log(yU_\tau^i/\nu_\delta)$  where  $U_\tau^i$  is the equivalent

incompressible friction velocity. Values of  $U_\tau^i$  were derived from the skin friction coefficient  $C_{f_p}$  using the formula

$$U_\tau^i = U_\delta \left( \frac{C_{f_p}}{2} \right)^{\frac{1}{2}} \left( 1 + 0.2M_\delta^2 \right)^{\frac{1}{4}} . \quad (26)$$

$C_{f_p}$  was obtained by treating the pitot tube when in contact with the wall as a Preston tube and using the calculation method described in section 3.3.

The results are plotted separately for three regions. Fig 18 shows the undisturbed velocity profiles just ahead of the interaction region. These profiles were used to define the undisturbed conditions of Table 1. The profiles far downstream of the interaction region are shown in Fig 19. Fig 20 shows typical profiles just downstream of the main interaction region.

#### 4.5.3 The law of the wall

Figs 18 to 20 show typical 'law of the wall' fits for small values of  $y$  (the distance from the wall). The law of the wall is defined in the form adopted by Winter and Gaudet<sup>25</sup> as

$$\frac{U}{U_\tau^i} = \frac{1}{\kappa} \ln \left( \frac{yU_\tau^i}{\nu_\delta} \right) + \phi(0) , \quad (27)$$

which may be expressed as

$$\frac{U}{U_\tau^i} = A \log \left( \frac{yU_\tau^i}{\nu_\delta} \right) + B . \quad (28)$$

The results have been compared with Winter and Gaudet's incompressible law of the wall

$$\frac{U}{U_\tau^i} = 6.05 \log \left( \frac{yU_\tau^i}{\nu_\delta} \right) + 4.05 , \quad (29)$$

and with Coles' incompressible form (equation (5))

$$\frac{U}{U_\tau} = 5.62 \log \left( \frac{yU_\tau}{\nu_\delta} \right) + 5.0 .$$

Coles' incompressible law of the wall is usually applied to compressible flow by making use of the Van Driest<sup>26</sup> transformation. It was therefore necessary to confirm that the transformations of Van Driest and Winter and Gaudet gave similar results when applied to the compressible profiles of the present experiment. Two profiles were checked and are plotted using both transformations in Figs 18 and 19. The first profile had a free-stream Mach number of 1.54 and was in the undisturbed region ahead of the

interaction region, while the second profile had a free-stream Mach number of 0.83 and was from a pitot traverse made 2759 mm downstream of the normal shock wave. It can be seen that both transformations gave identical values of A and B although the wake components were very different at the free-stream Mach number of 1.54 (Fig 18). Because both transformations gave identical values of A and B Coles' incompressible law of the wall has been presented in the form adopted by Winter and Gaudet.

It would appear from Fig 18 that within the data scatter there is little to choose between the forms of the law of the wall due to Coles and due to Winter and Gaudet.

The average fit made to all the profiles ahead of the interaction region is

$$\frac{U}{U_{\tau}^i} = 6.16 \log \frac{yU_{\tau}^i}{\nu_{\delta}} + 3.6 \quad (30)$$

which is somewhat closer to the latter.

However behind the normal shock wave (Figs 19 and 20) the average fit becomes

$$\frac{U}{U_{\tau}^i} = 4.77 \log \frac{yU_{\tau}^i}{\nu_{\delta}} + 6.6 \quad (31)$$

which is quite different from equation (30).

Equations (30) and (31) were obtained by fitting the best straight lines (using the method of least squares) to the linear logarithmic regions close to the wall and averaging the results ahead of, and downstream of, the normal shock wave. Straight line fitting was not attempted when there were less than eight measured points in the linear region, or when the pitot traverse results contained reversed flow. The two traverse positions that were closest to the wall were omitted when fitting best straight lines.

Fig 21 shows the variation of A and B with streamwise position for each undisturbed free stream condition. It demonstrates most clearly the reduction in A accompanied by an increase in B for the boundary-layer traverse positions downstream of the normal shock wave. There does not seem to be any consistent variation of A and B with Reynolds number.

It would appear therefore that either large perturbations or normal pressure gradients affect the law of the wall, in a way which implies an increase in the eddy viscosity.

#### 4.5.4 Departures from equilibrium and the law of the wake

An attempt has been made to demonstrate violent departures of the flow from equilibrium by extracting from the measurements the parameters used to describe the equilibrium locus in integral models of turbulent boundary layers. The analysis is further extended in terms of the character and magnitude of the wake component.

In order to deal with separated flows, East, Smith and Merryman<sup>27</sup> redefined the usual parameters

$$G = \frac{\bar{H} - 1}{\bar{H}} \sqrt{\frac{2}{C_f}} , \quad (32)$$

$$\Pi = - \frac{2\delta^*}{C_f U_\delta} \frac{dU_\delta}{dX} \quad (33)$$

as

$$E_f^i = \frac{1}{G^2} , \quad (34)$$

and

$$E_p^i = \frac{\Pi}{G^2} , \quad (35)$$

thus removing the difficulty created as the skin friction coefficient passes through zero and becomes negative. With an empirically derived allowance for compressibility, the parameters become

$$E_f = \frac{1 + 0.04M_\delta^2}{G^2} \quad (36)$$

$$E_p = \frac{\Pi}{G^2} (1 + 0.04M_\delta^2) . \quad (37)$$

In Fig 22, the loci for the measured boundary layer developments are compared with the equilibrium locus

$$E_f = 0.024 - 0.8E_p \quad (38)$$

which is substantiated by experiment for attached flow and tentatively assumed in Ref 27 to remain valid in separated flow.

Points to the right and left of the equilibrium locus correspond respectively to stronger and weaker adverse pressure gradients than those appropriate to equilibrium flow. Negative values of  $E_p$  represent favourable pressure gradients, while negative values of  $E_f$  represent separation.

In Fig 22 the results for each set of test conditions have been plotted using symbols to represent the following regions

- A represents equilibrium conditions ahead of the main interaction;
- B represents the strongly adverse pressure gradient under the leading compression (which causes separation at  $M = 1.5$ );
- C represents the rapid recovery just downstream of the normal shock wave;
- D represents the remainder of the flow which might be expected to approach equilibrium conditions.

Points on the loci where there are changes from one region to the next are indicated by the numerals 1 to 3.



The loci show that region A is approximately in equilibrium but the rapid rise of  $E_p$  while  $E_f$  only falls slowly in region B indicates that the boundary layer lags in its response to the strong adverse pressure gradient under the leading compression. In region C,  $E_p$  recovers rapidly to the equilibrium locus but then overshoots before returning.  $E_f$  only starts to increase after  $E_p$  has overshoot the equilibrium locus and this again indicates a lag in the response of the boundary layer to a change in pressure gradient. The failure of the boundary layer to return to the equilibrium locus far downstream (in region D) may be interpreted as a further indication of the persistently disruptive effect of the shock-wave boundary-layer interactions on the velocity profiles already detected in the law of the wall as shown in Fig 21.

On the other hand the wake components of the profiles, remain fairly close to the standard shape as shown in Figs 23 and 24. In these figures the normalised wake components have been plotted in the following way. Fig 23a shows the undisturbed wake components in region A, and the results under the first compression through which it is possible to fit a law of the wall are shown in Fig 23b. Fig 24a-c has been produced by grouping similar normalised wakes into one diagram. In fact Fig 24a&b covers the rapid recovery region C together with the beginning of D, while Fig 24c covers the downstream part of region D.

According to Winter and Gaudet<sup>25</sup> the law of the wake for compressible boundary layers in zero pressure gradients is

$$\frac{\Delta U}{U_\tau^i} = 0.89 \left[ 1 + \sin \frac{\pi}{0.707} \left( \frac{y}{\delta_{0.999}} - 0.483 \right) \right] . \quad (39)$$

which after normalisation and allowance for the difference between  $\delta_{0.999}$  and  $\delta_{0.995}$  becomes

$$\left( \frac{\Delta U}{U_\tau^i} \right)_N = 0.5 \left[ 1 + \sin \frac{\pi}{0.818} \left( \frac{y}{\delta_{0.995}} - 0.529 \right) \right] , \quad (40)$$

where the normalised wake component  $\left( \Delta U / U_\tau^i \right)_N$  has been obtained by dividing the wake component by the maximum value for each traverse. The shape of the normalised wake components has been plotted in Figs 23 and 24. On each figure a curve in the form of equation (40) is shown with the constants adjusted to fit the particular set of results.

The maximum values of the wake component for each traverse  $\left( \Delta U / U_\tau^i \right)_{\max}$  are plotted in Fig 25 against  $E_f$ . In Fig 25a the results for regions A and B ahead of the normal shock wave are given while the results downstream of the normal shock wave (in regions C and D) are shown in Fig 25b. It will be seen in Fig 25a that apart from the boundary layer profiles that have been perturbed by the leading edge of the strong compression, the maximum values of the wake components are in good agreement with the locus obtained from the equilibrium family of boundary layers described by East, Sawyer and Nash<sup>28</sup>. However, in Fig 25b for locations downstream of the disruptive effect of the strong pressure gradient (points in the regions C and D downstream of the normal shock wave) the results depart considerably from the equilibrium locus.

The different behaviour upstream and downstream of the shock wave is illustrated further in Fig 26 where calculated values of  $J$  and  $K$  are plotted against the equilibrium parameter  $E_f$ . The values of  $J$  and  $K$  were obtained by fitting sine waves of the form

$$\left(\frac{\Delta U}{U_f^i}\right)_N = 0.5 \left[ 1 + \sin \frac{\pi}{J} \left( \frac{y}{\delta_{0.995}} - K \right) \right], \quad (41)$$

to the wake components for each boundary layer profile.

It should be noted that because of the quantity of data recorded, the values of  $\left(\Delta U/U_f^i\right)_{\max}$  were taken at that  $y$ -position of the pitot probe which gave a maximum value rather than estimating the true value by curve fitting. This in part accounts for the spread of values of  $J$ . No attempt was made to investigate the region B under the first compression.

However in the undisturbed equilibrium boundary layers of region A, the averaged values of  $J$  and  $K$  result in a normalised law of the wake

$$\left(\frac{\Delta U}{U_f^i}\right)_N = 0.5 \left[ 1 + \sin \frac{\pi}{0.819} \left( \frac{y}{\delta_{0.995}} - 0.494 \right) \right] \quad (42)$$

which is extremely close to Winter and Gaudet's law (equation (40)). The average value of  $\left(\Delta U/U_f^i\right)_{\max}$  for region A is 2.23 which is rather higher than Winter and Gaudet's value of 1.78 (equation (39)).

In the region downstream of the shock wave (Fig 26b) the parameters  $J$  and  $K$  show an appreciable variation with  $E_f$ . Thus in this region the velocity profiles cannot be represented by a family having either a standard law of the wall (section 4.5.3) or a standard form of the law of the wake.

## 5 CONCLUSIONS

Seven flows have been studied involving the interaction of normal shock waves with nominally two-dimensional turbulent boundary layers over a range of Mach numbers of 1.3 to 1.5 and of Reynolds numbers based on an effective streamwise run of  $10 \times 10^6$  to  $30 \times 10^6$ . The data extend from 700 mm upstream to 3000 mm downstream of the normal shock-wave position. These distances are equivalent to respectively 90 and 400 times the undisturbed boundary layer displacement thickness.

Oil flow investigations on the floor under the main interaction region indicate a highly three-dimensional flow at  $M = 1.5$ , but the results and momentum balance calculations support the view that this three-dimensionality is confined to the separation region. This region is very shallow having a depth of less than 10 mm and streamwise extent of 300 mm while the flow in the region of the tunnel centre line is tolerably two-dimensional, except in the immediate regions of the saddle points at the start and end of the separation. Further downstream of the main interaction region, the momentum balance calculations indicate a slight flow divergence over the width of the tunnel of between  $7^\circ$  at  $M = 1.3$  to  $15^\circ$  at  $M = 1.5$ .

In calculating the momentum balance, use has been made of corrected static pressure measurements and an attempt has been made to follow the recent ideas of matching the free-stream conditions with the viscous layer by defining an equivalent inviscid flow.

A method has been evolved for correcting the static pressure measurements made with the twin static pressure probe used in the experiment, and static pressure distributions normal to the wall within the main shock-wave boundary-layer interaction are presented. Combined with pitot measurements this enables the Mach number distribution to be obtained.

The results agree with the laser measurements of East<sup>3</sup> which cover a more limited area. The present experiment has also produced more detail of the separated region. Good agreement is also noted with Kooi's<sup>7</sup> results at  $M = 1.4$ .

All the measurements confirm that the flow has not stabilised after 3 m downstream of the normal shock wave (or 400 times the undisturbed displacement thickness). Here the thin shear layer which is produced at the bifurcation point of the shock waves at  $M = 1.4$  and 1.5 is intact and there are still velocity gradients across the tunnel in the inviscid flow. Also the boundary-layer profiles have not recovered to the equilibrium shapes.

The analysis in terms of the law of the wall and the law of the wake for the region ahead of the interaction agree fairly closely with Winter and Gaudet (equation (29)) and Gaudet (equation (5)). However the evidence downstream of the normal shock wave suggests that the law of the wall has been changed by the large perturbations or normal pressure gradients. However a single law of the wall may be used for the whole region behind the main disturbance.

A normalised version of Winter and Gaudet's law of the wake (equation (40)) provides a fair estimate for the shape of the normalised wake components ahead of the normal shock wave. The disruptive effects of the normal shock waves appear mainly as changes in amplitude of the normalised wake components, but the form of the wake component is also changed.

Apart from the boundary layers immediately affected by the leading edge of the first compression, the maximum values of the wake function ahead of the normal shock wave have a similar correlation with the equilibrium function  $E_f$  (equation (36)) as the equilibrium family of flows of East, Sawyer and Nash<sup>28</sup>. Although the maximum values of the wake functions downstream of the normal shock wave also correlate with  $E_f$ , they correlate in a quite different way from that expected for equilibrium boundary layers.

## Appendix

### STATIC PRESSURE PROBE CORRECTIONS

#### A.1 Calibration measurements

As stated previously (section 2.2.4) the corrections to be applied to the static pressure probes were based on limited measurements made in the free stream at transonic speeds together with the results of the calibrations of the twin static pressure probe by traverses through the floor boundary layers at free-stream Mach numbers between 0.66 and 0.88. Additional information was derived during the actual experiment from the static and pitot traverses ahead of the interaction region at free-stream Mach numbers of 1.3, 1.4 and 1.5. Data was also used from the static and pitot traverses made through the boundary layer 1 to 3 m downstream of the normal shock wave at  $M = 1.3$ . It was assumed that for all these regions the static pressure for each traverse was constant and equal to the wall value,  $p_w$ .

The results of the free-stream calibrations are shown in Fig 27 where the differences between the measured and actual static pressures are presented as pressure coefficients based on local conditions plotted against Mach number. Also (shown dotted) are the calibrations after three stages of smoothing which were used to correct the static pressure readings made under the severe velocity gradients of the region investigated (section A.2.2). There was no apparent Reynolds number effect on the calibrations but time limitations precluded much use of the single static pressure probes. The correction method described, therefore applies only to the twin static pressure probe. No static measurements were made at  $M = 1.4$  for a unit Reynolds number of  $3.5 \times 10^6/m$ .

#### A.2 The correction method applied to the twin static pressure probe

Fig 28a&b shows typical static pressure measurement errors incurred while making boundary layer traverses with the twin static pressure probe. The boundary layers had constant static pressures normal to the wall.

The errors have been presented as the differences between the measured and actual static pressures and are shown as pressure coefficients based on local conditions. They are plotted against the distance from the wall,  $y$ , non-dimensionalised by dividing by the boundary layer thickness  $\delta_{0.995}$ .

Fig 28a shows typical errors when the maximum Mach number is less than the critical value of 1.098 (the point at which the free-stream calibration errors are shown in Fig 27, to become negligible). The errors have a different character if the maximum Mach number for the traverse is above the critical value as shown in Fig 28b. It is therefore convenient to divide the errors to be corrected into two categories:

- (1) when the outer static pressure probe is at a Mach number of less than or equal to 1.098;
- (2) when the outer static pressure probe is at a Mach number greater than 1.098.

This is a not unreasonable assumption because the main source of error in the free-stream calibrations and the static traverse measurements made away from the influence of the wall, can be shown to be mostly due to the interconnecting stem between the inner and outer static pressure probes (see Fig 27 and Read, Pope and Cooksey<sup>29</sup>, pp 102&103). Therefore the main correction to be applied to the inner static probe depends on some estimate of the mean Mach number over the connecting stem provided the static pressure probes are both at Mach numbers below the critical 1.098. If however, the outer static probe is at a Mach number above this critical value, then there is no interference associated with the interconnecting stem in the region of the outer static probe. In this case a suitable course of action is to use the local Mach number to estimate the correction due to the interconnecting stem on the pressure measured by the inner static probe.

It is now proposed to deal with the errors in more detail by considering the three regions A, B and C indicated in Fig 28 in conjunction with the Mach number of the outer static pressure probe.

#### A.2.1 Region A

The error in this region is treated as arising mainly from wall interference. There is however some compressibility effect. The errors are presented in law of the wall terms for correlation purposes (Figs 29 and 30). Fig 29 shows the accumulated errors resulting from the subsonic boundary-layer traverses, while Fig 30 shows the errors resulting from the undisturbed boundary-layer traverses ahead of the interaction region at free-stream Mach numbers of 1.3, 1.4 and 1.5. To calculate the corrections, the errors of region A may be added to those of region B. However because the errors of regions B and C are based on local conditions rather than the conditions at the edge of the boundary layer used for region A, the region A errors are multiplied by a factor  $(M/M_0)^2$  to bring them into line.

Thus the corrections needed for the static pressure measurements made in region A are given by

$$C_{PA} = \frac{P_m - P}{\frac{1}{2}\rho U^2} = C_i \left( \frac{M_0}{M} \right)^2 f_n \left( \frac{yU_\tau}{\nu_\tau}, M \right).$$

##### A.2.1.1 Outer static pressure probe at $M \leq 1.098$

The measurement errors shown in Fig 29 have been presented as

$$\left( \frac{P_m - P_w}{\frac{1}{2}\rho_\tau U_\tau^2} \right) \frac{1}{C_f}$$

and plotted against  $yU_\tau/\nu_\tau$ . The corrections needed are actually fairly small (for the Mach numbers are low) and so a single correction has been used and this is represented by the continuous line in the figure. The correction is given by

$$C_{p_A} = 15C_f \left(\frac{M_\infty}{M}\right)^2 \quad \text{when } \frac{yU_\infty}{v_\infty} < 644$$

$$C_{p_A} = C_f \left(\frac{M_\infty}{M}\right)^2 \left[ 50.37 - 5.469 \ln\left(\frac{yU_\infty}{v_\infty}\right) \right] \quad \text{when } 644 \leq \frac{yU_\infty}{v_\infty} < 1000$$

$$C_{p_A} = 0 \quad \text{when } \frac{yU_\infty}{v_\infty} \geq 1000 .$$

#### A.2.1.2 Outer static pressure probe at $M > 1.098$

Fig 30 shows the pressure measurement errors plotted in similar terms to those used in section A.2.1.1. Here the results are strongly Mach-number dependent. The corrections have been applied on the assumption that the pressure measurement errors in Fig 30 have a linear relation with Mach number for constant  $yU_\infty/v_\infty$ . The slopes and zero intercepts of this linear variation are then assumed to be entirely dependent upon  $yU_\infty/v_\infty$ . The corrections which are shown by the continuous lines in Fig 30 are given by

$$C_{p_A} = FC_f \left(\frac{M_\infty}{M}\right)^2 \left[ M - 0.2725 - 0.1153 \ln\left(\frac{yU_\infty}{v_\infty}\right) \right]$$

$$\text{where } F = 19.33 \ln\left(\frac{yU_\infty}{v_\infty}\right) - 433.5 \quad \text{when } \frac{yU_\infty}{v_\infty} \leq 7660$$

$$F = 692.7 \ln\left(\frac{yU_\infty}{v_\infty}\right) - 6456 \quad \text{when } 7660 < \frac{yU_\infty}{v_\infty} < 11200$$

$$F = 0 \quad \text{when } \frac{yU_\infty}{v_\infty} \geq 11200 .$$

This correction is based on rather limited evidence but the magnitude is small and the probable accuracy of the correction is within 1½% of the true static pressure.

#### A.2.2 Regions B and C

The errors in these regions are treated as arising from a combination of shear flow and compressibility effects. It would therefore be expected that there would be an error which would correlate with  $y/\delta_{0.995}$  and a larger error due to the geometry of the twin static pressure probe, which would correlate with Mach number. As stated in section A.2 the greater part of the latter error is due to the stem interconnecting the inner and outer static pressure probes, and the necessary correction depends on an estimate of Mach number and a form of the free-stream calibration of the twin static probe.

In fact, the average Mach number of the inner and outer static probes is used to give the necessary correction to the static pressure measured by the inner probe, when the outer probe is below the critical Mach number of 1.098. In all other instances the local Mach number is used to obtain the correction needed to the measured static pressure.

This applies to both the inner and outer static probes. The local Mach number is always used for the outer static pressure probe because it is normally in a region where the Mach number gradient normal to the wall is small.

It was found that the free-stream calibration overcorrected the static pressure measurement errors, and so a compromise calibration was used (shown dotted in Fig 27a) which involved three stages of smoothing. It may be noted from Fig 16a-f that the critical Mach number is only encountered ahead of and in the immediate vicinity of the main interaction region. The location of the point for critical Mach number is close to the wall for stations upstream of the influence of the normal shock wave. The environment is therefore one of severe shear strains and velocity gradients and the smoothing exercise is probably justified as it only affects the free-stream calibration in the region of the critical Mach number.

The form of the corrections is given by

$$C_{P_B} = \text{fn}\left(M_I, M_U, \frac{y}{\delta_{0.995}}\right)$$

$$C_{P_C} = \text{fn}\left(M_U, \frac{y}{\delta_{0.995}}\right) .$$

#### A.2.2.1 Outer static pressure probe at $M \leq 1.098$

The corrections are calculated in terms of local density and velocity. The modified calibration curves (shown dotted in Fig 27) are used to obtain  $(p_m - p/\frac{1}{2}\rho U^2)$  from  $\text{fn}(M)$  and the modification to the free-stream calibration due to probe position is shown in Fig 31.

Thus the total correction is given by

$$C_{P_B} = \text{fn}\left(\frac{M_I + M_U}{2}\right) \times 0.94 \left[ \sin\left\{0.665 \left(\frac{y}{\delta_{0.995}} - 0.15\right)\right\} \right]^{\frac{1}{2}}$$

$$C_{P_C} = \text{fn}(M_U) \times 0.94 \left[ \sin\left\{0.665 \left(\frac{y}{\delta_{0.995}} - 0.15\right)\right\} \right]^{\frac{1}{2}}$$

$$C_{P_B} = 0 \quad \text{if } \frac{y}{\delta_{0.995}} < 0.15 .$$

#### A.2.2.2 Outer static pressure probe at $M > 1.098$

$$C_{P_B} = \text{fn}(M_I) \times 0.94 \left[ \sin\left\{0.665 \left(\frac{y}{\delta_{0.995}} - 0.15\right)\right\} \right]^{\frac{1}{2}}$$

$$C_{p_C} = f_n(M_U) \cdot 0.94 \left[ \sin \left\{ 0.665 \left( \frac{y}{0.495} - 0.15 \right) \right\} \right]^{\frac{1}{2}}$$

$$C_{p_B} = 0 \quad \text{if} \quad \frac{y}{0.495} < 0.15 .$$

### A.2.3 Total corrections

$$\text{Inner tube} \quad C_{p_I} = C_{p_A} + C_{p_B} = \frac{p_m - p}{\frac{1}{2} \rho U^2}$$

$$\text{Outer tube} \quad C_{p_U} = C_{p_C} = \frac{p_m - p}{\frac{1}{2} \rho U^2} .$$

### A.3 Applying the corrections

The following describes how the static pressure corrections are calculated and applied:

- (1) Calculate the Mach number at each measuring station from interpolated pitot and wall pressure measurements. Calculate  $y/\delta_{0.995}$ ,  $C_f$  and  $y(U_\tau/\nu_\tau)$ .
- (2) Calculate the static pressure corrections and subtract from the measured values.
- (3) Recalculate the new Mach number using the new static pressure and the interpolated pitot measurement.

Steps (2) and (3) are repeated until the difference between the new and old Mach number is less than 0.001. A suitable damping factor is needed to prevent oscillations in the calculation.

- (4) Record the corrected Mach number and static pressure.

Fig 32 shows the effect of the correction on static pressures measured ahead and downstream of the interaction region where the static pressures may be expected to be nearly uniform across the boundary layer thickness. It will be seen that the static pressure errors have been reduced to  $1\frac{1}{2}\%$  of the true static pressure.

### A.4 Transferring the corrected static pressures to the pitot traverse measurements

The final stage of the procedure is to interpolate in the distribution of static pressure to obtain values at the location of the pitot-pressure measurements.

The calculated static pressures for each static pressure traverse are smoothed and transferred to a carpet plot of static pressure against streamwise position as shown in Fig 33. The appropriate static pressures are then transferred from the carpet plot for each pitot traverse. A final stage of smoothing ensures that the final static pressure curves are asymptotic to the wall static pressure within a few millimetres of the tunnel floor.

The corrected static pressure results may be seen in Fig 15a&b.



Table 1

TEST CONDITIONS

$M_0$	$Re/m \times 10^{-6}$	$Re \delta^* \times 10^{-3}$	$Re \theta \times 10^{-3}$	$Re \lambda \times 10^{-6}$	Distance of throat ahead of window centreline (m)	Effective turbulent run ahead of window centreline (m)
1.270	3.66	29.1	14.1	11.2	2.78	3.25
1.272	10.21	68.2	33.8	31.2	2.78	3.23
1.373	3.67	30.0	13.6	10.9	2.84	3.17
1.386	10.03	68.2	31.6	29.5	2.84	3.14
1.522	3.51	28.1	11.8	9.5	2.86	2.97
1.531	6.47	46.1	20.2	17.3	2.87	2.95
1.538	9.96	68.7	29.2	27.9	2.87	3.02





Table 2 (continued)

N (NUMBER) = 13		10-25.7 L DEL 95%-42.8 MM		10-25.3 K DEL 95%-44.9 MM		10-25.3 L DEL 95%-45.3 MM		10-25.0 K DEL 95%-48.9 MM											
REQ/NO. 3 (REQUIRED) (MEASURED) P		REQ/NO. 3 (REQUIRED) (MEASURED) P		REQ/NO. 3 (REQUIRED) (MEASURED) P		REQ/NO. 3 (REQUIRED) (MEASURED) P		REQ/NO. 3 (REQUIRED) (MEASURED) P											
V (MM)	CONST N	U/E	REQD P	V (MM)	CONST N	U/E	REQD P	V (MM)	CONST N	U/E	REQD P	V (MM)	CONST N	U/E	REQD P	V (MM)	CONST N	U/E	REQD P
0.0	0.000	0.000	0.000	0.0	0.000	0.000	0.000	0.0	0.000	0.000	0.000	0.0	0.000	0.000	0.000	0.0	0.000	0.000	0.000
0.5	0.596	0.583	0.598	0.5	0.580	0.567	0.583	0.5	0.578	0.565	0.581	0.5	0.576	0.563	0.579	0.5	0.574	0.561	0.577
1.0	0.599	0.586	0.599	1.0	0.583	0.570	0.583	1.0	0.581	0.568	0.581	1.0	0.579	0.566	0.579	1.0	0.577	0.564	0.577
1.5	0.602	0.589	0.603	1.5	0.586	0.573	0.586	1.5	0.584	0.571	0.584	1.5	0.582	0.569	0.582	1.5	0.580	0.567	0.580
2.0	0.605	0.592	0.606	2.0	0.589	0.576	0.589	2.0	0.587	0.574	0.587	2.0	0.585	0.572	0.585	2.0	0.583	0.570	0.583
2.5	0.608	0.595	0.609	2.5	0.592	0.579	0.592	2.5	0.590	0.577	0.590	2.5	0.588	0.575	0.588	2.5	0.586	0.573	0.586
3.0	0.611	0.598	0.612	3.0	0.595	0.582	0.595	3.0	0.593	0.580	0.593	3.0	0.591	0.578	0.591	3.0	0.589	0.576	0.589
3.5	0.614	0.601	0.613	3.5	0.598	0.585	0.598	3.5	0.596	0.583	0.596	3.5	0.594	0.581	0.594	3.5	0.592	0.579	0.592
4.0	0.617	0.604	0.614	4.0	0.601	0.588	0.601	4.0	0.599	0.586	0.599	4.0	0.597	0.584	0.597	4.0	0.595	0.582	0.595
4.5	0.620	0.607	0.617	4.5	0.604	0.591	0.604	4.5	0.602	0.589	0.602	4.5	0.600	0.587	0.600	4.5	0.598	0.585	0.598
5.0	0.623	0.610	0.619	5.0	0.607	0.594	0.607	5.0	0.605	0.592	0.605	5.0	0.603	0.590	0.603	5.0	0.601	0.588	0.601
5.5	0.626	0.613	0.621	5.5	0.610	0.597	0.610	5.5	0.608	0.595	0.608	5.5	0.606	0.593	0.606	5.5	0.604	0.591	0.604
6.0	0.629	0.616	0.624	6.0	0.613	0.600	0.613	6.0	0.611	0.598	0.611	6.0	0.609	0.596	0.609	6.0	0.607	0.594	0.607
6.5	0.632	0.619	0.627	6.5	0.616	0.603	0.616	6.5	0.614	0.601	0.614	6.5	0.612	0.599	0.612	6.5	0.610	0.597	0.610
7.0	0.635	0.622	0.629	7.0	0.619	0.606	0.619	7.0	0.617	0.604	0.617	7.0	0.615	0.602	0.615	7.0	0.613	0.600	0.613
7.5	0.638	0.625	0.631	7.5	0.622	0.609	0.622	7.5	0.620	0.607	0.620	7.5	0.618	0.605	0.618	7.5	0.616	0.603	0.616
8.0	0.641	0.628	0.634	8.0	0.625	0.612	0.625	8.0	0.623	0.610	0.623	8.0	0.621	0.608	0.621	8.0	0.619	0.606	0.619
8.5	0.644	0.631	0.637	8.5	0.628	0.615	0.628	8.5	0.626	0.613	0.626	8.5	0.624	0.611	0.624	8.5	0.622	0.609	0.622
9.0	0.647	0.634	0.640	9.0	0.631	0.618	0.631	9.0	0.629	0.616	0.629	9.0	0.627	0.614	0.627	9.0	0.625	0.612	0.625
9.5	0.650	0.637	0.643	9.5	0.634	0.621	0.634	9.5	0.632	0.619	0.632	9.5	0.630	0.617	0.630	9.5	0.628	0.615	0.628
10.0	0.653	0.640	0.646	10.0	0.637	0.624	0.637	10.0	0.635	0.622	0.635	10.0	0.633	0.620	0.633	10.0	0.631	0.618	0.631
10.5	0.656	0.643	0.649	10.5	0.640	0.627	0.640	10.5	0.638	0.625	0.638	10.5	0.636	0.623	0.636	10.5	0.634	0.621	0.634
11.0	0.659	0.646	0.651	11.0	0.643	0.630	0.643	11.0	0.641	0.628	0.641	11.0	0.639	0.626	0.639	11.0	0.637	0.624	0.637
11.5	0.662	0.649	0.654	11.5	0.646	0.633	0.646	11.5	0.644	0.631	0.644	11.5	0.642	0.629	0.642	11.5	0.640	0.627	0.640
12.0	0.665	0.652	0.657	12.0	0.649	0.636	0.649	12.0	0.647	0.634	0.647	12.0	0.645	0.632	0.645	12.0	0.643	0.630	0.643
12.5	0.668	0.655	0.660	12.5	0.652	0.639	0.652	12.5	0.650	0.637	0.650	12.5	0.648	0.635	0.648	12.5	0.646	0.633	0.646
13.0	0.671	0.658	0.663	13.0	0.655	0.642	0.655	13.0	0.653	0.640	0.653	13.0	0.651	0.638	0.651	13.0	0.649	0.636	0.649
13.5	0.674	0.661	0.666	13.5	0.658	0.645	0.658	13.5	0.656	0.643	0.656	13.5	0.654	0.641	0.654	13.5	0.652	0.639	0.652
14.0	0.677	0.664	0.669	14.0	0.661	0.648	0.661	14.0	0.659	0.646	0.659	14.0	0.657	0.644	0.657	14.0	0.655	0.642	0.655
14.5	0.680	0.667	0.672	14.5	0.664	0.651	0.664	14.5	0.662	0.649	0.662	14.5	0.660	0.647	0.660	14.5	0.658	0.645	0.658
15.0	0.683	0.670	0.675	15.0	0.667	0.654	0.667	15.0	0.665	0.652	0.665	15.0	0.663	0.650	0.663	15.0	0.661	0.648	0.661
15.5	0.686	0.673	0.678	15.5	0.670	0.657	0.670	15.5	0.668	0.655	0.668	15.5	0.666	0.653	0.666	15.5	0.664	0.651	0.664
16.0	0.689	0.676	0.681	16.0	0.673	0.660	0.673	16.0	0.671	0.658	0.671	16.0	0.669	0.656	0.669	16.0	0.667	0.654	0.667
16.5	0.692	0.679	0.684	16.5	0.676	0.663	0.676	16.5	0.674	0.661	0.674	16.5	0.672	0.659	0.672	16.5	0.670	0.657	0.670
17.0	0.695	0.682	0.687	17.0	0.679	0.666	0.679	17.0	0.677	0.664	0.677	17.0	0.675	0.662	0.675	17.0	0.673	0.660	0.673
17.5	0.698	0.685	0.690	17.5	0.682	0.671	0.682	17.5	0.680	0.667	0.680	17.5	0.678	0.665	0.678	17.5	0.676	0.663	0.676
18.0	0.701	0.688	0.693	18.0	0.685	0.674	0.685	18.0	0.683	0.670	0.683	18.0	0.681	0.668	0.681	18.0	0.679	0.666	0.679
18.5	0.704	0.691	0.696	18.5	0.688	0.677	0.688	18.5	0.686	0.673	0.686	18.5	0.684	0.671	0.684	18.5	0.682	0.669	0.682
19.0	0.707	0.694	0.699	19.0	0.691	0.680	0.691	19.0	0.689	0.676	0.689	19.0	0.687	0.674	0.687	19.0	0.685	0.672	0.685
19.5	0.710	0.697	0.702	19.5	0.694	0.683	0.694	19.5	0.692	0.679	0.692	19.5	0.690	0.677	0.690	19.5	0.688	0.675	0.688
20.0	0.713	0.700	0.705	20.0	0.697	0.686	0.697	20.0	0.695	0.682	0.695	20.0	0.693	0.680	0.693	20.0	0.691	0.678	0.691
20.5	0.716	0.703	0.708	20.5	0.700	0.689	0.700	20.5	0.698	0.685	0.698	20.5	0.696	0.683	0.696	20.5	0.694	0.681	0.694
21.0	0.719	0.706	0.711	21.0	0.703	0.692	0.703	21.0	0.701	0.688	0.701	21.0	0.699	0.686	0.699	21.0	0.697	0.684	0.697
21.5	0.722	0.709	0.714	21.5	0.706	0.695	0.706	21.5	0.704	0.691	0.704	21.5	0.702	0.689	0.702	21.5	0.700	0.687	0.700
22.0	0.725	0.712	0.717	22.0	0.709	0.698	0.709	22.0	0.707	0.694	0.707	22.0	0.705	0.692	0.705	22.0	0.703	0.690	0.703
22.5	0.728	0.715	0.720	22.5	0.712	0.701	0.712	22.5	0.710	0.697	0.710	22.5	0.708	0.695	0.708	22.5	0.706	0.693	0.706
23.0	0.731	0.718	0.723	23.0	0.715	0.704	0.715	23.0	0.713	0.700	0.713	23.0	0.711	0.698	0.711	23.0	0.709	0.696	0.709
23.5	0.734	0.721	0.726	23.5	0.718	0.707	0.718	23.5	0.716	0.703	0.716	23.5	0.714	0.701	0.714	23.5	0.712	0.699	0.712
24.0	0.737	0.724	0.729	24.0	0.721	0.710	0.721	24.0	0.719	0.706	0.719	24.0	0.717	0.704	0.717	24.0	0.715	0.702	0.715
24.5	0.740	0.727	0.732	24.5	0.724	0.713	0.724	24.5	0.722	0.709	0.722	24.5	0.720	0.707	0.720	24.5	0.718	0.705	0.718
25.0	0.743	0.730	0.735	25.0	0.727	0.716	0.727	25.0	0.725	0.712	0.725	25.0	0.723	0.710	0.723	25.0	0.721	0.708	0.721
25.5	0.746	0.733	0.738	25.5	0.730	0.719	0.730	25.5	0.728	0.715	0.728	25.5	0.726	0.713	0.726	25.5	0.724	0.711	0.724
26.0	0.749	0.736	0.741	26.0	0.733	0.722	0.733	26.0	0.731	0.718	0.731	26.0	0.729	0.716	0.729	26.0	0.727	0.714	0.727
26.5	0.752	0.739	0.744	26.5	0.736	0.725	0.736	26.5	0.734	0.721	0.734	26.5	0.732	0.719	0.732	26.5	0.730	0.717	0.730
27.0	0.755	0.742	0.747	27.0	0.739	0.728	0.739	27.0	0.737	0.724	0.737	27.0	0.735	0.722	0.735	27.0	0.733	0.720	0.733
27.5	0.758	0.745	0.750	27.5	0.742	0.731	0.742	27.5	0.740	0.727	0.740	27.5	0.738	0.725	0.738	27.5	0.736	0.723	0.736
28.0	0.761	0.748	0.753	28.0	0.745	0.734	0.745	28.0	0.743	0.730	0.743	28.0	0.741	0.728	0.741	28.0	0.739	0.726	0.739
28.5	0.764	0.751	0.756	28.5	0.748	0.737	0.748	28.5	0.746	0.733	0.746	28.5	0.744	0.731	0.744	28.5	0.742	0.729	0.742
29.0	0.767	0.754	0.759	29.0	0.751	0.740	0.751	29.0	0.749	0.736	0.749	29.0	0.747	0.734	0.747	29.0	0.745	0.732	0.745
29.5	0.770	0.757	0.762	29.5	0.754	0.743	0.754	29.5	0.752	0.739	0.752	29.5							







R. MONTANA 113  
 XE 2785 MW (MEASURED P) 19-291.7 k DEL 995-115 0 MW  
 RE-76-3 541076 (MEASURED P) RE-40 889 (MEASURED P)

LONESTAR		MEASURED P	
Y (MW)	H (H)	VALUE	PLANT
0.06	0.0000	0.0000	0.0000
0.06	0.4322	0.5279	0.6006
0.06	0.4462	0.5403	0.6006
1.06	0.4500	0.5540	0.6006
1.06	0.4672	0.5646	0.6006
1.47	0.4738	0.5777	0.6006
1.67	0.4895	0.5904	0.6006
2.21	0.5024	0.6052	0.6006
4.06	0.5124	0.6178	0.6006
7.17	0.5275	0.6338	0.6006
7.70	0.5387	0.6466	0.6006
4.56	0.5546	0.6648	0.6006
6.56	0.5747	0.6971	0.6006
8.67	0.5945	0.7395	0.6006
10.66	0.6081	0.7845	0.6006
12.66	0.6147	0.8117	0.6006
14.67	0.6274	0.8414	0.6006
16.66	0.6279	0.8463	0.6006
18.66	0.6405	0.8807	0.6006
20.70	0.6454	0.8856	0.6006
25.71	0.6622	0.9259	0.6006
30.66	0.6681	0.9381	0.6006
35.67	0.6753	0.9593	0.6006
40.66	0.7087	1.0146	0.6006
45.66	0.7225	1.0488	0.6006
50.70	0.7367	1.0824	0.6006
55.75	0.7510	1.1162	0.6006
60.66	0.7662	1.1502	0.6006
70.75	0.7923	1.2193	0.6006
80.71	0.8173	1.2877	0.6006
90.66	0.8333	1.3540	0.6006
101.43	0.8547	1.4247	0.6006
111.43	0.8645	1.4645	0.6006
121.47	0.8676	1.4676	0.6006
131.43	0.8690	1.4690	0.6006
141.47	0.8687	1.4687	0.6006
151.47	0.8676	1.4676	0.6006
156.52	0.8642	1.4642	0.6006
161.47	0.8449	1.4649	0.6006
171.50	0.8632	1.4632	0.6006
181.46	0.8418	1.4618	0.6006
191.47	0.8676	1.4676	0.6006

L











M. MONTHLY (1.1)									
K=125 MM					K=174 MM				
DEL. 995-52.9 MM					DEL. 995-52.9 MM				
MEAS. 9.84418 G. (MEASURED P.)					MEAS. 9.84418 G. (MEASURED P.)				
Y. (MM)	M	U. (E)	P. (PTO)	P. (PTO)	Y. (MM)	M	U. (E)	P. (PTO)	P. (PTO)
0.00	0.0000	0.0000	0.0000	0.0000	0.00	0.0000	0.0000	0.0000	0.0000
0.01	0.2775	0.1138	0.2775	0.1138	0.01	0.2775	0.1138	0.2775	0.1138
0.02	0.5550	0.2276	0.5550	0.2276	0.02	0.5550	0.2276	0.5550	0.2276
0.03	0.8325	0.3414	0.8325	0.3414	0.03	0.8325	0.3414	0.8325	0.3414
0.04	1.1100	0.4552	1.1100	0.4552	0.04	1.1100	0.4552	1.1100	0.4552
0.05	1.3875	0.5690	1.3875	0.5690	0.05	1.3875	0.5690	1.3875	0.5690
0.06	1.6650	0.6828	1.6650	0.6828	0.06	1.6650	0.6828	1.6650	0.6828
0.07	1.9425	0.7966	1.9425	0.7966	0.07	1.9425	0.7966	1.9425	0.7966
0.08	2.2200	0.9104	2.2200	0.9104	0.08	2.2200	0.9104	2.2200	0.9104
0.09	2.4975	1.0242	2.4975	1.0242	0.09	2.4975	1.0242	2.4975	1.0242
0.10	2.7750	1.1380	2.7750	1.1380	0.10	2.7750	1.1380	2.7750	1.1380
0.11	3.0525	1.2518	3.0525	1.2518	0.11	3.0525	1.2518	3.0525	1.2518
0.12	3.3300	1.3656	3.3300	1.3656	0.12	3.3300	1.3656	3.3300	1.3656
0.13	3.6075	1.4794	3.6075	1.4794	0.13	3.6075	1.4794	3.6075	1.4794
0.14	3.8850	1.5932	3.8850	1.5932	0.14	3.8850	1.5932	3.8850	1.5932
0.15	4.1625	1.7070	4.1625	1.7070	0.15	4.1625	1.7070	4.1625	1.7070
0.16	4.4400	1.8208	4.4400	1.8208	0.16	4.4400	1.8208	4.4400	1.8208
0.17	4.7175	1.9346	4.7175	1.9346	0.17	4.7175	1.9346	4.7175	1.9346
0.18	5.0000	2.0484	5.0000	2.0484	0.18	5.0000	2.0484	5.0000	2.0484
0.19	5.2775	2.1622	5.2775	2.1622	0.19	5.2775	2.1622	5.2775	2.1622
0.20	5.5550	2.2760	5.5550	2.2760	0.20	5.5550	2.2760	5.5550	2.2760
0.21	5.8325	2.3898	5.8325	2.3898	0.21	5.8325	2.3898	5.8325	2.3898
0.22	6.1100	2.5036	6.1100	2.5036	0.22	6.1100	2.5036	6.1100	2.5036
0.23	6.3875	2.6174	6.3875	2.6174	0.23	6.3875	2.6174	6.3875	2.6174
0.24	6.6650	2.7312	6.6650	2.7312	0.24	6.6650	2.7312	6.6650	2.7312
0.25	6.9425	2.8450	6.9425	2.8450	0.25	6.9425	2.8450	6.9425	2.8450
0.26	7.2200	2.9588	7.2200	2.9588	0.26	7.2200	2.9588	7.2200	2.9588
0.27	7.4975	3.0726	7.4975	3.0726	0.27	7.4975	3.0726	7.4975	3.0726
0.28	7.7750	3.1864	7.7750	3.1864	0.28	7.7750	3.1864	7.7750	3.1864
0.29	8.0525	3.3002	8.0525	3.3002	0.29	8.0525	3.3002	8.0525	3.3002
0.30	8.3300	3.4140	8.3300	3.4140	0.30	8.3300	3.4140	8.3300	3.4140
0.31	8.6075	3.5278	8.6075	3.5278	0.31	8.6075	3.5278	8.6075	3.5278
0.32	8.8850	3.6416	8.8850	3.6416	0.32	8.8850	3.6416	8.8850	3.6416
0.33	9.1625	3.7554	9.1625	3.7554	0.33	9.1625	3.7554	9.1625	3.7554
0.34	9.4400	3.8692	9.4400	3.8692	0.34	9.4400	3.8692	9.4400	3.8692
0.35	9.7175	3.9830	9.7175	3.9830	0.35	9.7175	3.9830	9.7175	3.9830
0.36	10.0000	4.0968	10.0000	4.0968	0.36	10.0000	4.0968	10.0000	4.0968
0.37	10.2775	4.2106	10.2775	4.2106	0.37	10.2775	4.2106	10.2775	4.2106
0.38	10.5550	4.3244	10.5550	4.3244	0.38	10.5550	4.3244	10.5550	4.3244
0.39	10.8325	4.4382	10.8325	4.4382	0.39	10.8325	4.4382	10.8325	4.4382
0.40	11.1100	4.5520	11.1100	4.5520	0.40	11.1100	4.5520	11.1100	4.5520
0.41	11.3875	4.6658	11.3875	4.6658	0.41	11.3875	4.6658	11.3875	4.6658
0.42	11.6650	4.7796	11.6650	4.7796	0.42	11.6650	4.7796	11.6650	4.7796
0.43	11.9425	4.8934	11.9425	4.8934	0.43	11.9425	4.8934	11.9425	4.8934
0.44	12.2200	5.0072	12.2200	5.0072	0.44	12.2200	5.0072	12.2200	5.0072
0.45	12.4975	5.1210	12.4975	5.1210	0.45	12.4975	5.1210	12.4975	5.1210
0.46	12.7750	5.2348	12.7750	5.2348	0.46	12.7750	5.2348	12.7750	5.2348
0.47	13.0525	5.3486	13.0525	5.3486	0.47	13.0525	5.3486	13.0525	5.3486
0.48	13.3300	5.4624	13.3300	5.4624	0.48	13.3300	5.4624	13.3300	5.4624
0.49	13.6075	5.5762	13.6075	5.5762	0.49	13.6075	5.5762	13.6075	5.5762
0.50	13.8850	5.6900	13.8850	5.6900	0.50	13.8850	5.6900	13.8850	5.6900
0.51	14.1625	5.8038	14.1625	5.8038	0.51	14.1625	5.8038	14.1625	5.8038
0.52	14.4400	5.9176	14.4400	5.9176	0.52	14.4400	5.9176	14.4400	5.9176
0.53	14.7175	6.0314	14.7175	6.0314	0.53	14.7175	6.0314	14.7175	6.0314
0.54	15.0000	6.1452	15.0000	6.1452	0.54	15.0000	6.1452	15.0000	6.1452
0.55	15.2775	6.2590	15.2775	6.2590	0.55	15.2775	6.2590	15.2775	6.2590
0.56	15.5550	6.3728	15.5550	6.3728	0.56	15.5550	6.3728	15.5550	6.3728
0.57	15.8325	6.4866	15.8325	6.4866	0.57	15.8325	6.4866	15.8325	6.4866
0.58	16.1100	6.6004	16.1100	6.6004	0.58	16.1100	6.6004	16.1100	6.6004
0.59	16.3875	6.7142	16.3875	6.7142	0.59	16.3875	6.7142	16.3875	6.7142
0.60	16.6650	6.8280	16.6650	6.8280	0.60	16.6650	6.8280	16.6650	6.8280
0.61	16.9425	6.9418	16.9425	6.9418	0.61	16.9425	6.9418	16.9425	6.9418
0.62	17.2200	7.0556	17.2200	7.0556	0.62	17.2200	7.0556	17.2200	7.0556
0.63	17.4975	7.1694	17.4975	7.1694	0.63	17.4975	7.1694	17.4975	7.1694
0.64	17.7750	7.2832	17.7750	7.2832	0.64	17.7750	7.2832	17.7750	7.2832
0.65	18.0525	7.3970	18.0525	7.3970	0.65	18.0525	7.3970	18.0525	7.3970
0.66	18.3300	7.5108	18.3300	7.5108	0.66	18.3300	7.5108	18.3300	7.5108
0.67	18.6075	7.6246	18.6075	7.6246	0.67	18.6075	7.6246	18.6075	7.6246
0.68	18.8850	7.7384	18.8850	7.7384	0.68	18.8850	7.7384	18.8850	7.7384
0.69	19.1625	7.8522	19.1625	7.8522	0.69	19.1625	7.8522	19.1625	7.8522
0.70	19.4400	7.9660	19.4400	7.9660	0.70	19.4400	7.9660	19.4400	7.9660
0.71	19.7175	8.0798	19.7175	8.0798	0.71	19.7175	8.0798	19.7175	8.0798
0.72	20.0000	8.1936	20.0000	8.1936	0.72	20.0000	8.1936	20.0000	8.1936
0.73	20.2775	8.3074	20.2775	8.3074	0.73	20.2775	8.3074	20.2775	8.3074
0.74	20.5550	8.4212	20.5550	8.4212	0.74	20.5550	8.4212	20.5550	8.4212
0.75	20.8325	8.5350	20.8325	8.5350	0.75	20.8325	8.5350	20.8325	8.5350
0.76	21.1100	8.6488	21.1100	8.6488	0.76	21.1100	8.6488	21.1100	8.6488
0.77	21.3875	8.7626	21.3875	8.7626	0.77	21.3875	8.7626	21.3875	8.7626
0.78	21.6650	8.8764	21.6650	8.8764	0.78	21.6650	8.8764	21.6650	8.8764
0.79	21.9425	8.9902	21.9425	8.9902	0.79	21.9425	8.9902	21.9425	8.9902
0.80	22.2200	9.1040	22.2200	9.1040	0.80	22.2200	9.1040	22.2200	9.1040
0.81	22.4975	9.2178	22.4975	9.2178	0.81	22.4975	9.2178	22.4975	9.2178
0.82	22.7750	9.3316	22.7750	9.3316	0.82	22.7750	9.3316	22.7750	9.3316
0.83	23.0525	9.4454	23.0525	9.4454	0.83	23.0525	9.4454	23.0525	9.4454
0.84	23.3300	9.5592	23.3300	9.5592	0.84	23.3300	9.5592	23.3300	9.5592
0.85	23.6075	9.6730	23.6075	9.6730	0.85	23.6075	9.6730	23.6075	9.6730
0.86	23.8850	9.7868	23.8850	9.7868	0.86	23.8850	9.7868	23.8850	9.7868
0.87	24.1625	9.9006	24.1625	9.9006	0.87	24.1625	9.9006	24.1625	9.9006
0.88	24.4400	10.0144	24.4400	10.0144	0.88	24.4400	10.0144	24.4400	10.0144
0.89	24.7175	10.1282	24.7175	10.1282	0.89	24.7175	10.1282	24.7175	10.1282
0.90	25.0000	10.2420	25.0000	10.2420	0.90	25.0000	10.2420	25.0000	10.2420
0.91	25.2775	10.3558	25.2775	10.3558	0.91	25.2775	10.3558	25.2775	10.3558
0.92	25.5550	10.4696	25.5550	10.4696	0.92	25.5550	10.4696	25.5550	10.4696
0.93	25.8325	10.5834	25.8325	10.5834	0.93	25.8325	10.5834	25.8325	10.5834
0.94	26.1100	10.6972	26.1100	10.6972	0.94	26.1100	10.6972	26.1100	10.6972
0.95	26.3875	10.8110	26.3875	10.8110	0.95	26.3875	10.8110	26.3875	10.8110
0.96	26.6650	10.9248	26.6650	10.9248	0.96	26.6650	10.9248	26.6650	10.9248
0.97	26.9425	11.0386	26.9425	11.0386	0.97	26.9425	11.0386	26.9425	11.0386
0.98	27.2200	11.1524	27.2200	11.1524	0.98	27.2200	11.1524	27.2200	11.1524
0.99	27.4975	11.2662	27.4975	11.2662	0.99	27.4975	11.2662	27.4975	11.2662
1.00	27.7750	11.3800	27.7750	11.3800	1.00	27.7750	11.3800	27.7750	11.3800



11 MONTHS (1-1)

10-26 7 K DEL 995-63 2 P  
RE-9 74418 S (MEASURED P) ME-913 (MEASURED P)

V (M)	CONST P		MEASURED P		P (M)	U (E)	P (M)	U (E)	P (M)	U (E)
	M	U (E)	M	U (E)						
0.00	0.000	0.000	0.000	0.000	0.000	0.000	0.000	0.000	0.000	0.000
0.05	0.791	0.659	0.791	0.659	0.791	0.659	0.791	0.659	0.791	0.659
0.10	0.001	0.079	0.001	0.079	0.001	0.079	0.001	0.079	0.001	0.079
0.15	0.024	0.179	0.024	0.179	0.024	0.179	0.024	0.179	0.024	0.179
0.20	0.050	0.279	0.050	0.279	0.050	0.279	0.050	0.279	0.050	0.279
0.25	0.076	0.379	0.076	0.379	0.076	0.379	0.076	0.379	0.076	0.379
0.30	0.102	0.479	0.102	0.479	0.102	0.479	0.102	0.479	0.102	0.479
0.35	0.128	0.579	0.128	0.579	0.128	0.579	0.128	0.579	0.128	0.579
0.40	0.154	0.679	0.154	0.679	0.154	0.679	0.154	0.679	0.154	0.679
0.45	0.180	0.779	0.180	0.779	0.180	0.779	0.180	0.779	0.180	0.779
0.50	0.206	0.879	0.206	0.879	0.206	0.879	0.206	0.879	0.206	0.879
0.55	0.232	0.979	0.232	0.979	0.232	0.979	0.232	0.979	0.232	0.979
0.60	0.258	1.079	0.258	1.079	0.258	1.079	0.258	1.079	0.258	1.079
0.65	0.284	1.179	0.284	1.179	0.284	1.179	0.284	1.179	0.284	1.179
0.70	0.310	1.279	0.310	1.279	0.310	1.279	0.310	1.279	0.310	1.279
0.75	0.336	1.379	0.336	1.379	0.336	1.379	0.336	1.379	0.336	1.379
0.80	0.362	1.479	0.362	1.479	0.362	1.479	0.362	1.479	0.362	1.479
0.85	0.388	1.579	0.388	1.579	0.388	1.579	0.388	1.579	0.388	1.579
0.90	0.414	1.679	0.414	1.679	0.414	1.679	0.414	1.679	0.414	1.679
0.95	0.440	1.779	0.440	1.779	0.440	1.779	0.440	1.779	0.440	1.779
1.00	0.466	1.879	0.466	1.879	0.466	1.879	0.466	1.879	0.466	1.879
1.05	0.492	1.979	0.492	1.979	0.492	1.979	0.492	1.979	0.492	1.979
1.10	0.518	2.079	0.518	2.079	0.518	2.079	0.518	2.079	0.518	2.079
1.15	0.544	2.179	0.544	2.179	0.544	2.179	0.544	2.179	0.544	2.179
1.20	0.570	2.279	0.570	2.279	0.570	2.279	0.570	2.279	0.570	2.279
1.25	0.596	2.379	0.596	2.379	0.596	2.379	0.596	2.379	0.596	2.379
1.30	0.622	2.479	0.622	2.479	0.622	2.479	0.622	2.479	0.622	2.479
1.35	0.648	2.579	0.648	2.579	0.648	2.579	0.648	2.579	0.648	2.579
1.40	0.674	2.679	0.674	2.679	0.674	2.679	0.674	2.679	0.674	2.679
1.45	0.700	2.779	0.700	2.779	0.700	2.779	0.700	2.779	0.700	2.779
1.50	0.726	2.879	0.726	2.879	0.726	2.879	0.726	2.879	0.726	2.879
1.55	0.752	2.979	0.752	2.979	0.752	2.979	0.752	2.979	0.752	2.979
1.60	0.778	3.079	0.778	3.079	0.778	3.079	0.778	3.079	0.778	3.079
1.65	0.804	3.179	0.804	3.179	0.804	3.179	0.804	3.179	0.804	3.179
1.70	0.830	3.279	0.830	3.279	0.830	3.279	0.830	3.279	0.830	3.279
1.75	0.856	3.379	0.856	3.379	0.856	3.379	0.856	3.379	0.856	3.379
1.80	0.882	3.479	0.882	3.479	0.882	3.479	0.882	3.479	0.882	3.479
1.85	0.908	3.579	0.908	3.579	0.908	3.579	0.908	3.579	0.908	3.579
1.90	0.934	3.679	0.934	3.679	0.934	3.679	0.934	3.679	0.934	3.679
1.95	0.960	3.779	0.960	3.779	0.960	3.779	0.960	3.779	0.960	3.779
2.00	0.986	3.879	0.986	3.879	0.986	3.879	0.986	3.879	0.986	3.879
2.05	1.012	3.979	1.012	3.979	1.012	3.979	1.012	3.979	1.012	3.979
2.10	1.038	4.079	1.038	4.079	1.038	4.079	1.038	4.079	1.038	4.079
2.15	1.064	4.179	1.064	4.179	1.064	4.179	1.064	4.179	1.064	4.179
2.20	1.090	4.279	1.090	4.279	1.090	4.279	1.090	4.279	1.090	4.279
2.25	1.116	4.379	1.116	4.379	1.116	4.379	1.116	4.379	1.116	4.379
2.30	1.142	4.479	1.142	4.479	1.142	4.479	1.142	4.479	1.142	4.479
2.35	1.168	4.579	1.168	4.579	1.168	4.579	1.168	4.579	1.168	4.579
2.40	1.194	4.679	1.194	4.679	1.194	4.679	1.194	4.679	1.194	4.679
2.45	1.220	4.779	1.220	4.779	1.220	4.779	1.220	4.779	1.220	4.779
2.50	1.246	4.879	1.246	4.879	1.246	4.879	1.246	4.879	1.246	4.879
2.55	1.272	4.979	1.272	4.979	1.272	4.979	1.272	4.979	1.272	4.979
2.60	1.298	5.079	1.298	5.079	1.298	5.079	1.298	5.079	1.298	5.079
2.65	1.324	5.179	1.324	5.179	1.324	5.179	1.324	5.179	1.324	5.179
2.70	1.350	5.279	1.350	5.279	1.350	5.279	1.350	5.279	1.350	5.279
2.75	1.376	5.379	1.376	5.379	1.376	5.379	1.376	5.379	1.376	5.379
2.80	1.402	5.479	1.402	5.479	1.402	5.479	1.402	5.479	1.402	5.479
2.85	1.428	5.579	1.428	5.579	1.428	5.579	1.428	5.579	1.428	5.579
2.90	1.454	5.679	1.454	5.679	1.454	5.679	1.454	5.679	1.454	5.679
2.95	1.480	5.779	1.480	5.779	1.480	5.779	1.480	5.779	1.480	5.779
3.00	1.506	5.879	1.506	5.879	1.506	5.879	1.506	5.879	1.506	5.879
3.05	1.532	5.979	1.532	5.979	1.532	5.979	1.532	5.979	1.532	5.979
3.10	1.558	6.079	1.558	6.079	1.558	6.079	1.558	6.079	1.558	6.079
3.15	1.584	6.179	1.584	6.179	1.584	6.179	1.584	6.179	1.584	6.179
3.20	1.610	6.279	1.610	6.279	1.610	6.279	1.610	6.279	1.610	6.279
3.25	1.636	6.379	1.636	6.379	1.636	6.379	1.636	6.379	1.636	6.379
3.30	1.662	6.479	1.662	6.479	1.662	6.479	1.662	6.479	1.662	6.479
3.35	1.688	6.579	1.688	6.579	1.688	6.579	1.688	6.579	1.688	6.579
3.40	1.714	6.679	1.714	6.679	1.714	6.679	1.714	6.679	1.714	6.679
3.45	1.740	6.779	1.740	6.779	1.740	6.779	1.740	6.779	1.740	6.779
3.50	1.766	6.879	1.766	6.879	1.766	6.879	1.766	6.879	1.766	6.879
3.55	1.792	6.979	1.792	6.979	1.792	6.979	1.792	6.979	1.792	6.979
3.60	1.818	7.079	1.818	7.079	1.818	7.079	1.818	7.079	1.818	7.079
3.65	1.844	7.179	1.844	7.179	1.844	7.179	1.844	7.179	1.844	7.179
3.70	1.870	7.279	1.870	7.279	1.870	7.279	1.870	7.279	1.870	7.279
3.75	1.896	7.379	1.896	7.379	1.896	7.379	1.896	7.379	1.896	7.379
3.80	1.922	7.479	1.922	7.479	1.922	7.479	1.922	7.479	1.922	7.479
3.85	1.948	7.579	1.948	7.579	1.948	7.579	1.948	7.579	1.948	7.579
3.90	1.974	7.679	1.974	7.679	1.974	7.679	1.974	7.679	1.974	7.679
3.95	2.000	7.779	2.000	7.779	2.000	7.779	2.000	7.779	2.000	7.779
4.00	2.026	7.879	2.026	7.879	2.026	7.879	2.026	7.879	2.026	7.879
4.05	2.052	7.979	2.052	7.979	2.052	7.979	2.052	7.979	2.052	7.979
4.10	2.078	8.079	2.078	8.079	2.078	8.079	2.078	8.079	2.078	8.079
4.15	2.104	8.179	2.104	8.179	2.104	8.179	2.104	8.179	2.104	8.179
4.20	2.130	8.279	2.130	8.279	2.130	8.279	2.130	8.279	2.130	8.279
4.25	2.156	8.379	2.156	8.379	2.156	8.379	2.156	8.379	2.156	8.379
4.30	2.182	8.479	2.182	8.479	2.182	8.479	2.182	8.479	2.182	8.479
4.35	2.208	8.579	2.208	8.579	2.208	8.579	2.208	8.579	2.208	8.579
4.40	2.234	8.679	2.234	8.679	2.234	8.679	2.234	8.679	2.234	8.679
4.45	2.260	8.779	2.260	8.779	2.260	8.779	2.260	8.779	2.260	8.779
4.50	2.286	8.879	2.286	8.879	2.286	8.879	2.286	8.879	2.286	8.879
4.55	2.312	8.979	2.312	8.979	2.312	8.979	2.312	8.979	2.312	8.979
4.60	2.338	9.079	2.338	9.079	2.338	9.079	2.338	9.079	2.338	9.079
4.65	2.364	9.179	2.364	9.179	2.364	9.179	2.364	9.179	2.364	9.179
4.70	2.390	9.279	2.390	9.279	2.390	9.279	2.390	9.279	2.390	9.279
4.75	2.416	9.379	2.416	9.379	2.416	9.379	2.416	9.379	2.416	9.379
4.80	2.442	9.479	2.442	9.479	2.442	9.479	2.442	9.479	2.442	9.479
4.85	2.468	9.579	2.468	9.579	2.468	9.579	2.468	9.579	2.468	9.579
4.90	2.494	9.679	2.494	9.679	2.494	9.679	2.494	9.679	2.494	9.679
4.95	2.520	9.779	2.520	9.779	2.520	9.779	2.520	9.779	2.520	9.779
5.00	2.546	9.879	2.546	9.879	2.546	9.879	2.546	9.879	2.546	9.879

11 MONTHS (1-1)

10-26 8 K DEL 995-63 2 P  
RE-9 74418 S (MEASURED P) ME-913 (MEASURED P)

V (M)	CONST P		MEASURED P		P (M)	U (E)	P (M)	U (E)	P (M)	U (E)
	M	U (E)	M	U (E)						
0.00	0.000	0.000	0.000	0.000	0.000	0.000	0.000	0.000	0.000	0.000
0.05	0.791	0.659	0.791	0.659	0.791	0.659	0.791	0.659	0.791	





M (NUMBER) = 1.1

26-1278 W  
DEL 955-24.6 W  
RE-9 50410.6 (REQUIRED P)

Table with 10 columns: Y (W), N, UVE, P, UVE, P, P, UVE, P, P. Rows contain numerical data for various parameters.

M (NUMBER) = 1.1

26-1279 W  
DEL 955-24.6 W  
RE-9 50410.6 (REQUIRED P)

Table with 10 columns: Y (W), N, UVE, P, UVE, P, P, UVE, P, P. Rows contain numerical data for various parameters.

M (NUMBER) = 1.1

26-1280 W  
DEL 955-24.6 W  
RE-9 50410.6 (REQUIRED P)

Table with 10 columns: Y (W), N, UVE, P, UVE, P, P, UVE, P, P. Rows contain numerical data for various parameters.

M (NUMBER) = 1.1

26-1281 W  
DEL 955-24.6 W  
RE-9 50410.6 (REQUIRED P)

Table with 10 columns: Y (W), N, UVE, P, UVE, P, P, UVE, P, P. Rows contain numerical data for various parameters.

M (NUMBER) = 1.1

26-1282 W  
DEL 955-24.6 W  
RE-9 50410.6 (REQUIRED P)

Table with 10 columns: Y (W), N, UVE, P, UVE, P, P, UVE, P, P. Rows contain numerical data for various parameters.

M (NUMBER) = 1.1

26-1283 W  
DEL 955-24.6 W  
RE-9 50410.6 (REQUIRED P)

Table with 10 columns: Y (W), N, UVE, P, UVE, P, P, UVE, P, P. Rows contain numerical data for various parameters.

continued

N (NORMAL) = 1.3

IN 2729 IN 78-294 S K DEL 955-100 0 194  
 RE/AF 9 344176 (MEASURED P) RE-# 838 (MEASURED P)

Y (IND)	N	CONST	PA	MEASURED P	UAVE	N	UAVE	P/P10	P/P10
0.00	0.0000	0.0000	0.0000	0.0000	0.0000	0.0000	0.0000	0.0000	0.0000
0.05	0.4514	0.5636	0.4514	0.5636	0.6299	0.6299	0.6299	0.6299	0.6299
0.10	0.8928	1.1272	0.8928	1.1272	0.6299	0.6299	0.6299	0.6299	0.6299
0.15	1.3342	1.6908	1.3342	1.6908	0.6299	0.6299	0.6299	0.6299	0.6299
0.20	1.7756	2.2544	1.7756	2.2544	0.6299	0.6299	0.6299	0.6299	0.6299
0.25	2.2170	2.8180	2.2170	2.8180	0.6299	0.6299	0.6299	0.6299	0.6299
0.30	2.6584	3.3816	2.6584	3.3816	0.6299	0.6299	0.6299	0.6299	0.6299
0.35	3.1000	3.9452	3.1000	3.9452	0.6299	0.6299	0.6299	0.6299	0.6299
0.40	3.5414	4.5088	3.5414	4.5088	0.6299	0.6299	0.6299	0.6299	0.6299
0.45	3.9828	5.0724	3.9828	5.0724	0.6299	0.6299	0.6299	0.6299	0.6299
0.50	4.4242	5.6360	4.4242	5.6360	0.6299	0.6299	0.6299	0.6299	0.6299
0.55	4.8656	6.2000	4.8656	6.2000	0.6299	0.6299	0.6299	0.6299	0.6299
0.60	5.3070	6.7636	5.3070	6.7636	0.6299	0.6299	0.6299	0.6299	0.6299
0.65	5.7484	7.3272	5.7484	7.3272	0.6299	0.6299	0.6299	0.6299	0.6299
0.70	6.1898	7.8908	6.1898	7.8908	0.6299	0.6299	0.6299	0.6299	0.6299
0.75	6.6312	8.4544	6.6312	8.4544	0.6299	0.6299	0.6299	0.6299	0.6299
0.80	7.0726	9.0180	7.0726	9.0180	0.6299	0.6299	0.6299	0.6299	0.6299
0.85	7.5140	9.5816	7.5140	9.5816	0.6299	0.6299	0.6299	0.6299	0.6299
0.90	7.9554	10.1452	7.9554	10.1452	0.6299	0.6299	0.6299	0.6299	0.6299
0.95	8.3968	10.7088	8.3968	10.7088	0.6299	0.6299	0.6299	0.6299	0.6299
1.00	8.8382	11.2724	8.8382	11.2724	0.6299	0.6299	0.6299	0.6299	0.6299
1.05	9.2796	11.8360	9.2796	11.8360	0.6299	0.6299	0.6299	0.6299	0.6299
1.10	9.7210	12.4000	9.7210	12.4000	0.6299	0.6299	0.6299	0.6299	0.6299
1.15	10.1624	12.9636	10.1624	12.9636	0.6299	0.6299	0.6299	0.6299	0.6299
1.20	10.6038	13.5272	10.6038	13.5272	0.6299	0.6299	0.6299	0.6299	0.6299
1.25	11.0452	14.0908	11.0452	14.0908	0.6299	0.6299	0.6299	0.6299	0.6299
1.30	11.4866	14.6544	11.4866	14.6544	0.6299	0.6299	0.6299	0.6299	0.6299
1.35	11.9280	15.2180	11.9280	15.2180	0.6299	0.6299	0.6299	0.6299	0.6299
1.40	12.3694	15.7816	12.3694	15.7816	0.6299	0.6299	0.6299	0.6299	0.6299
1.45	12.8108	16.3452	12.8108	16.3452	0.6299	0.6299	0.6299	0.6299	0.6299
1.50	13.2522	16.9088	13.2522	16.9088	0.6299	0.6299	0.6299	0.6299	0.6299
1.55	13.6936	17.4724	13.6936	17.4724	0.6299	0.6299	0.6299	0.6299	0.6299
1.60	14.1350	18.0360	14.1350	18.0360	0.6299	0.6299	0.6299	0.6299	0.6299
1.65	14.5764	18.6000	14.5764	18.6000	0.6299	0.6299	0.6299	0.6299	0.6299
1.70	15.0178	19.1636	15.0178	19.1636	0.6299	0.6299	0.6299	0.6299	0.6299
1.75	15.4592	19.7272	15.4592	19.7272	0.6299	0.6299	0.6299	0.6299	0.6299
1.80	15.9006	20.2908	15.9006	20.2908	0.6299	0.6299	0.6299	0.6299	0.6299
1.85	16.3420	20.8544	16.3420	20.8544	0.6299	0.6299	0.6299	0.6299	0.6299
1.90	16.7834	21.4180	16.7834	21.4180	0.6299	0.6299	0.6299	0.6299	0.6299
1.95	17.2248	21.9816	17.2248	21.9816	0.6299	0.6299	0.6299	0.6299	0.6299
2.00	17.6662	22.5452	17.6662	22.5452	0.6299	0.6299	0.6299	0.6299	0.6299
2.05	18.1076	23.1088	18.1076	23.1088	0.6299	0.6299	0.6299	0.6299	0.6299
2.10	18.5490	23.6724	18.5490	23.6724	0.6299	0.6299	0.6299	0.6299	0.6299
2.15	18.9904	24.2360	18.9904	24.2360	0.6299	0.6299	0.6299	0.6299	0.6299
2.20	19.4318	24.8000	19.4318	24.8000	0.6299	0.6299	0.6299	0.6299	0.6299
2.25	19.8732	25.3636	19.8732	25.3636	0.6299	0.6299	0.6299	0.6299	0.6299
2.30	20.3146	25.9272	20.3146	25.9272	0.6299	0.6299	0.6299	0.6299	0.6299
2.35	20.7560	26.4908	20.7560	26.4908	0.6299	0.6299	0.6299	0.6299	0.6299
2.40	21.1974	27.0544	21.1974	27.0544	0.6299	0.6299	0.6299	0.6299	0.6299
2.45	21.6388	27.6180	21.6388	27.6180	0.6299	0.6299	0.6299	0.6299	0.6299
2.50	22.0802	28.1816	22.0802	28.1816	0.6299	0.6299	0.6299	0.6299	0.6299
2.55	22.5216	28.7452	22.5216	28.7452	0.6299	0.6299	0.6299	0.6299	0.6299
2.60	22.9630	29.3088	22.9630	29.3088	0.6299	0.6299	0.6299	0.6299	0.6299
2.65	23.4044	29.8724	23.4044	29.8724	0.6299	0.6299	0.6299	0.6299	0.6299
2.70	23.8458	30.4360	23.8458	30.4360	0.6299	0.6299	0.6299	0.6299	0.6299
2.75	24.2872	31.0000	24.2872	31.0000	0.6299	0.6299	0.6299	0.6299	0.6299
2.80	24.7286	31.5636	24.7286	31.5636	0.6299	0.6299	0.6299	0.6299	0.6299
2.85	25.1700	32.1272	25.1700	32.1272	0.6299	0.6299	0.6299	0.6299	0.6299
2.90	25.6114	32.6908	25.6114	32.6908	0.6299	0.6299	0.6299	0.6299	0.6299
2.95	26.0528	33.2544	26.0528	33.2544	0.6299	0.6299	0.6299	0.6299	0.6299
3.00	26.4942	33.8180	26.4942	33.8180	0.6299	0.6299	0.6299	0.6299	0.6299
3.05	26.9356	34.3816	26.9356	34.3816	0.6299	0.6299	0.6299	0.6299	0.6299
3.10	27.3770	34.9452	27.3770	34.9452	0.6299	0.6299	0.6299	0.6299	0.6299
3.15	27.8184	35.5088	27.8184	35.5088	0.6299	0.6299	0.6299	0.6299	0.6299
3.20	28.2598	36.0724	28.2598	36.0724	0.6299	0.6299	0.6299	0.6299	0.6299
3.25	28.7012	36.6360	28.7012	36.6360	0.6299	0.6299	0.6299	0.6299	0.6299
3.30	29.1426	37.2000	29.1426	37.2000	0.6299	0.6299	0.6299	0.6299	0.6299
3.35	29.5840	37.7636	29.5840	37.7636	0.6299	0.6299	0.6299	0.6299	0.6299
3.40	30.0254	38.3272	30.0254	38.3272	0.6299	0.6299	0.6299	0.6299	0.6299
3.45	30.4668	38.8908	30.4668	38.8908	0.6299	0.6299	0.6299	0.6299	0.6299
3.50	30.9082	39.4544	30.9082	39.4544	0.6299	0.6299	0.6299	0.6299	0.6299
3.55	31.3496	40.0180	31.3496	40.0180	0.6299	0.6299	0.6299	0.6299	0.6299
3.60	31.7910	40.5816	31.7910	40.5816	0.6299	0.6299	0.6299	0.6299	0.6299
3.65	32.2324	41.1452	32.2324	41.1452	0.6299	0.6299	0.6299	0.6299	0.6299
3.70	32.6738	41.7088	32.6738	41.7088	0.6299	0.6299	0.6299	0.6299	0.6299
3.75	33.1152	42.2724	33.1152	42.2724	0.6299	0.6299	0.6299	0.6299	0.6299
3.80	33.5566	42.8360	33.5566	42.8360	0.6299	0.6299	0.6299	0.6299	0.6299
3.85	33.9980	43.4000	33.9980	43.4000	0.6299	0.6299	0.6299	0.6299	0.6299
3.90	34.4394	43.9636	34.4394	43.9636	0.6299	0.6299	0.6299	0.6299	0.6299
3.95	34.8808	44.5272	34.8808	44.5272	0.6299	0.6299	0.6299	0.6299	0.6299
4.00	35.3222	45.0908	35.3222	45.0908	0.6299	0.6299	0.6299	0.6299	0.6299
4.05	35.7636	45.6544	35.7636	45.6544	0.6299	0.6299	0.6299	0.6299	0.6299
4.10	36.2050	46.2180	36.2050	46.2180	0.6299	0.6299	0.6299	0.6299	0.6299
4.15	36.6464	46.7816	36.6464	46.7816	0.6299	0.6299	0.6299	0.6299	0.6299
4.20	37.0878	47.3452	37.0878	47.3452	0.6299	0.6299	0.6299	0.6299	0.6299
4.25	37.5292	47.9088	37.5292	47.9088	0.6299	0.6299	0.6299	0.6299	0.6299
4.30	37.9706	48.4724	37.9706	48.4724	0.6299	0.6299	0.6299	0.6299	0.6299
4.35	38.4120	49.0360	38.4120	49.0360	0.6299	0.6299	0.6299	0.6299	0.6299
4.40	38.8534	49.6000	38.8534	49.6000	0.6299	0.6299	0.6299	0.6299	0.6299
4.45	39.2948	50.1636	39.2948	50.1636	0.6299	0.6299	0.6299	0.6299	0.6299
4.50	39.7362	50.7272	39.7362	50.7272	0.6299	0.6299	0.6299	0.6299	0.6299
4.55	40.1776	51.2908	40.1776	51.2908	0.6299	0.6299	0.6299	0.6299	0.6299
4.60	40.6190	51.8544	40.6190	51.8544	0.6299	0.6299	0.6299	0.6299	0.6299
4.65	41.0604	52.4180	41.0604	52.4180	0.6299	0.6299	0.6299	0.6299	0.6299
4.70	41.5018	52.9816	41.5018	52.9816	0.6299	0.6299	0.6299	0.6299	0.6299
4.75	41.9432	53.5452	41.9432	53.5452	0.6299	0.6299	0.6299	0.6299	0.6299
4.80	42.3846	54.1088	42.3846	54.1088	0.6299	0.6299	0.6299	0.6299	0.6299
4.85	42.8260	54.6724	42.8260	54.6724	0.6299	0.6299	0.6299	0.6299	0.6299
4.90	43.2674	55.2360	43.2674	55.2360	0.6299	0.6299	0.6299	0.6299	0.6299
4.95	43.7088	55.8000	43.7088	55.8000	0.6299	0.6299	0.6299	0.6299	0.6299
5.00	44.1502	56.3636	44.1502	56.3636	0.6299	0.6299	0.6299	0.6299	0.6299
5.05	44.5916	56.9272	44.5916	56.9272	0.6299	0.6299	0.6299	0.6299	0.6299
5.10	45.0330	57.4908	45.0330	57.4908	0.6299	0.6299	0.6299	0.6299	0.6299
5.15	45.4744	58.0544	45.4744	58.0544	0.6299	0.6299	0.6299	0.6299	0.6299
5.2									







Table 2. (continued)

R (MONTH) = 1.4									
R = 1.0		R = 1.2		R = 1.4		R = 1.6		R = 1.8	
Y (MM)	U (MM)	Y (MM)	U (MM)	Y (MM)	U (MM)	Y (MM)	U (MM)	Y (MM)	U (MM)
0.0	0.000	0.0	0.000	0.0	0.000	0.0	0.000	0.0	0.000
0.1	0.232	0.1	0.232	0.1	0.232	0.1	0.232	0.1	0.232
0.2	0.464	0.2	0.464	0.2	0.464	0.2	0.464	0.2	0.464
0.3	0.696	0.3	0.696	0.3	0.696	0.3	0.696	0.3	0.696
0.4	0.928	0.4	0.928	0.4	0.928	0.4	0.928	0.4	0.928
0.5	1.160	0.5	1.160	0.5	1.160	0.5	1.160	0.5	1.160
0.6	1.392	0.6	1.392	0.6	1.392	0.6	1.392	0.6	1.392
0.7	1.624	0.7	1.624	0.7	1.624	0.7	1.624	0.7	1.624
0.8	1.856	0.8	1.856	0.8	1.856	0.8	1.856	0.8	1.856
0.9	2.088	0.9	2.088	0.9	2.088	0.9	2.088	0.9	2.088
1.0	2.320	1.0	2.320	1.0	2.320	1.0	2.320	1.0	2.320
1.1	2.552	1.1	2.552	1.1	2.552	1.1	2.552	1.1	2.552
1.2	2.784	1.2	2.784	1.2	2.784	1.2	2.784	1.2	2.784
1.3	3.016	1.3	3.016	1.3	3.016	1.3	3.016	1.3	3.016
1.4	3.248	1.4	3.248	1.4	3.248	1.4	3.248	1.4	3.248
1.5	3.480	1.5	3.480	1.5	3.480	1.5	3.480	1.5	3.480
1.6	3.712	1.6	3.712	1.6	3.712	1.6	3.712	1.6	3.712
1.7	3.944	1.7	3.944	1.7	3.944	1.7	3.944	1.7	3.944
1.8	4.176	1.8	4.176	1.8	4.176	1.8	4.176	1.8	4.176
1.9	4.408	1.9	4.408	1.9	4.408	1.9	4.408	1.9	4.408
2.0	4.640	2.0	4.640	2.0	4.640	2.0	4.640	2.0	4.640
2.1	4.872	2.1	4.872	2.1	4.872	2.1	4.872	2.1	4.872
2.2	5.104	2.2	5.104	2.2	5.104	2.2	5.104	2.2	5.104
2.3	5.336	2.3	5.336	2.3	5.336	2.3	5.336	2.3	5.336
2.4	5.568	2.4	5.568	2.4	5.568	2.4	5.568	2.4	5.568
2.5	5.800	2.5	5.800	2.5	5.800	2.5	5.800	2.5	5.800
2.6	6.032	2.6	6.032	2.6	6.032	2.6	6.032	2.6	6.032
2.7	6.264	2.7	6.264	2.7	6.264	2.7	6.264	2.7	6.264
2.8	6.496	2.8	6.496	2.8	6.496	2.8	6.496	2.8	6.496
2.9	6.728	2.9	6.728	2.9	6.728	2.9	6.728	2.9	6.728
3.0	6.960	3.0	6.960	3.0	6.960	3.0	6.960	3.0	6.960
3.1	7.192	3.1	7.192	3.1	7.192	3.1	7.192	3.1	7.192
3.2	7.424	3.2	7.424	3.2	7.424	3.2	7.424	3.2	7.424
3.3	7.656	3.3	7.656	3.3	7.656	3.3	7.656	3.3	7.656
3.4	7.888	3.4	7.888	3.4	7.888	3.4	7.888	3.4	7.888
3.5	8.120	3.5	8.120	3.5	8.120	3.5	8.120	3.5	8.120
3.6	8.352	3.6	8.352	3.6	8.352	3.6	8.352	3.6	8.352
3.7	8.584	3.7	8.584	3.7	8.584	3.7	8.584	3.7	8.584
3.8	8.816	3.8	8.816	3.8	8.816	3.8	8.816	3.8	8.816
3.9	9.048	3.9	9.048	3.9	9.048	3.9	9.048	3.9	9.048
4.0	9.280	4.0	9.280	4.0	9.280	4.0	9.280	4.0	9.280
4.1	9.512	4.1	9.512	4.1	9.512	4.1	9.512	4.1	9.512
4.2	9.744	4.2	9.744	4.2	9.744	4.2	9.744	4.2	9.744
4.3	9.976	4.3	9.976	4.3	9.976	4.3	9.976	4.3	9.976
4.4	10.208	4.4	10.208	4.4	10.208	4.4	10.208	4.4	10.208
4.5	10.440	4.5	10.440	4.5	10.440	4.5	10.440	4.5	10.440
4.6	10.672	4.6	10.672	4.6	10.672	4.6	10.672	4.6	10.672
4.7	10.904	4.7	10.904	4.7	10.904	4.7	10.904	4.7	10.904
4.8	11.136	4.8	11.136	4.8	11.136	4.8	11.136	4.8	11.136
4.9	11.368	4.9	11.368	4.9	11.368	4.9	11.368	4.9	11.368
5.0	11.600	5.0	11.600	5.0	11.600	5.0	11.600	5.0	11.600
5.1	11.832	5.1	11.832	5.1	11.832	5.1	11.832	5.1	11.832
5.2	12.064	5.2	12.064	5.2	12.064	5.2	12.064	5.2	12.064
5.3	12.296	5.3	12.296	5.3	12.296	5.3	12.296	5.3	12.296
5.4	12.528	5.4	12.528	5.4	12.528	5.4	12.528	5.4	12.528
5.5	12.760	5.5	12.760	5.5	12.760	5.5	12.760	5.5	12.760
5.6	12.992	5.6	12.992	5.6	12.992	5.6	12.992	5.6	12.992
5.7	13.224	5.7	13.224	5.7	13.224	5.7	13.224	5.7	13.224
5.8	13.456	5.8	13.456	5.8	13.456	5.8	13.456	5.8	13.456
5.9	13.688	5.9	13.688	5.9	13.688	5.9	13.688	5.9	13.688
6.0	13.920	6.0	13.920	6.0	13.920	6.0	13.920	6.0	13.920
6.1	14.152	6.1	14.152	6.1	14.152	6.1	14.152	6.1	14.152
6.2	14.384	6.2	14.384	6.2	14.384	6.2	14.384	6.2	14.384
6.3	14.616	6.3	14.616	6.3	14.616	6.3	14.616	6.3	14.616
6.4	14.848	6.4	14.848	6.4	14.848	6.4	14.848	6.4	14.848
6.5	15.080	6.5	15.080	6.5	15.080	6.5	15.080	6.5	15.080
6.6	15.312	6.6	15.312	6.6	15.312	6.6	15.312	6.6	15.312
6.7	15.544	6.7	15.544	6.7	15.544	6.7	15.544	6.7	15.544
6.8	15.776	6.8	15.776	6.8	15.776	6.8	15.776	6.8	15.776
6.9	16.008	6.9	16.008	6.9	16.008	6.9	16.008	6.9	16.008
7.0	16.240	7.0	16.240	7.0	16.240	7.0	16.240	7.0	16.240
7.1	16.472	7.1	16.472	7.1	16.472	7.1	16.472	7.1	16.472
7.2	16.704	7.2	16.704	7.2	16.704	7.2	16.704	7.2	16.704
7.3	16.936	7.3	16.936	7.3	16.936	7.3	16.936	7.3	16.936
7.4	17.168	7.4	17.168	7.4	17.168	7.4	17.168	7.4	17.168
7.5	17.400	7.5	17.400	7.5	17.400	7.5	17.400	7.5	17.400
7.6	17.632	7.6	17.632	7.6	17.632	7.6	17.632	7.6	17.632
7.7	17.864	7.7	17.864	7.7	17.864	7.7	17.864	7.7	17.864
7.8	18.096	7.8	18.096	7.8	18.096	7.8	18.096	7.8	18.096
7.9	18.328	7.9	18.328	7.9	18.328	7.9	18.328	7.9	18.328
8.0	18.560	8.0	18.560	8.0	18.560	8.0	18.560	8.0	18.560
8.1	18.792	8.1	18.792	8.1	18.792	8.1	18.792	8.1	18.792
8.2	19.024	8.2	19.024	8.2	19.024	8.2	19.024	8.2	19.024
8.3	19.256	8.3	19.256	8.3	19.256	8.3	19.256	8.3	19.256
8.4	19.488	8.4	19.488	8.4	19.488	8.4	19.488	8.4	19.488
8.5	19.720	8.5	19.720	8.5	19.720	8.5	19.720	8.5	19.720
8.6	19.952	8.6	19.952	8.6	19.952	8.6	19.952	8.6	19.952
8.7	20.184	8.7	20.184	8.7	20.184	8.7	20.184	8.7	20.184
8.8	20.416	8.8	20.416	8.8	20.416	8.8	20.416	8.8	20.416
8.9	20.648	8.9	20.648	8.9	20.648	8.9	20.648	8.9	20.648
9.0	20.880	9.0	20.880	9.0	20.880	9.0	20.880	9.0	20.880
9.1	21.112	9.1	21.112	9.1	21.112	9.1	21.112	9.1	21.112
9.2	21.344	9.2	21.344	9.2	21.344	9.2	21.344	9.2	21.344
9.3	21.576	9.3	21.576	9.3	21.576	9.3	21.576	9.3	21.576
9.4	21.808	9.4	21.808	9.4	21.808	9.4	21.808	9.4	21.808
9.5	22.040	9.5	22.040	9.5	22.040	9.5	22.040	9.5	22.040
9.6	22.272	9.6	22.272	9.6	22.272	9.6	22.272	9.6	22.272
9.7	22.504	9.7	22.504	9.7	22.504	9.7	22.504	9.7	22.504
9.8	22.736	9.8	22.736	9.8	22.736	9.8	22.736	9.8	22.736
9.9	22.968	9.9	22.968	9.9	22.968	9.9	22.968	9.9	22.968
10.0	23.200	10.0	23.200	10.0	23.200	10.0	23.200	10.0	23.200

N (NUMBER) = 14  
 AT 250 MM DEL 395-41.1 (MEASURED P) DEL 395-42.0 MM  
 REFR 3.04176 (MEASURED P) REFR 3.040 (MEASURED P)

Y (MM)	CONST P1		MEASURED P		CONST P2		MEASURED P	
	N	UVE	N	UVE	N	UVE	N	UVE
0.00	0.0000	0.0000	0.0000	0.0000	0.0000	0.0000	0.0000	0.0000
0.05	0.295	0.213	0.295	0.213	0.295	0.213	0.295	0.213
0.10	0.580	0.426	0.580	0.426	0.580	0.426	0.580	0.426
0.15	0.865	0.639	0.865	0.639	0.865	0.639	0.865	0.639
0.20	1.150	0.852	1.150	0.852	1.150	0.852	1.150	0.852
0.25	1.435	1.065	1.435	1.065	1.435	1.065	1.435	1.065
0.30	1.720	1.278	1.720	1.278	1.720	1.278	1.720	1.278
0.35	2.005	1.491	2.005	1.491	2.005	1.491	2.005	1.491
0.40	2.290	1.704	2.290	1.704	2.290	1.704	2.290	1.704
0.45	2.575	1.917	2.575	1.917	2.575	1.917	2.575	1.917
0.50	2.860	2.130	2.860	2.130	2.860	2.130	2.860	2.130
0.55	3.145	2.343	3.145	2.343	3.145	2.343	3.145	2.343
0.60	3.430	2.556	3.430	2.556	3.430	2.556	3.430	2.556
0.65	3.715	2.769	3.715	2.769	3.715	2.769	3.715	2.769
0.70	4.000	2.982	4.000	2.982	4.000	2.982	4.000	2.982
0.75	4.285	3.195	4.285	3.195	4.285	3.195	4.285	3.195
0.80	4.570	3.408	4.570	3.408	4.570	3.408	4.570	3.408
0.85	4.855	3.621	4.855	3.621	4.855	3.621	4.855	3.621
0.90	5.140	3.834	5.140	3.834	5.140	3.834	5.140	3.834
0.95	5.425	4.047	5.425	4.047	5.425	4.047	5.425	4.047
1.00	5.710	4.260	5.710	4.260	5.710	4.260	5.710	4.260
1.05	5.995	4.473	5.995	4.473	5.995	4.473	5.995	4.473
1.10	6.280	4.686	6.280	4.686	6.280	4.686	6.280	4.686
1.15	6.565	4.899	6.565	4.899	6.565	4.899	6.565	4.899
1.20	6.850	5.112	6.850	5.112	6.850	5.112	6.850	5.112
1.25	7.135	5.325	7.135	5.325	7.135	5.325	7.135	5.325
1.30	7.420	5.538	7.420	5.538	7.420	5.538	7.420	5.538
1.35	7.705	5.751	7.705	5.751	7.705	5.751	7.705	5.751
1.40	7.990	5.964	7.990	5.964	7.990	5.964	7.990	5.964
1.45	8.275	6.177	8.275	6.177	8.275	6.177	8.275	6.177
1.50	8.560	6.390	8.560	6.390	8.560	6.390	8.560	6.390
1.55	8.845	6.603	8.845	6.603	8.845	6.603	8.845	6.603
1.60	9.130	6.816	9.130	6.816	9.130	6.816	9.130	6.816
1.65	9.415	7.029	9.415	7.029	9.415	7.029	9.415	7.029
1.70	9.700	7.242	9.700	7.242	9.700	7.242	9.700	7.242
1.75	9.985	7.455	9.985	7.455	9.985	7.455	9.985	7.455
1.80	10.270	7.668	10.270	7.668	10.270	7.668	10.270	7.668
1.85	10.555	7.881	10.555	7.881	10.555	7.881	10.555	7.881
1.90	10.840	8.094	10.840	8.094	10.840	8.094	10.840	8.094
1.95	11.125	8.307	11.125	8.307	11.125	8.307	11.125	8.307
2.00	11.410	8.520	11.410	8.520	11.410	8.520	11.410	8.520
2.05	11.695	8.733	11.695	8.733	11.695	8.733	11.695	8.733
2.10	11.980	8.946	11.980	8.946	11.980	8.946	11.980	8.946
2.15	12.265	9.159	12.265	9.159	12.265	9.159	12.265	9.159
2.20	12.550	9.372	12.550	9.372	12.550	9.372	12.550	9.372
2.25	12.835	9.585	12.835	9.585	12.835	9.585	12.835	9.585
2.30	13.120	9.798	13.120	9.798	13.120	9.798	13.120	9.798
2.35	13.405	10.011	13.405	10.011	13.405	10.011	13.405	10.011
2.40	13.690	10.224	13.690	10.224	13.690	10.224	13.690	10.224
2.45	13.975	10.437	13.975	10.437	13.975	10.437	13.975	10.437
2.50	14.260	10.650	14.260	10.650	14.260	10.650	14.260	10.650
2.55	14.545	10.863	14.545	10.863	14.545	10.863	14.545	10.863
2.60	14.830	11.076	14.830	11.076	14.830	11.076	14.830	11.076
2.65	15.115	11.289	15.115	11.289	15.115	11.289	15.115	11.289
2.70	15.400	11.502	15.400	11.502	15.400	11.502	15.400	11.502
2.75	15.685	11.715	15.685	11.715	15.685	11.715	15.685	11.715
2.80	15.970	11.928	15.970	11.928	15.970	11.928	15.970	11.928
2.85	16.255	12.141	16.255	12.141	16.255	12.141	16.255	12.141
2.90	16.540	12.354	16.540	12.354	16.540	12.354	16.540	12.354
2.95	16.825	12.567	16.825	12.567	16.825	12.567	16.825	12.567
3.00	17.110	12.780	17.110	12.780	17.110	12.780	17.110	12.780
3.05	17.395	12.993	17.395	12.993	17.395	12.993	17.395	12.993
3.10	17.680	13.206	17.680	13.206	17.680	13.206	17.680	13.206
3.15	17.965	13.419	17.965	13.419	17.965	13.419	17.965	13.419
3.20	18.250	13.632	18.250	13.632	18.250	13.632	18.250	13.632
3.25	18.535	13.845	18.535	13.845	18.535	13.845	18.535	13.845
3.30	18.820	14.058	18.820	14.058	18.820	14.058	18.820	14.058
3.35	19.105	14.271	19.105	14.271	19.105	14.271	19.105	14.271
3.40	19.390	14.484	19.390	14.484	19.390	14.484	19.390	14.484
3.45	19.675	14.697	19.675	14.697	19.675	14.697	19.675	14.697
3.50	19.960	14.910	19.960	14.910	19.960	14.910	19.960	14.910
3.55	20.245	15.123	20.245	15.123	20.245	15.123	20.245	15.123
3.60	20.530	15.336	20.530	15.336	20.530	15.336	20.530	15.336
3.65	20.815	15.549	20.815	15.549	20.815	15.549	20.815	15.549
3.70	21.100	15.762	21.100	15.762	21.100	15.762	21.100	15.762
3.75	21.385	15.975	21.385	15.975	21.385	15.975	21.385	15.975
3.80	21.670	16.188	21.670	16.188	21.670	16.188	21.670	16.188
3.85	21.955	16.401	21.955	16.401	21.955	16.401	21.955	16.401
3.90	22.240	16.614	22.240	16.614	22.240	16.614	22.240	16.614
3.95	22.525	16.827	22.525	16.827	22.525	16.827	22.525	16.827
4.00	22.810	17.040	22.810	17.040	22.810	17.040	22.810	17.040
4.05	23.095	17.253	23.095	17.253	23.095	17.253	23.095	17.253
4.10	23.380	17.466	23.380	17.466	23.380	17.466	23.380	17.466
4.15	23.665	17.679	23.665	17.679	23.665	17.679	23.665	17.679
4.20	23.950	17.892	23.950	17.892	23.950	17.892	23.950	17.892
4.25	24.235	18.105	24.235	18.105	24.235	18.105	24.235	18.105
4.30	24.520	18.318	24.520	18.318	24.520	18.318	24.520	18.318
4.35	24.805	18.531	24.805	18.531	24.805	18.531	24.805	18.531
4.40	25.090	18.744	25.090	18.744	25.090	18.744	25.090	18.744
4.45	25.375	18.957	25.375	18.957	25.375	18.957	25.375	18.957
4.50	25.660	19.170	25.660	19.170	25.660	19.170	25.660	19.170
4.55	25.945	19.383	25.945	19.383	25.945	19.383	25.945	19.383
4.60	26.230	19.596	26.230	19.596	26.230	19.596	26.230	19.596
4.65	26.515	19.809	26.515	19.809	26.515	19.809	26.515	19.809
4.70	26.800	20.022	26.800	20.022	26.800	20.022	26.800	20.022
4.75	27.085	20.235	27.085	20.235	27.085	20.235	27.085	20.235
4.80	27.370	20.448	27.370	20.448	27.370	20.448	27.370	20.448
4.85	27.655	20.661	27.655	20.661	27.655	20.661	27.655	20.661
4.90	27.940	20.874	27.940	20.874	27.940	20.874	27.940	20.874
4.95	28.225	21.087	28.225	21.087	28.225	21.087	28.225	21.087
5.00	28.510	21.300	28.510	21.300	28.510	21.300	28.510	21.300
5.05	28.795	21.513	28.795	21.513	28.795	21.513	28.795	21.513
5.10	29.080	21.726	29.080	21.726	29.080	21.726	29.080	21.726
5.15	29.365	21.939	29.365	21.939	29.365	21.939	29.365	21.939
5.20	29.650	22.152	29.650	22.152	29.650	22.152	29.650	22.152
5.25	29.935	22.365	29.935	22.365	29.935	22.365	29.935	22.365
5.30	30.220	22.578	30.220	22.578	30.220	22.578	30.220	22.578
5.35	30.505	22.791	30.505	22.791	30.505	22.791	30.505	22.791
5.40	30.790	23.004	30.790	23.004	30.790	23.004	30.790	23.004
5.45	31.075	23.217	31.075	23.217	31.075	23.217	31.075	23.217
5.50	31.360	23.430	31.360	23.430	31.360	23.430	31.360	23.430
5.55	31.645	23.643	31.645	23.643	31.645	23.643	31.645	23.643
5.60	31.930	23.856	31.930	23.856	31.930	23.856	31.930	23.856
5.65	32.215	24.069	32.215	24.069	32.215	24.069	32.215	24.069
5.70	32.500	24.282	32.500	24.282	32.500	24.282	32.500	24.282
5.75	32.785	24.495	32.785	24.495	32.785	24.495	32.785	24.495
5.80	33.070	24.708	33.070	24.708	33.070	24.708	33.070	24.708
5.85	33.355	24.921	33.355	24.921	33.355	24.921	33.355	24.921
5.90	33.640	25.134	33.640	25.134	33.640	25.134	33.640	25.134
5.95	33.925	25.347	33.925	25.347	33.925	25.347	33.925	25.347
6.00	34.210	25.560	34.210	25.560	34.210	25.560	34.210	25.560
6.05	34.495	25.773	34.495	25.773	34.495			













N. NUMBER = 14

X=24.000 DEL. 995= 46.000  
 DEL. 995= 25.000 MEASURED P. ME. 1.121 (REQUIRED P.)

Y. (NO)	CONST. P.	U. (E)	MEASURED P.	U. (E)	P. (P.1)	P. (P.10)
0.0	0.0000	0.0000	0.0000	0.0000	0.0000	0.0000
0.5	0.2162	0.2162	0.2162	0.2162	0.2162	0.2162
1.0	0.2337	0.2337	0.2337	0.2337	0.2337	0.2337
1.5	0.2507	0.2507	0.2507	0.2507	0.2507	0.2507
2.0	0.2671	0.2671	0.2671	0.2671	0.2671	0.2671
2.5	0.2830	0.2830	0.2830	0.2830	0.2830	0.2830
3.0	0.2984	0.2984	0.2984	0.2984	0.2984	0.2984
3.5	0.3133	0.3133	0.3133	0.3133	0.3133	0.3133
4.0	0.3277	0.3277	0.3277	0.3277	0.3277	0.3277
4.5	0.3416	0.3416	0.3416	0.3416	0.3416	0.3416
5.0	0.3550	0.3550	0.3550	0.3550	0.3550	0.3550
5.5	0.3679	0.3679	0.3679	0.3679	0.3679	0.3679
6.0	0.3803	0.3803	0.3803	0.3803	0.3803	0.3803
6.5	0.3922	0.3922	0.3922	0.3922	0.3922	0.3922
7.0	0.4036	0.4036	0.4036	0.4036	0.4036	0.4036
7.5	0.4145	0.4145	0.4145	0.4145	0.4145	0.4145
8.0	0.4249	0.4249	0.4249	0.4249	0.4249	0.4249
8.5	0.4348	0.4348	0.4348	0.4348	0.4348	0.4348
9.0	0.4442	0.4442	0.4442	0.4442	0.4442	0.4442
9.5	0.4531	0.4531	0.4531	0.4531	0.4531	0.4531
10.0	0.4615	0.4615	0.4615	0.4615	0.4615	0.4615
10.5	0.4694	0.4694	0.4694	0.4694	0.4694	0.4694
11.0	0.4768	0.4768	0.4768	0.4768	0.4768	0.4768
11.5	0.4837	0.4837	0.4837	0.4837	0.4837	0.4837
12.0	0.4901	0.4901	0.4901	0.4901	0.4901	0.4901
12.5	0.4960	0.4960	0.4960	0.4960	0.4960	0.4960
13.0	0.5014	0.5014	0.5014	0.5014	0.5014	0.5014
13.5	0.5073	0.5073	0.5073	0.5073	0.5073	0.5073
14.0	0.5127	0.5127	0.5127	0.5127	0.5127	0.5127
14.5	0.5176	0.5176	0.5176	0.5176	0.5176	0.5176
15.0	0.5220	0.5220	0.5220	0.5220	0.5220	0.5220
15.5	0.5269	0.5269	0.5269	0.5269	0.5269	0.5269
16.0	0.5313	0.5313	0.5313	0.5313	0.5313	0.5313
16.5	0.5362	0.5362	0.5362	0.5362	0.5362	0.5362
17.0	0.5406	0.5406	0.5406	0.5406	0.5406	0.5406
17.5	0.5455	0.5455	0.5455	0.5455	0.5455	0.5455
18.0	0.5509	0.5509	0.5509	0.5509	0.5509	0.5509
18.5	0.5558	0.5558	0.5558	0.5558	0.5558	0.5558
19.0	0.5602	0.5602	0.5602	0.5602	0.5602	0.5602
19.5	0.5651	0.5651	0.5651	0.5651	0.5651	0.5651
20.0	0.5695	0.5695	0.5695	0.5695	0.5695	0.5695
20.5	0.5744	0.5744	0.5744	0.5744	0.5744	0.5744
21.0	0.5788	0.5788	0.5788	0.5788	0.5788	0.5788
21.5	0.5837	0.5837	0.5837	0.5837	0.5837	0.5837
22.0	0.5881	0.5881	0.5881	0.5881	0.5881	0.5881
22.5	0.5920	0.5920	0.5920	0.5920	0.5920	0.5920
23.0	0.5964	0.5964	0.5964	0.5964	0.5964	0.5964
23.5	0.6003	0.6003	0.6003	0.6003	0.6003	0.6003
24.0	0.6047	0.6047	0.6047	0.6047	0.6047	0.6047
24.5	0.6086	0.6086	0.6086	0.6086	0.6086	0.6086
25.0	0.6120	0.6120	0.6120	0.6120	0.6120	0.6120
25.5	0.6159	0.6159	0.6159	0.6159	0.6159	0.6159
26.0	0.6193	0.6193	0.6193	0.6193	0.6193	0.6193
26.5	0.6232	0.6232	0.6232	0.6232	0.6232	0.6232
27.0	0.6271	0.6271	0.6271	0.6271	0.6271	0.6271
27.5	0.6305	0.6305	0.6305	0.6305	0.6305	0.6305
28.0	0.6344	0.6344	0.6344	0.6344	0.6344	0.6344
28.5	0.6383	0.6383	0.6383	0.6383	0.6383	0.6383
29.0	0.6422	0.6422	0.6422	0.6422	0.6422	0.6422
29.5	0.6461	0.6461	0.6461	0.6461	0.6461	0.6461
30.0	0.6495	0.6495	0.6495	0.6495	0.6495	0.6495
30.5	0.6534	0.6534	0.6534	0.6534	0.6534	0.6534
31.0	0.6573	0.6573	0.6573	0.6573	0.6573	0.6573
31.5	0.6612	0.6612	0.6612	0.6612	0.6612	0.6612
32.0	0.6651	0.6651	0.6651	0.6651	0.6651	0.6651
32.5	0.6690	0.6690	0.6690	0.6690	0.6690	0.6690
33.0	0.6729	0.6729	0.6729	0.6729	0.6729	0.6729
33.5	0.6768	0.6768	0.6768	0.6768	0.6768	0.6768
34.0	0.6807	0.6807	0.6807	0.6807	0.6807	0.6807
34.5	0.6846	0.6846	0.6846	0.6846	0.6846	0.6846
35.0	0.6885	0.6885	0.6885	0.6885	0.6885	0.6885
35.5	0.6924	0.6924	0.6924	0.6924	0.6924	0.6924
36.0	0.6963	0.6963	0.6963	0.6963	0.6963	0.6963
36.5	0.7002	0.7002	0.7002	0.7002	0.7002	0.7002
37.0	0.7041	0.7041	0.7041	0.7041	0.7041	0.7041
37.5	0.7080	0.7080	0.7080	0.7080	0.7080	0.7080
38.0	0.7119	0.7119	0.7119	0.7119	0.7119	0.7119
38.5	0.7158	0.7158	0.7158	0.7158	0.7158	0.7158
39.0	0.7197	0.7197	0.7197	0.7197	0.7197	0.7197
39.5	0.7236	0.7236	0.7236	0.7236	0.7236	0.7236
40.0	0.7275	0.7275	0.7275	0.7275	0.7275	0.7275
40.5	0.7314	0.7314	0.7314	0.7314	0.7314	0.7314
41.0	0.7353	0.7353	0.7353	0.7353	0.7353	0.7353
41.5	0.7392	0.7392	0.7392	0.7392	0.7392	0.7392
42.0	0.7431	0.7431	0.7431	0.7431	0.7431	0.7431
42.5	0.7470	0.7470	0.7470	0.7470	0.7470	0.7470
43.0	0.7509	0.7509	0.7509	0.7509	0.7509	0.7509
43.5	0.7548	0.7548	0.7548	0.7548	0.7548	0.7548
44.0	0.7587	0.7587	0.7587	0.7587	0.7587	0.7587
44.5	0.7626	0.7626	0.7626	0.7626	0.7626	0.7626
45.0	0.7665	0.7665	0.7665	0.7665	0.7665	0.7665
45.5	0.7704	0.7704	0.7704	0.7704	0.7704	0.7704
46.0	0.7743	0.7743	0.7743	0.7743	0.7743	0.7743
46.5	0.7782	0.7782	0.7782	0.7782	0.7782	0.7782
47.0	0.7821	0.7821	0.7821	0.7821	0.7821	0.7821
47.5	0.7860	0.7860	0.7860	0.7860	0.7860	0.7860
48.0	0.7899	0.7899	0.7899	0.7899	0.7899	0.7899
48.5	0.7938	0.7938	0.7938	0.7938	0.7938	0.7938
49.0	0.7977	0.7977	0.7977	0.7977	0.7977	0.7977
49.5	0.8016	0.8016	0.8016	0.8016	0.8016	0.8016
50.0	0.8055	0.8055	0.8055	0.8055	0.8055	0.8055

N. NUMBER = 14

X=40.000 DEL. 995= 44.200  
 DEL. 995= 24.000 MEASURED P. ME. 1.211 (REQUIRED P.)

Y. (NO)	CONST. P.	U. (E)	MEASURED P.	U. (E)	P. (P.1)	P. (P.10)
0.0	0.0000	0.0000	0.0000	0.0000	0.0000	0.0000
0.5	0.3481	0.3481	0.3481	0.3481	0.3481	0.3481
1.0	0.3591	0.3591	0.3591	0.3591	0.3591	0.3591
1.5	0.3705	0.3705	0.3705	0.3705	0.3705	0.3705
2.0	0.3823	0.3823	0.3823	0.3823	0.3823	0.3823
2.5	0.3945	0.3945	0.3945	0.3945	0.3945	0.3945
3.0	0.4071	0.4071	0.4071	0.4071	0.4071	0.4071
3.5	0.4201	0.4201	0.4201	0.4201	0.4201	0.4201
4.0	0.4335	0.4335	0.4335	0.4335	0.4335	0.4335
4.5	0.4473	0.4473	0.4473	0.4473	0.4473	0.4473
5.0	0.4615	0.4615	0.4615	0.4615	0.4615	0.4615
5.5	0.4761	0.4761	0.4761	0.4761	0.4761	0.4761
6.0	0.4911	0.4911	0.4911	0.4911	0.4911	0.4911
6.5	0.5065	0.5065	0.5065	0.5065	0.5065	0.5065
7.0	0.5223	0.5223	0.5223	0.5223	0.5223	0.5223
7.5	0.5385	0.5385	0.5385	0.5385	0.5385	0.5385
8.0	0.5551	0.5551	0.5551	0.5551	0.5551	0.5551
8.5	0.5721	0.5721	0.5721	0.5721	0.5721	0.5721
9.0	0.5895	0.5895	0.5895	0.5895	0.5895	0.5895
9.5	0.6073	0.6073	0.6073	0.6073	0.6073	0.6073
10.0	0.6255	0.6255	0.6255	0.6255	0.6255	0.6255
10.5	0.6441	0.6441	0.6441	0.6441	0.6441	0.6441
11.0	0.6631	0.6631	0.6631	0.6631	0.6631	0.6631
11.5	0.6825	0.6825	0.6825	0.6825	0.6825	0.6825
12.0	0.7023	0.7023	0.7023	0.7023	0.7023	0.7023
12.5	0.7225	0.7225	0.7225	0.7225	0.7225	0.7225
13.0	0.7431	0.7431	0.7431	0.7431	0.7431	0.7431
13.5	0.7641	0.7641	0.7641	0.7641	0.7641	0.7641
14.0	0.7855	0.7855	0.7855	0.7855	0.7855	0.7855
14.5	0.8073	0.8073	0.8073	0.8073	0.8073	0.8073
15.0	0.8295	0.8295	0.8295	0.8295	0.8295	0.8295
15.5	0.8521	0.8521	0.8521	0.8521	0.8521	0.8521
16.0	0.8751	0.8751	0.8751	0.8751	0.8751	0.8751
16.5	0.8985	0.8985	0.8985	0.8985	0.8985	0.8985
17.0	0.9223	0.9223	0.9223	0.9223	0.9223	0.9223
17.5	0.9465	0.9465	0.9465	0.9465	0.9465	0.9465
18.0	0.9711	0.9711	0.9711	0.9711	0.9711	0.9711
18.5	0.9961	0.9961	0.9961	0.9961	0.9961	0.9961
19.0	1.0215	1.0215	1.0215	1.0215	1.0215	1.0215
19.5	1.0473	1.0473	1.0473	1.0473	1.0473	1.0473
20.0	1.0735	1.0735	1.0735	1.0735	1.0735	1.0735
20.5	1.1001	1.1001	1.1001	1.1001	1.1001	1.1001
21.0	1.1271	1.1271	1.1271	1.1271	1.1271	1.1271
21.5	1.1545	1.1545	1.1545	1.1545	1.1545	1.1545
22.0	1.1823	1.1823	1.1823	1.1823	1.1823	1.1823
22.5	1.2105	1.2105	1.2105	1.2105	1.2105	1.2105
23.0	1.2391	1.2391	1.2391	1.2391	1.2391	1.2391
23.5	1.2681	1.2681	1.2681	1.2681	1.2681	1.2681
24.0	1.2975	1.2975	1.2975	1.2975	1.	



W. HADJIRI - 1.4

W. 137 W. DEL 995.43.000  
 DEL 995.43.000 (MEASURED P.)  
 DEL 995.43.000 (MEASURED P.)

Y	U	CONST	PH	MEASURED P	U	UVE	P	PI	PI
0.0	0.0	0.000	0.000	0.000	0.000	0.000	0.000	0.000	0.000
0.5	0.5	0.159	0.176	0.159	0.176	0.159	0.176	0.159	0.176
1.0	1.0	0.318	0.352	0.318	0.352	0.318	0.352	0.318	0.352
1.5	1.5	0.477	0.521	0.477	0.521	0.477	0.521	0.477	0.521
2.0	2.0	0.636	0.690	0.636	0.690	0.636	0.690	0.636	0.690
2.5	2.5	0.795	0.879	0.795	0.879	0.795	0.879	0.795	0.879
3.0	3.0	0.954	1.068	0.954	1.068	0.954	1.068	0.954	1.068
3.5	3.5	1.113	1.257	1.113	1.257	1.113	1.257	1.113	1.257
4.0	4.0	1.272	1.446	1.272	1.446	1.272	1.446	1.272	1.446
4.5	4.5	1.431	1.635	1.431	1.635	1.431	1.635	1.431	1.635
5.0	5.0	1.590	1.824	1.590	1.824	1.590	1.824	1.590	1.824
5.5	5.5	1.749	2.013	1.749	2.013	1.749	2.013	1.749	2.013
6.0	6.0	1.908	2.202	1.908	2.202	1.908	2.202	1.908	2.202
6.5	6.5	2.067	2.391	2.067	2.391	2.067	2.391	2.067	2.391
7.0	7.0	2.226	2.580	2.226	2.580	2.226	2.580	2.226	2.580
7.5	7.5	2.385	2.769	2.385	2.769	2.385	2.769	2.385	2.769
8.0	8.0	2.544	2.958	2.544	2.958	2.544	2.958	2.544	2.958
8.5	8.5	2.703	3.147	2.703	3.147	2.703	3.147	2.703	3.147
9.0	9.0	2.862	3.336	2.862	3.336	2.862	3.336	2.862	3.336
9.5	9.5	3.021	3.525	3.021	3.525	3.021	3.525	3.021	3.525
10.0	10.0	3.180	3.714	3.180	3.714	3.180	3.714	3.180	3.714
10.5	10.5	3.339	3.903	3.339	3.903	3.339	3.903	3.339	3.903
11.0	11.0	3.498	4.092	3.498	4.092	3.498	4.092	3.498	4.092
11.5	11.5	3.657	4.281	3.657	4.281	3.657	4.281	3.657	4.281
12.0	12.0	3.816	4.470	3.816	4.470	3.816	4.470	3.816	4.470
12.5	12.5	3.975	4.659	3.975	4.659	3.975	4.659	3.975	4.659
13.0	13.0	4.134	4.848	4.134	4.848	4.134	4.848	4.134	4.848
13.5	13.5	4.293	5.037	4.293	5.037	4.293	5.037	4.293	5.037
14.0	14.0	4.452	5.226	4.452	5.226	4.452	5.226	4.452	5.226
14.5	14.5	4.611	5.415	4.611	5.415	4.611	5.415	4.611	5.415
15.0	15.0	4.770	5.604	4.770	5.604	4.770	5.604	4.770	5.604
15.5	15.5	4.929	5.793	4.929	5.793	4.929	5.793	4.929	5.793
16.0	16.0	5.088	5.982	5.088	5.982	5.088	5.982	5.088	5.982
16.5	16.5	5.247	6.171	5.247	6.171	5.247	6.171	5.247	6.171
17.0	17.0	5.406	6.360	5.406	6.360	5.406	6.360	5.406	6.360
17.5	17.5	5.565	6.549	5.565	6.549	5.565	6.549	5.565	6.549
18.0	18.0	5.724	6.738	5.724	6.738	5.724	6.738	5.724	6.738
18.5	18.5	5.883	6.927	5.883	6.927	5.883	6.927	5.883	6.927
19.0	19.0	6.042	7.116	6.042	7.116	6.042	7.116	6.042	7.116
19.5	19.5	6.201	7.305	6.201	7.305	6.201	7.305	6.201	7.305
20.0	20.0	6.360	7.494	6.360	7.494	6.360	7.494	6.360	7.494
20.5	20.5	6.519	7.683	6.519	7.683	6.519	7.683	6.519	7.683
21.0	21.0	6.678	7.872	6.678	7.872	6.678	7.872	6.678	7.872
21.5	21.5	6.837	8.061	6.837	8.061	6.837	8.061	6.837	8.061
22.0	22.0	6.996	8.250	6.996	8.250	6.996	8.250	6.996	8.250
22.5	22.5	7.155	8.439	7.155	8.439	7.155	8.439	7.155	8.439
23.0	23.0	7.314	8.628	7.314	8.628	7.314	8.628	7.314	8.628
23.5	23.5	7.473	8.817	7.473	8.817	7.473	8.817	7.473	8.817
24.0	24.0	7.632	9.006	7.632	9.006	7.632	9.006	7.632	9.006
24.5	24.5	7.791	9.195	7.791	9.195	7.791	9.195	7.791	9.195
25.0	25.0	7.950	9.384	7.950	9.384	7.950	9.384	7.950	9.384
25.5	25.5	8.109	9.573	8.109	9.573	8.109	9.573	8.109	9.573
26.0	26.0	8.268	9.762	8.268	9.762	8.268	9.762	8.268	9.762
26.5	26.5	8.427	9.951	8.427	9.951	8.427	9.951	8.427	9.951
27.0	27.0	8.586	10.140	8.586	10.140	8.586	10.140	8.586	10.140
27.5	27.5	8.745	10.329	8.745	10.329	8.745	10.329	8.745	10.329
28.0	28.0	8.904	10.518	8.904	10.518	8.904	10.518	8.904	10.518
28.5	28.5	9.063	10.707	9.063	10.707	9.063	10.707	9.063	10.707
29.0	29.0	9.222	10.896	9.222	10.896	9.222	10.896	9.222	10.896
29.5	29.5	9.381	11.085	9.381	11.085	9.381	11.085	9.381	11.085
30.0	30.0	9.540	11.274	9.540	11.274	9.540	11.274	9.540	11.274
30.5	30.5	9.699	11.463	9.699	11.463	9.699	11.463	9.699	11.463
31.0	31.0	9.858	11.652	9.858	11.652	9.858	11.652	9.858	11.652
31.5	31.5	10.017	11.841	10.017	11.841	10.017	11.841	10.017	11.841
32.0	32.0	10.176	12.030	10.176	12.030	10.176	12.030	10.176	12.030
32.5	32.5	10.335	12.219	10.335	12.219	10.335	12.219	10.335	12.219
33.0	33.0	10.494	12.408	10.494	12.408	10.494	12.408	10.494	12.408
33.5	33.5	10.653	12.597	10.653	12.597	10.653	12.597	10.653	12.597
34.0	34.0	10.812	12.786	10.812	12.786	10.812	12.786	10.812	12.786
34.5	34.5	10.971	12.975	10.971	12.975	10.971	12.975	10.971	12.975
35.0	35.0	11.130	13.164	11.130	13.164	11.130	13.164	11.130	13.164
35.5	35.5	11.289	13.353	11.289	13.353	11.289	13.353	11.289	13.353
36.0	36.0	11.448	13.542	11.448	13.542	11.448	13.542	11.448	13.542
36.5	36.5	11.607	13.731	11.607	13.731	11.607	13.731	11.607	13.731
37.0	37.0	11.766	13.920	11.766	13.920	11.766	13.920	11.766	13.920
37.5	37.5	11.925	14.109	11.925	14.109	11.925	14.109	11.925	14.109
38.0	38.0	12.084	14.298	12.084	14.298	12.084	14.298	12.084	14.298
38.5	38.5	12.243	14.487	12.243	14.487	12.243	14.487	12.243	14.487
39.0	39.0	12.402	14.676	12.402	14.676	12.402	14.676	12.402	14.676
39.5	39.5	12.561	14.865	12.561	14.865	12.561	14.865	12.561	14.865
40.0	40.0	12.720	15.054	12.720	15.054	12.720	15.054	12.720	15.054
40.5	40.5	12.879	15.243	12.879	15.243	12.879	15.243	12.879	15.243
41.0	41.0	13.038	15.432	13.038	15.432	13.038	15.432	13.038	15.432
41.5	41.5	13.197	15.621	13.197	15.621	13.197	15.621	13.197	15.621
42.0	42.0	13.356	15.810	13.356	15.810	13.356	15.810	13.356	15.810
42.5	42.5	13.515	16.000	13.515	16.000	13.515	16.000	13.515	16.000
43.0	43.0	13.674	16.189	13.674	16.189	13.674	16.189	13.674	16.189
43.5	43.5	13.833	16.378	13.833	16.378	13.833	16.378	13.833	16.378
44.0	44.0	13.992	16.567	13.992	16.567	13.992	16.567	13.992	16.567
44.5	44.5	14.151	16.756	14.151	16.756	14.151	16.756	14.151	16.756
45.0	45.0	14.310	16.945	14.310	16.945	14.310	16.945	14.310	16.945
45.5	45.5	14.469	17.134	14.469	17.134	14.469	17.134	14.469	17.134
46.0	46.0	14.628	17.323	14.628	17.323	14.628	17.323	14.628	17.323
46.5	46.5	14.787	17.512	14.787	17.512	14.787	17.512	14.787	17.512
47.0	47.0	14.946	17.701	14.946	17.701	14.946	17.701	14.946	17.701
47.5	47.5	15.105	17.890	15.105	17.890	15.105	17.890	15.105	17.890
48.0	48.0	15.264	18.079	15.264	18.079	15.264	18.079	15.264	18.079
48.5	48.5	15.423	18.268	15.423	18.268	15.423	18.268	15.423	18.268
49.0	49.0	15.582	18.457	15.582	18.457	15.582	18.457	15.582	18.457
49.5	49.5	15.741	18.646	15.741	18.646	15.741	18.646	15.741	18.646
50.0	50.0	15.900	18.835	15.900	18.835	15.900	18.835	15.900	18.835
50.5	50.5	16.059	19.024	16.059	19.024	16.059	19.024	16.059	19.024
51.0	51.0	16.218	19.213	16.218	19.213	16.218	19.213	16.218	19.213
51.5	51.5	16.377	19.402	16.377	19.402	16.377	19.402	16.377	19.402
52.0	52.0	16.536	19.591	16.536	19.591	16.536	19.591	16.536	19.591
52.5	52.5	16.695	19.780	16.695	19.780	16.695	19.780	16.695	19.780
53.0	53.0	16.854	19.969	16.854	19.969	16.854	19.969	16.854	19.969
53.5	53.5	17.013	20.158	17.013	20.158	17.013	20.158	17.013	20.158
54.0	54.0	17.172	20.347	17.172	20.347	17.172	20.347	17.172	20.347
54.5	54.5	17.331	20.536	17.331	20.536	17.331	20.536	17.331	20.536
55.0	55.0	17.490	20.725	17.490	20.725	17.490	20.725	17.490	20.725
55.5	55.5	17.649	20.914	17.649	20.914	17.649	20.914	17.649	20.914
56.0	56.0	17.808	21.103	17.808	21.103	17.808	21.103	17.808	21.103
56.5	56.5	17.967							







Table 1 (continued)

N (NUMBER) = 14		DEL 995-118.1 MM		MEASURED P		DEL 995-118.1 MM		MEASURED P					
N (NUMBER) = 14		DEL 995-118.3 MM		MEASURED P		DEL 995-118.3 MM		MEASURED P					
N (NUMBER) = 14		DEL 995-113.9 MM		MEASURED P		DEL 995-113.9 MM		MEASURED P					
Y (MM)	CONST PN	N	UVE	N	UVE	P/P10	P1/P10	N	UVE	N	UVE	P/P10	P1/P10
0.0	0.000	0.000	0.000	0.000	0.000	0.000	0.000	0.000	0.000	0.000	0.000	0.000	0.000
0.6	0.427	0.372	0.447	0.372	0.447	0.372	0.447	0.372	0.447	0.372	0.447	0.372	0.447
1.2	0.854	0.744	0.894	0.744	0.894	0.744	0.894	0.744	0.894	0.744	0.894	0.744	0.894
1.8	1.281	1.111	1.341	1.111	1.341	1.111	1.341	1.111	1.341	1.111	1.341	1.111	1.341
2.4	1.708	1.478	1.898	1.478	1.898	1.478	1.898	1.478	1.898	1.478	1.898	1.478	1.898
3.0	2.135	1.825	2.375	1.825	2.375	1.825	2.375	1.825	2.375	1.825	2.375	1.825	2.375
3.6	2.562	2.252	2.802	2.252	2.802	2.252	2.802	2.252	2.802	2.252	2.802	2.252	2.802
4.2	2.989	2.679	3.232	2.679	3.232	2.679	3.232	2.679	3.232	2.679	3.232	2.679	3.232
4.8	3.416	3.106	3.662	3.106	3.662	3.106	3.662	3.106	3.662	3.106	3.662	3.106	3.662
5.4	3.843	3.533	4.092	3.533	4.092	3.533	4.092	3.533	4.092	3.533	4.092	3.533	4.092
6.0	4.270	3.960	4.522	3.960	4.522	3.960	4.522	3.960	4.522	3.960	4.522	3.960	4.522
6.6	4.697	4.387	4.952	4.387	4.952	4.387	4.952	4.387	4.952	4.387	4.952	4.387	4.952
7.2	5.124	4.814	5.382	4.814	5.382	4.814	5.382	4.814	5.382	4.814	5.382	4.814	5.382
7.8	5.551	5.241	5.812	5.241	5.812	5.241	5.812	5.241	5.812	5.241	5.812	5.241	5.812
8.4	5.978	5.668	6.242	5.668	6.242	5.668	6.242	5.668	6.242	5.668	6.242	5.668	6.242
9.0	6.405	6.095	6.672	6.095	6.672	6.095	6.672	6.095	6.672	6.095	6.672	6.095	6.672
9.6	6.832	6.522	7.102	6.522	7.102	6.522	7.102	6.522	7.102	6.522	7.102	6.522	7.102
10.2	7.259	6.949	7.532	6.949	7.532	6.949	7.532	6.949	7.532	6.949	7.532	6.949	7.532
10.8	7.686	7.376	7.962	7.376	7.962	7.376	7.962	7.376	7.962	7.376	7.962	7.376	7.962
11.4	8.113	7.803	8.392	7.803	8.392	7.803	8.392	7.803	8.392	7.803	8.392	7.803	8.392
12.0	8.540	8.230	8.822	8.230	8.822	8.230	8.822	8.230	8.822	8.230	8.822	8.230	8.822
12.6	8.967	8.657	9.252	8.657	9.252	8.657	9.252	8.657	9.252	8.657	9.252	8.657	9.252
13.2	9.394	9.084	9.682	9.084	9.682	9.084	9.682	9.084	9.682	9.084	9.682	9.084	9.682
13.8	9.821	9.511	10.112	9.511	10.112	9.511	10.112	9.511	10.112	9.511	10.112	9.511	10.112
14.4	10.248	9.938	10.542	9.938	10.542	9.938	10.542	9.938	10.542	9.938	10.542	9.938	10.542
15.0	10.675	10.365	10.972	10.365	10.972	10.365	10.972	10.365	10.972	10.365	10.972	10.365	10.972
15.6	11.102	10.792	11.402	10.792	11.402	10.792	11.402	10.792	11.402	10.792	11.402	10.792	11.402
16.2	11.529	11.219	11.832	11.219	11.832	11.219	11.832	11.219	11.832	11.219	11.832	11.219	11.832
16.8	11.956	11.646	12.262	11.646	12.262	11.646	12.262	11.646	12.262	11.646	12.262	11.646	12.262
17.4	12.383	12.073	12.692	12.073	12.692	12.073	12.692	12.073	12.692	12.073	12.692	12.073	12.692
18.0	12.810	12.500	13.122	12.500	13.122	12.500	13.122	12.500	13.122	12.500	13.122	12.500	13.122
18.6	13.237	12.927	13.552	12.927	13.552	12.927	13.552	12.927	13.552	12.927	13.552	12.927	13.552
19.2	13.664	13.354	13.982	13.354	13.982	13.354	13.982	13.354	13.982	13.354	13.982	13.354	13.982
19.8	14.091	13.781	14.412	13.781	14.412	13.781	14.412	13.781	14.412	13.781	14.412	13.781	14.412
20.4	14.518	14.208	14.842	14.208	14.842	14.208	14.842	14.208	14.842	14.208	14.842	14.208	14.842
21.0	14.945	14.635	15.272	14.635	15.272	14.635	15.272	14.635	15.272	14.635	15.272	14.635	15.272
21.6	15.372	15.062	15.702	15.062	15.702	15.062	15.702	15.062	15.702	15.062	15.702	15.062	15.702
22.2	15.799	15.489	16.132	15.489	16.132	15.489	16.132	15.489	16.132	15.489	16.132	15.489	16.132
22.8	16.226	15.916	16.562	15.916	16.562	15.916	16.562	15.916	16.562	15.916	16.562	15.916	16.562
23.4	16.653	16.343	16.992	16.343	16.992	16.343	16.992	16.343	16.992	16.343	16.992	16.343	16.992
24.0	17.080	16.770	17.422	16.770	17.422	16.770	17.422	16.770	17.422	16.770	17.422	16.770	17.422
24.6	17.507	17.197	17.852	17.197	17.852	17.197	17.852	17.197	17.852	17.197	17.852	17.197	17.852
25.2	17.934	17.624	18.282	17.624	18.282	17.624	18.282	17.624	18.282	17.624	18.282	17.624	18.282
25.8	18.361	18.051	18.712	18.051	18.712	18.051	18.712	18.051	18.712	18.051	18.712	18.051	18.712
26.4	18.788	18.478	19.142	18.478	19.142	18.478	19.142	18.478	19.142	18.478	19.142	18.478	19.142
27.0	19.215	18.905	19.572	18.905	19.572	18.905	19.572	18.905	19.572	18.905	19.572	18.905	19.572
27.6	19.642	19.332	20.002	19.332	20.002	19.332	20.002	19.332	20.002	19.332	20.002	19.332	20.002
28.2	20.069	19.759	20.432	19.759	20.432	19.759	20.432	19.759	20.432	19.759	20.432	19.759	20.432
28.8	20.496	20.186	20.862	20.186	20.862	20.186	20.862	20.186	20.862	20.186	20.862	20.186	20.862
29.4	20.923	20.613	21.292	20.613	21.292	20.613	21.292	20.613	21.292	20.613	21.292	20.613	21.292
30.0	21.350	21.040	21.722	21.040	21.722	21.040	21.722	21.040	21.722	21.040	21.722	21.040	21.722
30.6	21.777	21.467	22.152	21.467	22.152	21.467	22.152	21.467	22.152	21.467	22.152	21.467	22.152
31.2	22.204	21.894	22.582	21.894	22.582	21.894	22.582	21.894	22.582	21.894	22.582	21.894	22.582
31.8	22.631	22.321	23.012	22.321	23.012	22.321	23.012	22.321	23.012	22.321	23.012	22.321	23.012
32.4	23.058	22.748	23.442	22.748	23.442	22.748	23.442	22.748	23.442	22.748	23.442	22.748	23.442
33.0	23.485	23.175	23.872	23.175	23.872	23.175	23.872	23.175	23.872	23.175	23.872	23.175	23.872
33.6	23.912	23.602	24.302	23.602	24.302	23.602	24.302	23.602	24.302	23.602	24.302	23.602	24.302
34.2	24.339	24.029	24.732	24.029	24.732	24.029	24.732	24.029	24.732	24.029	24.732	24.029	24.732
34.8	24.766	24.456	25.162	24.456	25.162	24.456	25.162	24.456	25.162	24.456	25.162	24.456	25.162
35.4	25.193	24.883	25.592	24.883	25.592	24.883	25.592	24.883	25.592	24.883	25.592	24.883	25.592
36.0	25.620	25.310	26.022	25.310	26.022	25.310	26.022	25.310	26.022	25.310	26.022	25.310	26.022
36.6	26.047	25.737	26.452	25.737	26.452	25.737	26.452	25.737	26.452	25.737	26.452	25.737	26.452
37.2	26.474	26.164	26.882	26.164	26.882	26.164	26.882	26.164	26.882	26.164	26.882	26.164	26.882
37.8	26.901	26.591	27.312	26.591	27.312	26.591	27.312	26.591	27.312	26.591	27.312	26.591	27.312
38.4	27.328	27.018	27.742	27.018	27.742	27.018	27.742	27.018	27.742	27.018	27.742	27.018	27.742
39.0	27.755	27.445	28.172	27.445	28.172	27.445	28.172	27.445	28.172	27.445	28.172	27.445	28.172
39.6	28.182	27.872	28.602	27.872	28.602	27.872	28.602	27.872	28.602	27.872	28.602	27.872	28.602
40.2	28.609	28.299	29.032	28.299	29.032	28.299	29.032	28.299	29.032	28.299	29.032	28.299	29.032
40.8	29.036	28.726	29.462	28.726	29.462	28.726	29.462	28.726	29.462	28.726	29.462	28.726	29.462
41.4	29.463	29.153	29.892	29.153	29.892	29.153	29.892	29.153	29.892	29.153	29.892	29.153	29.892
42.0	29.890	29.580	30.322	29.580	30.322	29.580	30.322	29.580	30.322	29.580	30.322	29.580	30.322
42.6	30.317	30.007	30.752	30.007	30.752	30.007	30.752	30.007	30.752	30.007	30.752	30.007	30.752
43.2	30.744	30.434	31.182	30.434	31.182	30.434	31.182	30.434	31.182	30.434	31.182	30.434	31.182
43.8	31.171	30.861	31.612	30.861	31.612	30.861	31.612	30.861	31.612	30.861	31.612	30.861	31.612
44.4	31.598	31.288	32.042	31.288	32.042	31.288	32.042	31.288	32.042	31.288	32.042	31.288	32.042
45.0	32.025	31.715	32.472	31.715	32.472	31.715	32.472	31.715	32.472	31.715	32.472	31.715	32.472
45.6	32.452	32.142	32.902	32.142	32.902	32.142	32.902	32.142	32.902	32.142	32.902	32.142	32.902
46.2	32.879	32.569	33.332	32.569	33.332	32.569	33.332	32.569	33.33				

H. HEIGHT = 1.5  
X=276 MM DEL. 95% 37.4 MM  
RE. #= 3.5 (4) (6. (REQUIRED P.) RE. #1.522 (REQUIRED P.)

Table with columns: V (MM), CONST, N, U/E, REQUIRED P, P/FIT, P/FIT0. Rows 0-152.

H. HEIGHT = 1.5  
X=277 MM DEL. 95% 37.4 MM  
RE. #= 3.5 (4) (6. (REQUIRED P.) RE. #1.522 (REQUIRED P.)

Table with columns: V (MM), CONST, N, U/E, REQUIRED P, P/FIT, P/FIT0. Rows 0-152.

H. HEIGHT = 1.5  
X=278 MM DEL. 95% 34.5 MM  
RE. #= 3.5 (4) (6. (REQUIRED P.) RE. #1.540 (REQUIRED P.)

Table with columns: V (MM), CONST, N, U/E, REQUIRED P, P/FIT, P/FIT0. Rows 0-152.

H. HEIGHT = 1.5  
X=277 MM DEL. 95% 33.9 MM  
RE. #= 3.5 (4) (6. (REQUIRED P.) RE. #1.528 (REQUIRED P.)

Table with columns: V (MM), CONST, N, U/E, REQUIRED P, P/FIT, P/FIT0. Rows 0-152.

H. HEIGHT = 1.5  
X=276 MM DEL. 95% 34.5 MM  
RE. #= 3.5 (4) (6. (REQUIRED P.) RE. #1.540 (REQUIRED P.)

Table with columns: V (MM), CONST, N, U/E, REQUIRED P, P/FIT, P/FIT0. Rows 0-152.





R (MONTH) = 1.5  
G = 1.4 MM  
DELTA = 3.62418% (MEASURED P)  
DEL 995 = 79.2 MM  
ME = 1.185 (MEASURED P)

Y (MM)	CONST P/N		MEASURED P		Y (MM)	CONST P/N		MEASURED P	
	M	N	M	N		M	N	M	N
0 00	0.0000	0.0000	0.0000	0.0000	0 00	0.0000	0.0000	0.0000	0.0000
0 20	-0.0181	-0.0179	-0.0181	-0.0181	0 20	-0.0181	-0.0179	-0.0181	-0.0181
0 40	-0.0249	-0.0247	-0.0249	-0.0249	0 40	-0.0249	-0.0247	-0.0249	-0.0249
0 60	-0.0317	-0.0314	-0.0317	-0.0317	0 60	-0.0317	-0.0314	-0.0317	-0.0317
0 80	-0.0374	-0.0374	-0.0374	-0.0374	0 80	-0.0374	-0.0374	-0.0374	-0.0374
1 00	-0.0428	-0.0415	-0.0428	-0.0415	1 00	-0.0428	-0.0415	-0.0428	-0.0415
1 20	-0.0488	-0.0482	-0.0488	-0.0482	1 20	-0.0488	-0.0482	-0.0488	-0.0482
1 40	-0.0541	-0.0534	-0.0541	-0.0534	1 40	-0.0541	-0.0534	-0.0541	-0.0534
1 60	-0.0594	-0.0591	-0.0594	-0.0591	1 60	-0.0594	-0.0591	-0.0594	-0.0591
1 80	-0.0646	-0.0639	-0.0646	-0.0639	1 80	-0.0646	-0.0639	-0.0646	-0.0639
2 00	-0.0697	-0.0691	-0.0697	-0.0691	2 00	-0.0697	-0.0691	-0.0697	-0.0691
2 20	-0.0748	-0.0742	-0.0748	-0.0742	2 20	-0.0748	-0.0742	-0.0748	-0.0742
2 40	-0.0798	-0.0791	-0.0798	-0.0791	2 40	-0.0798	-0.0791	-0.0798	-0.0791
2 60	-0.0848	-0.0841	-0.0848	-0.0841	2 60	-0.0848	-0.0841	-0.0848	-0.0841
2 80	-0.0897	-0.0891	-0.0897	-0.0891	2 80	-0.0897	-0.0891	-0.0897	-0.0891
3 00	-0.0946	-0.0939	-0.0946	-0.0939	3 00	-0.0946	-0.0939	-0.0946	-0.0939
3 20	-0.0994	-0.0987	-0.0994	-0.0987	3 20	-0.0994	-0.0987	-0.0994	-0.0987
3 40	-0.1042	-0.1034	-0.1042	-0.1034	3 40	-0.1042	-0.1034	-0.1042	-0.1034
3 60	-0.1089	-0.1081	-0.1089	-0.1081	3 60	-0.1089	-0.1081	-0.1089	-0.1081
3 80	-0.1136	-0.1128	-0.1136	-0.1128	3 80	-0.1136	-0.1128	-0.1136	-0.1128
4 00	-0.1183	-0.1175	-0.1183	-0.1175	4 00	-0.1183	-0.1175	-0.1183	-0.1175
4 20	-0.1229	-0.1221	-0.1229	-0.1221	4 20	-0.1229	-0.1221	-0.1229	-0.1221
4 40	-0.1275	-0.1267	-0.1275	-0.1267	4 40	-0.1275	-0.1267	-0.1275	-0.1267
4 60	-0.1321	-0.1313	-0.1321	-0.1313	4 60	-0.1321	-0.1313	-0.1321	-0.1313
4 80	-0.1367	-0.1359	-0.1367	-0.1359	4 80	-0.1367	-0.1359	-0.1367	-0.1359
5 00	-0.1412	-0.1404	-0.1412	-0.1404	5 00	-0.1412	-0.1404	-0.1412	-0.1404
5 20	-0.1458	-0.1450	-0.1458	-0.1450	5 20	-0.1458	-0.1450	-0.1458	-0.1450
5 40	-0.1503	-0.1495	-0.1503	-0.1495	5 40	-0.1503	-0.1495	-0.1503	-0.1495
5 60	-0.1549	-0.1541	-0.1549	-0.1541	5 60	-0.1549	-0.1541	-0.1549	-0.1541
5 80	-0.1594	-0.1586	-0.1594	-0.1586	5 80	-0.1594	-0.1586	-0.1594	-0.1586
6 00	-0.1639	-0.1631	-0.1639	-0.1631	6 00	-0.1639	-0.1631	-0.1639	-0.1631
6 20	-0.1685	-0.1677	-0.1685	-0.1677	6 20	-0.1685	-0.1677	-0.1685	-0.1677
6 40	-0.1730	-0.1722	-0.1730	-0.1722	6 40	-0.1730	-0.1722	-0.1730	-0.1722
6 60	-0.1776	-0.1768	-0.1776	-0.1768	6 60	-0.1776	-0.1768	-0.1776	-0.1768
6 80	-0.1821	-0.1813	-0.1821	-0.1813	6 80	-0.1821	-0.1813	-0.1821	-0.1813
7 00	-0.1867	-0.1859	-0.1867	-0.1859	7 00	-0.1867	-0.1859	-0.1867	-0.1859
7 20	-0.1912	-0.1904	-0.1912	-0.1904	7 20	-0.1912	-0.1904	-0.1912	-0.1904
7 40	-0.1958	-0.1950	-0.1958	-0.1950	7 40	-0.1958	-0.1950	-0.1958	-0.1950
7 60	-0.2003	-0.1995	-0.2003	-0.1995	7 60	-0.2003	-0.1995	-0.2003	-0.1995
7 80	-0.2049	-0.2041	-0.2049	-0.2041	7 80	-0.2049	-0.2041	-0.2049	-0.2041
8 00	-0.2094	-0.2086	-0.2094	-0.2086	8 00	-0.2094	-0.2086	-0.2094	-0.2086
8 20	-0.2139	-0.2131	-0.2139	-0.2131	8 20	-0.2139	-0.2131	-0.2139	-0.2131
8 40	-0.2185	-0.2177	-0.2185	-0.2177	8 40	-0.2185	-0.2177	-0.2185	-0.2177
8 60	-0.2230	-0.2222	-0.2230	-0.2222	8 60	-0.2230	-0.2222	-0.2230	-0.2222
8 80	-0.2276	-0.2268	-0.2276	-0.2268	8 80	-0.2276	-0.2268	-0.2276	-0.2268
9 00	-0.2321	-0.2313	-0.2321	-0.2313	9 00	-0.2321	-0.2313	-0.2321	-0.2313
9 20	-0.2367	-0.2359	-0.2367	-0.2359	9 20	-0.2367	-0.2359	-0.2367	-0.2359
9 40	-0.2412	-0.2404	-0.2412	-0.2404	9 40	-0.2412	-0.2404	-0.2412	-0.2404
9 60	-0.2458	-0.2450	-0.2458	-0.2450	9 60	-0.2458	-0.2450	-0.2458	-0.2450
9 80	-0.2503	-0.2495	-0.2503	-0.2495	9 80	-0.2503	-0.2495	-0.2503	-0.2495
10 00	-0.2549	-0.2541	-0.2549	-0.2541	10 00	-0.2549	-0.2541	-0.2549	-0.2541
10 20	-0.2594	-0.2586	-0.2594	-0.2586	10 20	-0.2594	-0.2586	-0.2594	-0.2586
10 40	-0.2639	-0.2631	-0.2639	-0.2631	10 40	-0.2639	-0.2631	-0.2639	-0.2631
10 60	-0.2685	-0.2677	-0.2685	-0.2677	10 60	-0.2685	-0.2677	-0.2685	-0.2677
10 80	-0.2730	-0.2722	-0.2730	-0.2722	10 80	-0.2730	-0.2722	-0.2730	-0.2722
11 00	-0.2776	-0.2768	-0.2776	-0.2768	11 00	-0.2776	-0.2768	-0.2776	-0.2768
11 20	-0.2821	-0.2813	-0.2821	-0.2813	11 20	-0.2821	-0.2813	-0.2821	-0.2813
11 40	-0.2867	-0.2859	-0.2867	-0.2859	11 40	-0.2867	-0.2859	-0.2867	-0.2859
11 60	-0.2912	-0.2904	-0.2912	-0.2904	11 60	-0.2912	-0.2904	-0.2912	-0.2904
11 80	-0.2958	-0.2950	-0.2958	-0.2950	11 80	-0.2958	-0.2950	-0.2958	-0.2950
12 00	-0.3003	-0.2995	-0.3003	-0.2995	12 00	-0.3003	-0.2995	-0.3003	-0.2995
12 20	-0.3049	-0.3041	-0.3049	-0.3041	12 20	-0.3049	-0.3041	-0.3049	-0.3041
12 40	-0.3094	-0.3086	-0.3094	-0.3086	12 40	-0.3094	-0.3086	-0.3094	-0.3086
12 60	-0.3139	-0.3131	-0.3139	-0.3131	12 60	-0.3139	-0.3131	-0.3139	-0.3131
12 80	-0.3185	-0.3177	-0.3185	-0.3177	12 80	-0.3185	-0.3177	-0.3185	-0.3177
13 00	-0.3230	-0.3222	-0.3230	-0.3222	13 00	-0.3230	-0.3222	-0.3230	-0.3222
13 20	-0.3276	-0.3268	-0.3276	-0.3268	13 20	-0.3276	-0.3268	-0.3276	-0.3268
13 40	-0.3321	-0.3313	-0.3321	-0.3313	13 40	-0.3321	-0.3313	-0.3321	-0.3313
13 60	-0.3367	-0.3359	-0.3367	-0.3359	13 60	-0.3367	-0.3359	-0.3367	-0.3359
13 80	-0.3412	-0.3404	-0.3412	-0.3404	13 80	-0.3412	-0.3404	-0.3412	-0.3404
14 00	-0.3458	-0.3450	-0.3458	-0.3450	14 00	-0.3458	-0.3450	-0.3458	-0.3450
14 20	-0.3503	-0.3495	-0.3503	-0.3495	14 20	-0.3503	-0.3495	-0.3503	-0.3495
14 40	-0.3549	-0.3541	-0.3549	-0.3541	14 40	-0.3549	-0.3541	-0.3549	-0.3541
14 60	-0.3594	-0.3586	-0.3594	-0.3586	14 60	-0.3594	-0.3586	-0.3594	-0.3586
14 80	-0.3639	-0.3631	-0.3639	-0.3631	14 80	-0.3639	-0.3631	-0.3639	-0.3631
15 00	-0.3685	-0.3677	-0.3685	-0.3677	15 00	-0.3685	-0.3677	-0.3685	-0.3677
15 20	-0.3730	-0.3722	-0.3730	-0.3722	15 20	-0.3730	-0.3722	-0.3730	-0.3722
15 40	-0.3776	-0.3768	-0.3776	-0.3768	15 40	-0.3776	-0.3768	-0.3776	-0.3768
15 60	-0.3821	-0.3813	-0.3821	-0.3813	15 60	-0.3821	-0.3813	-0.3821	-0.3813
15 80	-0.3867	-0.3859	-0.3867	-0.3859	15 80	-0.3867	-0.3859	-0.3867	-0.3859
16 00	-0.3912	-0.3904	-0.3912	-0.3904	16 00	-0.3912	-0.3904	-0.3912	-0.3904
16 20	-0.3958	-0.3950	-0.3958	-0.3950	16 20	-0.3958	-0.3950	-0.3958	-0.3950
16 40	-0.4003	-0.3995	-0.4003	-0.3995	16 40	-0.4003	-0.3995	-0.4003	-0.3995
16 60	-0.4049	-0.4041	-0.4049	-0.4041	16 60	-0.4049	-0.4041	-0.4049	-0.4041
16 80	-0.4094	-0.4086	-0.4094	-0.4086	16 80	-0.4094	-0.4086	-0.4094	-0.4086
17 00	-0.4139	-0.4131	-0.4139	-0.4131	17 00	-0.4139	-0.4131	-0.4139	-0.4131
17 20	-0.4185	-0.4177	-0.4185	-0.4177	17 20	-0.4185	-0.4177	-0.4185	-0.4177
17 40	-0.4230	-0.4222	-0.4230	-0.4222	17 40	-0.4230	-0.4222	-0.4230	-0.4222
17 60	-0.4276	-0.4268	-0.4276	-0.4268	17 60	-0.4276	-0.4268	-0.4276	-0.4268
17 80	-0.4321	-0.4313	-0.4321	-0.4313	17 80	-0.4321	-0.4313	-0.4321	-0.4313
18 00	-0.4367	-0.4359	-0.4367	-0.4359	18 00	-0.4367	-0.4359	-0.4367	-0.4359
18 20	-0.4412	-0.4404	-0.4412	-0.4404	18 20	-0.4412	-0.4404	-0.4412	-0.4404
18 40	-0.4458	-0.4450	-0.4458	-0.4450	18 40	-0.4458	-0.4450	-0.4458	-0.4450
18 60	-0.4503	-0.4495	-0.4503	-0.4495	18 60	-0.4503	-0.4495	-0.4503	-0.4495
18 80	-0.4549	-0.4541	-0.4549	-0.4541	18 80	-0.4549	-0.4541	-0.4549	-0.4541
19 00	-0.4594	-0.4586	-0.4594	-0.4586	19 00	-0.4594	-0.4586	-0.4594	-0.4586
19 20	-0.4639	-0.4631	-0.4639	-0.4631	19 20	-0.4639	-0.4631	-0.4639	-0.4631
19 40	-0.4685	-0.4677	-0.4685	-0.4677	19 40	-0.4685	-0.4677	-0.4685	-0.4677
19 60	-0.4730	-0.4722	-0.4730	-0.4722	19 60	-0.4730	-0.4722	-0.4730	-0.4722
19 80	-0.4776	-0.4768	-0.4776	-0.4768	19 80	-0.4776	-0.4768	-0.4776	-0.4768
20 00	-0.4821	-0.4813	-0.4821	-0.4813	20 00	-0.4821	-0.4813	-0.4821	-0.4813
20 20	-0.4867	-0.4859	-0.4867	-0.4859	20 20	-0.4867	-0.4859	-0.4867	-0.4859
20 40	-0.4912	-0.4904	-0.4912	-0.4904	20 40	-0.4912	-0.4904	-0.4912	-0.4904
20 60	-0.4958	-0.4950	-0.4958	-0.4950	20 60	-0.4958	-0.4950	-0.4958	-0.4950
20 80	-0.5003	-0.4995	-0.5003	-0.4995	20 80	-0.5003	-0.4995	-0.5003	-0.4995
21 00	-0.5049	-0.5041	-0.5049	-0.5041	21 00	-0.5049	-0.5041	-0.5049	-0.5041
21 20	-0.5094	-0.5086	-0.5094	-0.5086	21 20	-0.5094	-0.5086	-0.5094	-0.5086
21 40	-0.5139	-0.5131	-0.5139	-0.5131	21 40	-0.51			



H (CONTINUED) 1-15

X= 656 MM DEL 995-118.5 MM  
REF: 1.5418 G (MEASURED P) REF: 9.973 (MEASURED P)

Table with 10 columns: V (MM), CONST, M, UVE, REQUIRED P, M, UVE, P/P10, P/P10. Contains 100 rows of numerical data.

H (CONTINUED) 1-15

X= 740 MM DEL 995-118.5 MM  
REF: 1.5418 G (MEASURED P) REF: 9.973 (MEASURED P)

Table with 10 columns: V (MM), CONST, M, UVE, REQUIRED P, M, UVE, P/P10, P/P10. Contains 100 rows of numerical data.

H (CONTINUED) 1-15

X= 1043 MM DEL 995-120.0 MM  
REF: 1.4918 G (MEASURED P) REF: 9.911 (MEASURED P)

Table with 10 columns: V (MM), CONST, M, UVE, REQUIRED P, M, UVE, P/P10, P/P10. Contains 100 rows of numerical data.

H (CONTINUED) 1-15

X= 1279 MM DEL 995-119.5 MM  
REF: 1.4918 G (MEASURED P) REF: 9.911 (MEASURED P)

Table with 10 columns: V (MM), CONST, M, UVE, REQUIRED P, M, UVE, P/P10, P/P10. Contains 100 rows of numerical data.



W. NUMBER = 1.5

DEL 995-157.6 MM  
RES/NO. 3 25416.6 (MEASURED P)  
RES/NO. 875 (MEASURED P)

Y (MM)	H	CONST PM	U	MEASURED P	P	PI/PTO	PI/PTO
0.0	0.000	0.000	0.000	0.000	0.000	0.000	0.000
0.6	0.300	0.621	0.320	0.621	0.621	0.621	0.621
0.8	0.326	0.716	0.326	0.716	0.716	0.716	0.716
1.0	0.401	0.829	0.401	0.829	0.829	0.829	0.829
1.2	0.488	0.955	0.488	0.955	0.955	0.955	0.955
1.4	0.479	0.913	0.479	0.913	0.913	0.913	0.913
1.6	0.429	0.816	0.429	0.816	0.816	0.816	0.816
1.8	0.469	0.868	0.469	0.868	0.868	0.868	0.868
2.0	0.448	0.849	0.448	0.849	0.849	0.849	0.849
2.2	0.458	0.854	0.458	0.854	0.854	0.854	0.854
2.4	0.466	0.866	0.466	0.866	0.866	0.866	0.866
2.6	0.475	0.876	0.475	0.876	0.876	0.876	0.876
2.8	0.478	0.879	0.478	0.879	0.879	0.879	0.879
3.0	0.479	0.880	0.479	0.880	0.880	0.880	0.880
3.2	0.479	0.880	0.479	0.880	0.880	0.880	0.880
3.4	0.478	0.879	0.478	0.879	0.879	0.879	0.879
3.6	0.475	0.876	0.475	0.876	0.876	0.876	0.876
3.8	0.470	0.871	0.470	0.871	0.871	0.871	0.871
4.0	0.463	0.864	0.463	0.864	0.864	0.864	0.864
4.2	0.454	0.855	0.454	0.855	0.855	0.855	0.855
4.4	0.444	0.845	0.444	0.845	0.845	0.845	0.845
4.6	0.433	0.834	0.433	0.834	0.834	0.834	0.834
4.8	0.421	0.822	0.421	0.822	0.822	0.822	0.822
5.0	0.409	0.809	0.409	0.809	0.809	0.809	0.809
5.2	0.397	0.796	0.397	0.796	0.796	0.796	0.796
5.4	0.385	0.783	0.385	0.783	0.783	0.783	0.783
5.6	0.373	0.770	0.373	0.770	0.770	0.770	0.770
5.8	0.361	0.757	0.361	0.757	0.757	0.757	0.757
6.0	0.349	0.744	0.349	0.744	0.744	0.744	0.744
6.2	0.337	0.731	0.337	0.731	0.731	0.731	0.731
6.4	0.325	0.718	0.325	0.718	0.718	0.718	0.718
6.6	0.313	0.705	0.313	0.705	0.705	0.705	0.705
6.8	0.301	0.692	0.301	0.692	0.692	0.692	0.692
7.0	0.289	0.679	0.289	0.679	0.679	0.679	0.679
7.2	0.277	0.666	0.277	0.666	0.666	0.666	0.666
7.4	0.265	0.653	0.265	0.653	0.653	0.653	0.653
7.6	0.253	0.640	0.253	0.640	0.640	0.640	0.640
7.8	0.241	0.627	0.241	0.627	0.627	0.627	0.627
8.0	0.229	0.614	0.229	0.614	0.614	0.614	0.614
8.2	0.217	0.601	0.217	0.601	0.601	0.601	0.601
8.4	0.205	0.588	0.205	0.588	0.588	0.588	0.588
8.6	0.193	0.575	0.193	0.575	0.575	0.575	0.575
8.8	0.181	0.562	0.181	0.562	0.562	0.562	0.562
9.0	0.169	0.549	0.169	0.549	0.549	0.549	0.549
9.2	0.157	0.536	0.157	0.536	0.536	0.536	0.536
9.4	0.145	0.523	0.145	0.523	0.523	0.523	0.523
9.6	0.133	0.510	0.133	0.510	0.510	0.510	0.510
9.8	0.121	0.497	0.121	0.497	0.497	0.497	0.497
10.0	0.109	0.484	0.109	0.484	0.484	0.484	0.484

W. NUMBER = 1.5

DEL 995-172.7 MM  
RES/NO. 3 25416.6 (MEASURED P)  
RES/NO. 875 (MEASURED P)

Y (MM)	H	CONST PM	U	MEASURED P	P	PI/PTO	PI/PTO
0.0	0.000	0.000	0.000	0.000	0.000	0.000	0.000
0.6	0.331	0.687	0.331	0.687	0.687	0.687	0.687
0.8	0.485	0.962	0.485	0.962	0.962	0.962	0.962
1.0	0.418	0.817	0.418	0.817	0.817	0.817	0.817
1.2	0.423	0.823	0.423	0.823	0.823	0.823	0.823
1.4	0.431	0.828	0.431	0.828	0.828	0.828	0.828
1.6	0.442	0.834	0.442	0.834	0.834	0.834	0.834
1.8	0.454	0.839	0.454	0.839	0.839	0.839	0.839
2.0	0.465	0.845	0.465	0.845	0.845	0.845	0.845
2.2	0.476	0.850	0.476	0.850	0.850	0.850	0.850
2.4	0.485	0.855	0.485	0.855	0.855	0.855	0.855
2.6	0.495	0.860	0.495	0.860	0.860	0.860	0.860
2.8	0.519	0.870	0.519	0.870	0.870	0.870	0.870
3.0	0.524	0.874	0.524	0.874	0.874	0.874	0.874
3.2	0.541	0.884	0.541	0.884	0.884	0.884	0.884
3.4	0.546	0.887	0.546	0.887	0.887	0.887	0.887
3.6	0.558	0.894	0.558	0.894	0.894	0.894	0.894
3.8	0.570	0.901	0.570	0.901	0.901	0.901	0.901
4.0	0.582	0.908	0.582	0.908	0.908	0.908	0.908
4.2	0.594	0.915	0.594	0.915	0.915	0.915	0.915
4.4	0.606	0.922	0.606	0.922	0.922	0.922	0.922
4.6	0.618	0.929	0.618	0.929	0.929	0.929	0.929
4.8	0.630	0.936	0.630	0.936	0.936	0.936	0.936
5.0	0.642	0.943	0.642	0.943	0.943	0.943	0.943
5.2	0.654	0.950	0.654	0.950	0.950	0.950	0.950
5.4	0.666	0.957	0.666	0.957	0.957	0.957	0.957
5.6	0.678	0.964	0.678	0.964	0.964	0.964	0.964
5.8	0.690	0.971	0.690	0.971	0.971	0.971	0.971
6.0	0.702	0.978	0.702	0.978	0.978	0.978	0.978
6.2	0.714	0.985	0.714	0.985	0.985	0.985	0.985
6.4	0.726	0.992	0.726	0.992	0.992	0.992	0.992
6.6	0.738	0.999	0.738	0.999	0.999	0.999	0.999
6.8	0.750	1.006	0.750	1.006	1.006	1.006	1.006
7.0	0.762	1.013	0.762	1.013	1.013	1.013	1.013
7.2	0.774	1.020	0.774	1.020	1.020	1.020	1.020
7.4	0.786	1.027	0.786	1.027	1.027	1.027	1.027
7.6	0.798	1.034	0.798	1.034	1.034	1.034	1.034
7.8	0.810	1.041	0.810	1.041	1.041	1.041	1.041
8.0	0.822	1.048	0.822	1.048	1.048	1.048	1.048
8.2	0.834	1.055	0.834	1.055	1.055	1.055	1.055
8.4	0.846	1.062	0.846	1.062	1.062	1.062	1.062
8.6	0.858	1.069	0.858	1.069	1.069	1.069	1.069
8.8	0.870	1.076	0.870	1.076	1.076	1.076	1.076
9.0	0.882	1.083	0.882	1.083	1.083	1.083	1.083
9.2	0.894	1.090	0.894	1.090	1.090	1.090	1.090
9.4	0.906	1.097	0.906	1.097	1.097	1.097	1.097
9.6	0.918	1.104	0.918	1.104	1.104	1.104	1.104
9.8	0.930	1.111	0.930	1.111	1.111	1.111	1.111
10.0	0.942	1.118	0.942	1.118	1.118	1.118	1.118

W. NUMBER = 1.5

DEL 995-181.7 MM  
RES/NO. 3 25416.6 (MEASURED P)  
RES/NO. 875 (MEASURED P)

Y (MM)	H	CONST PM	U	MEASURED P	P	PI/PTO	PI/PTO
0.0	0.000	0.000	0.000	0.000	0.000	0.000	0.000
0.6	0.351	0.765	0.351	0.765	0.765	0.765	0.765
0.8	0.418	0.818	0.418	0.818	0.818	0.818	0.818
1.0	0.417	0.817	0.417	0.817	0.817	0.817	0.817
1.2	0.426	0.826	0.426	0.826	0.826	0.826	0.826
1.4	0.435	0.835	0.435	0.835	0.835	0.835	0.835
1.6	0.444	0.844	0.444	0.844	0.844	0.844	0.844
1.8	0.453	0.853	0.453	0.853	0.853	0.853	0.853
2.0	0.462	0.862	0.462	0.862	0.862	0.862	0.862
2.2	0.471	0.871	0.471	0.871	0.871	0.871	0.871
2.4	0.480	0.880	0.480	0.880	0.880	0.880	0.880
2.6	0.489	0.889	0.489	0.889	0.889	0.889	0.889
2.8	0.498	0.898	0.498	0.898	0.898	0.898	0.898
3.0	0.507	0.907	0.507	0.907	0.907	0.907	0.907
3.2	0.516	0.916	0.516	0.916	0.916	0.916	0.916
3.4	0.525	0.925	0.525	0.925	0.925	0.925	0.925
3.6	0.534	0.934	0.534	0.934	0.934	0.934	0.934
3.8	0.543	0.943	0.543	0.943	0.943	0.943	0.943
4.0	0.552	0.952	0.552	0.952	0.952	0.952	0.952
4.2	0.561	0.961	0.561	0.961	0.961	0.961	0.961
4.4	0.570	0.970	0.570	0.970	0.970	0.970	0.970
4.6	0.579	0.979	0.579	0.979	0.979	0.979	0.979
4.8	0.588	0.988	0.588	0.988	0.988	0.988	0.988
5.0	0.597	0.997	0.597	0.997	0.997	0.997	0.997
5.2	0.606	1.006	0.606	1.006	1.006	1.006	1.006
5.4	0.615	1.015	0.615	1.015	1.015	1.015	1.015
5.6	0.624	1.024	0.624	1.024	1.024	1.024	1.024
5.8	0.633	1.033	0.633	1.033	1.033	1.033	1.033
6.0	0.642	1.042	0.642	1.042	1.042	1.042	1.042
6.2	0.651	1.051	0.651	1.051	1.051	1.051	1.051
6.4	0.660	1.060	0.660	1.060	1.060	1.060	1.060
6.6	0.669	1.069	0.669	1.069	1.069	1.069	1.069
6.8	0.678	1.078	0.678	1.078	1.078	1.078	1.078
7.0	0.687	1.087	0.687	1.087	1.087	1.087	1.087
7.2	0.696	1.096	0.696	1.096	1.096	1.096	1.096
7.4	0.705	1.105	0.705	1.105	1.105	1.105	1.105
7.6	0.714	1.114	0.714	1.114	1.114	1.114	1.114
7.8	0.723	1.123	0.723	1.123	1.123	1.123	1.123
8.0	0.732	1.132	0.732	1.132	1.132	1.132	1.132
8.2	0.741	1.141	0.741	1.141	1.141	1.141	1.141
8.4	0.750	1.150	0.750	1.150	1.150	1.150	1.150
8.6	0.759	1.159	0.759	1.159			









H (NUMBER) = 1.5  
Z = 75.0 MI  
REF = 6.4641876 (MEASURED) P  
19-294 5 K DEL 955-113.4 MI  
MEAS (S) (MEASURED) P

Table with 12 columns: Y (MI), H, CONST, M, UAVE, M, UAVE, P/P10, P/P10. Rows 1-200.

H (NUMBER) = 1.5  
Z = 60.0 MI  
REF = 6.5548186 (MEASURED) P  
19-295 5 K DEL 955-104.4 MI  
MEAS (S) (MEASURED) P

Table with 12 columns: Y (MI), H, CONST, M, UAVE, M, UAVE, P/P10, P/P10. Rows 1-200.

H (NUMBER) = 1.5  
Z = 45.0 MI  
REF = 6.5941876 (MEASURED) P  
19-296 2 K DEL 955-92.0 MI  
MEAS (S) (MEASURED) P

Table with 12 columns: Y (MI), H, CONST, M, UAVE, M, UAVE, P/P10, P/P10. Rows 1-200.

H (NUMBER) = 1.5  
Z = 30.0 MI  
REF = 6.5941876 (MEASURED) P  
19-296 6 K DEL 955-78.0 MI  
MEAS (S) (MEASURED) P

Table with 12 columns: Y (MI), H, CONST, M, UAVE, M, UAVE, P/P10, P/P10. Rows 1-200.

H (MIDLINE) = 1.5  
X= 2265 MM DEL 995-127.4 MM  
RE=0.30410'S (MEASURED P.) RE=0.911 (MEASURED P.)

Table with 10 columns: Y (MM), H, CONST PH, U/E, H, U/E, H, U/E, P/P10, P/P10. Contains 20 rows of data.

H (MIDLINE) = 1.5  
X= 1776 MM DEL 995-153.1 MM  
RE=0.60410'S (MEASURED P.) RE=0.856 (MEASURED P.)

Table with 10 columns: Y (MM), H, CONST PH, U/E, H, U/E, H, U/E, P/P10, P/P10. Contains 20 rows of data.

H (MIDLINE) = 1.5  
X= 1236 MM DEL 995-135.9 MM  
RE=0.620410'S (MEASURED P.) RE=0.889 (MEASURED P.)

Table with 10 columns: Y (MM), H, CONST PH, U/E, H, U/E, H, U/E, P/P10, P/P10. Contains 20 rows of data.

H (MIDLINE) = 1.5  
X= 1050 MM DEL 995-127.4 MM  
RE=0.620410'S (MEASURED P.) RE=0.911 (MEASURED P.)

Table with 10 columns: Y (MM), H, CONST PH, U/E, H, U/E, H, U/E, P/P10, P/P10. Contains 20 rows of data.





Table 2 (Continued)

H (NORMAL)= 1.5		H (NORMAL)= 1.5		H (NORMAL)= 1.5		H (NORMAL)= 1.5		H (NORMAL)= 1.5	
X=75 MI DEL 95% 33.3 MI RE/NO 9 504/176 (REQUIRED P)		X=50 MI DEL 95% 23.3 MI RE/NO 9 504/176 (REQUIRED P)		X=25 MI DEL 95% 13.3 MI RE/NO 9 504/176 (REQUIRED P)		X=45 MI DEL 95% 33.3 MI RE/NO 9 504/176 (REQUIRED P)		X=65 MI DEL 95% 33.3 MI RE/NO 9 504/176 (REQUIRED P)	
Y (MI)	CONST	H	U/E	REQUIRED P	Y (MI)	CONST	H	U/E	REQUIRED P
0.00	0.0000	0.0000	0.0000	0.0000	0.00	0.0000	0.0000	0.0000	0.0000
0.05	0.0122	0.0018	0.0122	0.0018	0.05	0.0136	0.0029	0.0136	0.0029
0.10	0.0477	0.0261	0.0477	0.0261	0.10	0.0542	0.0542	0.0542	0.0542
0.15	0.0774	0.0441	0.0774	0.0441	0.15	0.0855	0.0855	0.0855	0.0855
0.20	0.0939	0.0564	0.0939	0.0564	0.20	0.1131	0.1131	0.1131	0.1131
0.25	0.1032	0.0644	0.1032	0.0644	0.25	0.1368	0.1368	0.1368	0.1368
0.30	0.1095	0.0700	0.1095	0.0700	0.30	0.1575	0.1575	0.1575	0.1575
0.35	0.1135	0.0742	0.1135	0.0742	0.35	0.1755	0.1755	0.1755	0.1755
0.40	0.1158	0.0773	0.1158	0.0773	0.40	0.1905	0.1905	0.1905	0.1905
0.45	0.1168	0.0797	0.1168	0.0797	0.45	0.2031	0.2031	0.2031	0.2031
0.50	0.1168	0.0814	0.1168	0.0814	0.50	0.2130	0.2130	0.2130	0.2130
0.55	0.1158	0.0823	0.1158	0.0823	0.55	0.2205	0.2205	0.2205	0.2205
0.60	0.1135	0.0823	0.1135	0.0823	0.60	0.2259	0.2259	0.2259	0.2259
0.65	0.1095	0.0814	0.1095	0.0814	0.65	0.2296	0.2296	0.2296	0.2296
0.70	0.1032	0.0797	0.1032	0.0797	0.70	0.2316	0.2316	0.2316	0.2316
0.75	0.0939	0.0773	0.0939	0.0773	0.75	0.2319	0.2319	0.2319	0.2319
0.80	0.0855	0.0742	0.0855	0.0742	0.80	0.2313	0.2313	0.2313	0.2313
0.85	0.0774	0.0700	0.0774	0.0700	0.85	0.2296	0.2296	0.2296	0.2296
0.90	0.0690	0.0658	0.0690	0.0658	0.90	0.2268	0.2268	0.2268	0.2268
0.95	0.0606	0.0615	0.0606	0.0615	0.95	0.2229	0.2229	0.2229	0.2229
1.00	0.0522	0.0572	0.0522	0.0572	1.00	0.2180	0.2180	0.2180	0.2180
1.05	0.0438	0.0529	0.0438	0.0529	1.05	0.2122	0.2122	0.2122	0.2122
1.10	0.0354	0.0486	0.0354	0.0486	1.10	0.2056	0.2056	0.2056	0.2056
1.15	0.0270	0.0443	0.0270	0.0443	1.15	0.1982	0.1982	0.1982	0.1982
1.20	0.0186	0.0400	0.0186	0.0400	1.20	0.1900	0.1900	0.1900	0.1900
1.25	0.0102	0.0357	0.0102	0.0357	1.25	0.1810	0.1810	0.1810	0.1810
1.30	0.0018	0.0314	0.0018	0.0314	1.30	0.1713	0.1713	0.1713	0.1713
1.35	0.0000	0.0271	0.0000	0.0271	1.35	0.1610	0.1610	0.1610	0.1610
1.40	0.0000	0.0228	0.0000	0.0228	1.40	0.1502	0.1502	0.1502	0.1502
1.45	0.0000	0.0185	0.0000	0.0185	1.45	0.1390	0.1390	0.1390	0.1390
1.50	0.0000	0.0142	0.0000	0.0142	1.50	0.1275	0.1275	0.1275	0.1275
1.55	0.0000	0.0099	0.0000	0.0099	1.55	0.1158	0.1158	0.1158	0.1158
1.60	0.0000	0.0056	0.0000	0.0056	1.60	0.1039	0.1039	0.1039	0.1039
1.65	0.0000	0.0013	0.0000	0.0013	1.65	0.0918	0.0918	0.0918	0.0918
1.70	0.0000	0.0000	0.0000	0.0000	1.70	0.0795	0.0795	0.0795	0.0795
1.75	0.0000	0.0000	0.0000	0.0000	1.75	0.0670	0.0670	0.0670	0.0670
1.80	0.0000	0.0000	0.0000	0.0000	1.80	0.0544	0.0544	0.0544	0.0544
1.85	0.0000	0.0000	0.0000	0.0000	1.85	0.0418	0.0418	0.0418	0.0418
1.90	0.0000	0.0000	0.0000	0.0000	1.90	0.0292	0.0292	0.0292	0.0292
1.95	0.0000	0.0000	0.0000	0.0000	1.95	0.0166	0.0166	0.0166	0.0166
2.00	0.0000	0.0000	0.0000	0.0000	2.00	0.0040	0.0040	0.0040	0.0040
2.05	0.0000	0.0000	0.0000	0.0000	2.05	0.0000	0.0000	0.0000	0.0000
2.10	0.0000	0.0000	0.0000	0.0000	2.10	0.0000	0.0000	0.0000	0.0000
2.15	0.0000	0.0000	0.0000	0.0000	2.15	0.0000	0.0000	0.0000	0.0000
2.20	0.0000	0.0000	0.0000	0.0000	2.20	0.0000	0.0000	0.0000	0.0000
2.25	0.0000	0.0000	0.0000	0.0000	2.25	0.0000	0.0000	0.0000	0.0000
2.30	0.0000	0.0000	0.0000	0.0000	2.30	0.0000	0.0000	0.0000	0.0000
2.35	0.0000	0.0000	0.0000	0.0000	2.35	0.0000	0.0000	0.0000	0.0000
2.40	0.0000	0.0000	0.0000	0.0000	2.40	0.0000	0.0000	0.0000	0.0000
2.45	0.0000	0.0000	0.0000	0.0000	2.45	0.0000	0.0000	0.0000	0.0000
2.50	0.0000	0.0000	0.0000	0.0000	2.50	0.0000	0.0000	0.0000	0.0000
2.55	0.0000	0.0000	0.0000	0.0000	2.55	0.0000	0.0000	0.0000	0.0000
2.60	0.0000	0.0000	0.0000	0.0000	2.60	0.0000	0.0000	0.0000	0.0000
2.65	0.0000	0.0000	0.0000	0.0000	2.65	0.0000	0.0000	0.0000	0.0000
2.70	0.0000	0.0000	0.0000	0.0000	2.70	0.0000	0.0000	0.0000	0.0000
2.75	0.0000	0.0000	0.0000	0.0000	2.75	0.0000	0.0000	0.0000	0.0000
2.80	0.0000	0.0000	0.0000	0.0000	2.80	0.0000	0.0000	0.0000	0.0000
2.85	0.0000	0.0000	0.0000	0.0000	2.85	0.0000	0.0000	0.0000	0.0000
2.90	0.0000	0.0000	0.0000	0.0000	2.90	0.0000	0.0000	0.0000	0.0000
2.95	0.0000	0.0000	0.0000	0.0000	2.95	0.0000	0.0000	0.0000	0.0000
3.00	0.0000	0.0000	0.0000	0.0000	3.00	0.0000	0.0000	0.0000	0.0000
3.05	0.0000	0.0000	0.0000	0.0000	3.05	0.0000	0.0000	0.0000	0.0000
3.10	0.0000	0.0000	0.0000	0.0000	3.10	0.0000	0.0000	0.0000	0.0000
3.15	0.0000	0.0000	0.0000	0.0000	3.15	0.0000	0.0000	0.0000	0.0000
3.20	0.0000	0.0000	0.0000	0.0000	3.20	0.0000	0.0000	0.0000	0.0000
3.25	0.0000	0.0000	0.0000	0.0000	3.25	0.0000	0.0000	0.0000	0.0000
3.30	0.0000	0.0000	0.0000	0.0000	3.30	0.0000	0.0000	0.0000	0.0000
3.35	0.0000	0.0000	0.0000	0.0000	3.35	0.0000	0.0000	0.0000	0.0000
3.40	0.0000	0.0000	0.0000	0.0000	3.40	0.0000	0.0000	0.0000	0.0000
3.45	0.0000	0.0000	0.0000	0.0000	3.45	0.0000	0.0000	0.0000	0.0000
3.50	0.0000	0.0000	0.0000	0.0000	3.50	0.0000	0.0000	0.0000	0.0000
3.55	0.0000	0.0000	0.0000	0.0000	3.55	0.0000	0.0000	0.0000	0.0000
3.60	0.0000	0.0000	0.0000	0.0000	3.60	0.0000	0.0000	0.0000	0.0000
3.65	0.0000	0.0000	0.0000	0.0000	3.65	0.0000	0.0000	0.0000	0.0000
3.70	0.0000	0.0000	0.0000	0.0000	3.70	0.0000	0.0000	0.0000	0.0000
3.75	0.0000	0.0000	0.0000	0.0000	3.75	0.0000	0.0000	0.0000	0.0000
3.80	0.0000	0.0000	0.0000	0.0000	3.80	0.0000	0.0000	0.0000	0.0000
3.85	0.0000	0.0000	0.0000	0.0000	3.85	0.0000	0.0000	0.0000	0.0000
3.90	0.0000	0.0000	0.0000	0.0000	3.90	0.0000	0.0000	0.0000	0.0000
3.95	0.0000	0.0000	0.0000	0.0000	3.95	0.0000	0.0000	0.0000	0.0000
4.00	0.0000	0.0000	0.0000	0.0000	4.00	0.0000	0.0000	0.0000	0.0000
4.05	0.0000	0.0000	0.0000	0.0000	4.05	0.0000	0.0000	0.0000	0.0000
4.10	0.0000	0.0000	0.0000	0.0000	4.10	0.0000	0.0000	0.0000	0.0000
4.15	0.0000	0.0000	0.0000	0.0000	4.15	0.0000	0.0000	0.0000	0.0000
4.20	0.0000	0.0000	0.0000	0.0000	4.20	0.0000	0.0000	0.0000	0.0000
4.25	0.0000	0.0000	0.0000	0.0000	4.25	0.0000	0.0000	0.0000	0.0000
4.30	0.0000	0.0000	0.0000	0.0000	4.30	0.0000	0.0000	0.0000	0.0000
4.35	0.0000	0.0000	0.0000	0.0000	4.35	0.0000	0.0000	0.0000	0.0000
4.40	0.0000	0.0000	0.0000	0.0000	4.40	0.0000	0.0000	0.0000	0.0000
4.45	0.0000	0.0000	0.0000	0.0000	4.45	0.0000	0.0000	0.0000	0.0000
4.50	0.0000	0.0000	0.0000	0.0000	4.50	0.0000	0.0000	0.0000	0.0000
4.55	0.0000	0.0000	0.0000	0.0000	4.55	0.0000	0.0000	0.0000	0.0000
4.60	0.0000	0.0000	0.0000	0.0000	4.60	0.0000	0.0000	0.0000	0.0000
4.65	0.0000	0.0000	0.0000	0.0000	4.65	0.0000	0.0000	0.0000	0.0000
4.70	0.0000	0.0000	0.0000	0.0000	4.70	0.0000	0.0000	0.0000	0.0000
4.75	0.0000	0.0000	0.0000	0.0000	4.75	0.0000	0.0000	0.0000	0.0000
4.80	0.0000	0.0000	0.0000	0.0000	4.80	0.0000	0.0000	0.0000	0.0000
4.85	0.0000	0.0000	0.0000	0.0000	4.85	0.0000	0.0000	0.0000	0.0000
4.90	0.0000	0.0000	0.0000	0.0000	4.90	0.0000	0.0000	0.0000	0.0000
4.95	0.0000	0.0000	0.0000	0.0000	4.95	0.0000	0.0000	0.0000	0.0000
5.00	0.0000	0.0000	0.0000	0.0000	5.00	0.0000	0.0000	0.0000	0.0000

DELTA = 0.0001

N CONTINUED = 1.5

X= 170 MM  
RE= 9.50410'S (MEASURED P)  
DEL 995= 33.9 MM  
HE= 1.542 (MEASURED P)

V (MM)	CONST PM		MEASURED P		PPFD	PI/PTD
	N	U/E	N	U/E		
0.0	0.0000	0.0000	0.0000	0.0000	0.252	0.252
0.5	0.794	0.938	0.794	0.938	0.252	0.252
1.0	0.810	0.652	0.810	0.652	0.252	0.252
1.5	0.820	0.478	0.820	0.478	0.252	0.252
1.9	0.826	0.342	0.826	0.342	0.252	0.252
2.3	0.829	0.245	0.829	0.245	0.252	0.252
2.7	0.831	0.180	0.831	0.180	0.252	0.252
3.1	0.832	0.135	0.832	0.135	0.252	0.252
3.5	0.833	0.100	0.833	0.100	0.252	0.252
3.9	0.834	0.075	0.834	0.075	0.252	0.252
4.3	0.835	0.055	0.835	0.055	0.252	0.252
4.7	0.836	0.040	0.836	0.040	0.252	0.252
5.1	0.837	0.030	0.837	0.030	0.252	0.252
5.5	0.838	0.022	0.838	0.022	0.252	0.252
5.9	0.839	0.016	0.839	0.016	0.252	0.252
6.3	0.840	0.011	0.840	0.011	0.252	0.252
6.7	0.841	0.007	0.841	0.007	0.252	0.252
7.1	0.842	0.005	0.842	0.005	0.252	0.252
7.5	0.843	0.003	0.843	0.003	0.252	0.252
7.9	0.844	0.002	0.844	0.002	0.252	0.252
8.3	0.845	0.001	0.845	0.001	0.252	0.252
8.7	0.846	0.000	0.846	0.000	0.252	0.252
9.1	0.847	0.000	0.847	0.000	0.252	0.252
9.5	0.848	0.000	0.848	0.000	0.252	0.252
9.9	0.849	0.000	0.849	0.000	0.252	0.252
10.3	0.850	0.000	0.850	0.000	0.252	0.252
10.7	0.851	0.000	0.851	0.000	0.252	0.252
11.1	0.852	0.000	0.852	0.000	0.252	0.252
11.5	0.853	0.000	0.853	0.000	0.252	0.252
11.9	0.854	0.000	0.854	0.000	0.252	0.252
12.3	0.855	0.000	0.855	0.000	0.252	0.252
12.7	0.856	0.000	0.856	0.000	0.252	0.252
13.1	0.857	0.000	0.857	0.000	0.252	0.252
13.5	0.858	0.000	0.858	0.000	0.252	0.252
13.9	0.859	0.000	0.859	0.000	0.252	0.252
14.3	0.860	0.000	0.860	0.000	0.252	0.252
14.7	0.861	0.000	0.861	0.000	0.252	0.252
15.1	0.862	0.000	0.862	0.000	0.252	0.252
15.5	0.863	0.000	0.863	0.000	0.252	0.252
15.9	0.864	0.000	0.864	0.000	0.252	0.252
16.3	0.865	0.000	0.865	0.000	0.252	0.252
16.7	0.866	0.000	0.866	0.000	0.252	0.252
17.1	0.867	0.000	0.867	0.000	0.252	0.252
17.5	0.868	0.000	0.868	0.000	0.252	0.252
17.9	0.869	0.000	0.869	0.000	0.252	0.252
18.3	0.870	0.000	0.870	0.000	0.252	0.252
18.7	0.871	0.000	0.871	0.000	0.252	0.252
19.1	0.872	0.000	0.872	0.000	0.252	0.252
19.5	0.873	0.000	0.873	0.000	0.252	0.252
19.9	0.874	0.000	0.874	0.000	0.252	0.252
20.3	0.875	0.000	0.875	0.000	0.252	0.252
20.7	0.876	0.000	0.876	0.000	0.252	0.252
21.1	0.877	0.000	0.877	0.000	0.252	0.252
21.5	0.878	0.000	0.878	0.000	0.252	0.252
21.9	0.879	0.000	0.879	0.000	0.252	0.252
22.3	0.880	0.000	0.880	0.000	0.252	0.252
22.7	0.881	0.000	0.881	0.000	0.252	0.252
23.1	0.882	0.000	0.882	0.000	0.252	0.252
23.5	0.883	0.000	0.883	0.000	0.252	0.252
23.9	0.884	0.000	0.884	0.000	0.252	0.252
24.3	0.885	0.000	0.885	0.000	0.252	0.252
24.7	0.886	0.000	0.886	0.000	0.252	0.252
25.1	0.887	0.000	0.887	0.000	0.252	0.252
25.5	0.888	0.000	0.888	0.000	0.252	0.252
25.9	0.889	0.000	0.889	0.000	0.252	0.252
26.3	0.890	0.000	0.890	0.000	0.252	0.252
26.7	0.891	0.000	0.891	0.000	0.252	0.252
27.1	0.892	0.000	0.892	0.000	0.252	0.252
27.5	0.893	0.000	0.893	0.000	0.252	0.252
27.9	0.894	0.000	0.894	0.000	0.252	0.252
28.3	0.895	0.000	0.895	0.000	0.252	0.252
28.7	0.896	0.000	0.896	0.000	0.252	0.252
29.1	0.897	0.000	0.897	0.000	0.252	0.252
29.5	0.898	0.000	0.898	0.000	0.252	0.252
29.9	0.899	0.000	0.899	0.000	0.252	0.252
30.3	0.900	0.000	0.900	0.000	0.252	0.252
30.7	0.901	0.000	0.901	0.000	0.252	0.252
31.1	0.902	0.000	0.902	0.000	0.252	0.252
31.5	0.903	0.000	0.903	0.000	0.252	0.252
31.9	0.904	0.000	0.904	0.000	0.252	0.252
32.3	0.905	0.000	0.905	0.000	0.252	0.252
32.7	0.906	0.000	0.906	0.000	0.252	0.252
33.1	0.907	0.000	0.907	0.000	0.252	0.252
33.5	0.908	0.000	0.908	0.000	0.252	0.252
33.9	0.909	0.000	0.909	0.000	0.252	0.252
34.3	0.910	0.000	0.910	0.000	0.252	0.252
34.7	0.911	0.000	0.911	0.000	0.252	0.252
35.1	0.912	0.000	0.912	0.000	0.252	0.252
35.5	0.913	0.000	0.913	0.000	0.252	0.252
35.9	0.914	0.000	0.914	0.000	0.252	0.252
36.3	0.915	0.000	0.915	0.000	0.252	0.252
36.7	0.916	0.000	0.916	0.000	0.252	0.252
37.1	0.917	0.000	0.917	0.000	0.252	0.252
37.5	0.918	0.000	0.918	0.000	0.252	0.252
37.9	0.919	0.000	0.919	0.000	0.252	0.252
38.3	0.920	0.000	0.920	0.000	0.252	0.252
38.7	0.921	0.000	0.921	0.000	0.252	0.252
39.1	0.922	0.000	0.922	0.000	0.252	0.252
39.5	0.923	0.000	0.923	0.000	0.252	0.252
39.9	0.924	0.000	0.924	0.000	0.252	0.252
40.3	0.925	0.000	0.925	0.000	0.252	0.252
40.7	0.926	0.000	0.926	0.000	0.252	0.252
41.1	0.927	0.000	0.927	0.000	0.252	0.252
41.5	0.928	0.000	0.928	0.000	0.252	0.252
41.9	0.929	0.000	0.929	0.000	0.252	0.252
42.3	0.930	0.000	0.930	0.000	0.252	0.252
42.7	0.931	0.000	0.931	0.000	0.252	0.252
43.1	0.932	0.000	0.932	0.000	0.252	0.252
43.5	0.933	0.000	0.933	0.000	0.252	0.252
43.9	0.934	0.000	0.934	0.000	0.252	0.252
44.3	0.935	0.000	0.935	0.000	0.252	0.252
44.7	0.936	0.000	0.936	0.000	0.252	0.252
45.1	0.937	0.000	0.937	0.000	0.252	0.252
45.5	0.938	0.000	0.938	0.000	0.252	0.252
45.9	0.939	0.000	0.939	0.000	0.252	0.252
46.3	0.940	0.000	0.940	0.000	0.252	0.252
46.7	0.941	0.000	0.941	0.000	0.252	0.252
47.1	0.942	0.000	0.942	0.000	0.252	0.252
47.5	0.943	0.000	0.943	0.000	0.252	0.252
47.9	0.944	0.000	0.944	0.000	0.252	0.252
48.3	0.945	0.000	0.945	0.000	0.252	0.252
48.7	0.946	0.000	0.946	0.000	0.252	0.252
49.1	0.947	0.000	0.947	0.000	0.252	0.252
49.5	0.948	0.000	0.948	0.000	0.252	0.252
49.9	0.949	0.000	0.949	0.000	0.252	0.252
50.3	0.950	0.000	0.950	0.000	0.252	0.252
50.7	0.951	0.000	0.951	0.000	0.252	0.252
51.1	0.952	0.000	0.952	0.000	0.252	0.252
51.5	0.953	0.000	0.953	0.000	0.252	0.252
51.9	0.954	0.000	0.954	0.000	0.252	0.252
52.3	0.955	0.000	0.955	0.000	0.252	0.252
52.7	0.956	0.000	0.956	0.000	0.252	0.252
53.1	0.957	0.000	0.957	0.000	0.252	0.252
53.5	0.958	0.000	0.958	0.000	0.252	0.252
53.9	0.959	0.000	0.959	0.000	0.252	0.252
54.3	0.960	0.000	0.960	0.000	0.252	0.252
54.7	0.961	0.000	0.961	0.000	0.252	0.252
55.1	0.962	0.000	0.962	0.000	0.252	0.252
55.5	0.963	0.000	0.963	0.000	0.252	0.252
55.9	0.964	0.000	0.964	0.000	0.252	0.252
56.3	0.965	0.000	0.965	0.000	0.252	0.252
56.7	0.966	0.000	0.966	0.000	0.252	0.252
57.1	0.967	0.000	0.967	0.000	0.252	0.252
57.5	0.968	0.000	0.968	0.000	0.252	0.252
57.9	0.969	0.000	0.969	0.000	0.252	0.252
58.3	0.970	0.000	0.970	0.000	0.252	0.252
58.7	0.971	0.000	0.971	0.000	0.252	0.252
59.1	0.972	0.000	0.972	0.000	0.252	0.252
59.5	0.973	0.000	0.973	0.000	0.252	0.252
59.9	0.974	0.000	0.974	0.000	0.252	0.252
60.3	0.975	0.000	0.975	0.000	0.252	0.252
60.7	0.976	0.000	0.976	0.000	0.252	0.252
61.1	0.977	0.000	0.977	0.000	0.252	0.252
61.5	0.978	0.000	0.978	0.000	0.252	0.252
61.9	0.979	0.000	0.979	0.000	0.252	0.252
62.3	0.980	0.000	0.980	0.000	0.252	0.252
62.7	0.981	0.000	0.981	0.000	0.252	0.252
63.1	0.982	0.000	0.982	0.000	0.252	0.252
63.5	0.983	0.000	0.983	0.000	0.252	0.252
63.9	0.984	0.000	0.984	0.000	0.252	0.252
64.3	0.985	0.000	0.985	0.000	0.252	0.252
64.7	0.986	0.000	0.986	0.000	0.252	0.252
65.1	0.987	0.000	0.987	0.000	0.2	



Table 2. (continued)

N (OBSERVED) = 15

X = 22 MI DEL 95% - 24.7 MI  
REPAIRS 40417'S (MEASURED P) RE = 1.272 (MEASURED P)

Y (MI) N UAVE N UAVE P P10 P100

Table with 6 columns: Y (MI), N, UAVE, N, UAVE, P, P10, P100. Rows 1-200 showing data for 22 miles.

N (OBSERVED) = 15

X = 23 MI DEL 95% - 26.8 MI  
REPAIRS 41417'S (MEASURED P) RE = 1.233 (MEASURED P)

Y (MI) N UAVE N UAVE P P10 P100

Table with 6 columns: Y (MI), N, UAVE, N, UAVE, P, P10, P100. Rows 1-200 showing data for 23 miles.

N (OBSERVED) = 15

X = 24 MI DEL 95% - 28.3 MI  
REPAIRS 42417'S (MEASURED P) RE = 1.198 (MEASURED P)

Y (MI) N UAVE N UAVE P P10 P100

Table with 6 columns: Y (MI), N, UAVE, N, UAVE, P, P10, P100. Rows 1-200 showing data for 24 miles.

N (OBSERVED) = 15

X = 24 MI DEL 95% - 24.5 MI  
REPAIRS 43417'S (MEASURED P) RE = 1.155 (MEASURED P)

Y (MI) N UAVE N UAVE P P10 P100

Table with 6 columns: Y (MI), N, UAVE, N, UAVE, P, P10, P100. Rows 1-200 showing data for 24 miles.

R (CONTINUED) = 1.5  
A= 270 MW  
DEL 955-04.5 MW  
RE 1-102 (REQUIRED P)

Table with columns: Y (MW), CONST MW, MEASURED P, UAVE, PPTO, PI, PPTO. Rows 1-280.

R (CONTINUED) = 1.5  
A= 222 MW  
DEL 955-04.9 MW  
RE 1-101 (REQUIRED P)

Table with columns: Y (MW), CONST MW, MEASURED P, UAVE, PPTO, PI, PPTO. Rows 1-280.

R (CONTINUED) = 1.5  
A= 225 MW  
DEL 955-78.0 MW  
RE 1-104 (REQUIRED P)

Table with columns: Y (MW), CONST MW, MEASURED P, UAVE, PPTO, PI, PPTO. Rows 1-280.

R (CONTINUED) = 1.5  
A= 230 MW  
DEL 955-09.6 MW  
RE 1-101 (REQUIRED P)

Table with columns: Y (MW), CONST MW, MEASURED P, UAVE, PPTO, PI, PPTO. Rows 1-280.















82099

Table 3 (continued)

$M_0 = 1.373 \quad Re/m = 3.67 \times 10^6$

X DEL 95 MM	CONSTANT PM										MEASURED P										CALCULATED P									
	DEL 95 MM	RE/M X10 <sup>-6</sup>	ME MM	DEL* MM	THETA MM	H MM	HBR MM	HI MM	DELE MM	OPP X10 <sup>-3</sup>	CF X10 <sup>-3</sup>	RE/M X10 <sup>-6</sup>	ME MM	DEL* MM	THETA MM	H MM	HBR MM	HI MM	CF X10 <sup>-3</sup>	DELBR MM	THETABR MM	H MM	HBR MM							
-712.0	34.1	1.64	1.413	6.516	2.927	2.227	1.366	9.425	5.26	2.091	2.198	1.64	1.413	6.516	2.927	2.227	1.366	9.425	2.198	6.516	2.927	2.227	1.366	9.425	2.198					
-710.0	34.1	1.61	1.414	6.595	2.961	2.227	1.365	9.289	5.32	2.093	2.189	1.61	1.414	6.594	2.961	2.227	1.365	9.290	2.189	6.594	2.961	2.227	1.365	9.290	2.189					
-220.0	38.7	1.64	1.395	7.542	3.402	2.217	1.316	9.160	6.09	2.019	2.092	1.64	1.395	7.542	3.402	2.217	1.316	9.160	2.092	7.542	3.402	2.217	1.316	9.160	2.092					
-222.0	39.4	1.67	1.377	8.100	3.661	2.213	1.329	8.590	6.53	1.894	1.978	1.67	1.377	8.100	3.661	2.213	1.329	8.590	1.978	8.100	3.661	2.213	1.329	8.590	1.978					
-191.0	39.4	1.67	1.373	8.179	3.699	2.211	1.332	8.441	6.59	1.965	1.966	1.67	1.373	8.179	3.699	2.211	1.332	8.441	1.966	8.179	3.699	2.211	1.332	8.441	1.966					
-173.0	39.2	1.68	1.370	8.345	3.767	2.215	1.338	8.191	6.70	1.891	1.939	1.68	1.370	8.345	3.767	2.215	1.338	8.191	1.939	8.345	3.767	2.215	1.338	8.191	1.939					
-148.0	40.4	1.65	1.350	8.647	3.913	2.210	1.352	8.114	6.93	1.819	1.879	1.65	1.350	8.647	3.913	2.210	1.352	8.114	1.879	8.647	3.913	2.210	1.352	8.114	1.879					
-123.0	39.9	1.61	1.279	9.479	4.277	2.216	1.423	7.112	7.45	1.448	1.501	1.61	1.279	9.479	4.277	2.216	1.423	7.113	1.501	9.479	4.277	2.216	1.423	7.113	1.501					
-104.0	41.5	1.64	1.232	10.935	4.820	2.269	1.507	6.341	8.24	1.149	1.191	1.64	1.232	10.935	4.820	2.269	1.507	6.341	1.191	10.935	4.820	2.269	1.507	6.341	1.191					
-76.0	44.3	1.65	1.194	12.790	5.461	2.342	1.600	5.769	9.17	0.899	0.954	1.65	1.194	12.790	5.461	2.342	1.600	5.770	0.954	12.790	5.461	2.342	1.600	5.770	0.954					
-58.0	49.1	1.65	1.155	15.154	6.144	2.467	1.736	5.525	10.10	0.710	0.669	1.65	1.155	15.154	6.144	2.467	1.736	5.525	0.669	15.154	6.144	2.467	1.736	5.525	0.669					
-27.0	53.4	1.62	1.129	17.855	6.814	2.620	1.885	5.216	10.90	0.602	0.555	1.62	1.129	17.855	6.814	2.620	1.885	5.216	0.555	17.855	6.814	2.620	1.885	5.216	0.555					
-3.0	54.6	1.63	1.103	20.402	7.382	2.764	2.027	4.632	11.70	0.470	0.410	1.63	1.103	20.402	7.382	2.764	2.027	4.632	0.410	20.402	7.382	2.764	2.027	4.632	0.410					
22.0	57.4	1.67	1.065	22.618	7.834	2.807	2.147	4.440	12.28	0.304	0.312	1.67	1.065	22.618	7.834	2.807	2.147	4.440	0.312	22.618	7.834	2.807	2.147	4.440	0.312					
71.0	61.0	1.65	1.055	25.587	8.417	3.040	2.304	4.207	13.02	0.344	0.283	1.65	1.055	25.587	8.417	3.040	2.304	4.207	0.283	25.587	8.417	3.040	2.304	4.207	0.283					
120.0	63.4	1.63	1.033	26.934	8.839	3.047	2.335	4.126	13.50	0.311	0.351	1.63	1.033	26.934	8.839	3.047	2.335	4.126	0.351	26.934	8.839	3.047	2.335	4.126	0.351					
169.0	65.1	1.64	1.023	27.107	9.233	2.936	2.255	4.115	14.22	0.414	0.373	1.64	1.023	27.107	9.233	2.936	2.255	4.115	0.373	27.107	9.233	2.936	2.255	4.115	0.373					
267.0	65.5	1.63	1.003	26.296	9.721	2.705	2.065	4.033	15.11	0.540	0.519	1.63	1.003	26.296	9.721	2.705	2.065	4.033	0.519	26.296	9.721	2.705	2.065	4.033	0.519					
463.0	71.0	1.59	0.972	25.073	10.602	2.365	1.830	4.520	16.36	0.794	0.843	1.59	0.972	25.073	10.602	2.365	1.830	4.521	0.843	25.073	10.602	2.365	1.830	4.521	0.843					
756.0	82.6	1.56	0.940	21.200	11.266	2.059	1.600	5.273	18.71	1.168	1.190	1.56	0.940	21.200	11.266	2.059	1.600	5.273	1.190	21.200	11.266	2.059	1.600	5.273	1.190					
1062.0	92.7	1.54	0.916	22.329	11.040	1.806	1.471	5.943	20.22	1.444	1.462	1.54	0.916	22.329	11.040	1.806	1.471	5.943	1.462	22.329	11.040	1.806	1.471	5.943	1.462					
1204.0	101.4	1.50	0.905	21.752	12.137	1.792	1.399	6.562	21.00	1.704	1.700	1.50	0.905	21.752	12.137	1.792	1.399	6.562	1.700	21.752	12.137	1.792	1.399	6.562	1.700					
1776.0	117.6	1.43	0.878	21.700	12.916	1.606	1.327	7.419	22.08	1.998	1.975	1.43	0.878	21.700	12.916	1.606	1.327	7.419	1.975	21.700	12.916	1.606	1.327	7.419	1.975					
2267.0	129.2	1.39	0.861	22.111	13.503	1.620	1.280	7.804	24.32	2.131	2.119	1.39	0.861	22.111	13.503	1.620	1.280	7.804	2.119	22.111	13.503	1.620	1.280	7.804	2.119					
2752.0	137.4	1.33	0.839	22.253	14.000	1.509	1.270	8.225	25.26	2.105	2.109	1.33	0.839	22.253	14.000	1.509	1.270	8.225	2.109	22.253	14.000	1.509	1.270	8.225	2.109					

Table 3 (continued)

$$M_0 = 1.386 \quad Re/m = 10.0 \times 10^6$$

CONSTANT PM										MEASURED P										CALCULATED P										
X	DEL 955	RE/M	ME	DEL*	THETA	H	HEAR	HI	DELE	OPP	OF	RE/M	ME	DEL*	THETA	H	HEAR	HI	OF	DELE	THETA	H	HEAR	HI	OF	DELE	THETA	H	HEAR	
MM	MM	X10-6	MM	MM	MM	MM	MM	MM	MM	X10+3	X10+3	X10-6	MM	MM	MM	MM	MM	MM	X10+3	MM	MM	MM	MM	MM	MM	MM	MM	MM	MM	MM
-72.0	32.4	9.92	1.420	5.660	2.504	2.190	1.273	18.348	4.68	1.891	1.787	9.92	1.420	5.660	2.504	2.190	1.273	18.348	4.68	1.891	1.787	5.660	2.504	2.190	1.273	5.660	2.504	2.190	1.273	
-63.0	33.0	9.97	1.425	5.819	2.633	2.193	1.271	18.244	4.81	1.894	1.797	9.97	1.425	5.819	2.633	2.193	1.271	18.244	4.81	1.894	1.797	5.819	2.633	2.193	1.271	5.819	2.633	2.193	1.271	
-53.0	34.2	9.96	1.417	6.086	2.779	2.190	1.276	18.115	5.03	1.837	1.757	9.96	1.417	6.086	2.779	2.190	1.276	18.115	5.03	1.837	1.757	6.086	2.779	2.190	1.276	6.086	2.779	2.190	1.276	
-43.0	34.4	9.95	1.414	6.292	2.873	2.190	1.279	9.784	5.20	1.823	1.729	9.95	1.414	6.292	2.873	2.190	1.279	9.784	5.20	1.823	1.729	6.292	2.873	2.190	1.279	6.292	2.873	2.190	1.279	
-34.0	35.4	9.96	1.408	6.466	2.970	2.177	1.275	9.743	5.37	1.816	1.776	9.96	1.408	6.466	2.970	2.177	1.275	9.743	5.37	1.816	1.776	6.466	2.970	2.177	1.275	6.466	2.970	2.177	1.275	
-25.0	35.1	9.99	1.406	6.600	3.028	2.180	1.279	9.413	5.47	1.818	1.746	9.99	1.406	6.600	3.028	2.180	1.279	9.413	5.47	1.818	1.746	6.600	3.028	2.180	1.279	6.600	3.028	2.180	1.279	
-16.0	36.6	10.00	1.396	6.742	3.109	2.169	1.280	9.604	5.62	1.779	1.766	10.00	1.396	6.742	3.109	2.169	1.280	9.604	5.62	1.779	1.766	6.742	3.109	2.169	1.280	6.742	3.109	2.169	1.280	
-28.0	37.0	10.03	1.386	6.890	3.158	2.158	1.282	9.586	5.73	1.750	1.733	10.03	1.386	6.890	3.158	2.158	1.282	9.586	5.73	1.750	1.733	6.890	3.158	2.158	1.282	6.890	3.158	2.158	1.282	
-19.0	37.5	10.03	1.381	7.003	3.238	2.162	1.290	9.417	5.83	1.695	1.682	10.04	1.384	7.019	3.243	2.164	1.291	9.398	1.681	6.954	3.214	2.098	1.284	6.954	3.214	2.098	1.284			
-17.0	38.6	10.02	1.373	7.029	3.266	2.152	1.293	9.655	5.87	1.738	1.679	10.04	1.387	7.058	3.274	2.156	1.295	9.624	1.673	7.059	3.274	2.156	1.288	7.059	3.274	2.156	1.288			
-14.0	37.1	10.02	1.341	7.211	3.379	2.134	1.314	8.946	6.04	1.614	1.549	10.06	1.375	7.287	3.403	2.141	1.319	8.782	1.533	7.251	3.447	2.103	1.307	7.251	3.447	2.103	1.307			
-12.0	36.3	9.96	1.307	7.471	3.526	2.119	1.337	8.177	6.32	1.427	1.453	10.01	1.355	7.653	3.590	2.138	1.353	8.001	1.466	7.547	3.729	2.024	1.321	7.547	3.729	2.024	1.321			
-9.0	38.7	10.14	1.258	8.758	4.004	2.145	1.406	7.332	7.12	1.127	1.153	10.29	1.279	10.246	4.627	2.215	1.307	6.561	0.892	10.133	4.861	2.065	1.461	10.133	4.861	2.065	1.461			
-7.0	40.6	10.21	1.210	10.115	4.579	2.209	1.497	6.658	7.83	0.880	0.917	10.27	1.213	12.694	5.468	2.321	1.636	5.762	0.665	12.687	5.565	2.280	1.575	12.687	5.565	2.280	1.575			
-4.0	44.2	10.20	1.157	12.610	5.440	2.318	1.627	5.807	9.09	0.683	0.683	10.25	1.123	15.640	6.137	2.548	1.853	5.371	0.296	15.761	5.725	2.753	1.819	15.761	5.725	2.753	1.819			
-2.0	48.6	10.23	1.107	15.648	6.131	2.552	1.856	5.375	9.94	0.322	0.299	10.10	1.029	18.374	6.721	2.734	2.021	4.869	0.333	18.374	6.721	2.734	2.021	18.374	6.721	2.734	2.021			
1.0	51.1	10.20	1.061	18.261	6.748	2.706	1.997	4.867	10.79	0.206	0.321	9.95	1.015	22.066	7.697	2.971	2.264	4.344	0.228	22.066	7.697	2.971	2.264	22.066	7.697	2.971	2.264			
50.0	56.3	10.01	1.039	22.020	7.703	2.962	2.256	4.346	11.94	0.194	0.224	9.92	0.995	24.687	8.160	3.016	2.333	4.227	0.244	24.687	8.160	3.016	2.333	24.687	8.160	3.016	2.333			
140.0	60.5	9.97	1.012	24.694	8.161	3.015	2.330	4.127	13.17	0.257	0.264	9.92	0.988	25.124	8.572	2.931	2.281	4.127	0.266	25.124	8.572	2.931	2.281	25.124	8.572	2.931	2.281			
197.0	61.0	9.94	0.995	25.126	8.572	2.931	2.281	4.000	13.66	0.218	0.311	9.92	0.984	24.855	8.858	2.896	2.189	4.000	0.311	24.855	8.858	2.896	2.189	24.855	8.858	2.896	2.189			
246.0	61.3	9.93	0.973	24.200	9.097	2.669	2.065	4.063	14.15	0.400	0.378	9.92	0.973	24.279	9.097	2.669	2.065	4.070	0.378	24.279	9.097	2.669	2.065	24.279	9.097	2.669	2.065			
295.0	61.7	9.89	0.963	23.927	9.348	2.560	2.003	4.041	14.63	0.501	0.518	9.89	0.963	23.927	9.348	2.560	2.003	4.041	0.518	23.927	9.348	2.560	2.003	23.927	9.348	2.560	2.003			
342.0	63.5	9.89	0.956	23.492	9.499	2.473	1.936	4.212	14.96	0.533	0.508	9.89	0.956	23.492	9.499	2.473	1.936	4.212	0.508	23.492	9.499	2.473	1.936	23.492	9.499	2.473	1.936			
444.0	66.2	9.84	0.942	22.838	9.867	2.315	1.815	4.394	15.78	0.690	0.604	9.84	0.942	22.838	9.867	2.315	1.815	4.394	0.604	22.838	9.867	2.315	1.815	22.838	9.867	2.315	1.815			
539.0	70.2	9.80	0.931	21.976	10.065	2.183	1.713	4.791	16.37	0.819	0.821	9.88	0.931	21.976	10.065	2.183	1.713	4.791	0.821	21.976	10.065	2.183	1.713	21.976	10.065	2.183	1.713			
637.0	74.0	9.76	0.921	21.442	10.373	2.077	1.631	5.091	17.03	0.940	0.920	9.76	0.921	21.442	10.373	2.077	1.631	5.091	0.920	21.442	10.373	2.077	1.631	21.442	10.373	2.077	1.631			
755.0	76.7	9.74	0.912	20.997	10.583	1.999	1.571	5.304	17.53	1.107	1.011	9.74	0.912	20.997	10.583	1.999	1.571	5.304	1.011	20.997	10.583	1.999	1.571	20.997	10.583	1.999	1.571			
833.0	80.6	9.77	0.903	20.469	10.614	1.928	1.518	5.665	17.91	1.185	1.100	9.77	0.903	20.469	10.614	1.928	1.518	5.665	1.100	20.469	10.614	1.928	1.518	20.469	10.614	1.928	1.518			
931.0	86.1	9.57	0.895	20.146	10.729	1.878	1.400	6.147	18.26	1.247	1.185	9.57	0.895	20.146	10.729	1.878	1.400	6.147	1.185	20.146	10.729	1.878	1.400	20.146	10.729	1.878	1.400			
1027.0	89.5	9.82	0.890	20.118	10.978	1.833	1.445	6.320	18.05	1.262	1.210	9.82	0.890	20.118	10.977	1.833	1.445	6.320	1.210	20.118	10.977	1.833	1.445	20.118	10.977	1.833	1.445			
1755.0	107.1	9.24	0.856	19.400	11.073	1.634	1.297	7.306	21.28	1.067	1.794	9.24	0.856	19.400	11.073	1.634	1.297	7.306	1.794	19.400	11.073	1.634	1.297	19.400	11.073	1.634	1.297			
2244.0	113.9	9.10	0.832	18.988	11.804	1.575	1.262	8.075	21.28	1.900	1.948	9.10	0.832	18.988	11.804	1.575	1.262	8.075	1.948	18.988	11.804	1.575	1.262	18.988	11.804	1.575	1.262			
2733.0	116.3	8.92	0.808	17.901	11.670	1.534	1.241	8.432	21.22	2.023	1.935	8.92	0.808	17.901	11.670	1.534	1.241	8.432	1.935	17.901	11.670	1.534	1.241	17.901	11.670	1.534	1.241			
2933.0	118.1	8.80	0.799	17.693	11.617	1.523	1.237	8.643	21.17	2.001	1.941	8.80	0.799	17.693	11.617	1.523	1.237	8.643	1.941	17.693	11.617	1.523	1.237	17.693	11.617	1.523	1.237			



Table 3 (continued)

$$M_0 = 1.531 \quad Re/m = 6.47 \times 10^6$$

X MM	CONSTANT PM						MEASURED P						CALCULATED P														
	DEL 955 MM	RE/M X10 <sup>-6</sup>	ME MM	DEL* MM	TETA MM	H MM	HBR MM	HI MM	DEL MM	CF X10 <sup>-3</sup>	RE/M X10 <sup>-6</sup>	ME MM	DEL* MM	TETA MM	H MM	HBR MM	HI MM	DEL MM	CF X10 <sup>-3</sup>	RE/M X10 <sup>-6</sup>	ME MM	DEL* MM	TETA MM	H MM	HBR MM		
-315.0	33.4	6.45	1.544	6.492	2.746	2.364	1.278	9.799	4.97	1.944	1.959	6.45	1.544	6.492	2.746	2.364	1.278	9.799	1.959	6.45	1.544	6.492	2.746	2.364	1.278	9.799	1.959
-324.0	34.7	6.45	1.532	6.938	2.941	2.359	1.286	9.439	5.31	1.869	1.865	6.45	1.532	6.938	2.941	2.359	1.286	9.439	1.865	6.45	1.532	6.938	2.941	2.359	1.286	9.439	1.865
-371.0	36.5	6.47	1.531	7.128	3.023	2.358	1.286	9.716	5.46	1.854	1.888	6.47	1.531	7.128	3.023	2.358	1.286	9.716	1.888	6.47	1.531	7.128	3.023	2.358	1.286	9.716	1.888
-322.0	36.6	6.49	1.594	7.349	3.156	2.329	1.256	9.268	5.68	1.776	1.812	6.51	1.522	7.457	3.188	2.319	1.304	9.141	1.865	6.51	1.522	7.457	3.188	2.319	1.304	9.141	1.865
-399.0	37.0	6.45	1.461	7.457	3.266	2.283	1.317	9.044	5.83	1.640	1.697	6.50	1.527	7.868	3.393	2.319	1.346	8.585	1.673	6.50	1.527	7.868	3.393	2.319	1.346	8.585	1.673
-171.0	37.5	6.39	1.423	8.237	3.663	2.249	1.459	7.989	6.32	0.925	1.048	6.51	1.495	8.932	3.981	2.290	1.491	7.323	1.002	6.51	1.495	8.932	3.981	2.290	1.491	7.323	1.002
-148.0	36.7	6.50	1.244	10.313	4.122	2.582	1.694	6.402	6.93	0.212	0.332	6.54	1.288	10.392	4.148	2.585	1.692	6.342	0.326	6.54	1.288	10.392	4.148	2.585	1.692	6.342	0.326
-124.0	41.9	6.66	1.239	14.015	5.000	2.883	1.918	5.577	8.19	0.000	0.000	6.68	1.259	14.058	5.016	2.883	1.918	5.551	0.000	6.68	1.259	14.058	5.016	2.883	1.918	5.551	0.000
-101.0	46.9	6.66	1.287	17.434	5.592	3.118	2.189	5.269	8.98	0.000	0.000	6.70	1.294	17.459	5.602	3.116	2.156	5.255	0.000	6.70	1.294	17.459	5.602	3.116	2.156	5.255	0.000
-76.0	52.1	6.69	1.186	21.686	5.951	3.631	2.614	5.124	9.32	0.000	0.000	6.73	1.182	21.628	5.960	3.627	2.621	5.114	0.000	6.73	1.182	21.628	5.960	3.627	2.621	5.114	0.000
-52.0	60.6	6.72	1.164	27.952	6.744	4.144	3.048	4.841	10.45	0.000	0.000	6.73	1.182	27.785	6.865	4.036	2.978	4.792	0.000	6.73	1.182	27.785	6.865	4.036	2.978	4.792	0.000
-27.0	67.4	6.67	1.152	33.348	7.341	4.543	3.388	4.609	11.26	0.000	0.000	6.66	1.141	33.278	7.689	4.381	3.176	4.567	0.000	6.66	1.141	33.278	7.689	4.381	3.176	4.567	0.000
22.0	72.9	6.66	1.134	40.028	7.276	5.611	4.259	4.408	11.41	0.000	0.000	6.58	1.062	40.044	7.689	5.288	3.893	4.273	0.000	6.58	1.062	40.044	7.689	5.288	3.893	4.273	0.000
71.0	77.9	6.64	1.118	44.882	7.452	6.023	4.618	4.431	11.70	0.000	0.000	6.57	1.057	43.643	8.318	5.252	3.965	4.122	0.000	6.57	1.057	43.643	8.318	5.252	3.965	4.122	0.000
128.0	82.1	6.64	1.102	46.649	8.003	5.771	4.448	4.386	12.52	0.000	0.000	6.59	1.062	45.698	8.882	5.191	3.959	4.137	0.000	6.59	1.062	45.698	8.882	5.191	3.959	4.137	0.000
167.0	86.2	6.62	1.088	47.442	8.576	5.532	4.282	4.520	13.12	0.000	0.000	6.58	1.051	46.522	9.277	5.015	3.946	4.277	0.000	6.58	1.051	46.522	9.277	5.015	3.946	4.277	0.000
218.0	90.0	6.63	1.074	46.767	10.346	4.520	3.486	4.179	15.29	0.000	0.000	6.59	1.042	46.755	10.342	4.521	3.476	4.182	0.000	6.59	1.042	46.755	10.342	4.521	3.476	4.182	0.000
267.0	92.0	6.62	1.059	45.628	11.002	4.144	3.281	4.211	16.33	0.000	0.000	6.58	1.038	45.623	11.000	4.144	3.195	4.212	0.000	6.58	1.038	45.623	11.000	4.144	3.195	4.212	0.000
463.0	101.4	6.55	1.080	42.753	13.788	3.181	2.408	4.254	20.94	0.211	0.211	6.55	1.065	42.752	13.788	3.181	2.408	4.254	0.211	6.55	1.065	42.752	13.788	3.181	2.408	4.254	0.211
756.0	113.4	6.46	0.953	37.272	16.038	2.325	1.814	4.749	25.68	0.648	0.597	6.46	0.953	37.272	16.038	2.325	1.814	4.749	0.597	6.46	0.953	37.272	16.038	2.325	1.814	4.749	0.597
1050.0	127.4	6.38	0.911	33.889	16.846	2.012	1.503	5.551	27.92	0.990	1.007	6.38	0.911	33.889	16.846	2.012	1.503	5.551	1.007	6.38	0.911	33.889	16.846	2.012	1.503	5.551	1.007
1286.0	136.9	6.26	0.889	32.294	17.322	1.864	1.473	6.039	29.31	1.286	1.233	6.26	0.889	32.294	17.322	1.864	1.473	6.039	1.233	6.26	0.889	32.294	17.322	1.864	1.473	6.039	1.233
1776.0	153.1	6.08	0.856	31.245	18.312	1.706	1.360	6.654	32.06	1.652	1.593	6.08	0.856	31.245	18.312	1.706	1.360	6.654	1.593	6.08	0.856	31.245	18.312	1.706	1.360	6.654	1.593
2265.0	167.9	5.93	0.823	30.472	18.789	1.629	1.315	7.346	33.07	1.764	1.670	5.93	0.823	30.471	18.789	1.629	1.315	7.346	1.670	5.93	0.823	30.471	18.789	1.629	1.315	7.346	1.670
2752.0	175.4	5.77	0.796	29.015	18.454	1.572	1.283	7.932	33.23	1.812	1.744	5.77	0.796	29.015	18.454	1.572	1.283	7.932	1.744	5.77	0.796	29.015	18.454	1.572	1.283	7.932	1.744
2900.0	181.5	5.69	0.788	28.965	18.661	1.552	1.270	8.174	33.70	1.888	1.830	5.69	0.788	28.965	18.661	1.552	1.270	8.174	1.830	5.69	0.788	28.965	18.661	1.552	1.270	8.174	1.830





LIST OF SYMBOLS

(Bracketed symbols represent computer headings)

A,B		'law of the wall' constants in equation (28)
$C_f$	(CF)	local skin friction coefficient obtained from East's prediction of the law of the wall; see equation (6)
$C_{f_p}$	(CFP)	local skin friction coefficient based on Patel's Preston tube calibration as formulated by Head and Vasanta Ram; see section 3.3
$C_p$		pressure coefficient based on local conditions
d		probe diameter
D		constant in equation (6)
$E_f$		equilibrium factor in equation (36)
$E_p$		equilibrium factor in equation (37)
F		compressibility factor in equation (6)
G		Clauser shape parameter in equation (32)
h		distance of probe centre line above wall
H	(H)	boundary layer shape parameter in equations (9) and (13)
$\bar{H}$	(HBAR)	boundary layer shape parameter in equations (10), (14) and (20)
$H_1$	(HI)	boundary layer shape parameter $\frac{\delta_{0.995} - \delta^*}{\theta}$
J,K		normalised 'law of the wake' constants in equation (41)
l		effective turbulent run ahead of normal part of shock wave
M	(M)	Mach number
	(ME)	Mach number at edge of boundary layer
p	(P)	static pressure
	(PI)	equivalent inviscid static pressure
$P_{t0}$	(PTO)	tunnel total pressure
$P_{t1}$		local total pressure
Re	(RE)	unit Reynolds number; see equation (3)
T		temperature in Kelvins
	(TO)	total temperature in Kelvins
U		horizontal component of velocity
	(UE)	horizontal component of velocity at edge of boundary layer
$\Delta U$		wake component of velocity profile
$U_\tau$		friction velocity

LIST OF SYMBOLS (concluded)

$U_{\tau}^i$		equivalent incompressible friction velocity; see equation (26)
V		vertical component of velocity
X		streamwise position relative to the normal part of the main shock wave
y	(Y)	equivalent height above wall; see equations (1) and (2)
y*		non-dimensionalised y with respect to wall parameters in equation (6)
Z		distance perpendicular to flow but parallel to surface
$\delta$		boundary layer thickness
$\delta_{0.995}$	(DEL995)	boundary layer thickness at $U/U_{\delta} = 0.995$
$\delta_{0.999}$		boundary layer thickness at $U/U_{\delta} = 0.999$
$\delta_E$	(DELE)	boundary layer energy thickness; see equation (15)
$\bar{\delta}$	(DELBAR)	boundary layer thickness parameters; see equation (7)
$\delta^*$	(DEL*)	boundary layer displacement thickness; see equations (11) and (18)
$\theta$	(THETA)	boundary layer momentum thickness; see equations (12) and (13)
$\bar{\theta}$	(THETABAR)	boundary layer thickness parameter; see equation (8)
$\kappa$		mixing length constant in equation (27)
$\kappa$		surface curvature
$\mu$		viscosity of fluid
$\nu$		kinematic viscosity of fluid
$\Pi$		pressure gradient parameter for equilibrium flows; see equation (14)
		density

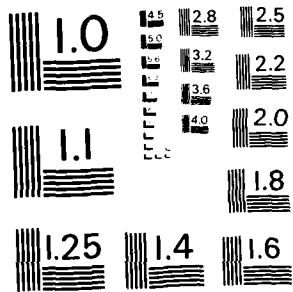
Subscripts

i	equivalent inviscid flow quantities
I	inner static pressure probe
m	measured quantities
N	normalised quantities
O	free-stream conditions before start of interaction
P	intermediate equivalent inviscid flow quantities
U	outer static pressure probe
w	wall conditions
A,B,C	regions in Fig 28a&b
e	edge of boundary layer conditions

Superscript

i	equivalent incompressible flow quantities
---	---





MICROCOPY RESOLUTION TEST CHART  
NATIONAL BUREAU OF STANDARDS - 1963 - A

REFERENCES

- | <u>No.</u> | <u>Author</u>  | <u>Title, etc</u>  |
|------------|--|--|
| 1          | J.B. Abbiss<br>L.F. East<br>C.R. Nash<br>P. Parker<br>E.R. Pyke<br>W.G. Sawyer | A study of the interaction of a normal shock wave and a turbulent boundary layer using a laser anemometer.<br>RAE Technical Report 75141 (1976)  |
| 2          | W.G. Sawyer<br>L.F. East<br>C.R. Nash  | A preliminary study of normal shock-wave turbulent boundary-layer interactions.<br>RAE Technical Memorandum Aero 1714 (1977)   |
| 3          | L.F. East  | The application of a laser anemometer to the investigation of shock-wave boundary-layer interactions.<br>AGARD CPP 193 (1976);<br>Also RAE Technical Memorandum Aero 1666 (1976)   |
| 4          | J.B. Abbiss<br>H.S. Dhadwal<br>P.R. Sharpe<br>M.P. Wright                      | Laser anemometry studies of a separated turbulent boundary layer in supersonic flow using a ten-nanosecond data acquisition system.<br>9th International Congress in Instrumentation in Aerospace Simulation Facilities (1981) |
| 5          | J. Seddon  | The flow produced by interaction of a turbulent boundary layer with a normal shock wave of strength sufficient to cause separation.<br>ARC R&M 3502 (1967)   |
| 6          | R.J. Vidal<br>C.E. Whittliff<br>P.A. Catlin<br>B.H. Sheen                      | Reynolds number effects on the shock wave turbulent boundary layer interaction at transonic speeds.<br>AIAA Paper 73-661 (1973)  |
| 7          | J.W. Kooi  | Experiment on transonic shock-wave boundary-layer interaction.<br>AGARD CPP 168 (1975)   |
| 8          | J. Delery  | Recherches sur l'interaction onde de choc-couche limite turbulente.<br>Onera TP 1976-135 (1976)  |
| 9          | C.F. Lo<br>F.L. Heltsley<br>M.C. Alstatt                                       | A study of laser velocimeter measurements in a viscous transonic flow.<br>AIAA Paper 76-333 (1976)   |
| 10         | H. Sobieczky<br>E. Stanewsky   | The design of transonic aerofoils under consideration of shock wave boundary layer interaction.<br>ICAS Paper 76-14 (1976)   |
| 11         | K.P. Burdges   | Experimental measurements of shock wave boundary layer interaction on a supercritical airfoil.<br>AIAA Paper 79-1499 (1979)  |

REFERENCES (continued)

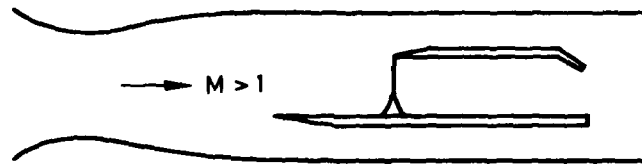
<u>No.</u>	<u>Author</u>	<u>Title, etc</u>
12	G.E. Gadd	Interactions between normal shock waves and turbulent boundary layers. ARC R&M 3262 (1961)
13	G.G. Mateer A. Brosch J.R. Viegas	A normal shock wave turbulent boundary layer interaction at transonic speeds. AIAA Paper 76-161 (1976)
14	E.P. Sutton	The development of slotted working-section liners for transonic operation of the RAE Bedford 3ft wind tunnel. ARC R&M 3085 (1955)
15	L.F. East	A representation of second-order boundary layer effects in the momentum integral equation and in viscous-inviscid interactions. RAE Technical Report 81002 (1981)
16	L.F. East	A prediction of the law of the wall in compressible three-dimensional turbulent boundary layers. RAE Technical Report 72178 (1972)
17	D.E. Coles	The turbulent boundary layer in a compressible fluid. Project Rand Report R-403-PR (1962)
18	Editors: D.E. Coles E.A. Hirst	Proceedings, Computation of turbulent boundary-layers. Vol.II. AFOSR-IFP Stanford Conference (1968)
19	D.F. Myring	The effects of normal pressure gradients on the boundary layer momentum integral equation. RAE Technical Report 68214 (1968)
20	P.H. Cook M.A. McDonald M.C.P. Firmin	Aerofoil RAE 2822 - pressure distributions and boundary layer and wake measurements. AGARD AR-138, Paper A6; Also RAE Technical Memorandum Aero 1725 (1979)
21	V.C. Patel	Calibration of the Preston tube and limitations on its use in pressure gradients. J. Fluid Mechanics, Vol.23, 1, pp.185-208 (1965)
22	M.R. Head V. Vasanta Ram	Improved presentation of Preston tube calibration. India Indian Inst. Tech., Kampur, Department of Aero Engineering, AE-10/1970. Also Aeronaut. Q. XXII, Vol.3 (1971)
23	F.W. Fenter C.J. Stalmach	The measurement of local turbulent skin friction at supersonic speeds by means of surface impact-pressure probes. J. Aero/Sp Sci. Vol.25, 12, pp.793-794 (1958)

REFERENCES (concluded)

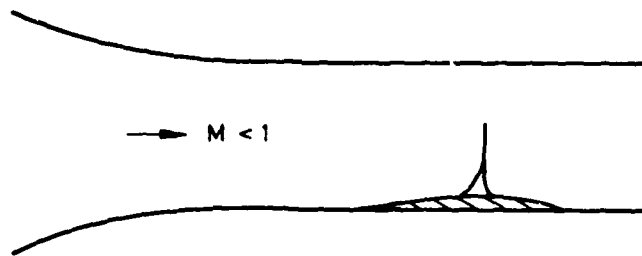
<u>No.</u>	<u>Author</u>	<u>Title, etc</u>
24	J.E. Green D.J. Weeks J.W.F. Brooman	Prediction of turbulent boundary layers and wakes in compressible flow by a lag-entrainment method. ARC R&M 3791 (1973)
25	K.G. Winter L. Gaudet	Turbulent boundary-layer studies at high Reynolds number at Mach numbers between 0.2 and 2.8. ARC R&M 3712 (1970)
26	E.R. van Driest	Turbulent boundary layer in compressible fluids. J. Aeronautical Sci., Vol.18, 3, pp.145-160 & 216 (1951)
27	L.F. East P.D. Smith P.J. Merryman	Prediction of the development of separated turbulent boundary layers by the lag-entrainment method. RAE Technical Report 77046 (1977)
28	L.F. East W.G. Sawyer C.R. Nash	An investigation of the structure of equilibrium turbulent boundary layers. RAE Technical Report 79040 (1979)
29	T.D. Reed T.C. Pope J.M. Cooksey	Calibration of transonic and supersonic wind tunnels. NASA Contractor Report 2920 (1977)

Reports quoted are not necessarily available to members of the public or commercial organisations.

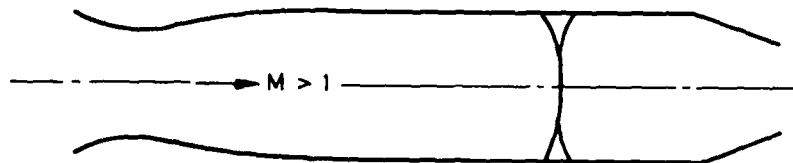
Fig 1a-c



a) Flat plate with shock-wave generator and downstream choking flap



b) Transonic bump



c) Conical shock in circular section

TR 82093

Fig 1a-c Three techniques for producing a normal shock-wave boundary-layer interaction



Fig 2

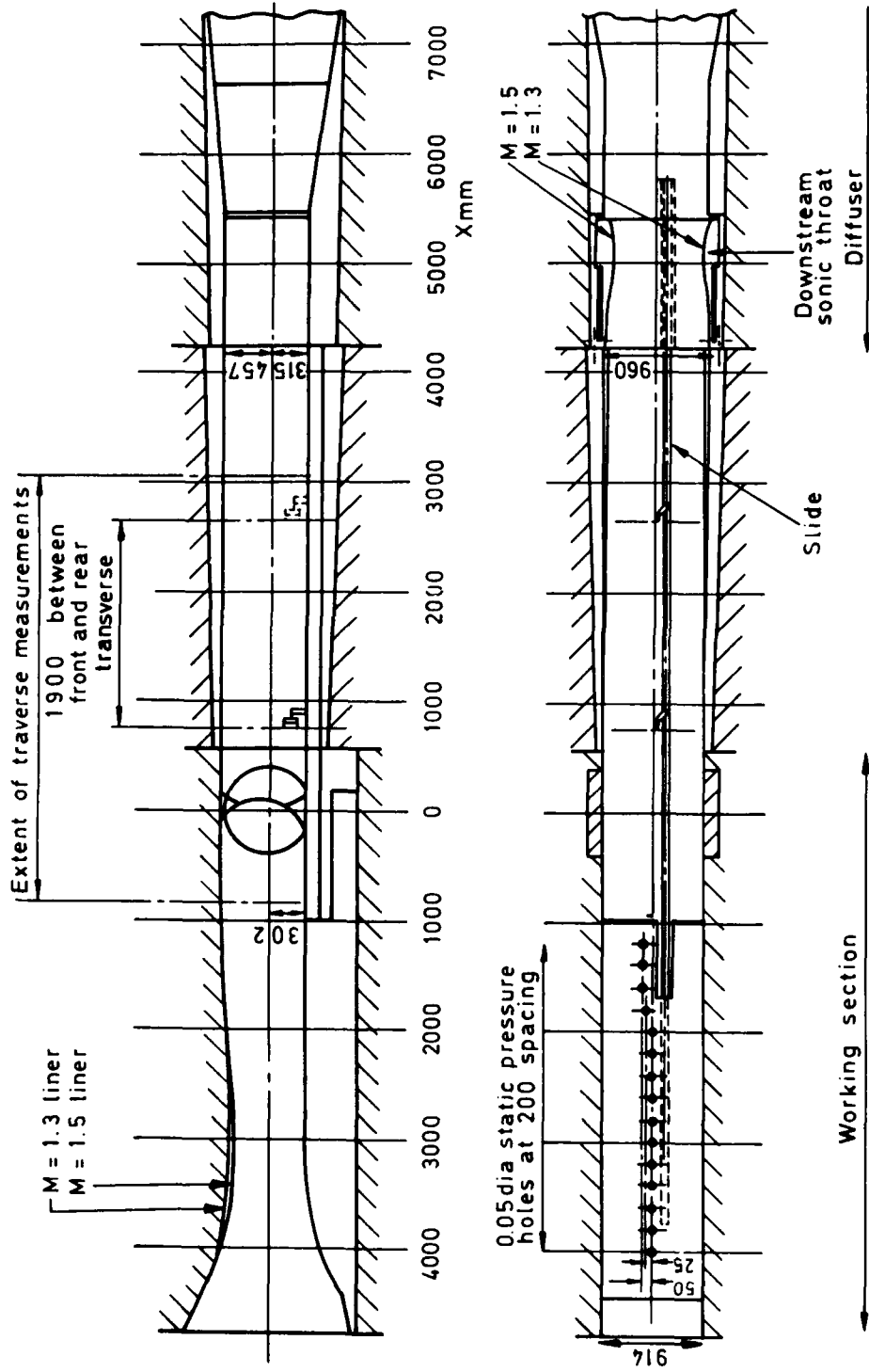


Fig 2 Experimental arrangement in the 3 ft x 3 ft wind tunnel

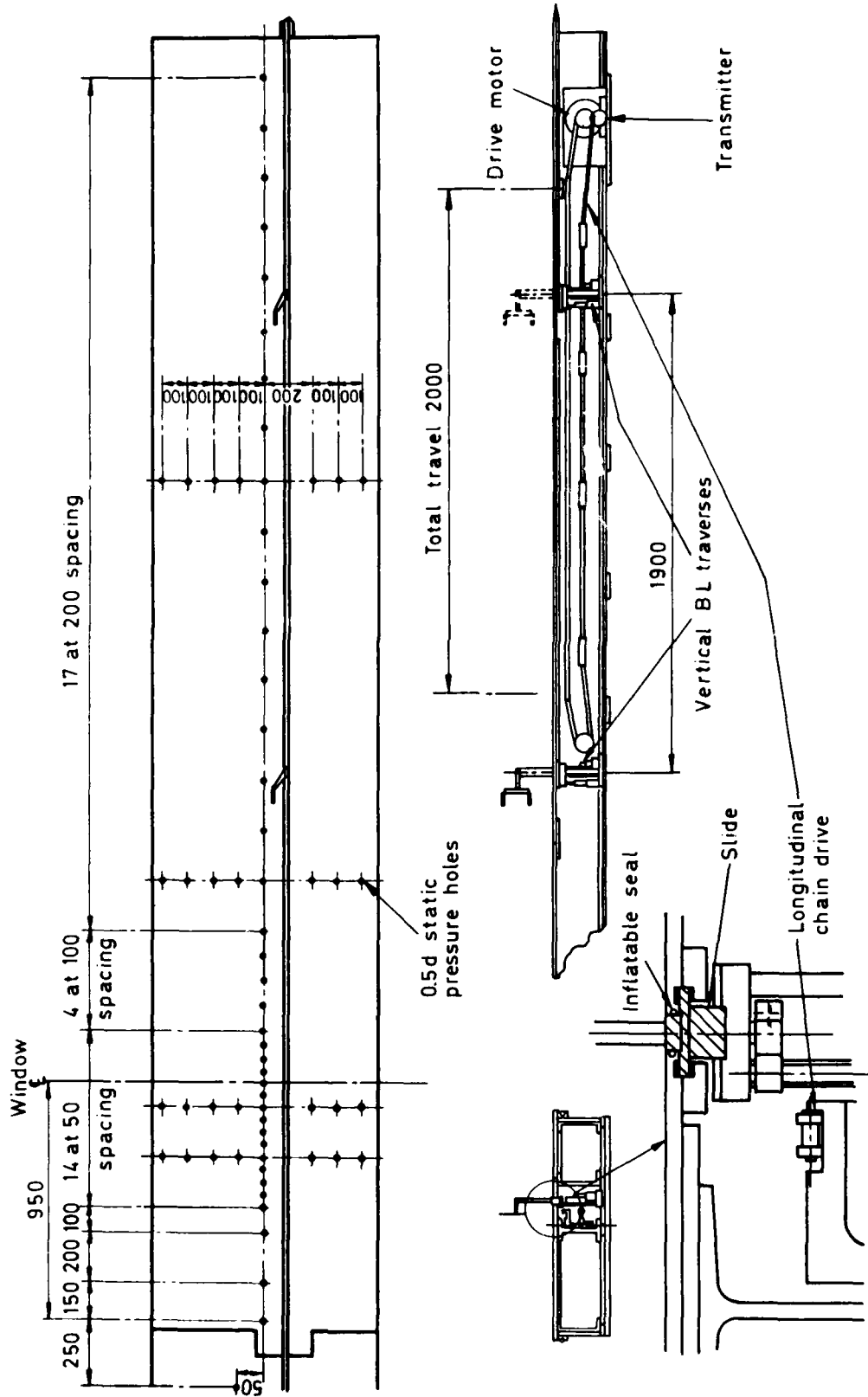


Fig 3

Fig 3 False floor and horizontal traverse mechanism

Fig 4

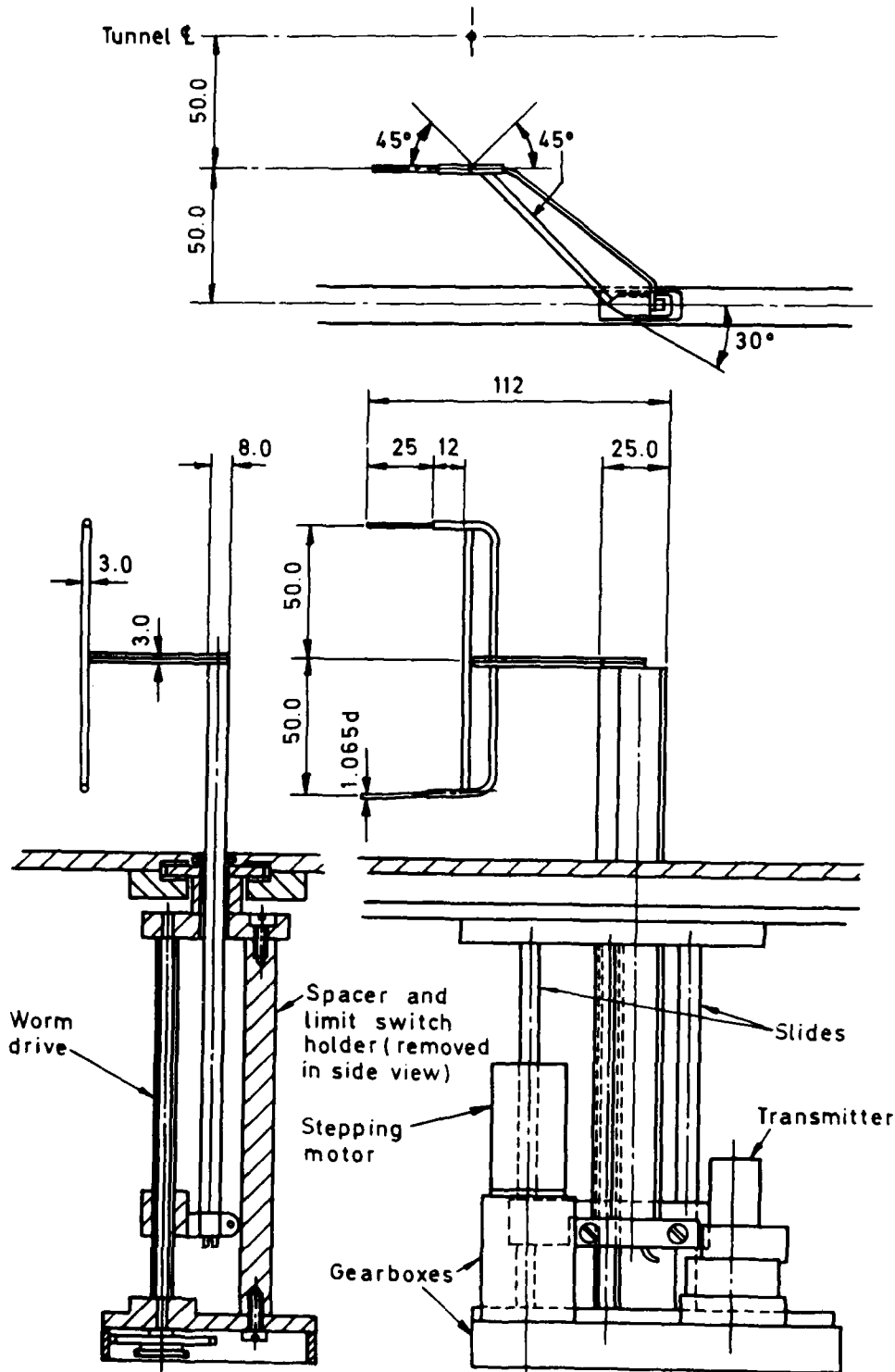


Fig 4 Pitot traverse mechanism and twin pitot probe

TR 82099

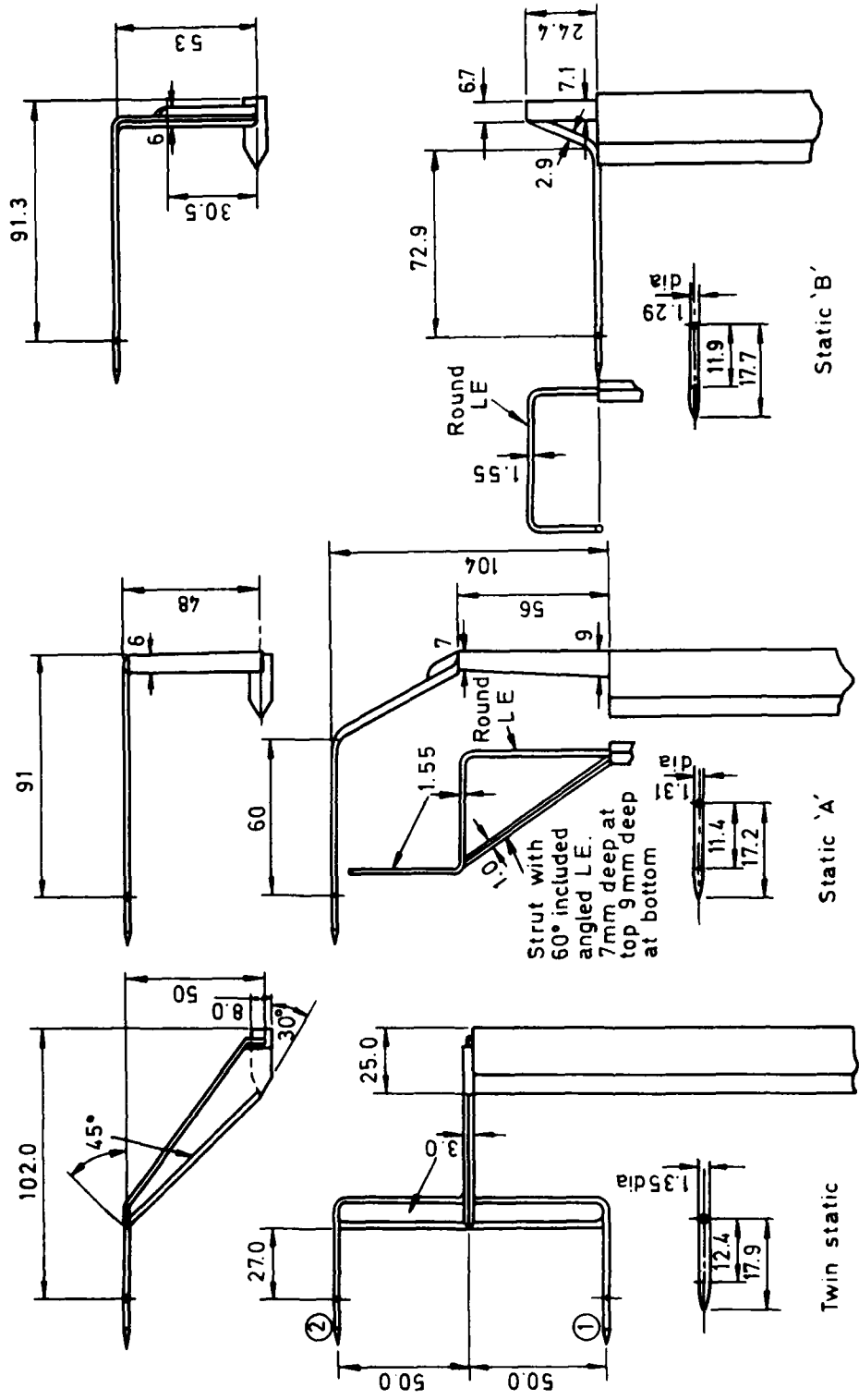


Fig 5 Details of static probes

Fig 5

Fig 6a

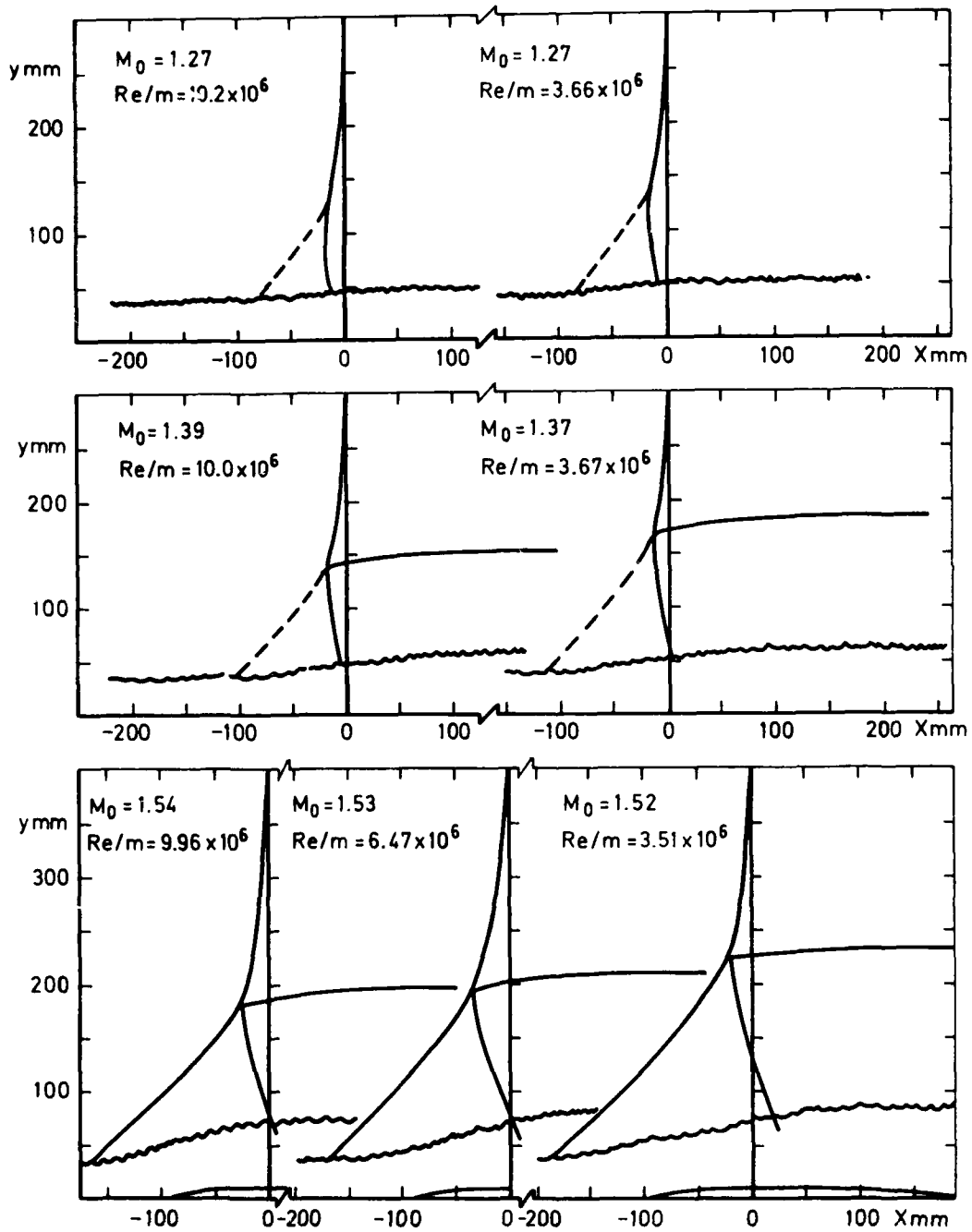
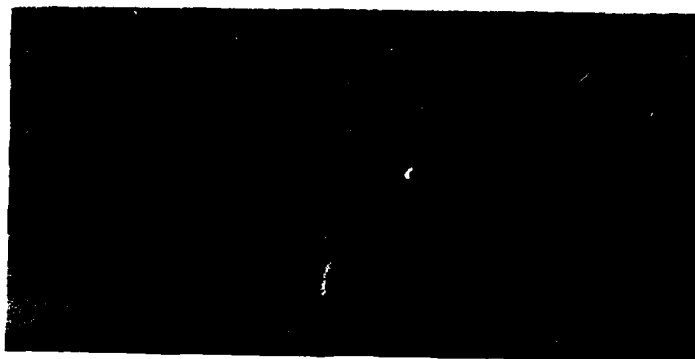


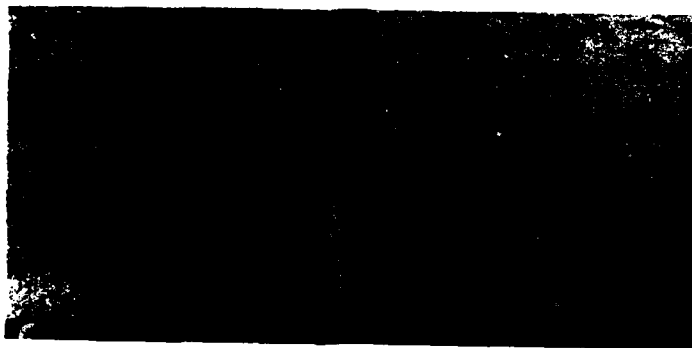
Fig 6a Normal shock-wave boundary-layer interactions

Fig 6b

$M_0 = 1.27$   
 $Re/m = 10.2 \times 10^6$



$M_0 = 1.39$   
 $Re/m = 10.0 \times 10^6$



$M_0 = 1.54$   
 $Re/m = 9.96 \times 10^6$

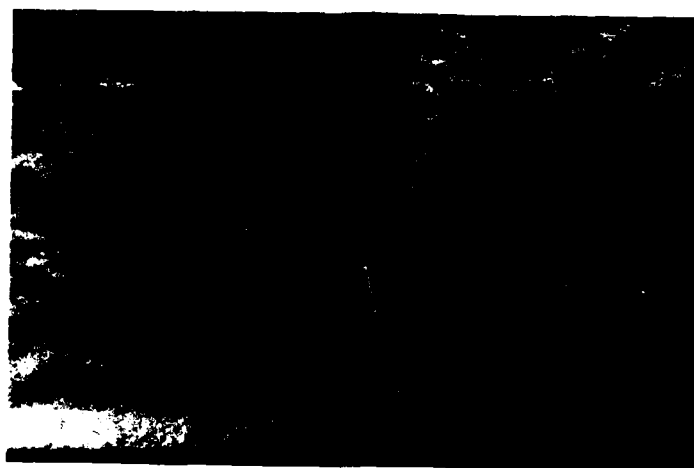
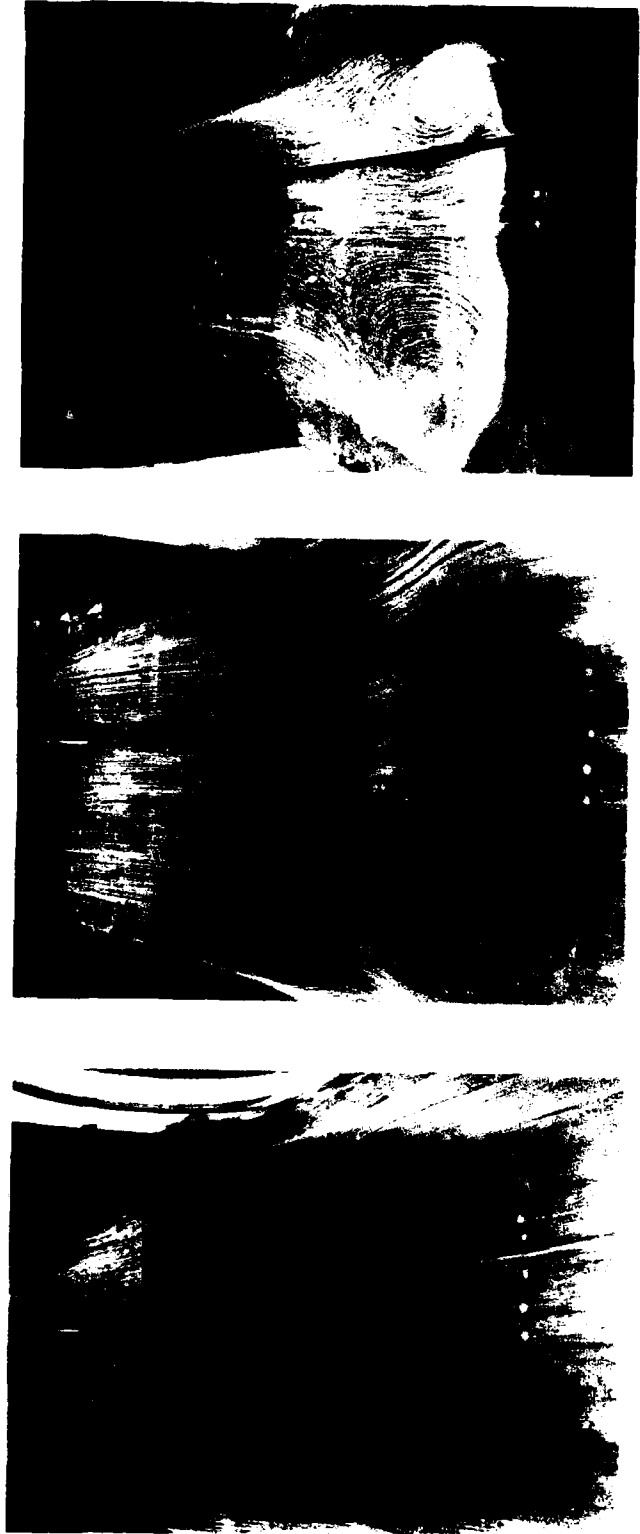


Fig 6b Schlieren photographs of normal shockwave boundary-layer interaction

Fig 7

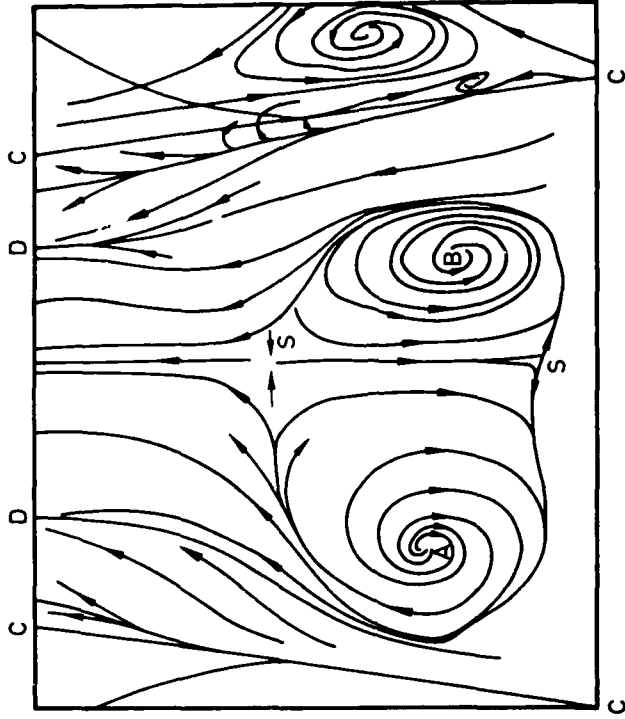
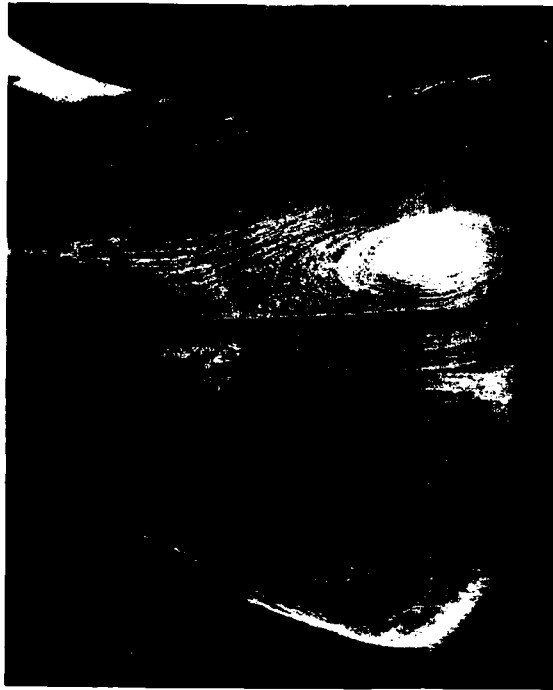


M = 1.5

M = 1.4

M = 1.3

Fig 7 Oil flow under interaction regions



- C Corners between floor and sidewalls
- A Attachment node
- B Separation node
- D Strong convergence lines
- S Saddle points

Fig 8 Oil flow under interaction region at  $M = 1.5$



Fig 9

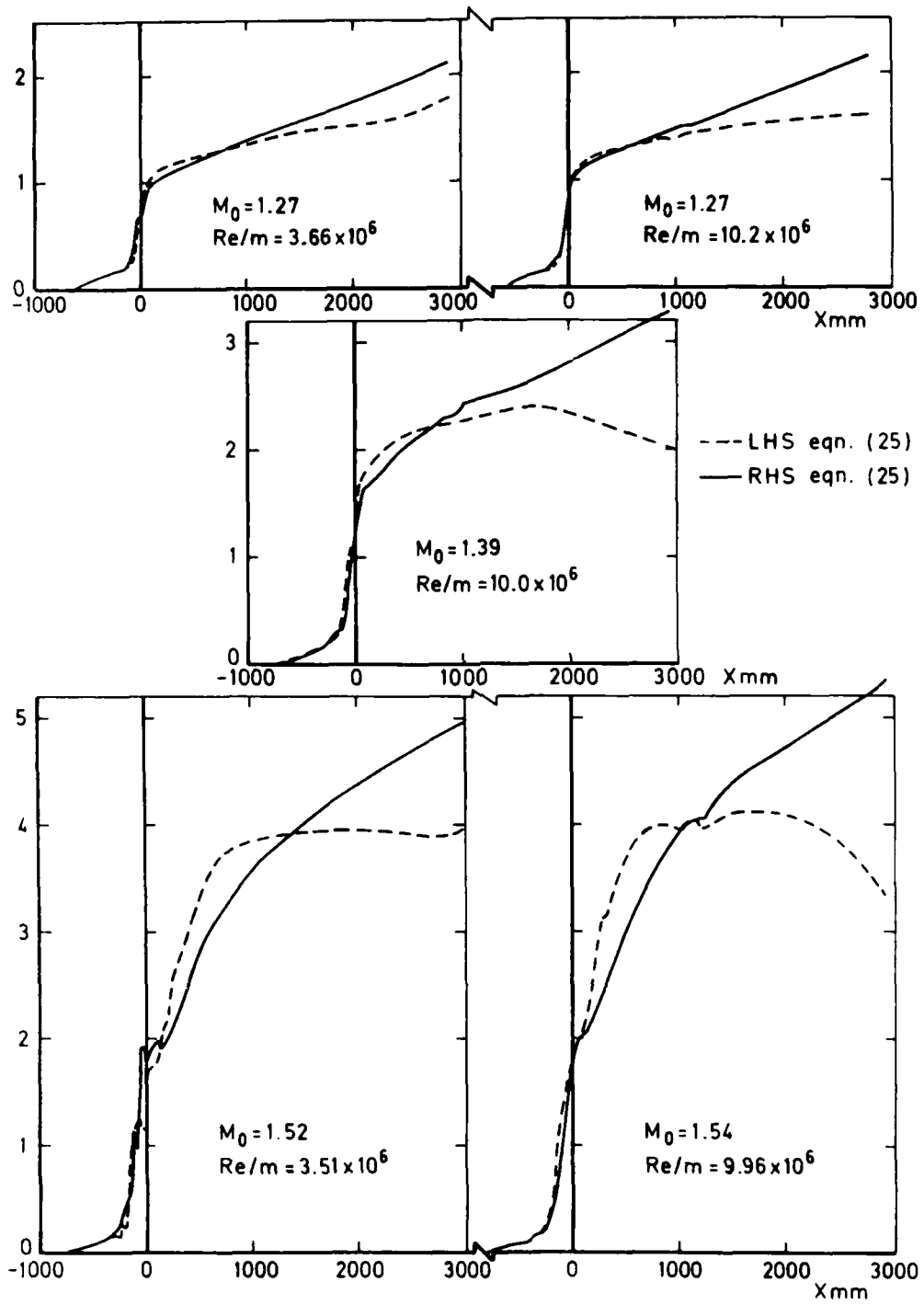


Fig 9 Momentum balance based on measured  $p$  + calculated  $p_i$  for  $X < 0$

TM 82094

Fig 10a

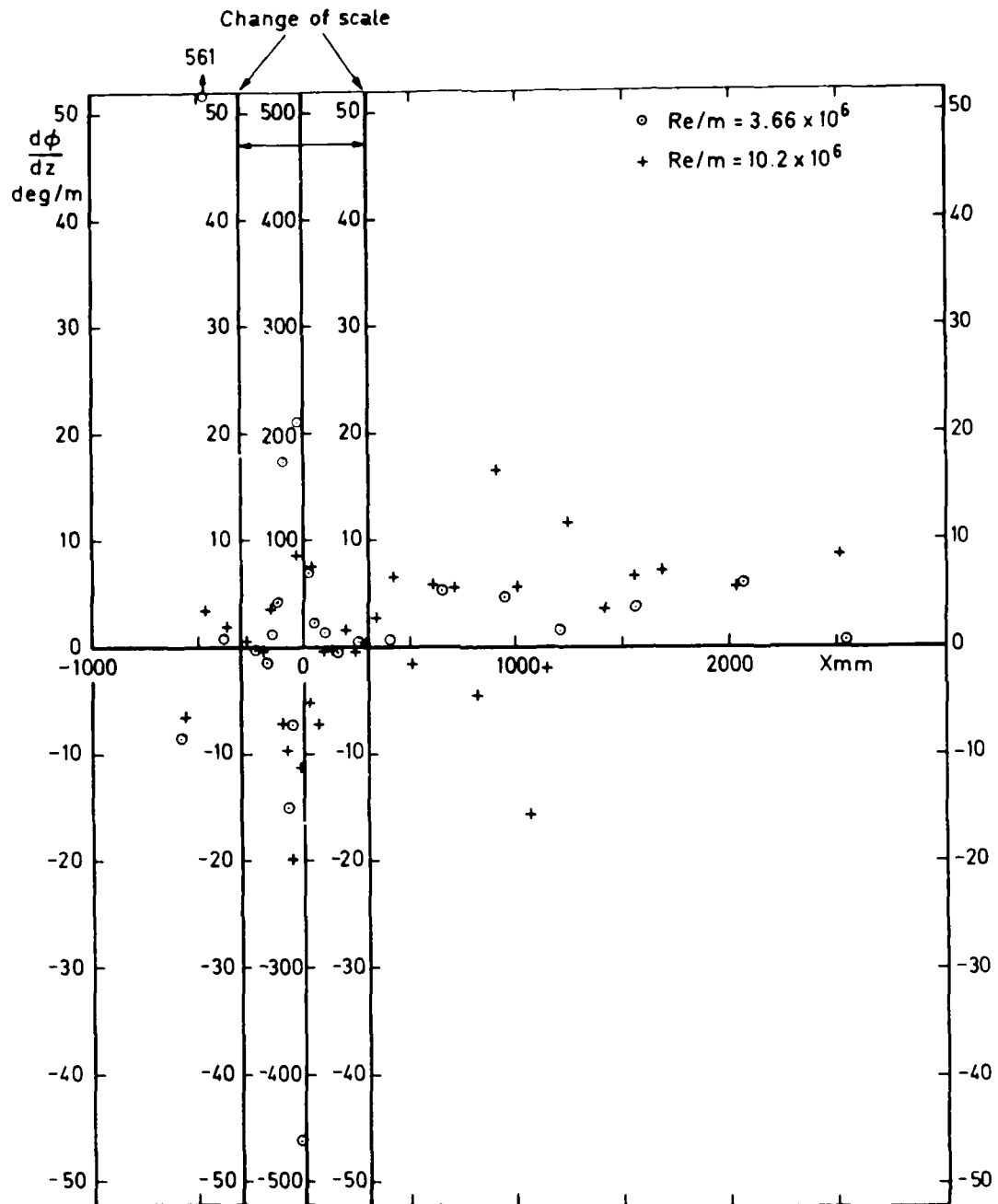


Fig 10a Flow divergence needed to balance momentum integral equation,  $M = 1.3$

Fig 10b

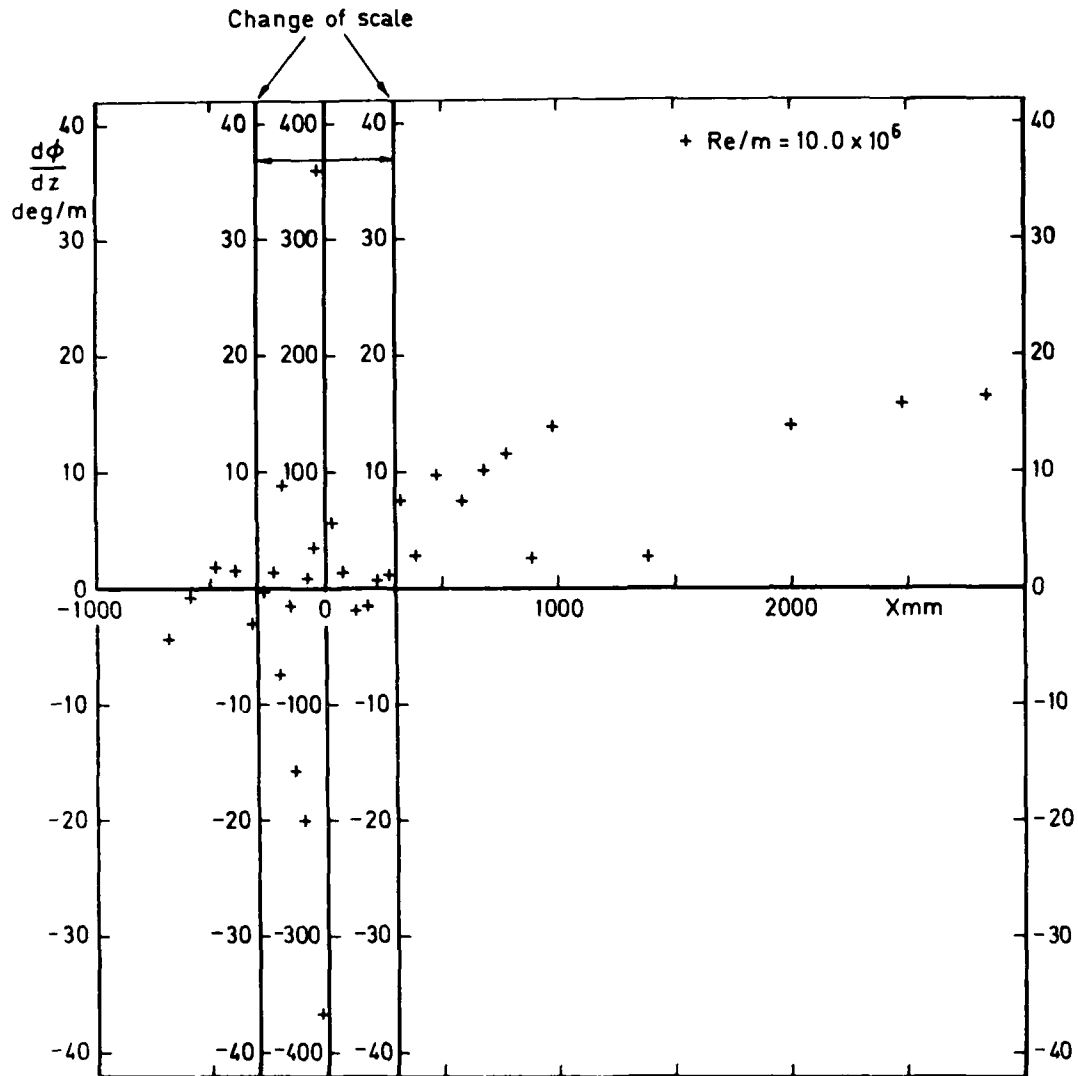


Fig 10b Flow divergence needed to balance momentum integral equation,  $M = 1.4$

Fig 10c

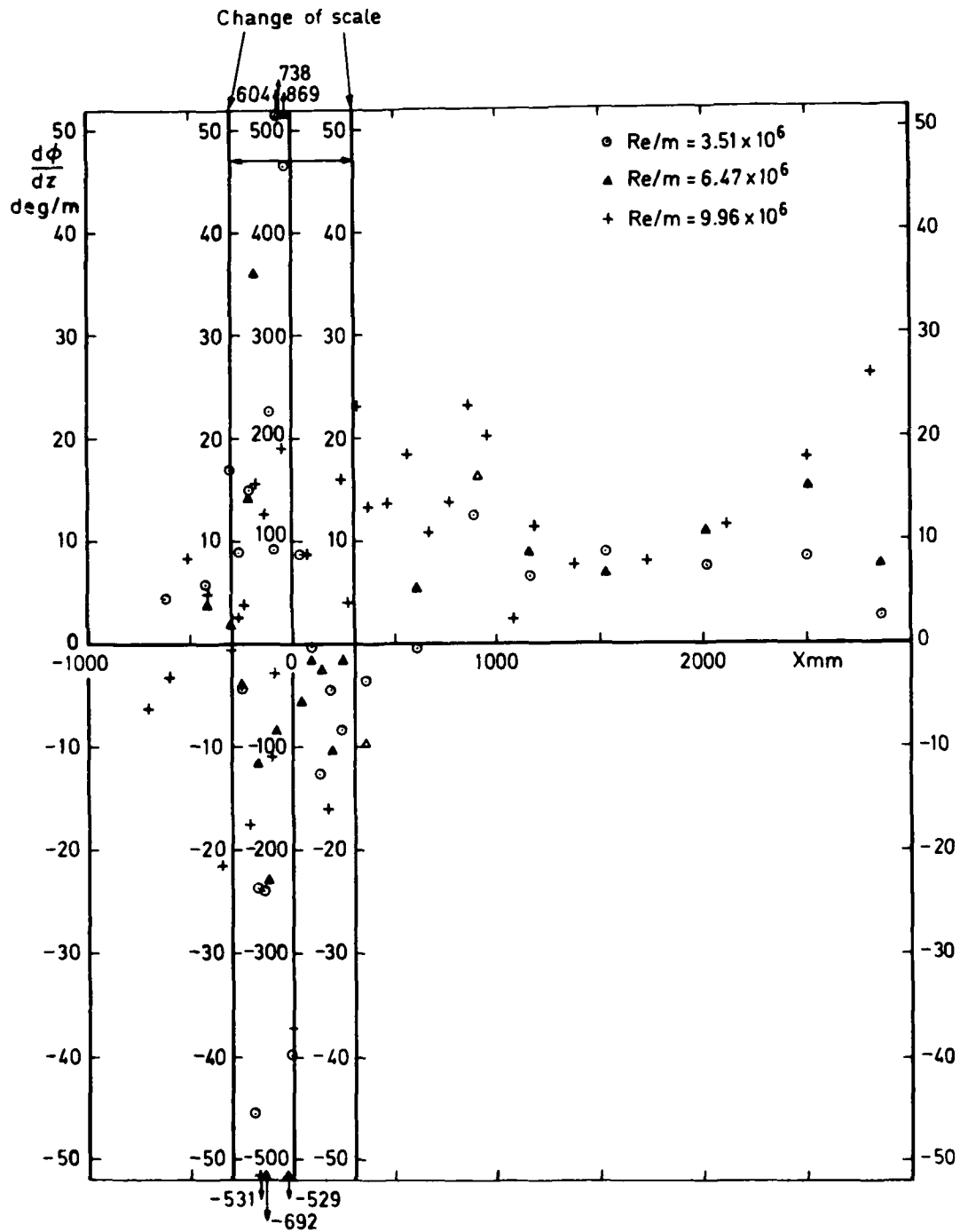


Fig 10c Flow divergence needed to balance momentum integral equation,  $M = 1.5$

Fig 11

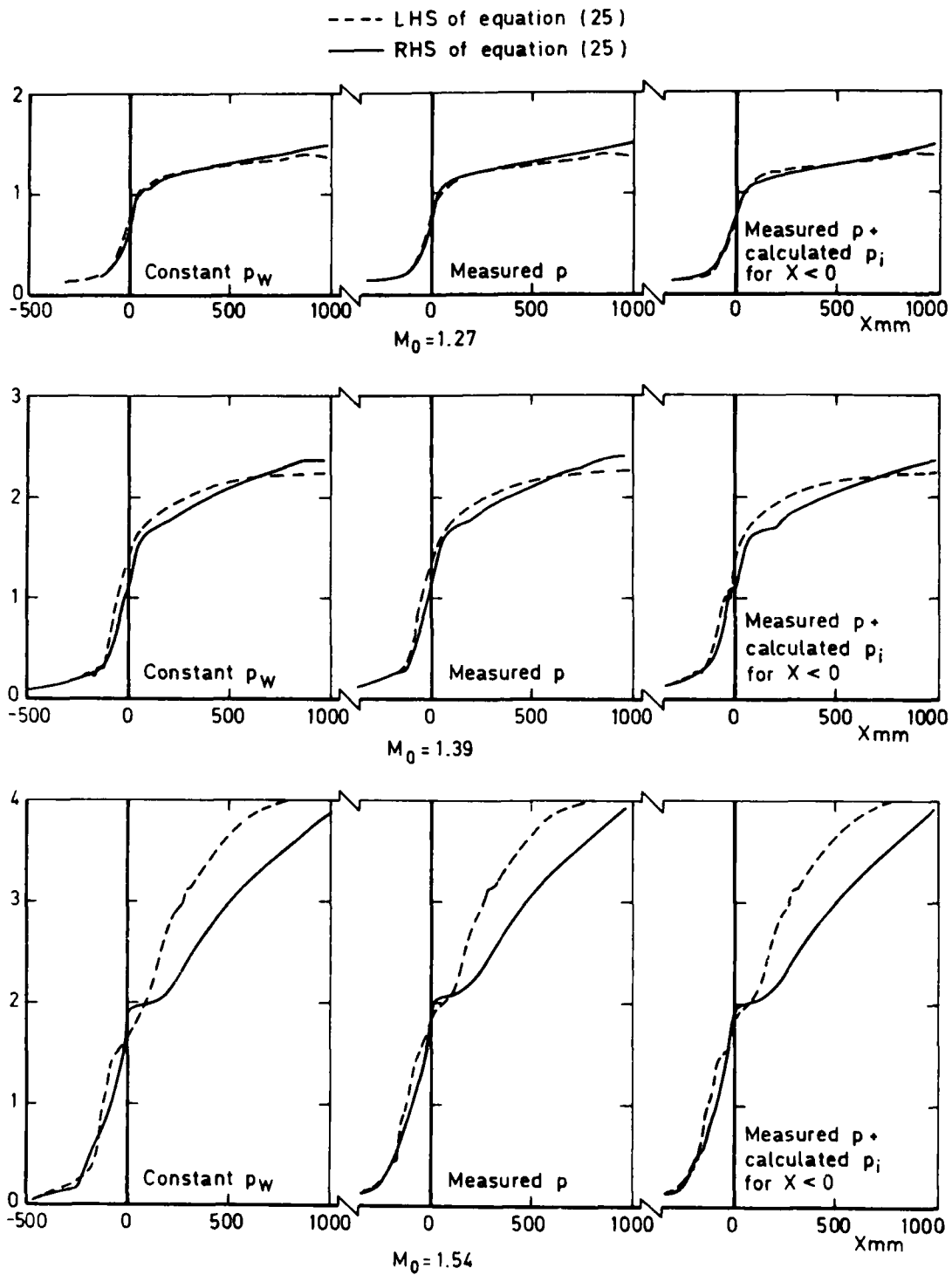


Fig 11 Comparison of momentum balance calculations at  $Re/m = 10 \times 10^6$

Fig 12

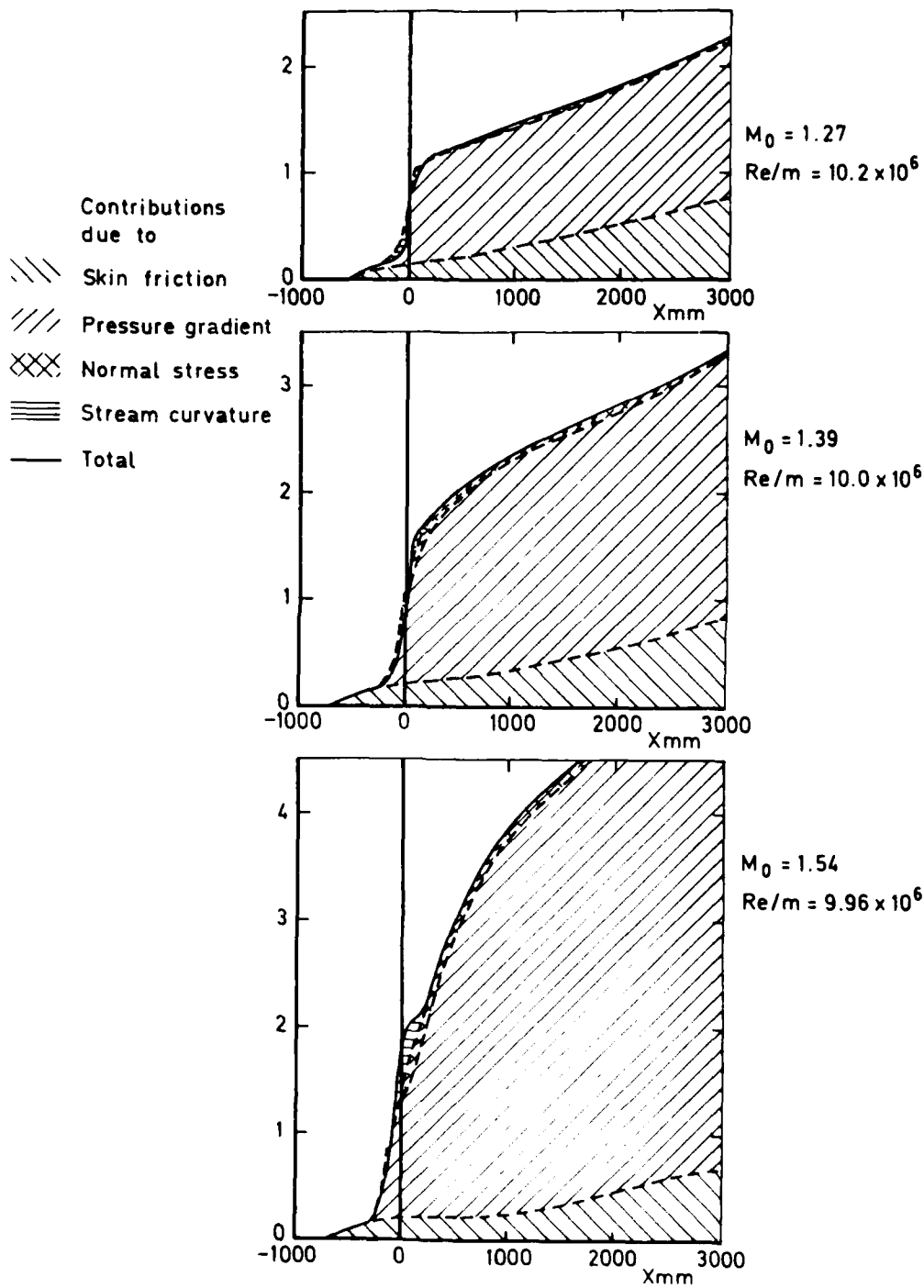


Fig 12 Composition of right hand side of momentum integral equation (measured  $p$  + calculated  $p_i$ )

Fig 13a

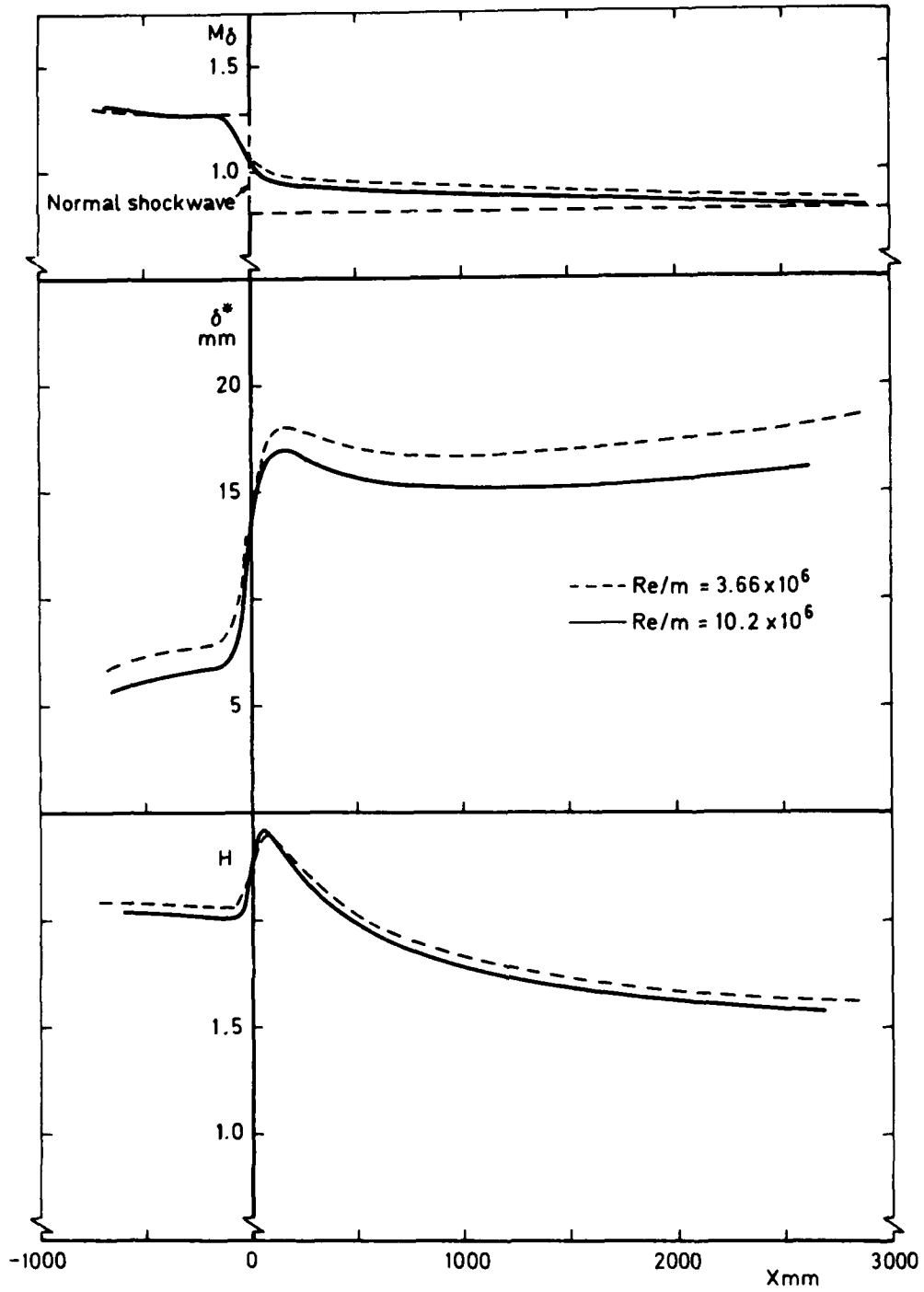


Fig 13a Boundary layer development ( $p = p_w$ )  $M = 1.3$

Fig 13a (concl'd)

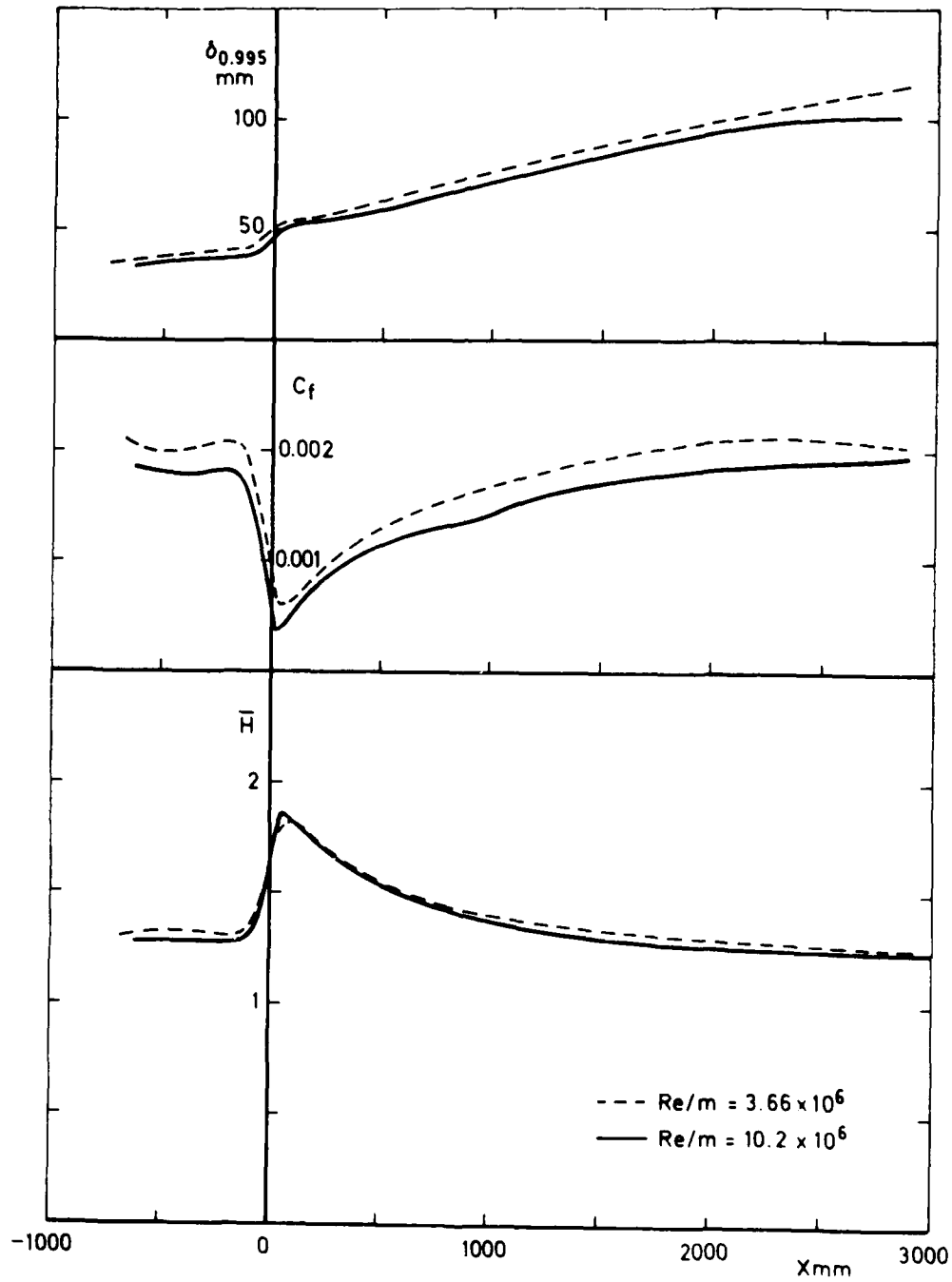


Fig 13a (concl'd) Boundary layer development ( $p = p_w$ )  $M = 1.3$



Fig 13b

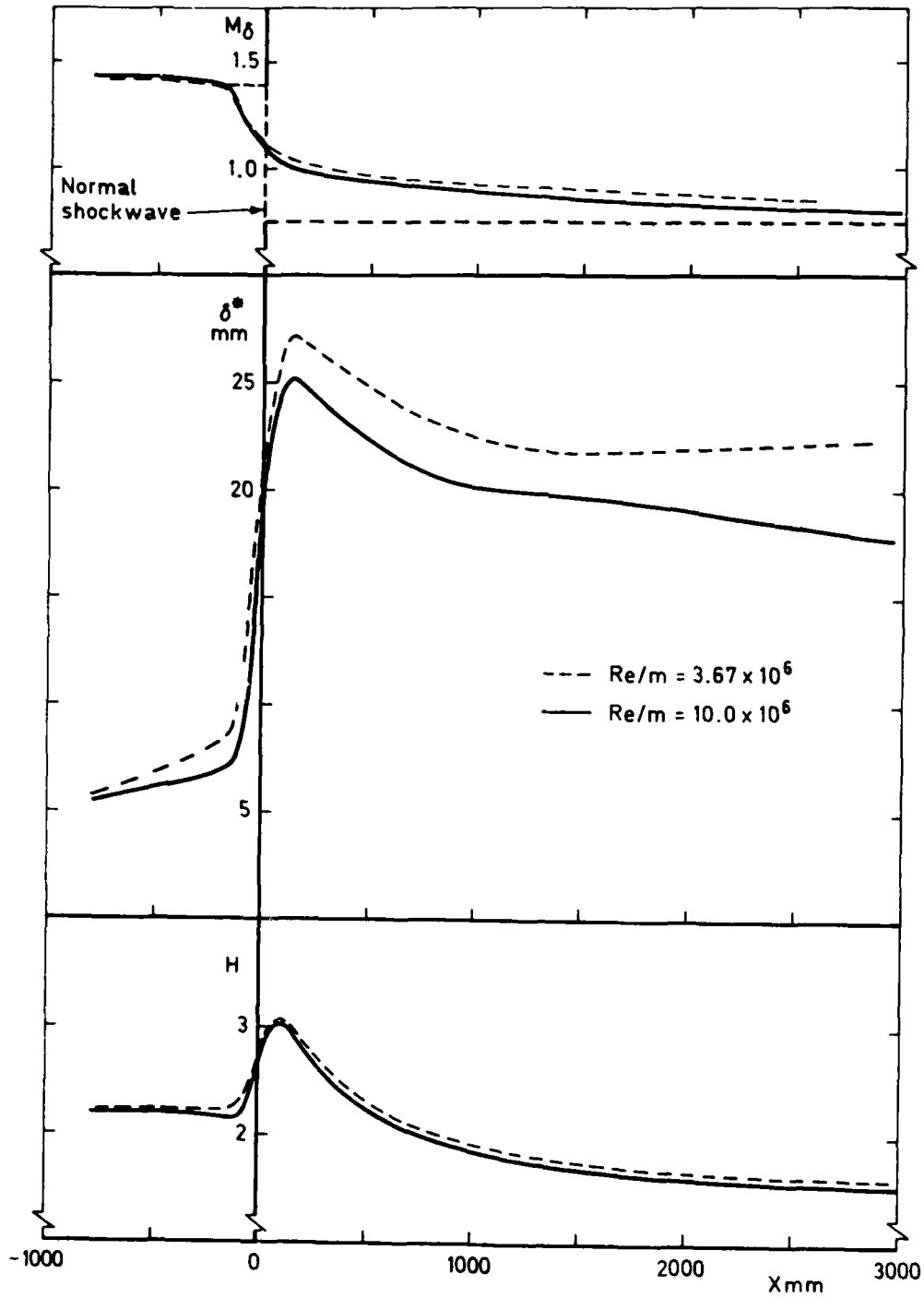


Fig 13b Boundary layer development ( $p = p_w$ )  $M = 1.4$

TR 82099

Fig 13b (concl'd)

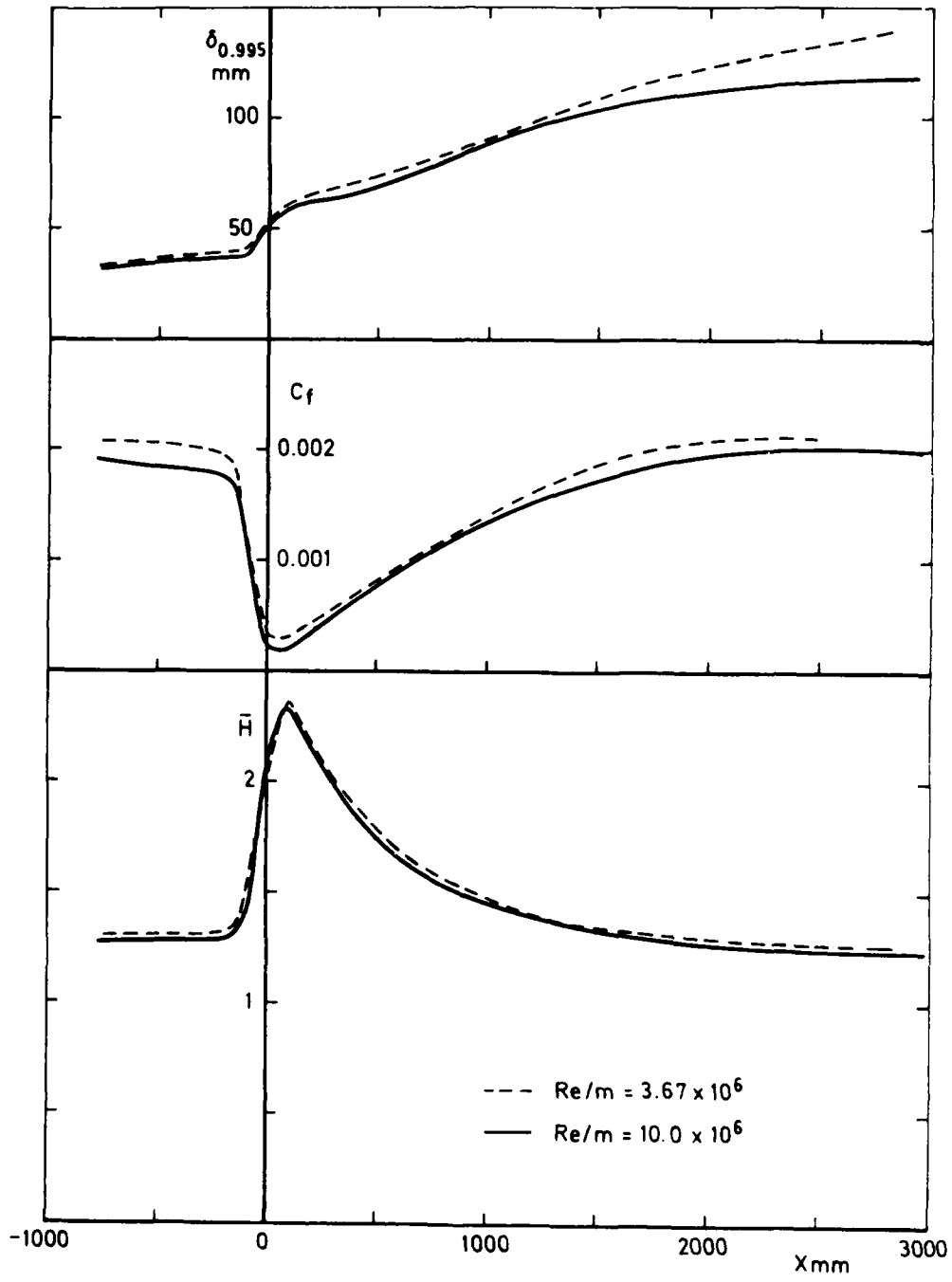


Fig 13b (concl'd) Boundary layer development ( $p = p_w$ )  $M = 1.4$

Fig 13c

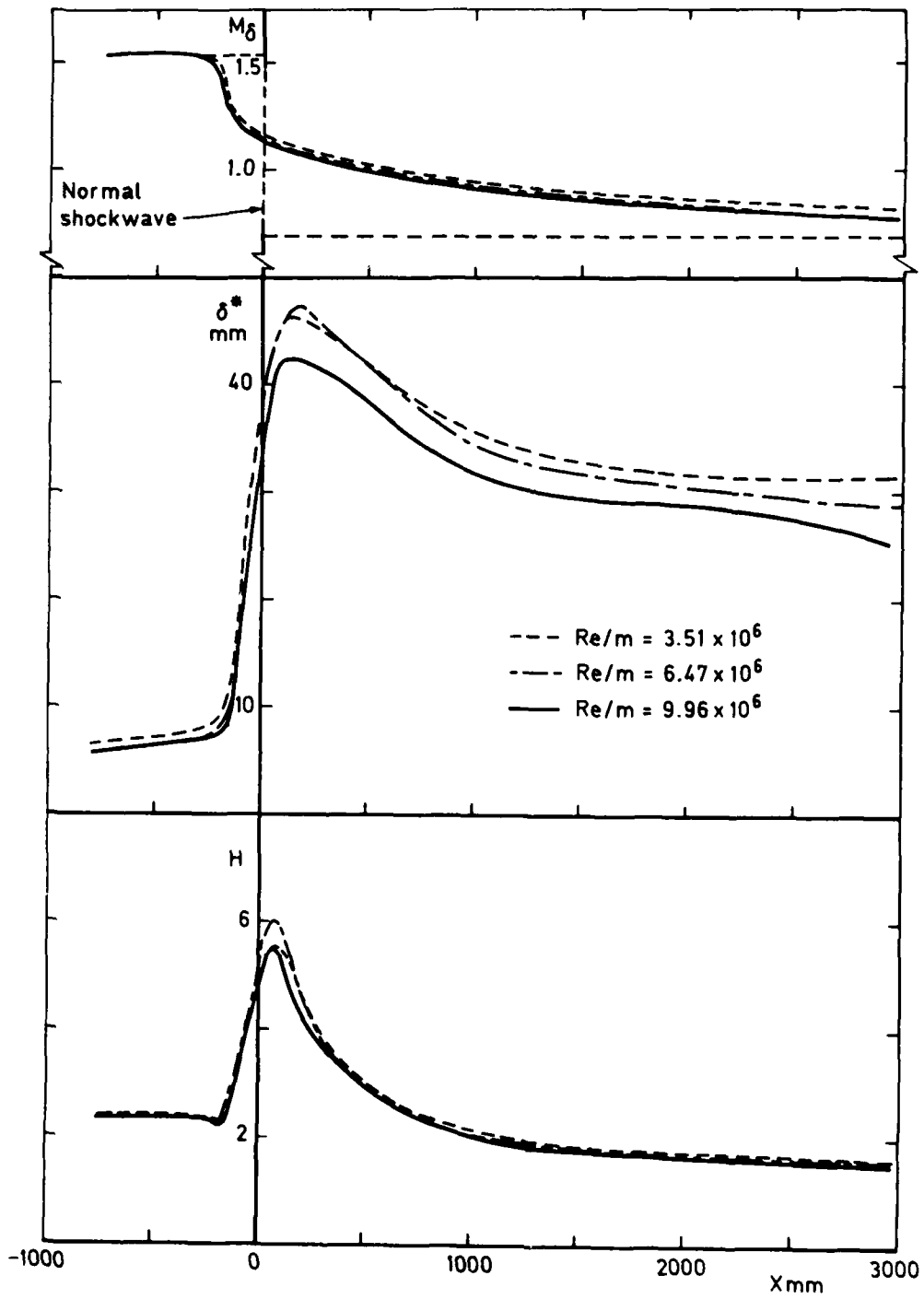


Fig 13c Boundary layer development ( $p = p_w$ )  $M = 1.5$

Fig 13c (concl'd)

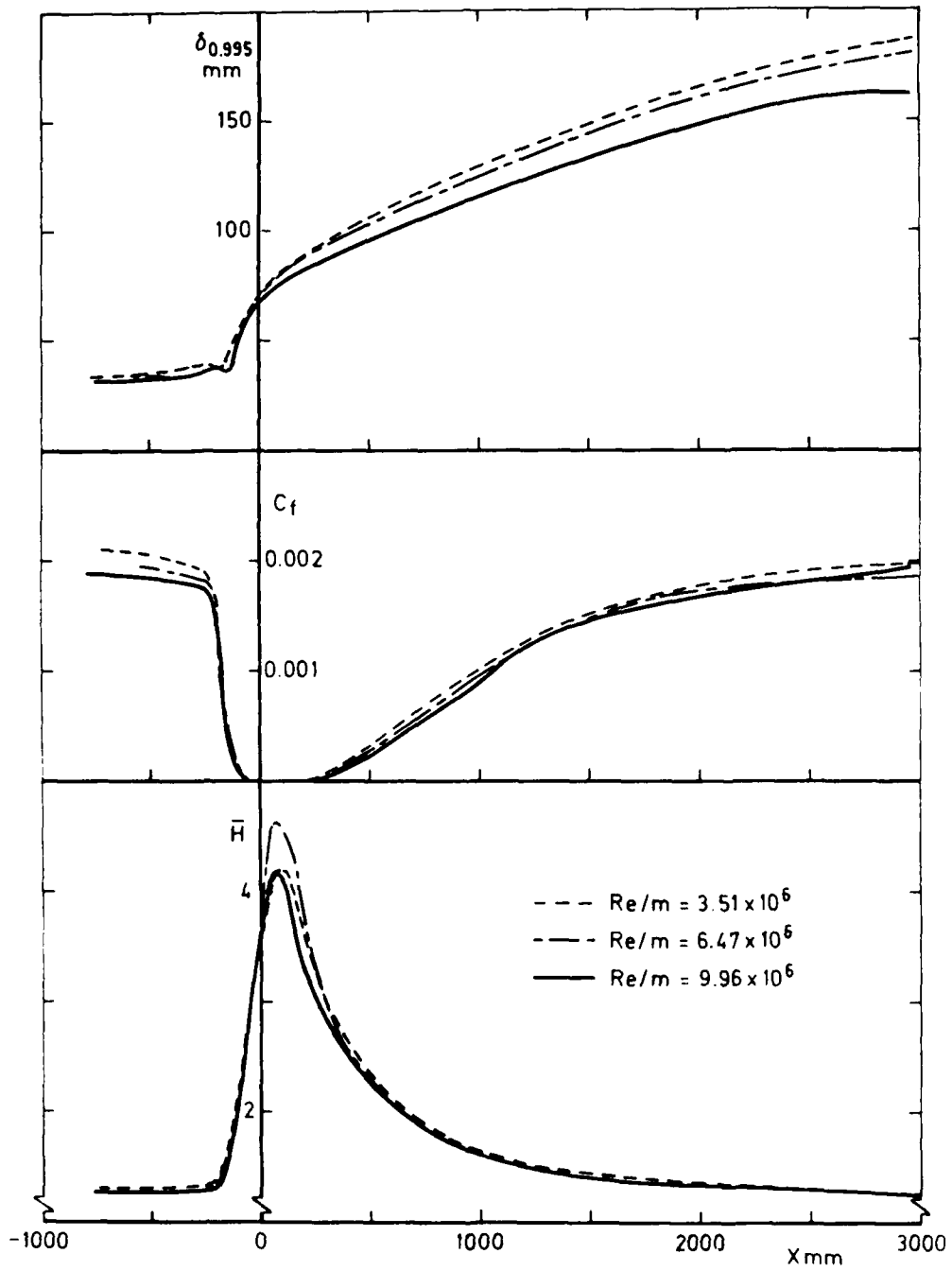


Fig 13c (concl'd) Boundary layer development ( $p = p_w$ )  $M = 1.5$

Fig 14a

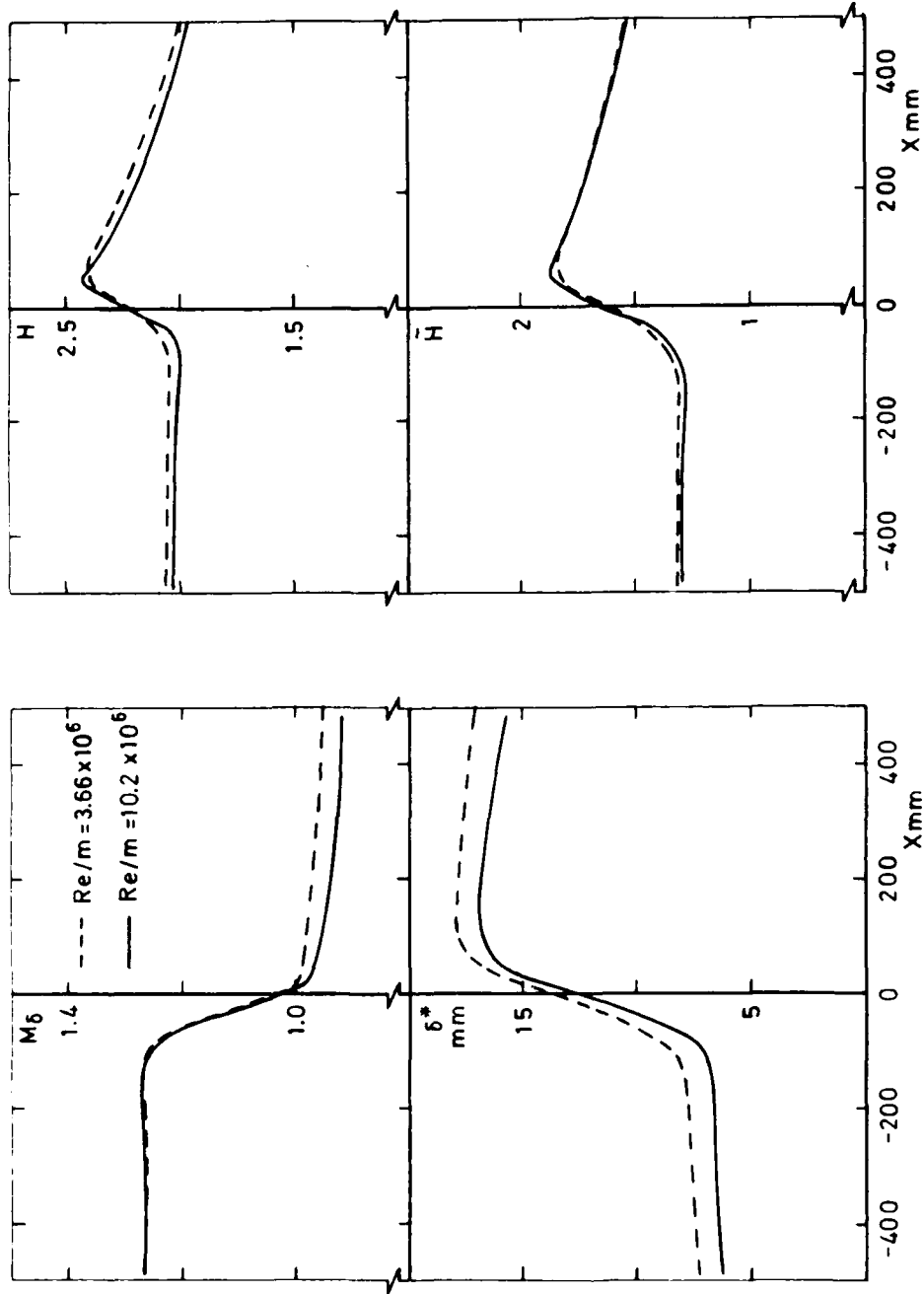


Fig 14a Boundary layer development (measured p)  $M = 1.3$

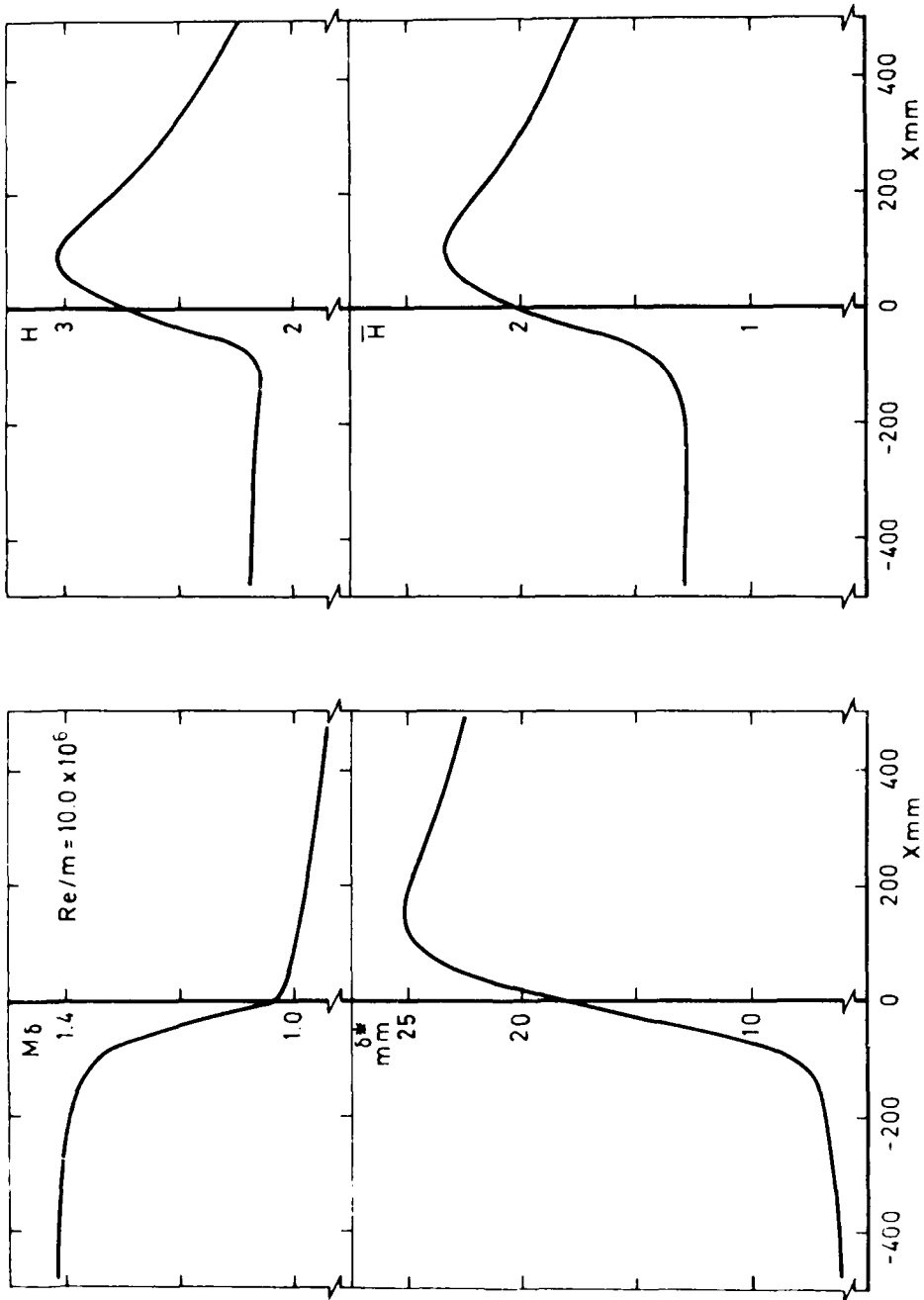


Fig 14b Boundary layer development (measured p) M = 1.4

Fig 14b

Fig 14c

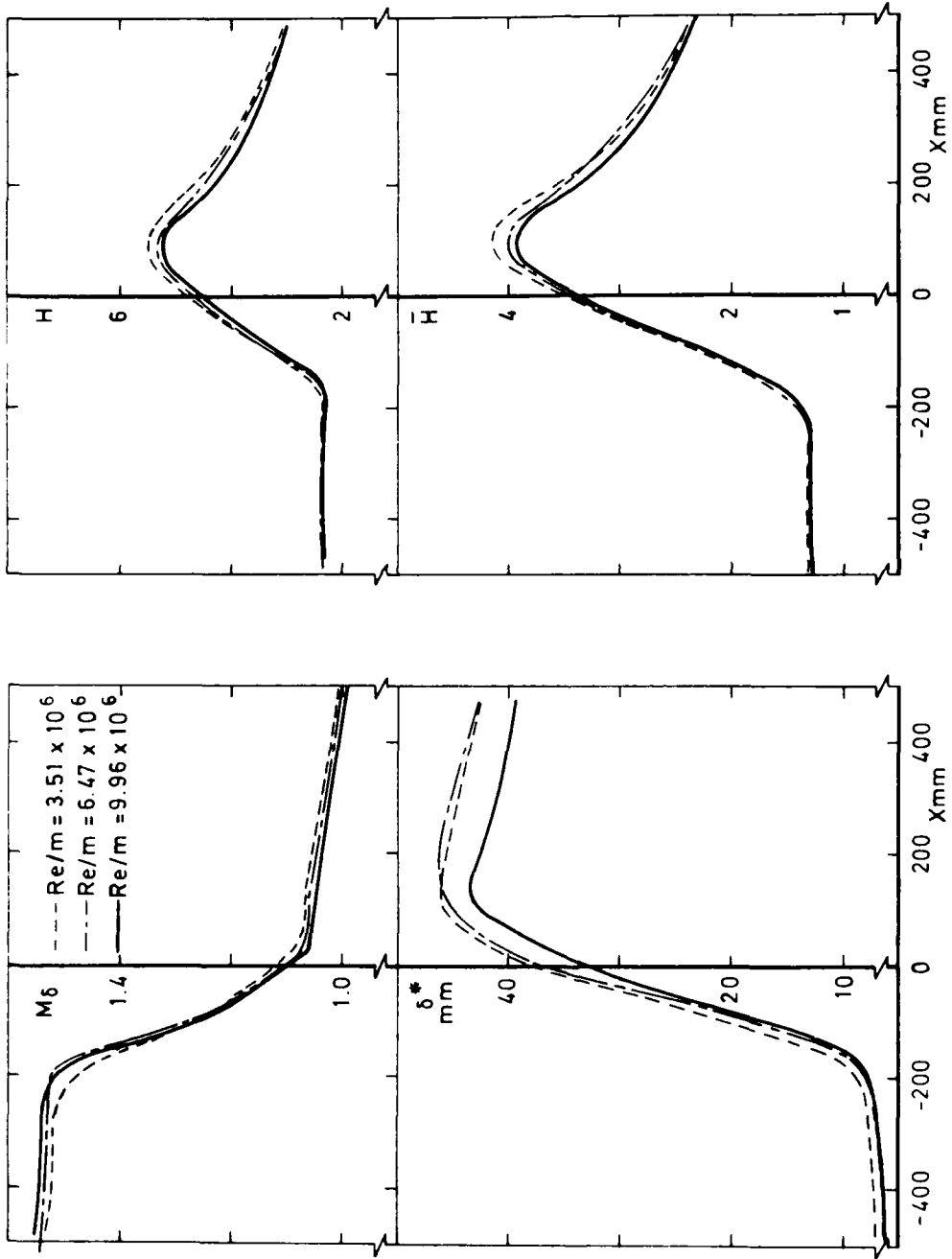


Fig 14c Boundary layer development (measured p)  $M = 1.5$

Fig 15a

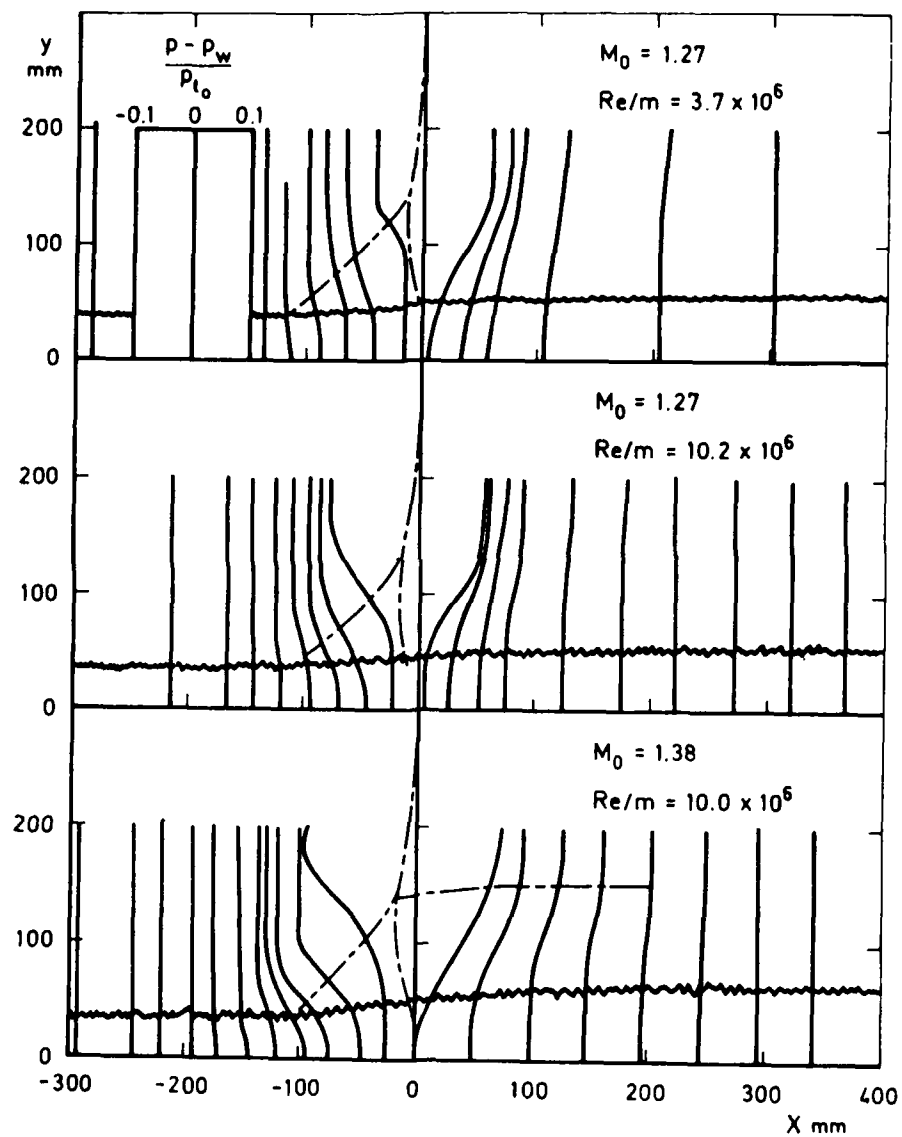


Fig 15a Measured static pressures



Fig 15b

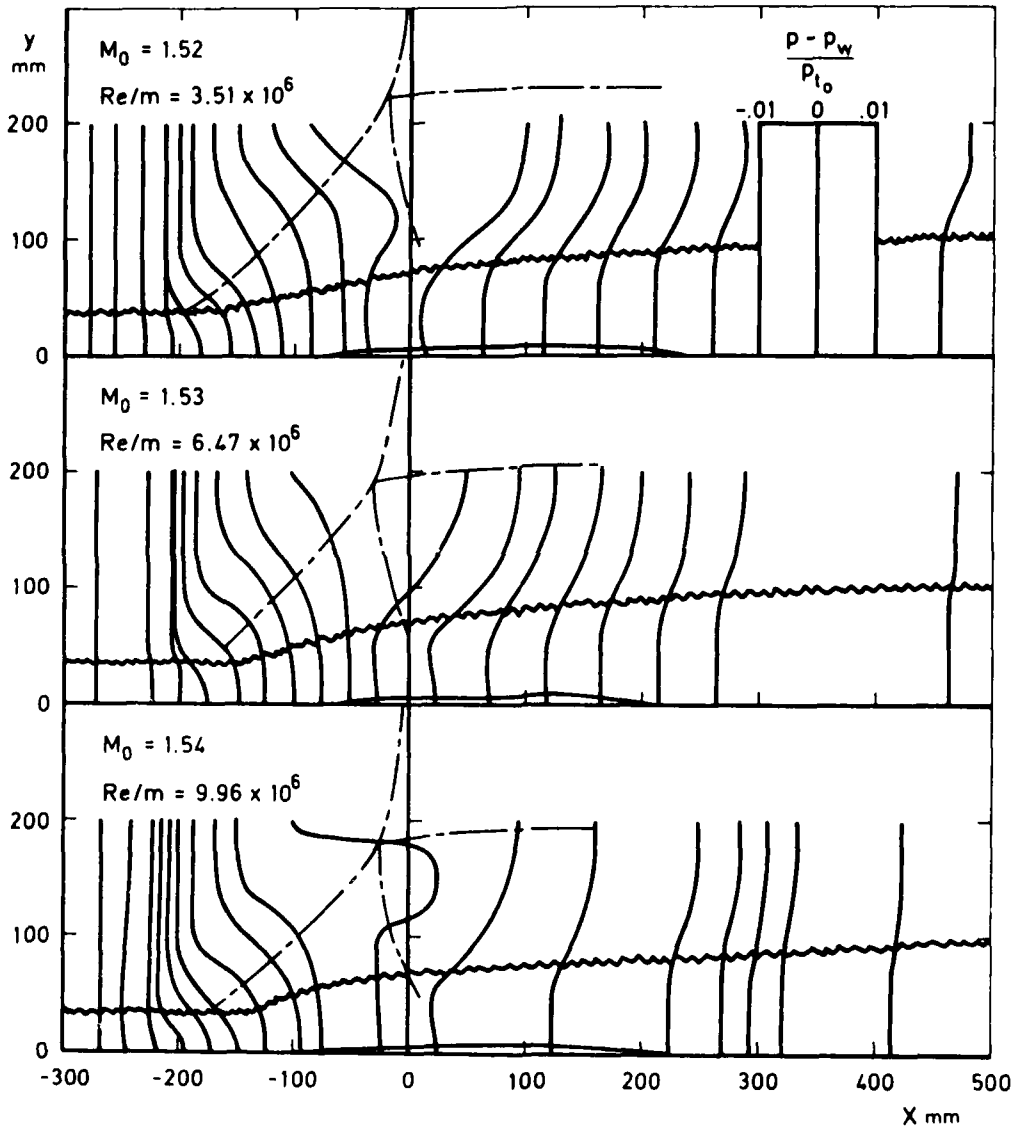


Fig 15b Measured static pressures

TH 82099

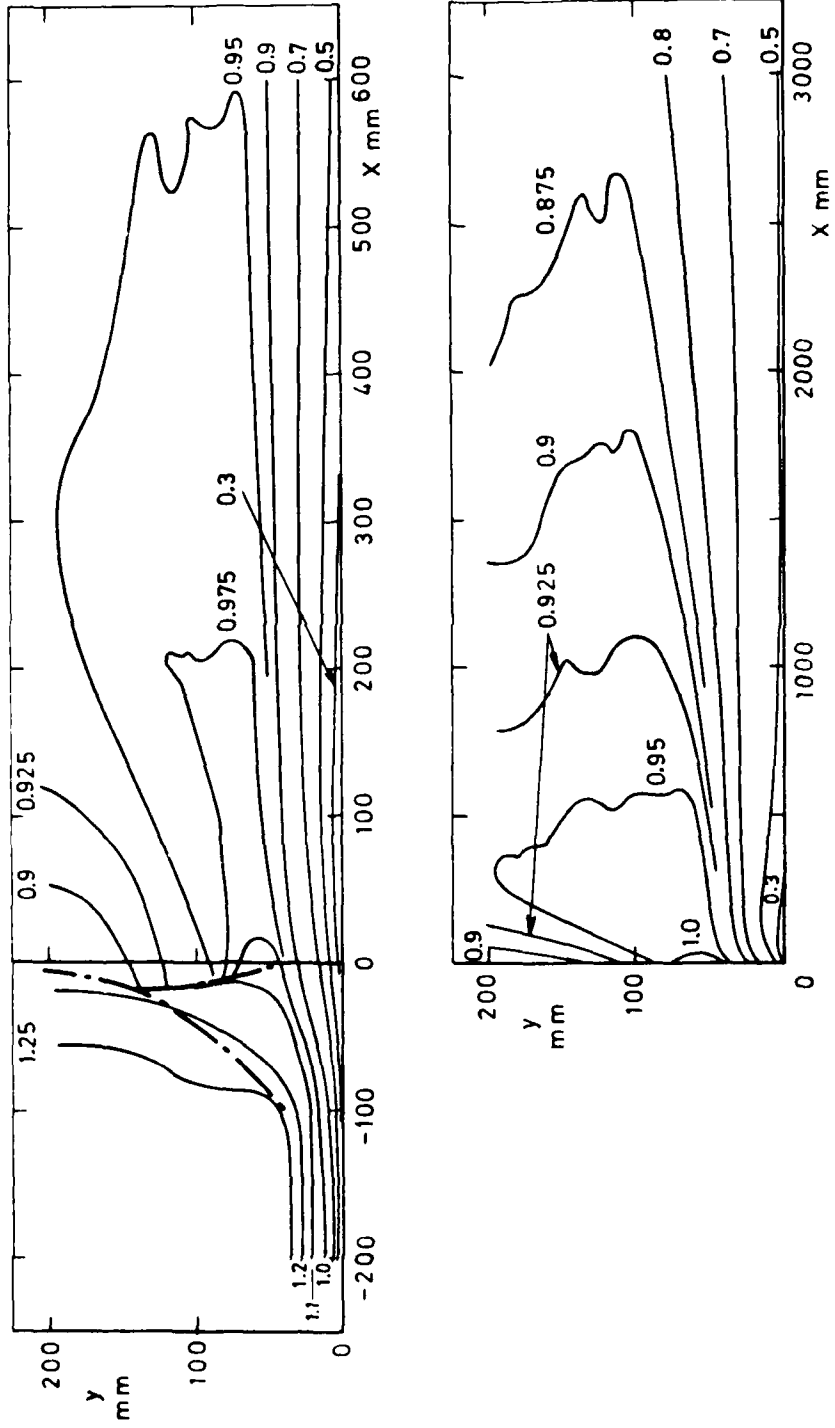


Fig 16a Mach number distribution,  $M_0 = 1.27$ ,  $Re/m = 3.66 \times 10^6$

Fig 16a

Fig 16b

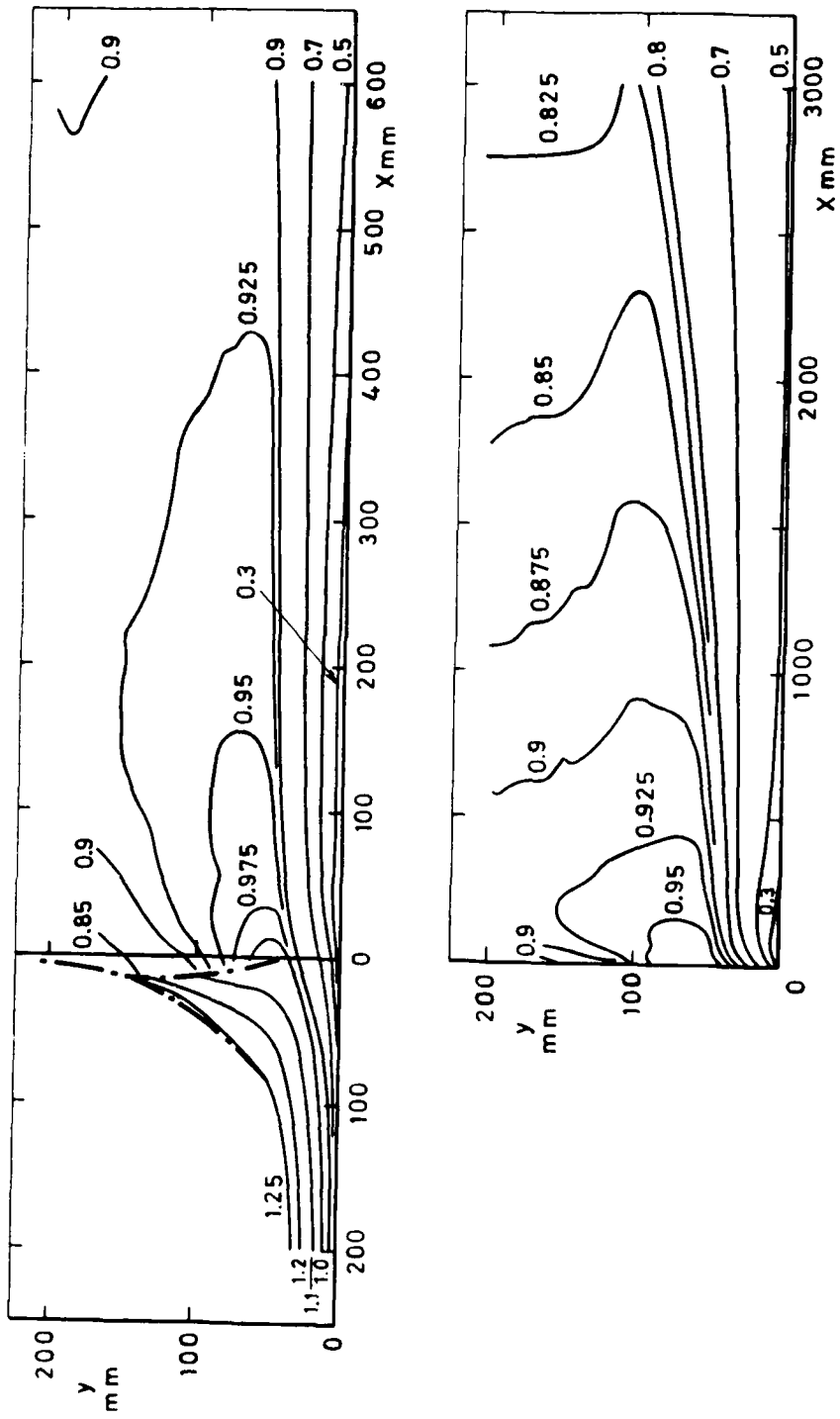


Fig 16b Mach number distribution,  $M_0 = 1.27$ ,  $Re/m = 10.2 \times 10^6$

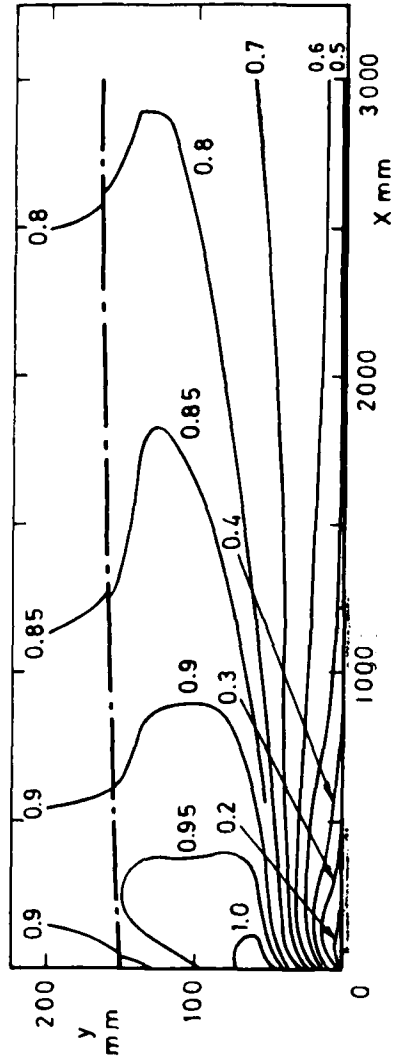
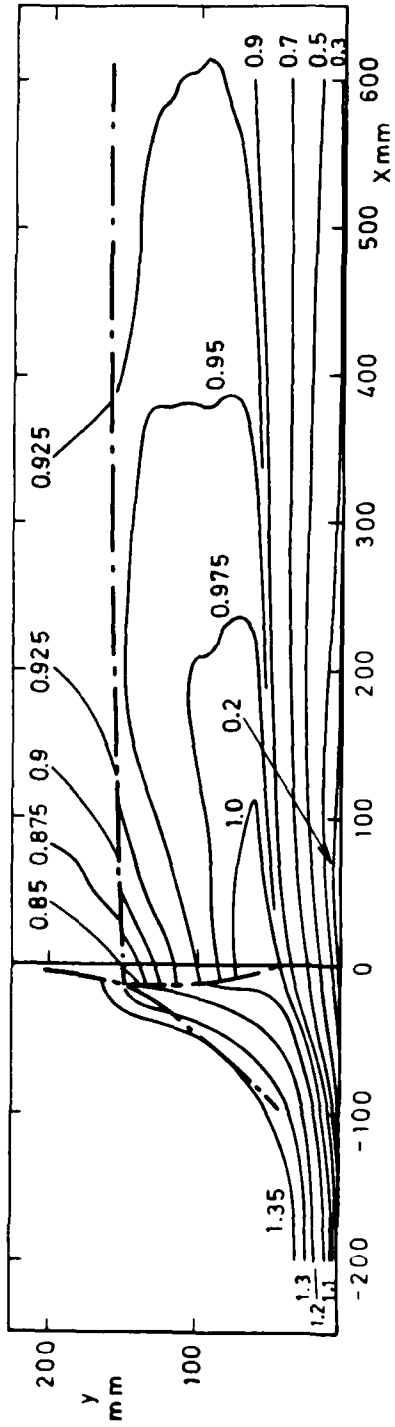


Fig 16c Mach number distribution,  $M_0 = 1.39$ ,  $Re/m = 10.0 \times 10^6$

Fig 16c

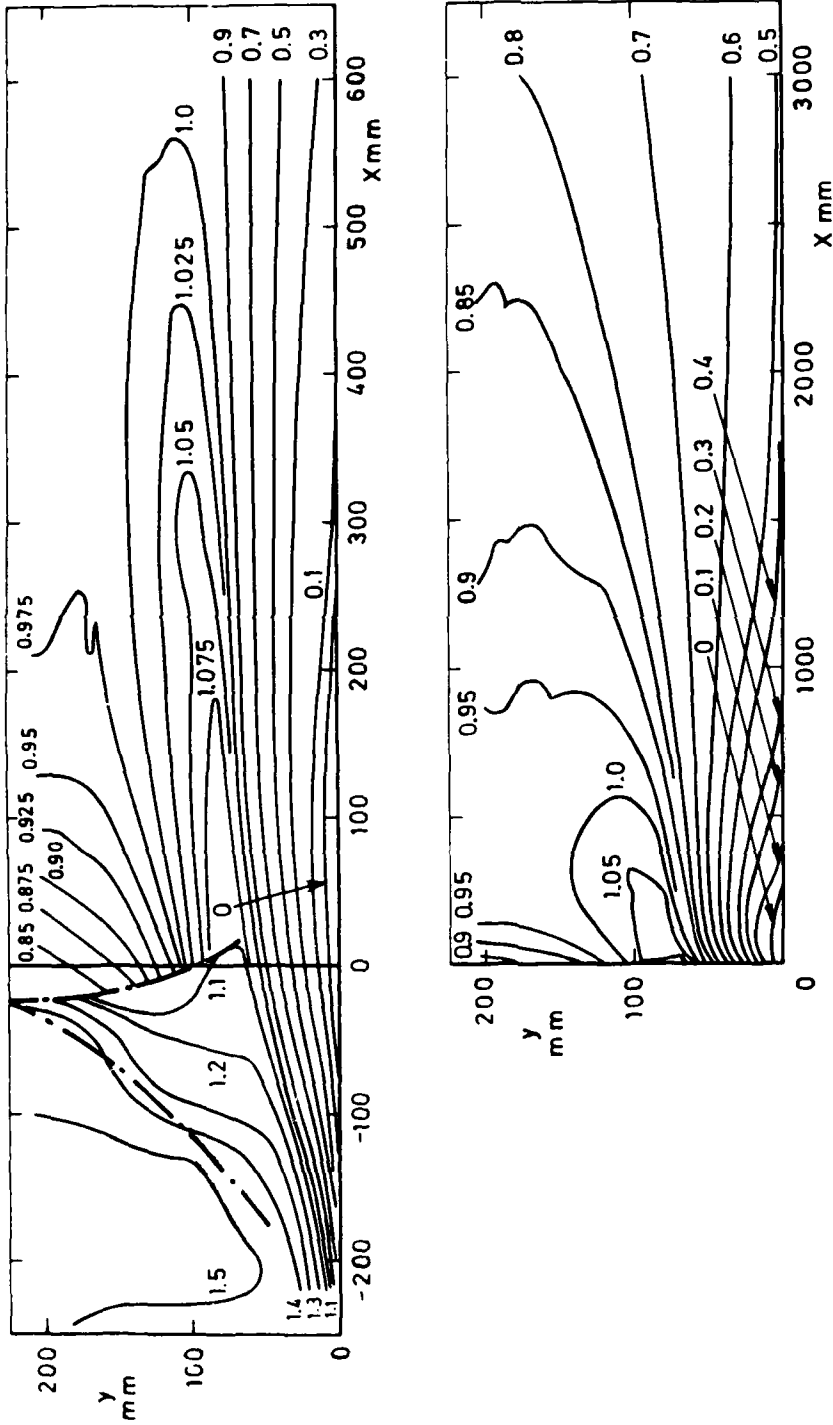


Fig 16d Mach number distribution,  $M_0 = 1.52$ ,  $Re/m = 3.51 \times 10^6$

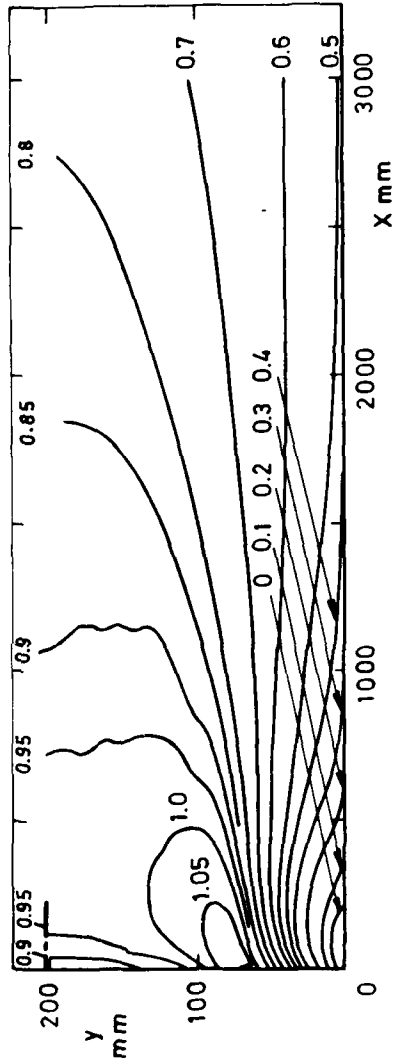
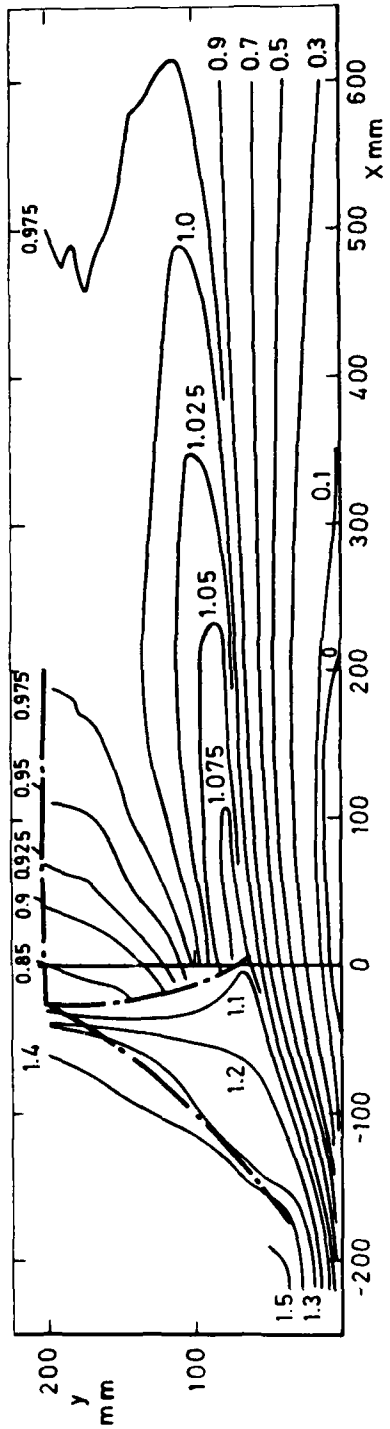


Fig 16e Mach number distribution,  $M_0 = 1.53$ ,  $Re/m = 6.47 \times 10^6$

Fig 16e

Fig 16f

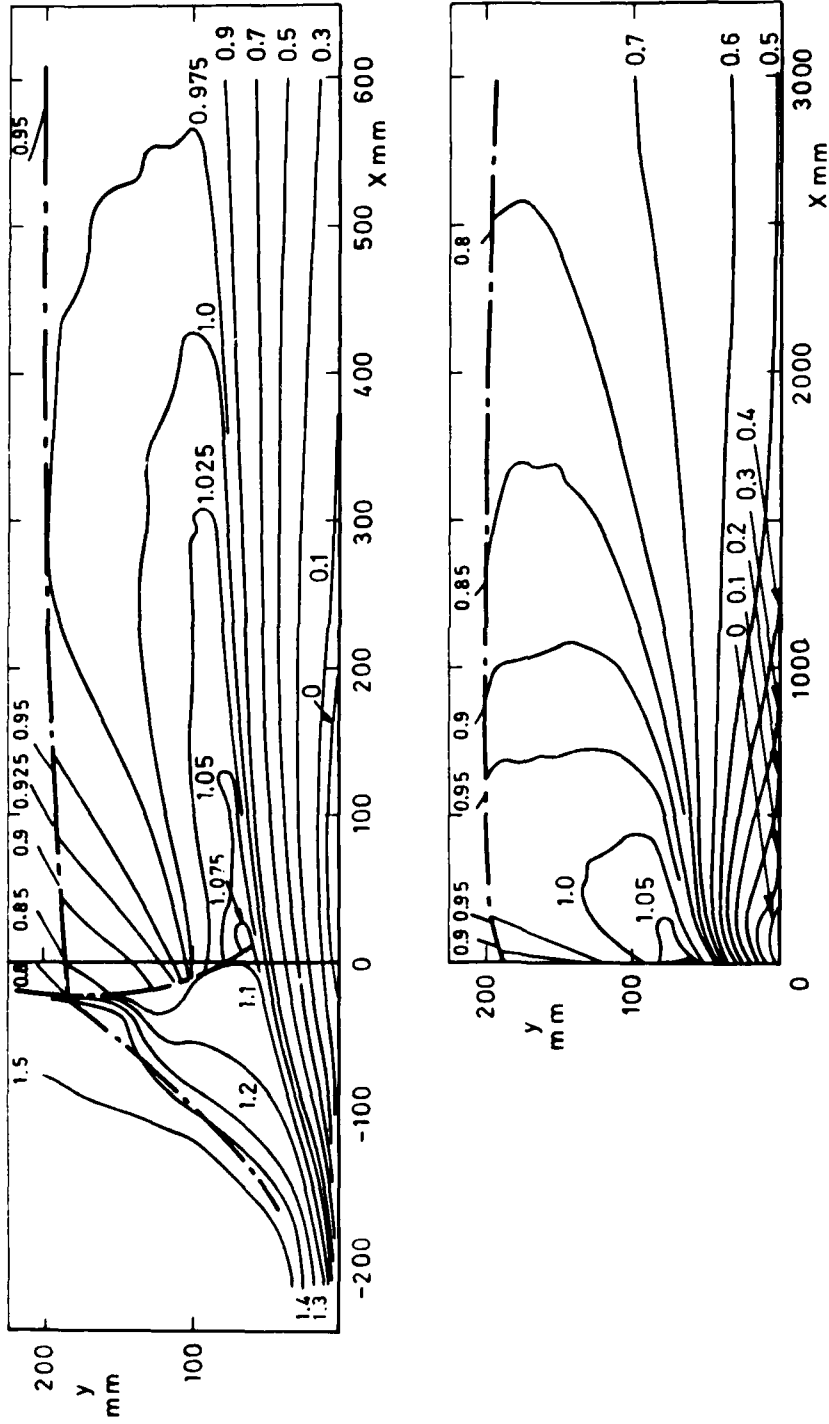


Fig 16f Mach number distribution,  $M_0 = 1.54$ ,  $Re/m = 9.96 \times 10^6$

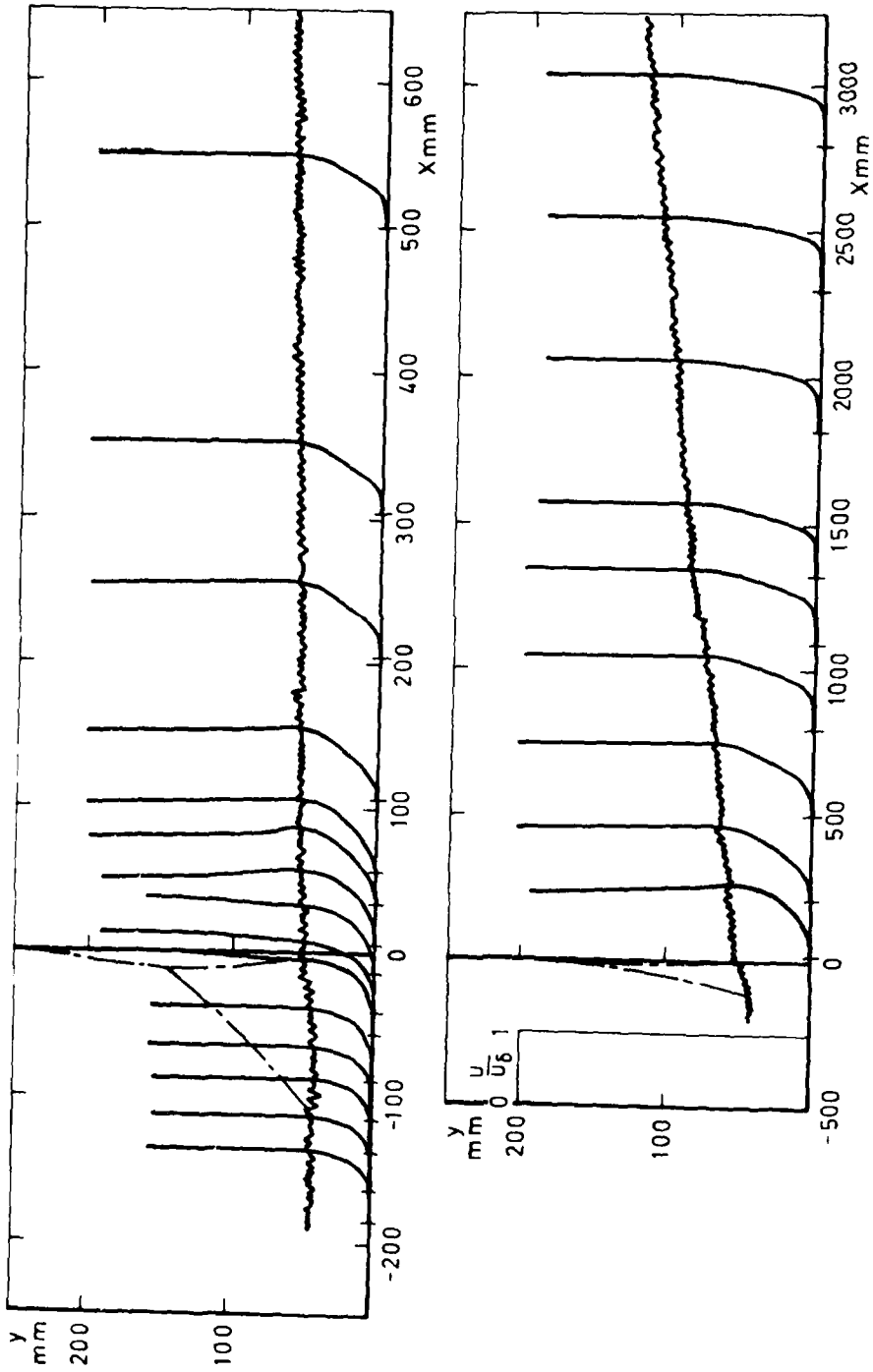


Fig 17a Velocity profiles,  $M_0 = 1.27$ ,  $Re/m = 3.66 \times 10^6$



Fig 17b

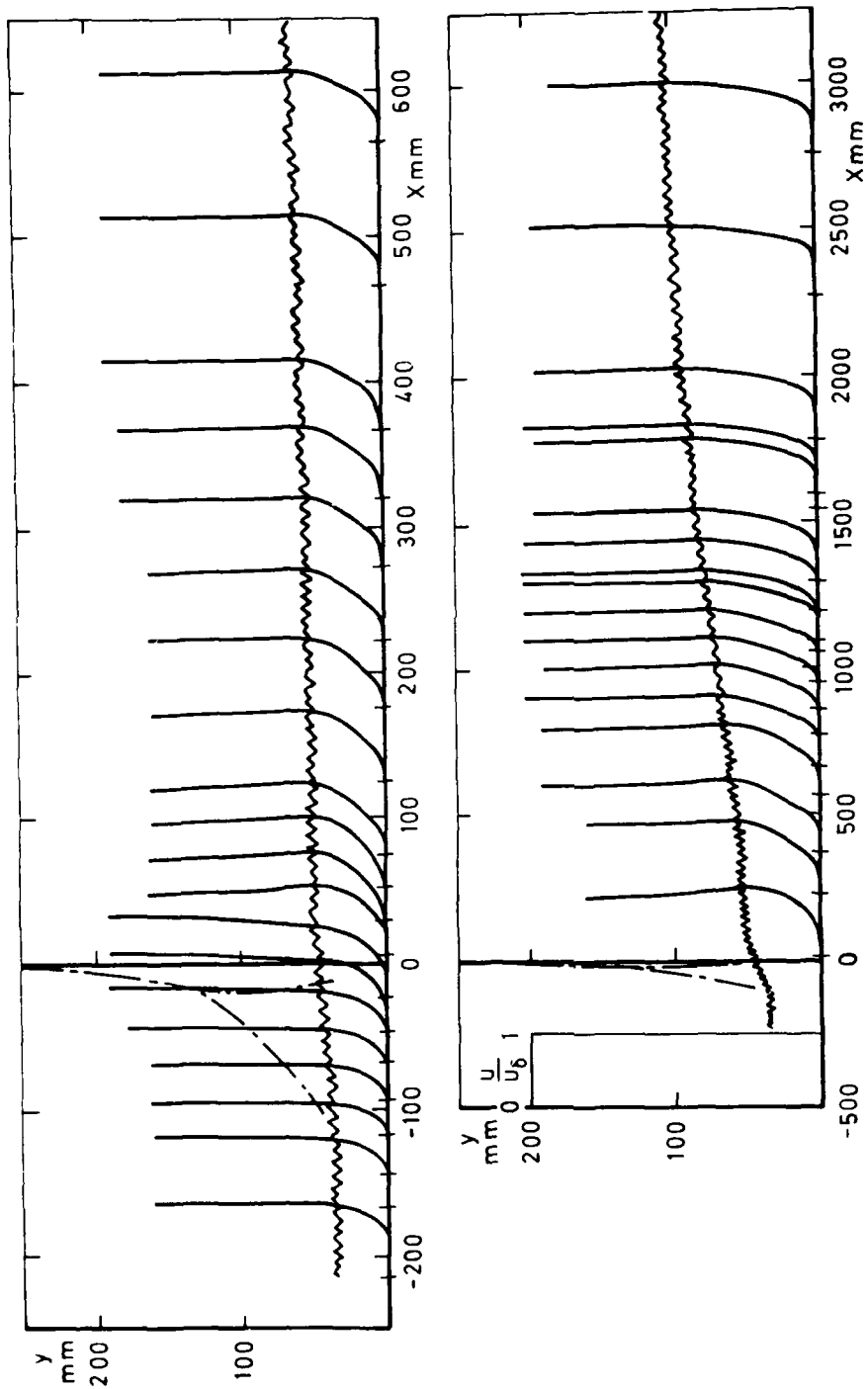


Fig 17b Velocity profiles,  $M_0 = 1.27$ ,  $Re/m = 10.2 \times 10^6$

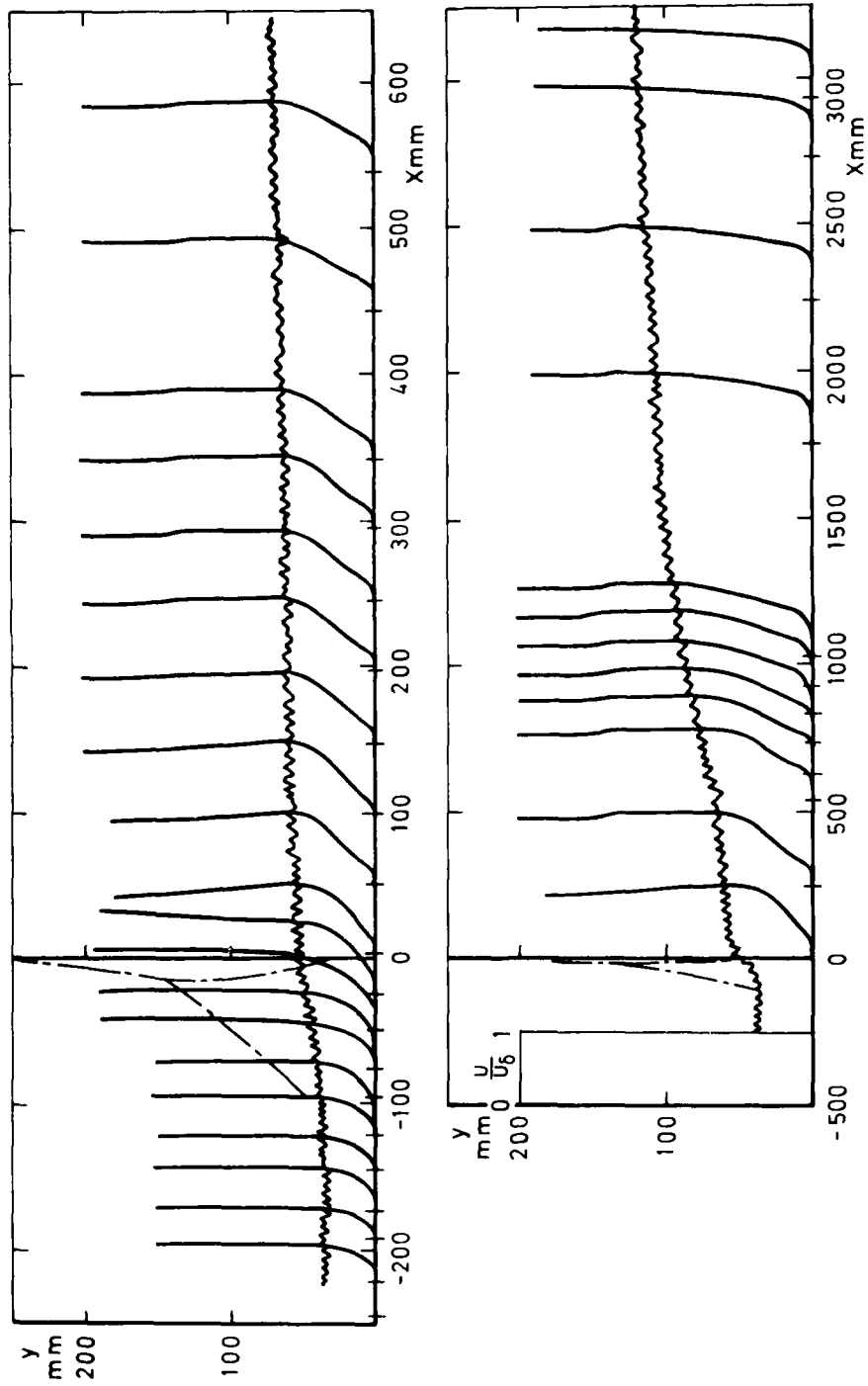


Fig 17c Velocity profiles,  $M_0 = 1.39$ ,  $Re/m = 10.0 \times 10^6$

Fig 17d

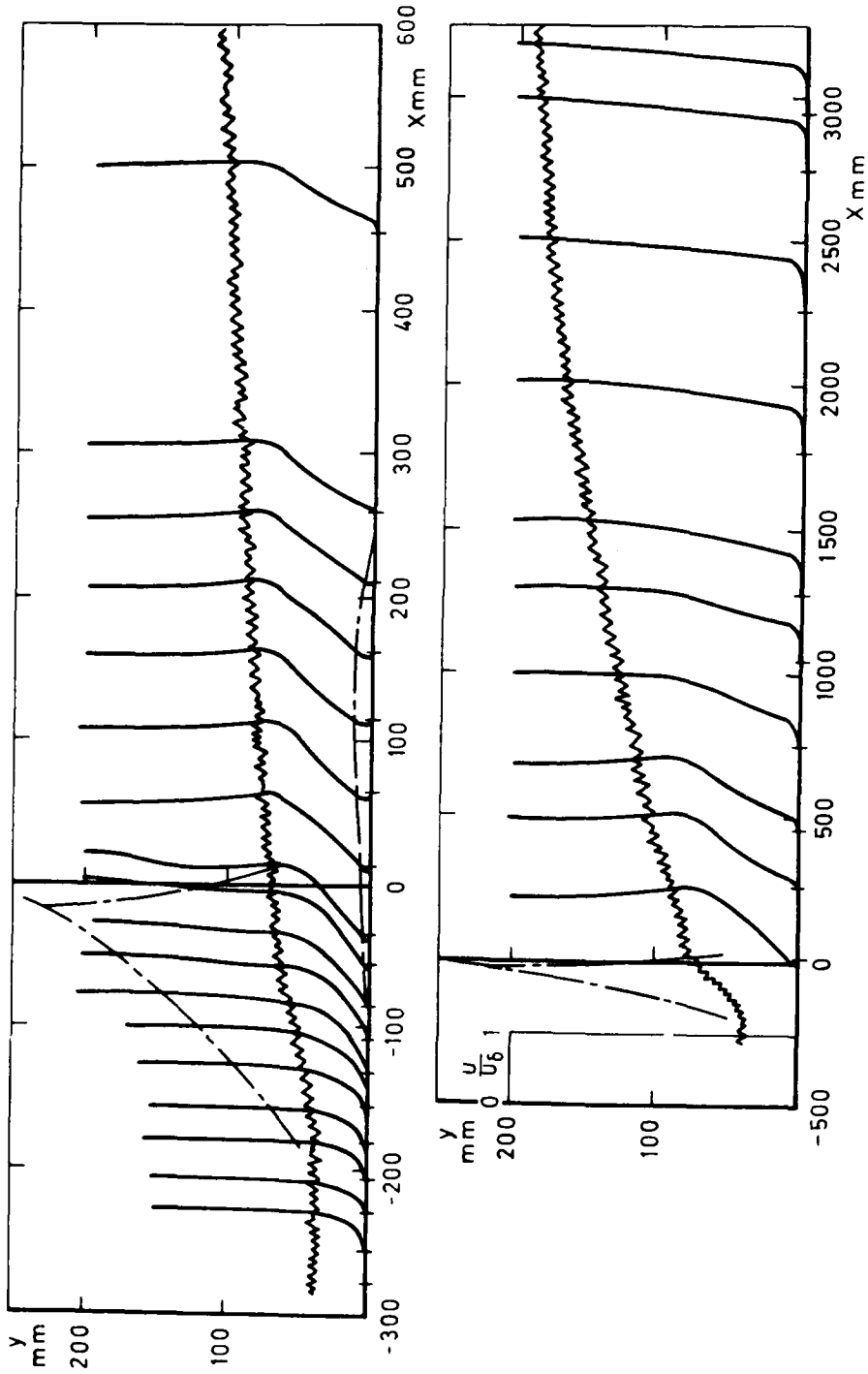


Fig 17d Velocity profiles,  $M_0 = 1.52$ ,  $Re/m = 3.51 \times 10^6$

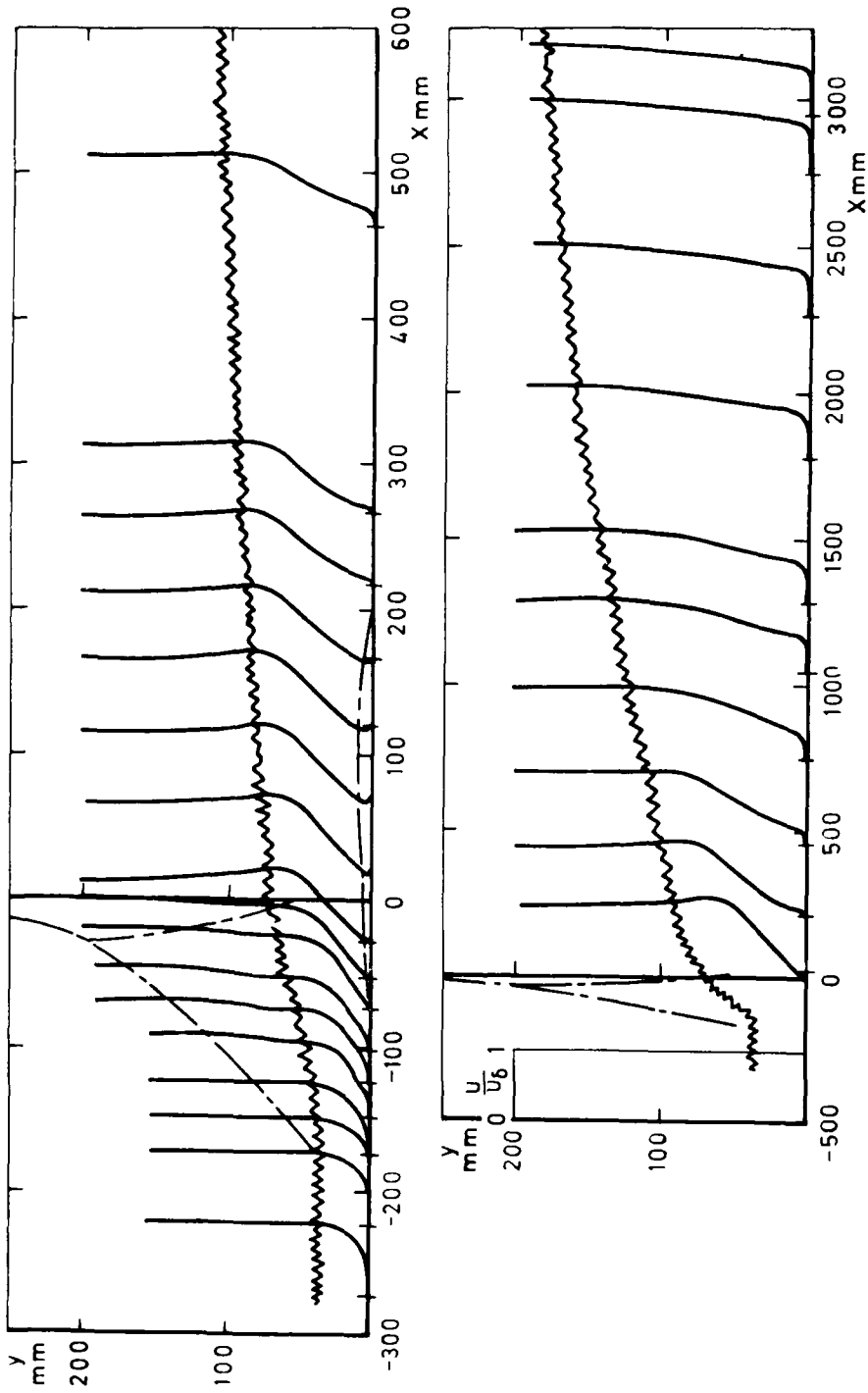


Fig 17e Velocity profiles,  $M_0 = 1.53$ ,  $Re/m = 6.47 \times 10^6$

Fig 17f

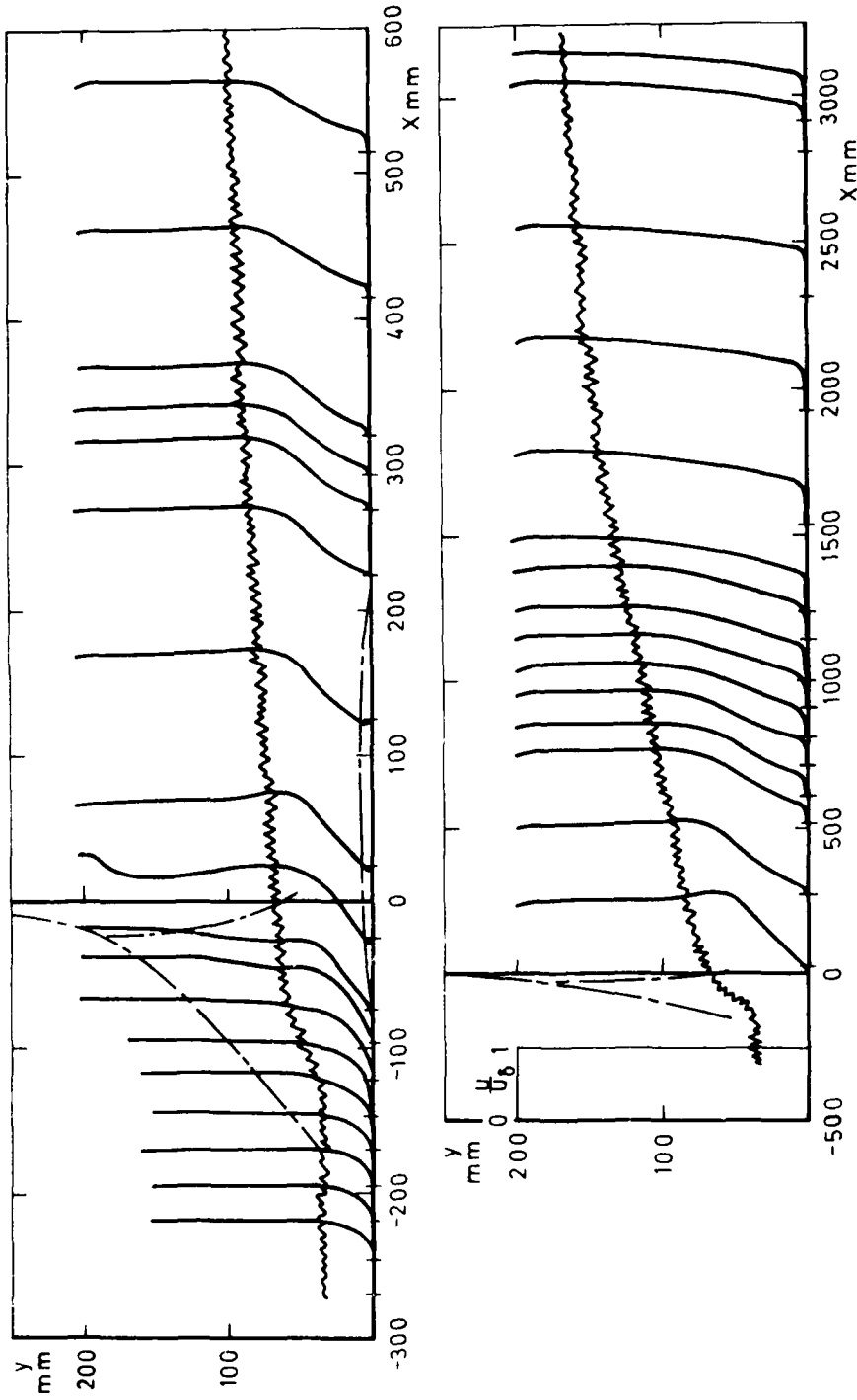


Fig 17f Velocity profiles,  $M_0 = 1.54$ ,  $Re/m = 9.96 \times 10^6$

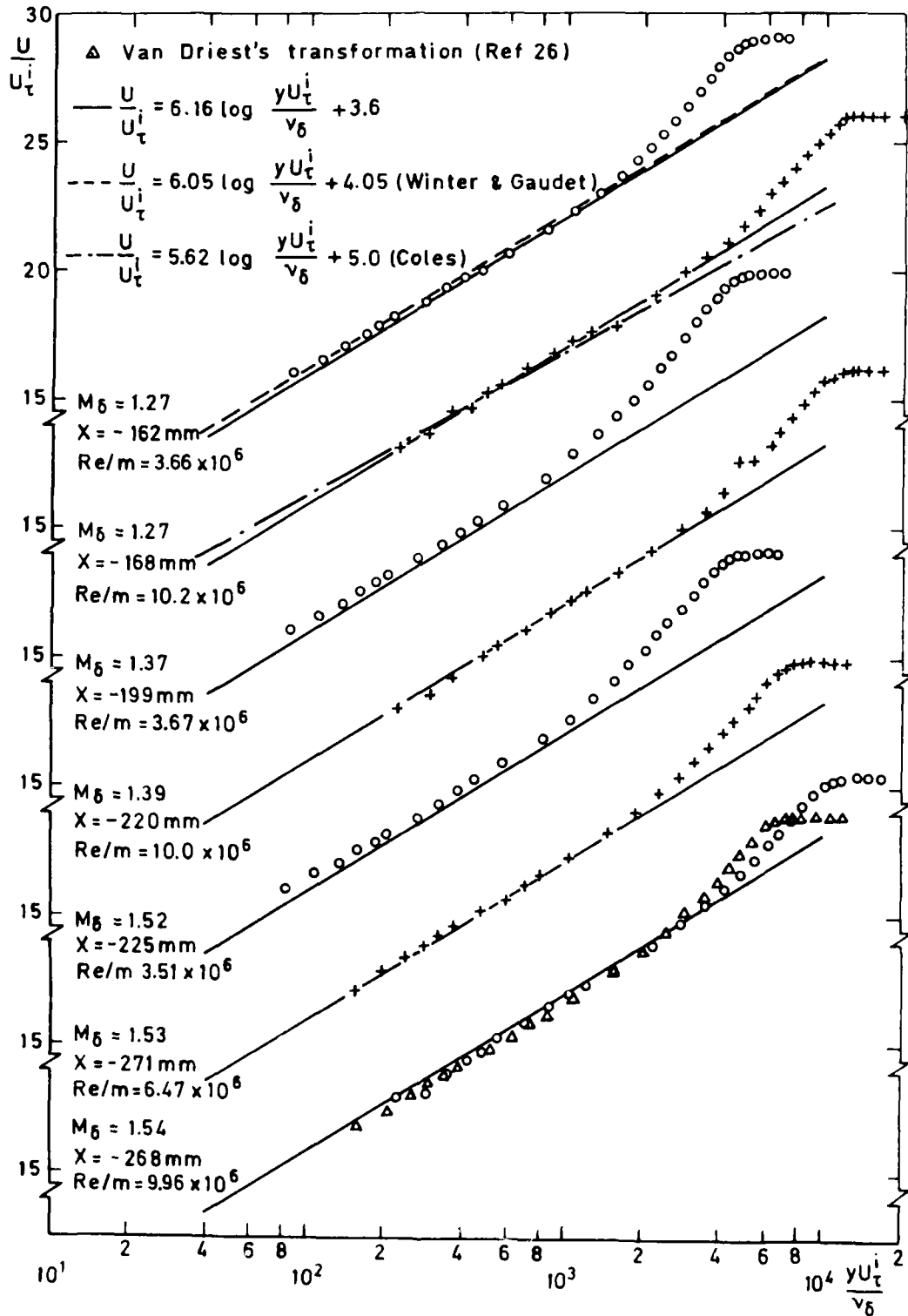


Fig 18 Logarithmic velocity profiles ahead of interaction (region A) (see Fig 22)

Fig 19

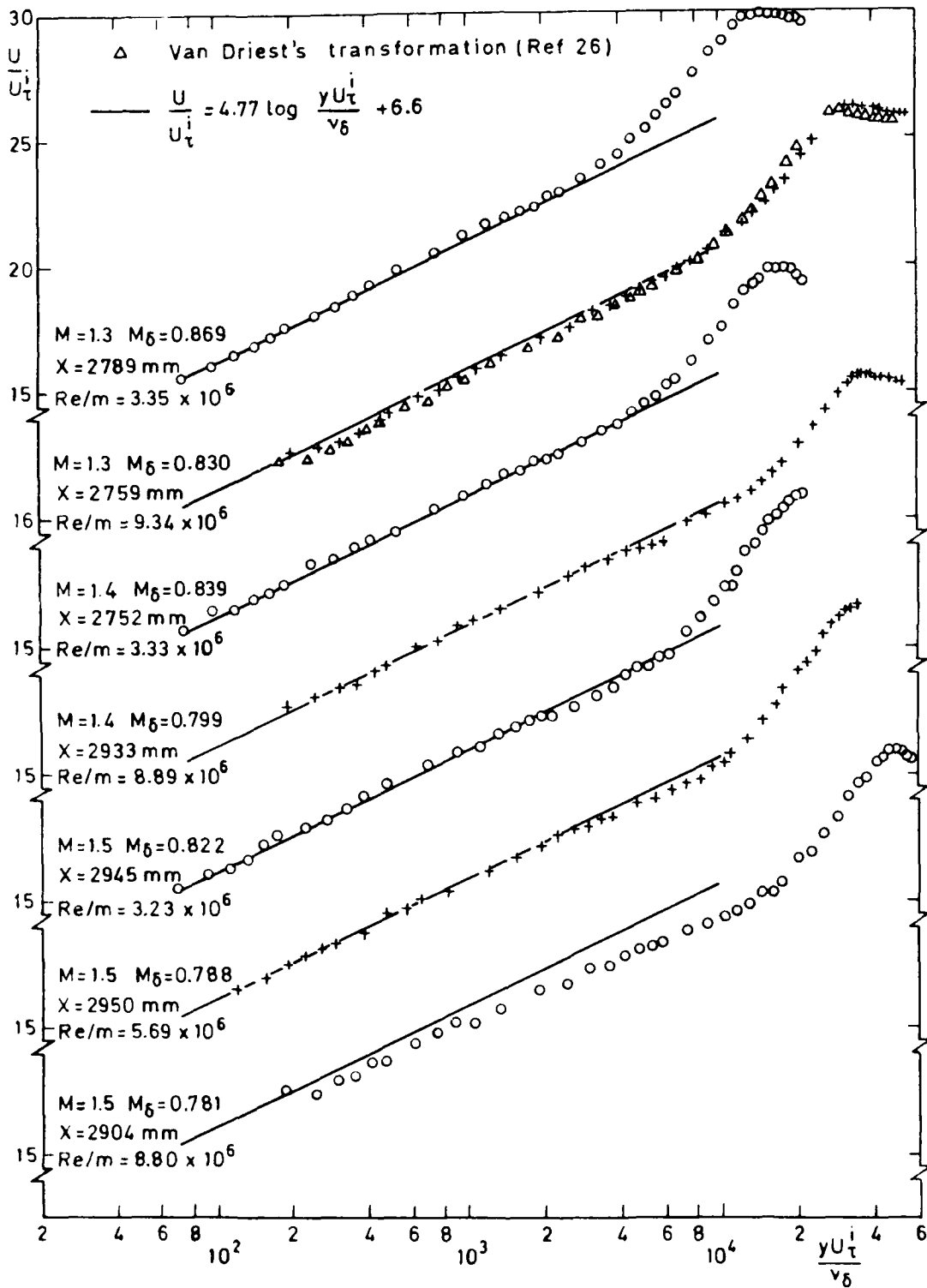


Fig 19 Logarithmic velocity profiles approx 3 m downstream of normal shock-wave (region D) (see Fig 22)

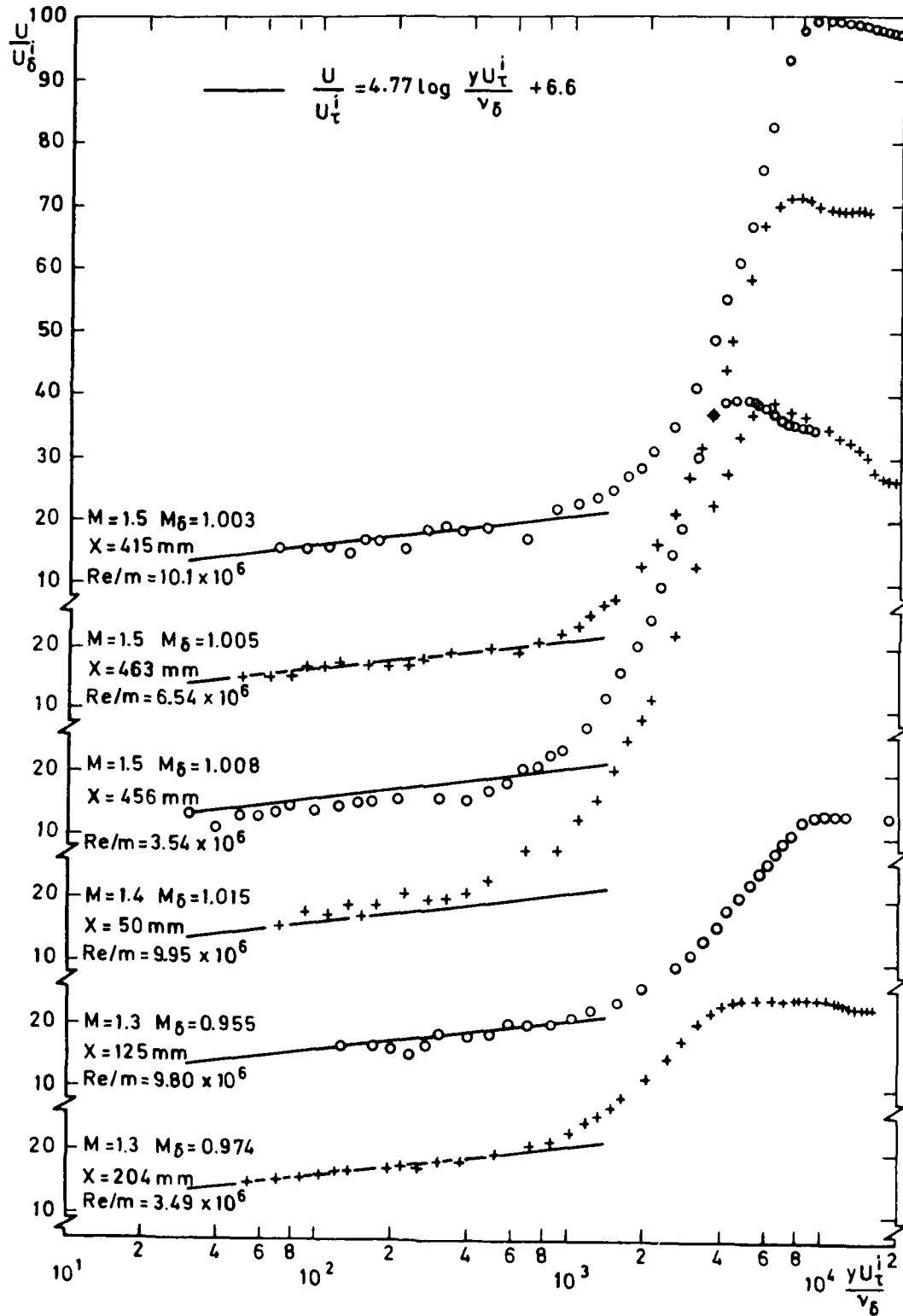


Fig 20 Logarithmic velocity profiles just downstream of normal shock-wave (region C) (see Fig 22)



Fig 21

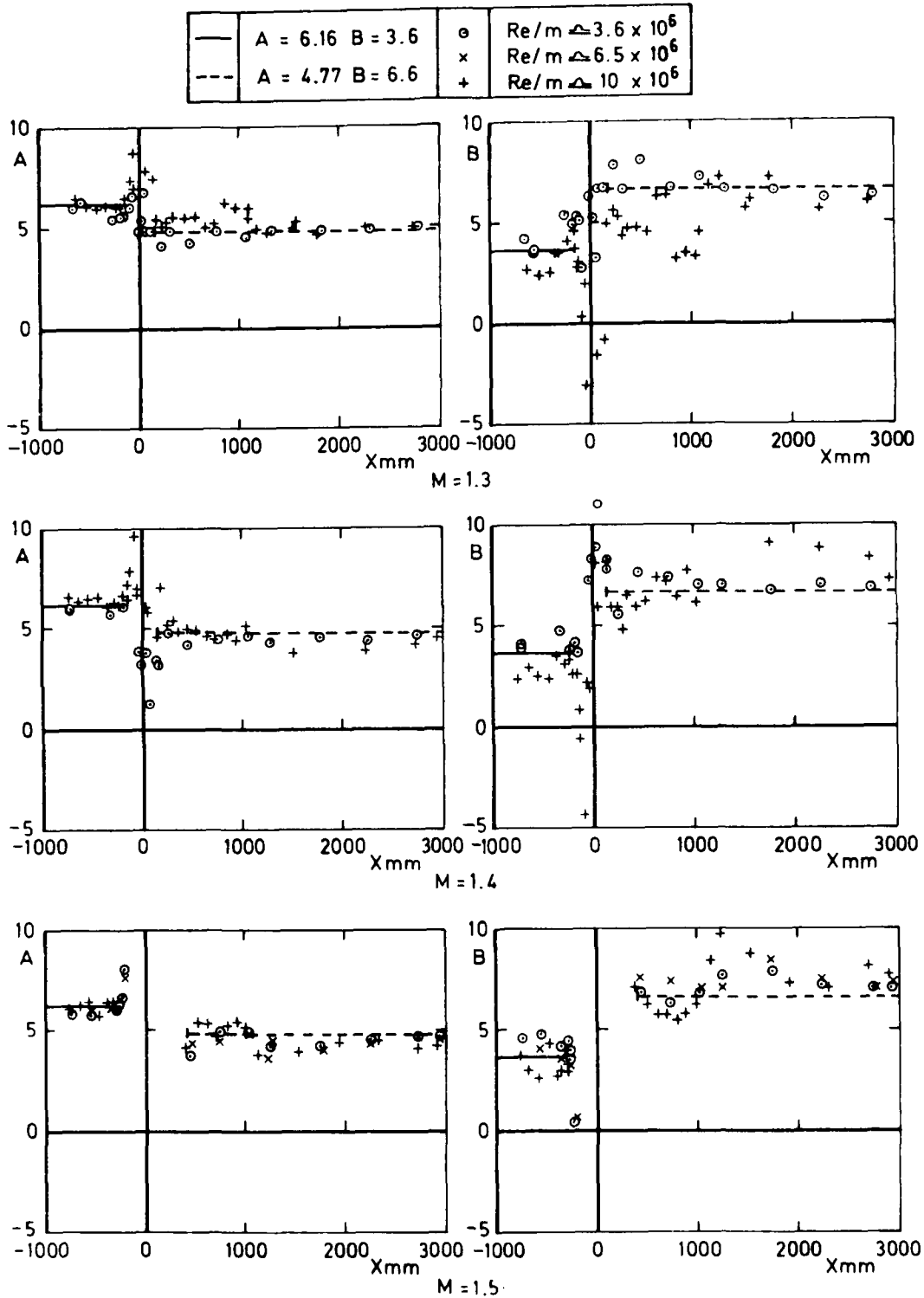


Fig 21 Variation of the constants A and B in the law of the wall  
 $(U/U_T^i = A \log yU_T^i/\nu_\delta + B)$

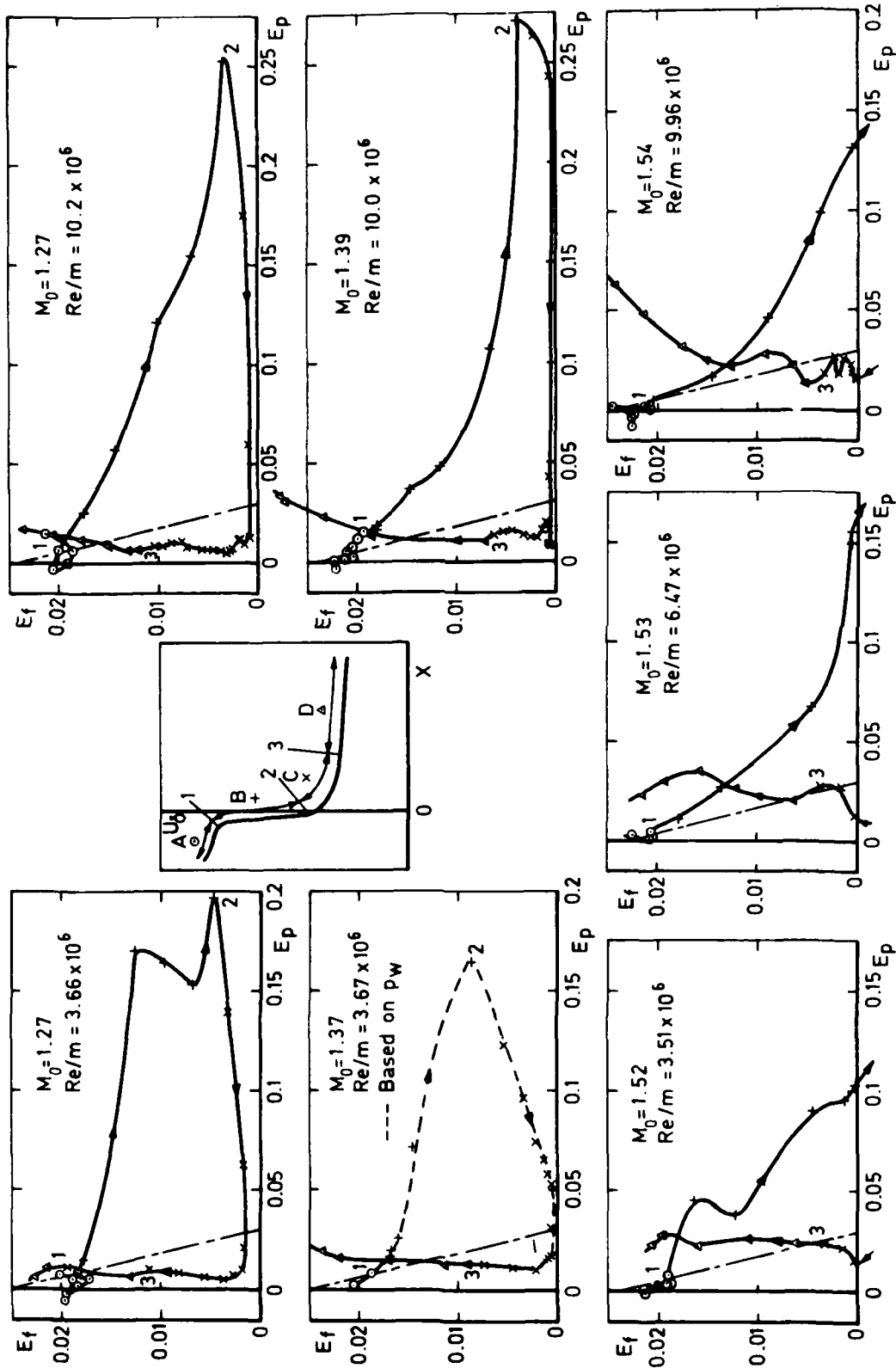


Fig 22

Fig 22 Equilibrium parameters

Fig 23a&b

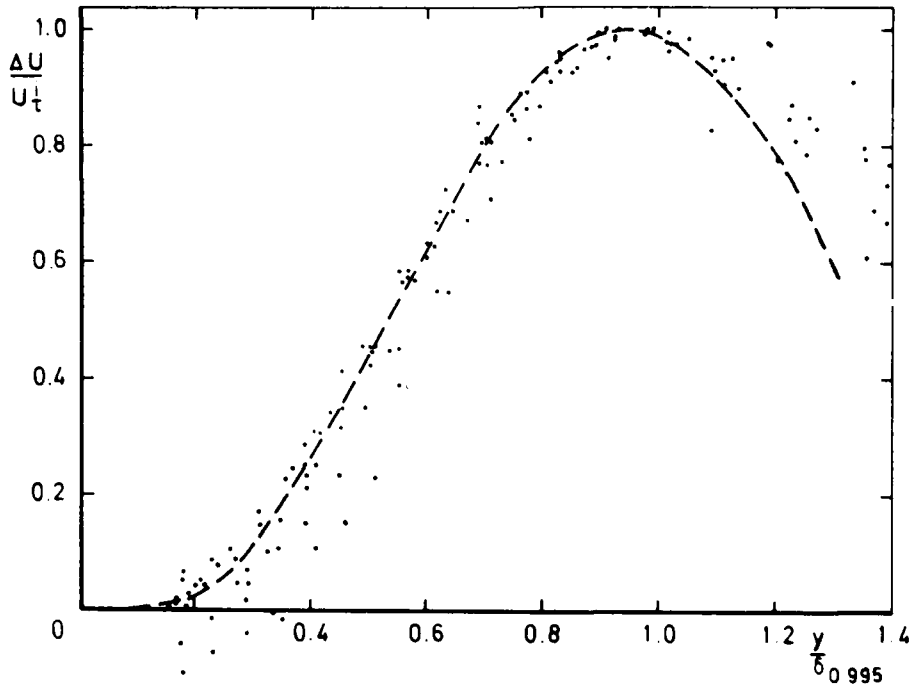
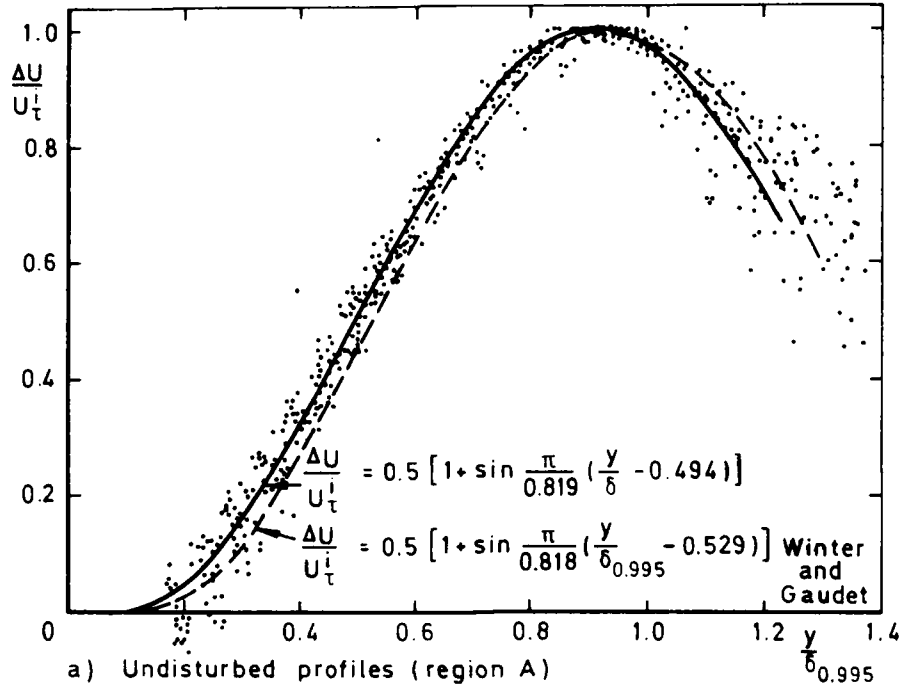
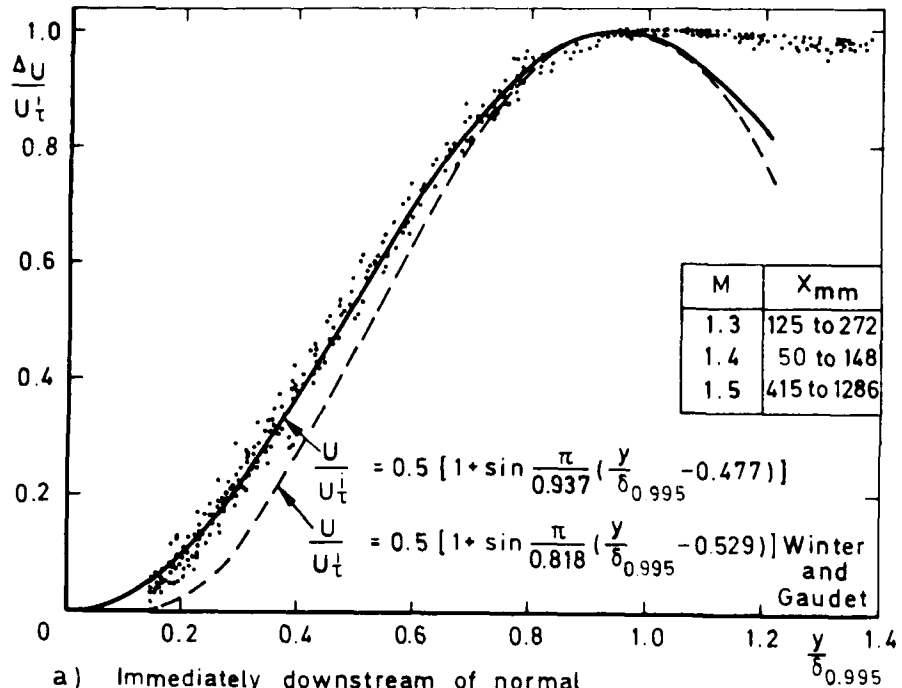
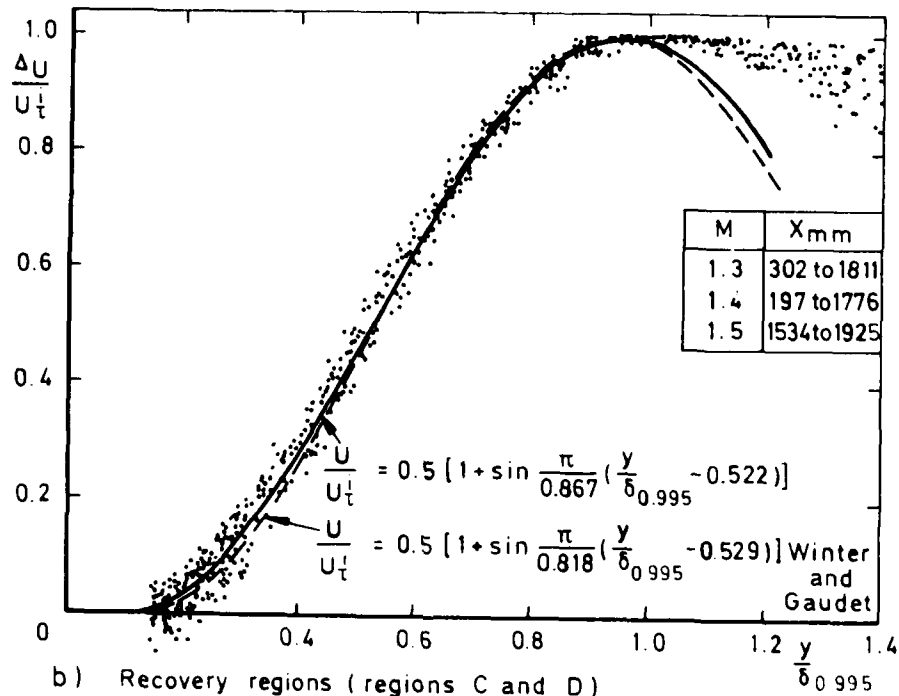


Fig 23a&b Wake components of velocity profiles ahead of shock-wave

Fig 24a&b



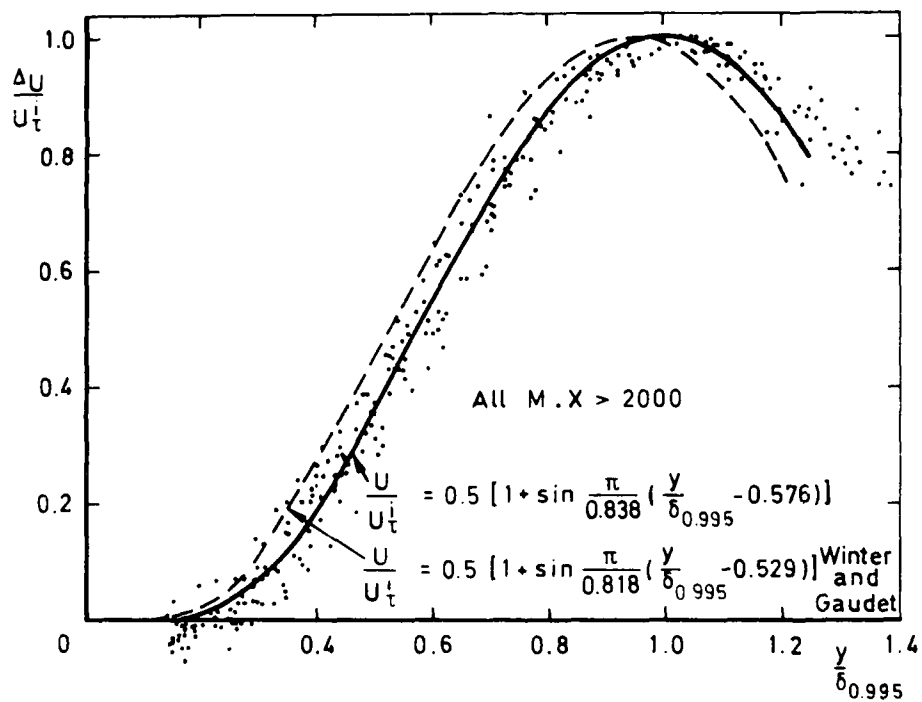
a) Immediately downstream of normal shock-wave (region C)



b) Recovery regions (regions C and D)

Fig 24a&b Wake components of velocity profiles downstream of shock-wave

Fig 24c



c)  $X > 2000\text{mm}$  (region D)

Fig 24c Wake components of velocity profiles downstream of shock-wave

Fig 25a&b

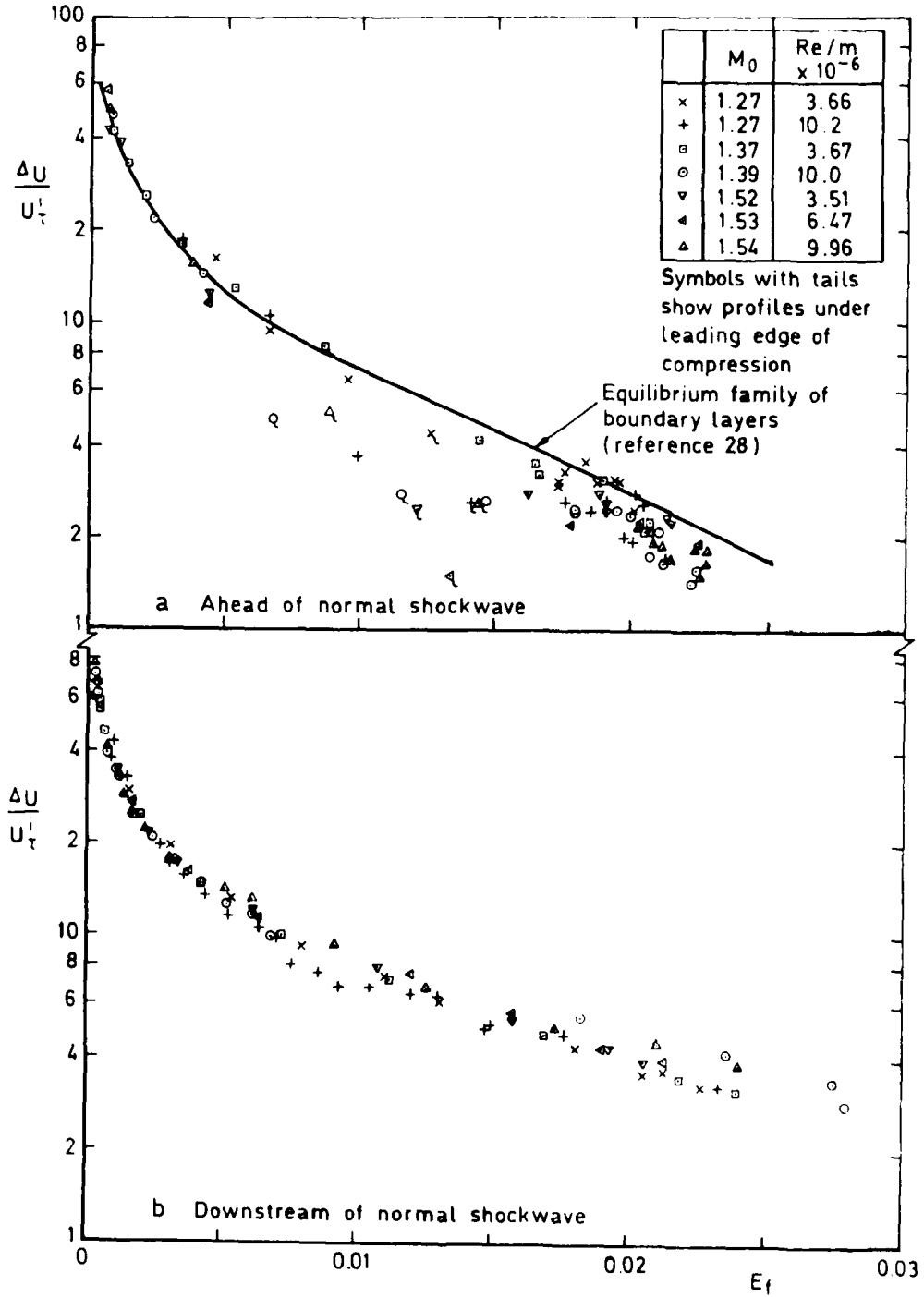
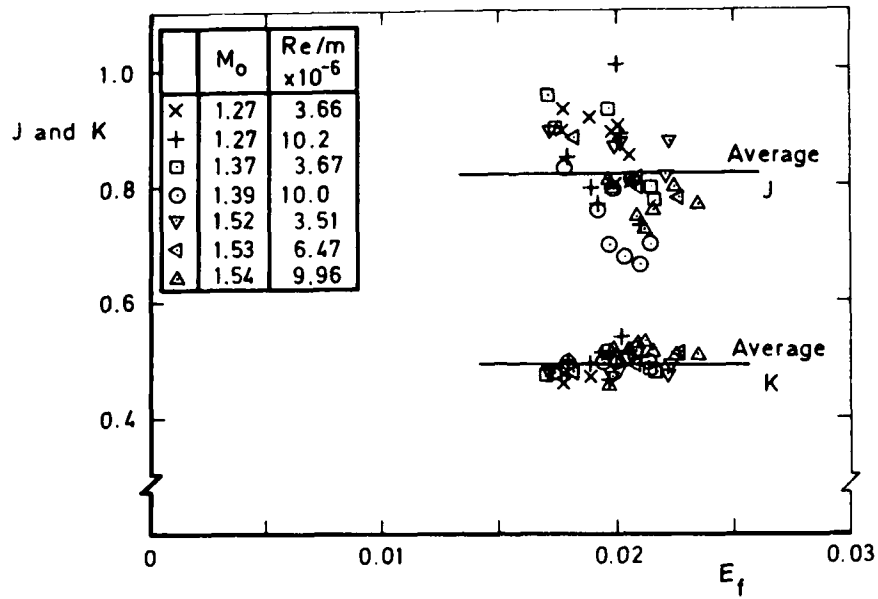
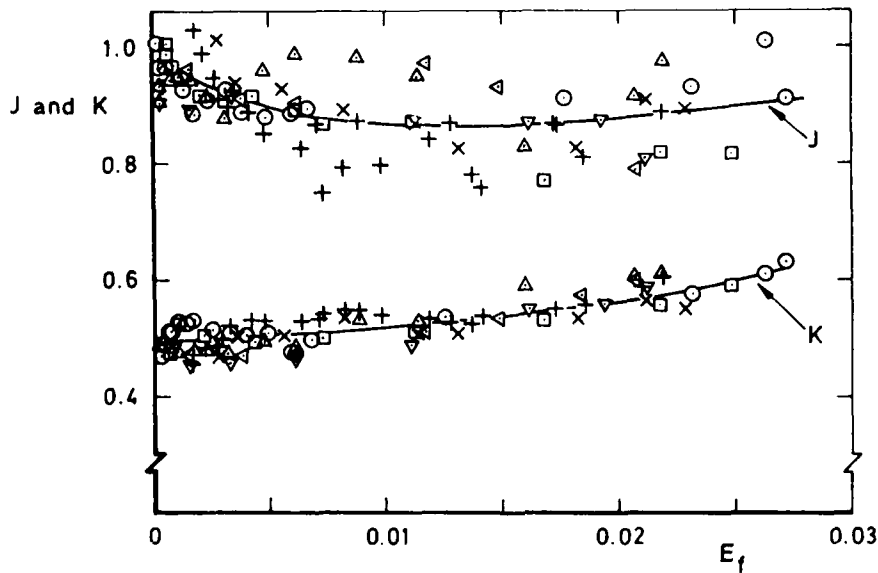


Fig 25a&b Maximum values of wake component

Fig 26a&b



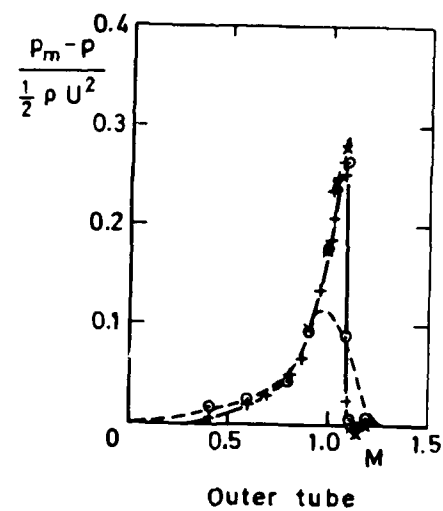
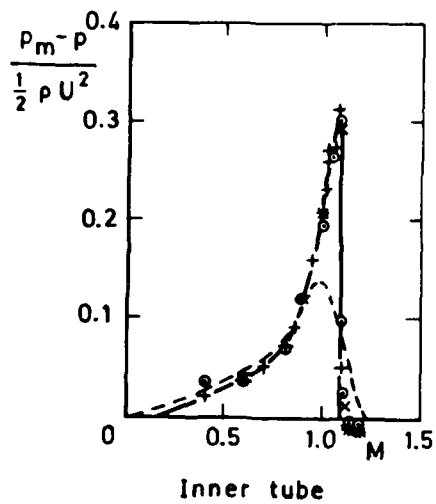
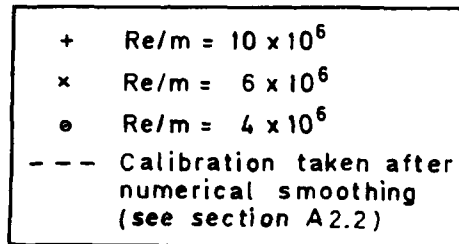
(a) Ahead of interaction



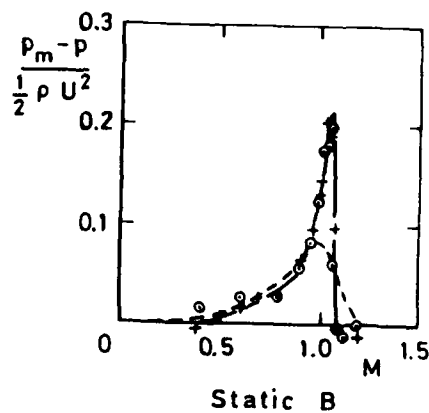
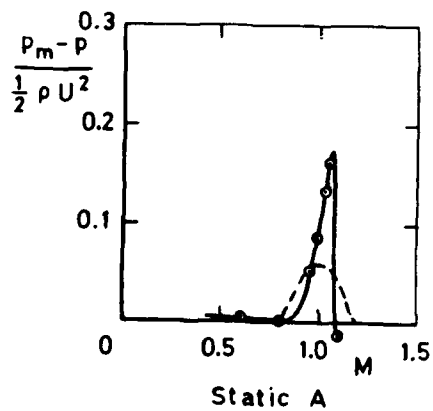
(b) Downstream of normal shockwave

Fig 26a&b Constants J and K in  $(\Delta U/U_r^i)_N = 0.5(1 + \sin \pi/J(\gamma/\delta_{0.995} - K))$

Fig 27a&b



a) Twin static

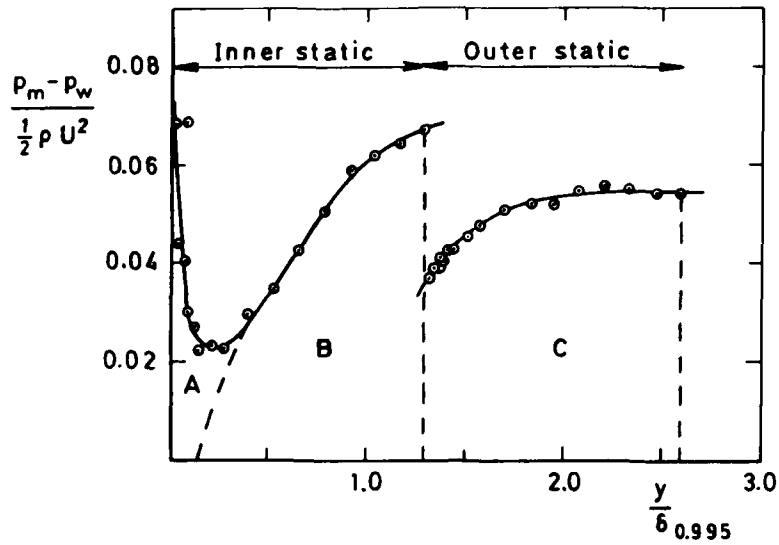


b) Single statics

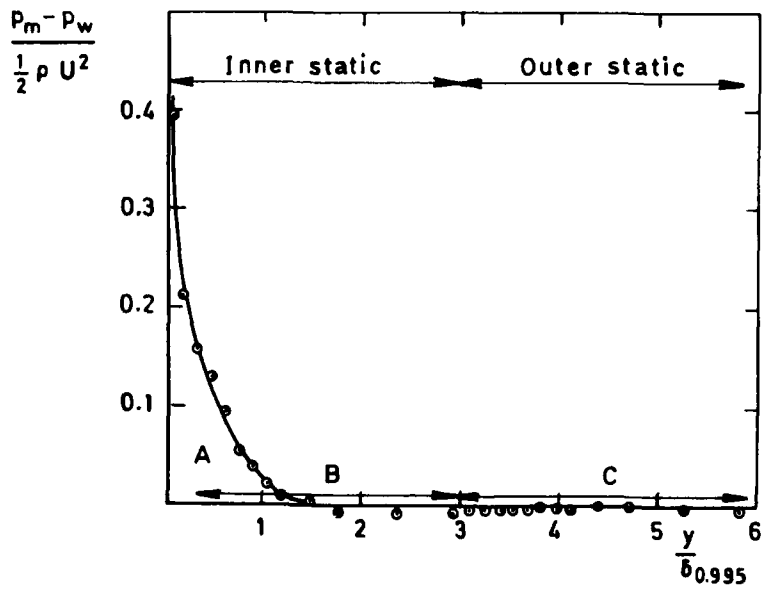
Fig 27a&b Free stream calibration of static probes



Fig 28a&b



a) Behind shockwave  
 $X = 1296 \text{ mm}$   $M_\delta = 0.887$



b) Ahead of shockwave  
 $X = -523 \text{ mm}$   $M_\delta = 1.284$

Fig 28a&b Typical static pressure measurement errors

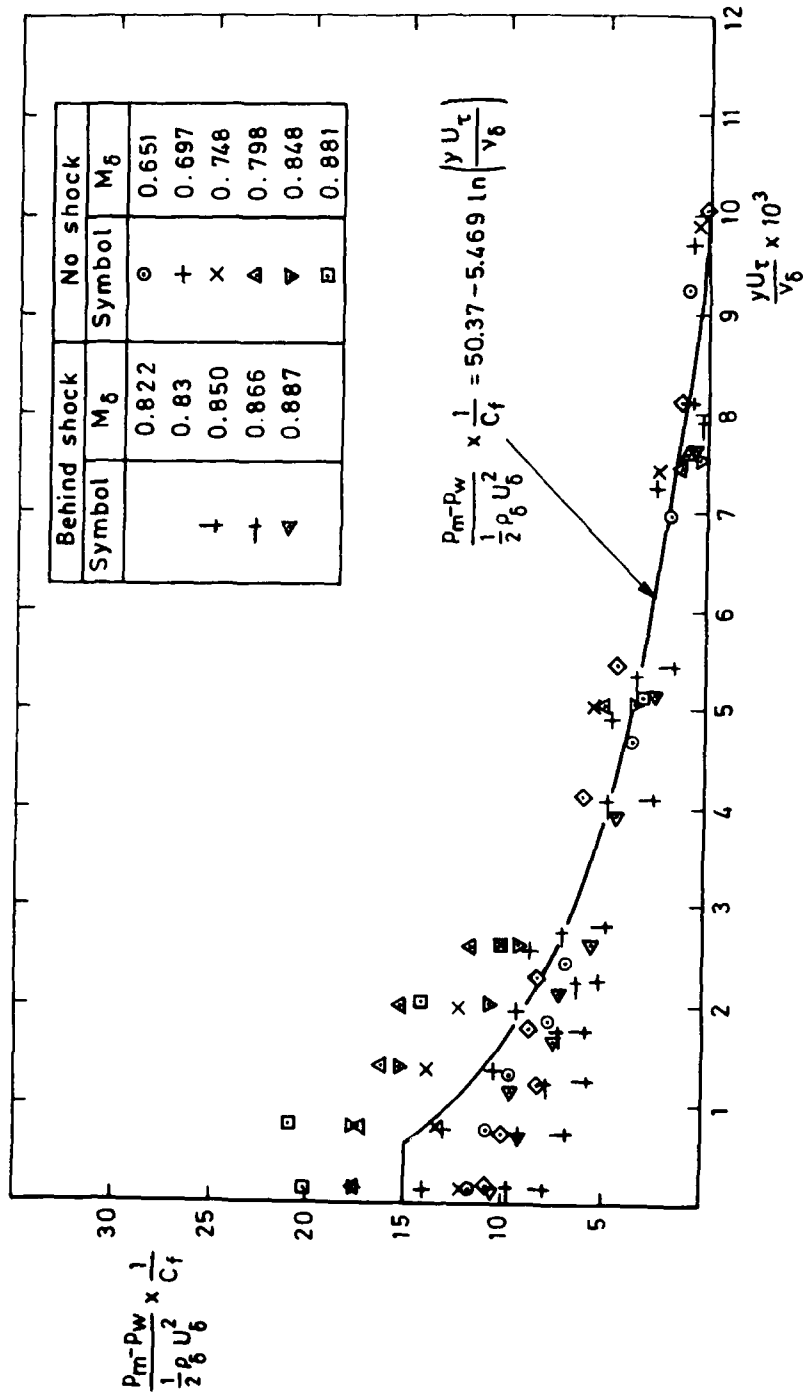


Fig 29 Wall/static interference errors,  $M_u \leq 1.098$

Fig 30

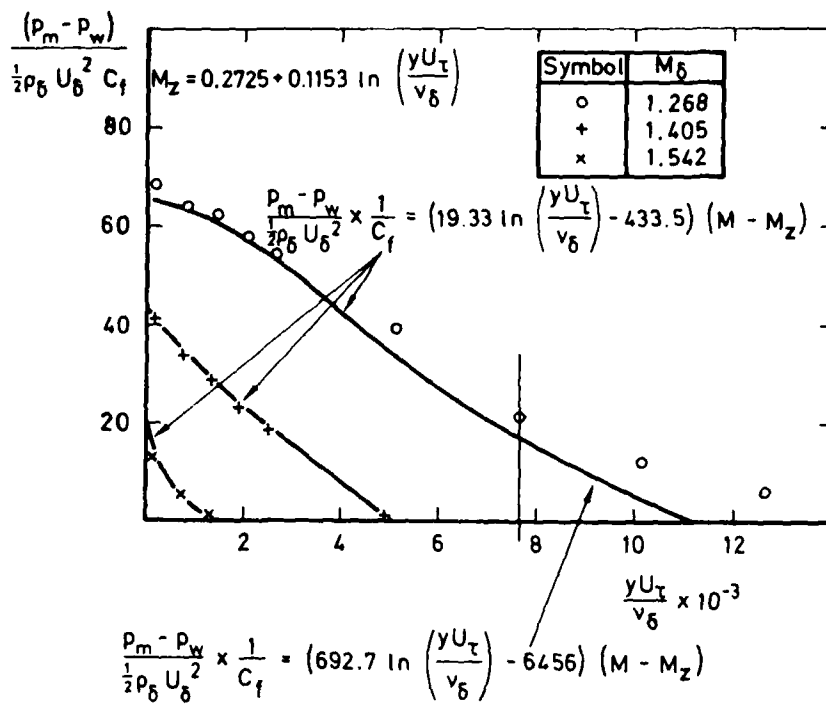
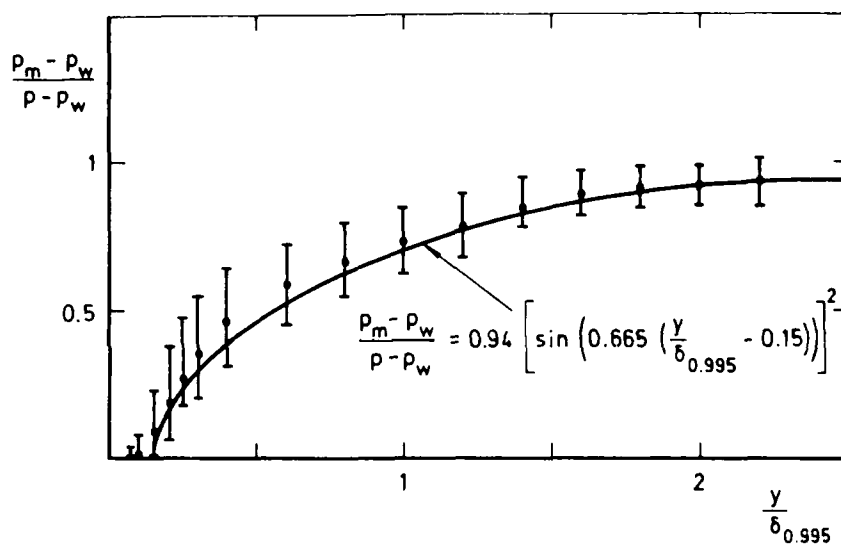


Fig 30 Wall/static interference errors,  $M_u \geq 1.098$

Fig 31



TR 82095

Fig 31 Modification to smoothed free stream static pressure calibration caused by probe position

Fig 32a&b

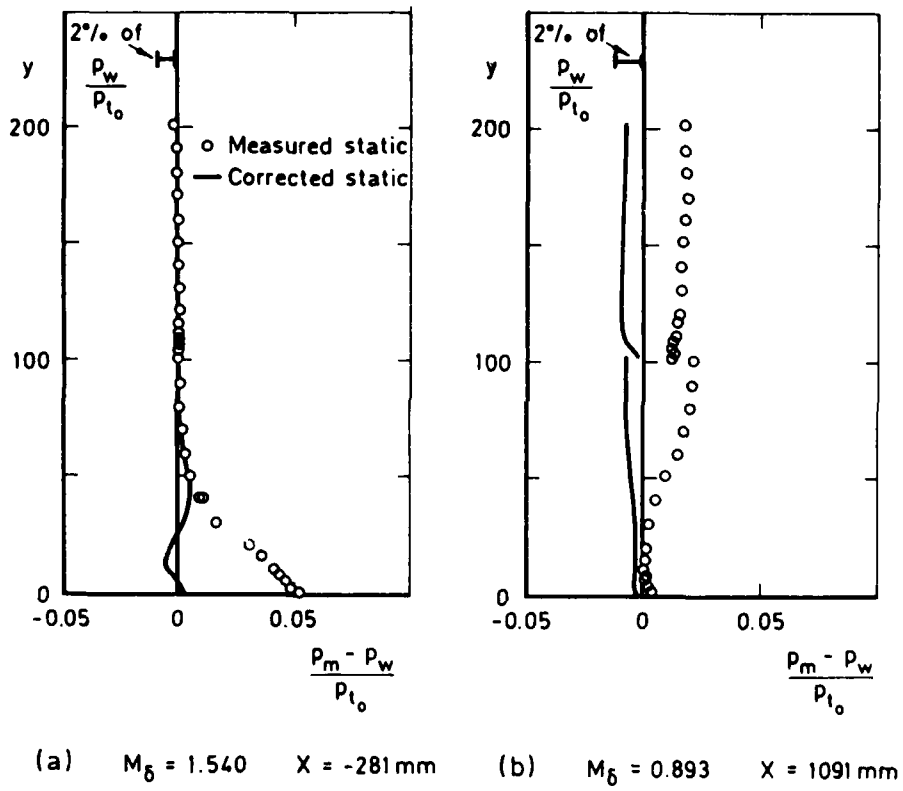


Fig 32a&b Typical corrected static pressures

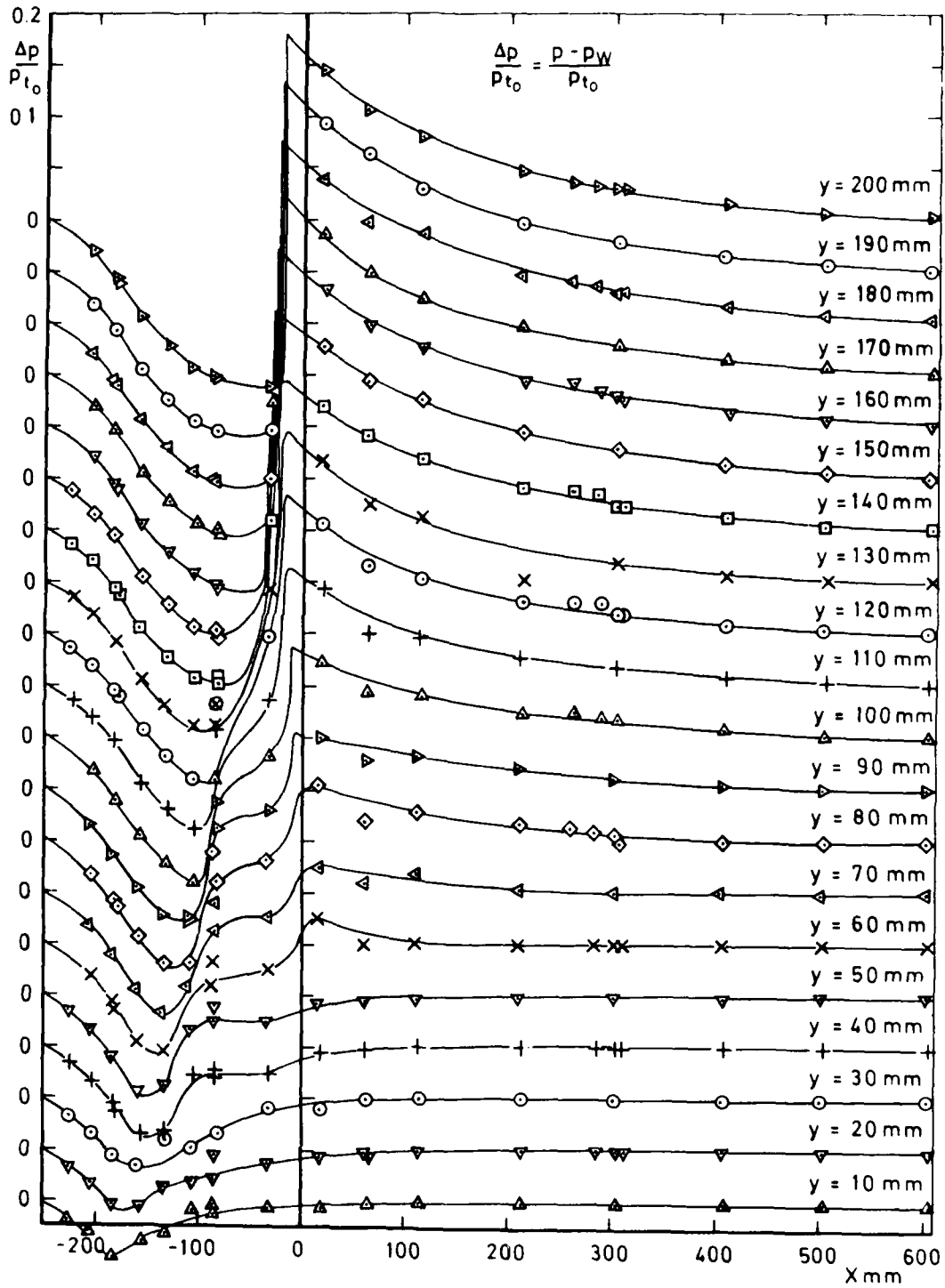


Fig 33 Smoothed static pressure distribution,  $M = 1.5$ ,  $Re = 10 \times 10^6/\text{mm}$

**REPORT DOCUMENTATION PAGE**

Overall security classification of this page

UNLIMITED

As far as possible this page should contain only unclassified information. If it is necessary to enter classified information, the box above must be marked to indicate the classification, e.g. Restricted, Confidential or Secret.

1. DRIC Reference (to be added by DRIC)	2. Originator's Reference RAE TR 82099	3. Agency Reference N/A	4. Report Security Classification/Marking  UNLIMITED
5. DRIC Code for Originator 7673000W	6. Originator (Corporate Author) Name and Location Royal Aircraft Establishment, Farnborough, Hants, UK		
5a. Sponsoring Agency's Code N/A	6a. Sponsoring Agency (Contract Authority) Name and Location N/A		
7. Title <b>A study of normal shock-wave turbulent boundary-layer interactions at Mach numbers of 1.3, 1.4 and 1.5</b>			
7a. (For Translations) Title in Foreign Language			
7b. (For Conference Papers) Title, Place and Date of Conference			
8. Author 1. Surname, Initials Sawyer, W.G.	9a. Author 2 Long, Carol J.	9b. Authors 3, 4 .... -	10. Date    Pages    Refs. October   153   29 1982
11. Contract Number N/A	12. Period N/A	13. Project -	14. Other Reference Nos. Aero 3532
15. Distribution statement (a) Controlled by - <b>RAL Aerodynamics</b> (b) Special limitations (if any) -			
16. Descriptors (Keywords)                      (Descriptors marked * are selected from TEST)  <b>Shock waves*. Turbulent boundary layers*. Boundary layer separation*.</b>			
17. Abstract  <p>This Report presents the results of a study of seven flows involving the interaction between a normal shock wave and a two-dimensional turbulent boundary layer. The measurements were made at free-stream Mach numbers of 1.3, 1.4 and 1.5 and at Reynolds numbers based on an effective streamwise run of <math>10 \times 10^6</math> to <math>30 \times 10^6</math>. The results were obtained from comprehensive traverses with both pitot and static probes.</p> <p>Standard boundary-layer integral parameters based on wall and measured static pressures are presented, together with velocity profiles and the Mach number distribution over the interaction region.</p> <p>An investigation has been made of the 'law of the wall' and the 'law of the wake' under the influence of strong normal pressure gradients.</p>			

END

DATE  
FILMED

9 - 83

DTI